ABSTRACT

KAZEM, HAMID. Shear Strengthening of Steel Bridge Girders Using Small-Diameter CFRP Strands. (Under the direction of Professor Sami H. Rizkalla)

There is a growing demand for strengthening steel structures and bridges due to increase of load demand and/or possible reduction of capacity caused by corrosion. Use of CFRP laminates with elastic modulus approximately equal to or higher than that of steel has been successfully used for flexural strengthening of steel structures; however, few researches explored the use of these materials for shear strengthening of steel structures and bridges. This thesis summarizes the findings of a comprehensive research program, including experimental and analytical studies undertaken to examine the use of small-diameter Carbon Fiber Reinforced Polymer (CFRP) strands for shear strengthening of steel structures and bridges. Most of the current research findings on the use of CFRP laminate revealed failure due to de-bonding since the laminates are only bonded to the substrate from one side. However, the small-diameter CFRP strands have revealed high bonding characteristics under flexural stresses. The experimental program examined the proposed strengthening system to increase the buckling capacity of steel plates subjected to uniaxial compressive stresses, relating to the principle compressive stresses arising from pure shear stress condition. A total 32 steel plates were tested under axial compressive loads to evaluate the increasing effects of plate slenderness ratio (h/t), CFRP elastic modulus, and strengthening reinforcement ratio on buckling capacity of the strengthened steel plate. The research then continued to examine the same strengthening system for increasing the shear capacity of steel plate by subjecting nine

steel plates to pure shear loading conditions. The effectiveness of strengthening reinforcement ratio and orientation of CFRP strands were determined in this phase. Nonlinear finite element (FE) models, calibrated by the experimental results were used to study different parameters that were not included in the experimental program. The FE models have also used to propose design guidelines for the strengthening system. Research findings indicated that the proposed system is effective for shear strengthening of steel structures and the material used eliminated the typical debonding failure, commonly observed for strengthening systems using CFRP laminates. Based on the research finding, design guidelines are recommended for the proposed strengthening system.

Shear Strengthening of Steel Bridge Girders Using Small-Diameter CFRP Strands

by
Hamid Kazem

A dissertation submitted to the Graduate Faculty of
North Carolina State University
in partial fulfillment of the
requirements for the Degree of
Doctor of Philosophy

Civil Engineering

Raleigh, North Carolina
2016

APPROVED BY:

Sami H. Rizkalla, Ph.D. Committee Chair	James Nau, Ph.D.
Gregory Lucier, Ph.D.	John Strenkowski, Ph.D.

DEDICATION

I dedicate this thesis to my beloved parents, Sodabeh Jafari Salim and Dr. Hossein Kazem and my beloved brother Navid Kazem, for their unwavering love, support and encouragement.

I also dedicate this dissertation to my family who have supported me throughout this long term study process. I give special thanks to my best friends, Nooshafarin Mohammadzadeh, Shahin Safavi, Mahboubeh Ameri, Mehran Jafari, Mahtab Fakhimi, Adele Moatti, Alireza Mashadi, Dr. Shayan Safavi, and Dr. Milad Hallaji encouraged and supported me during period of my PhD studies.

Thank you

BIOGRAPHY

Hamid Kazem started studying civil engineering in 2005 at Amirkabir University of Technology (Tehran Polytechnic), Tehran, Iran. In 2009, Hamid obtained his B.Sc. degree in with a grade distinction of honor and a scholastic rank as the second top student of his class. He was then waived taking M.Sc. entrance exam as talented student and started his graduate study at Amirkabir University of Technology (Tehran Polytechnic). In 2011, Hamid obtained his M.Sc. degree in Structural Engineering. During his studies, he started part-time work as a structural engineer at ZME consulting engineering company and continued for three years. Then, He joined as a full-time structural engineer at TSP consulting engineering firm specializing in structural analysis and design of buildings and bridges. In 2013, Hamid was awarded a scholarship to pursue a Ph.D. degree in the United States, which enabled him to enroll in the graduate program in structural engineering at North Carolina State University working under the direction of Professor Sami H. Rizkalla.

ACKNOWLEDGMENTS

I would like to thank my advisor and committee chair Dr. Sami Rizkalla for the extensive guidance, expertise, and advice he has given me throughout my graduate program. I would like to extend special thanks to Dr. James Nau for kindly accepting to be a member of my advisory committee. Thank you to Dr. Gregory Lucier for his guidance valuable support and expertise in many facets of this research program. I would like to express my thanks to Dr. John Strenkowski for his constructive comments.

Thanks to Nippon Steel and Sumikin Materials Company for their continued financial support of this research endeavor. Thanks to Jerry Atkinson, Jonathon McEntire and Benjamin Smith for their technical expertise and willingness to convey that expertise to performe experimental research. I also give special thanks to Dr. Hatem Seliem and Lucas Guaderrama for their efforts and advice throughout the first phase of this research program.

I would like to extend special thanks to all my colleagues and friends in the Constructed Facilities Laboratory (CFL) especially Dr. Dillon Lunn, Dr. Gautam Sopal, Mohamed Nafadi, Dr. Amir Botros, Griff Shapack, Omar Khalaf Allah, Cody Johnston, Oscar Santoyo-Apolonio, and Carlos Vega for their assistance during the experimental phase of this study. I would also like to acknowledge Wesley Ballew and Dr. Michael Borden for their advice in analytical section of the program.

Thank you to my family and friends for giving me support and encouragement in all that I do. Finally, I extend my heartfelt gratitude to my parents for all that they have done for me. Without you, this would not have been possible.

TABLE OF CONTENTS

LIST OF TABLES

LIST OF FIGURES

1 INTRODUCTION

1.1 RESEARCH OVERVIEW

Due to the known benefits of Fiber Reinforced Polymer (FRP) materials, their use for retrofitting (strengthening and repair) of concrete structures became a common practice. Accordingly, use of FRP material for steel structures is required due to increasing demand of traffic loads, corrosion and fatigue deterioration effects. The new bridge design codes require designing for higher vehicular live loads in comparison to that used in the initial design of the bridges. Therefore, production of high modulus Carbon FRP (CFRP) with elastic modulus higher than that of steel, offers a promising alternative for flexural and shear strengthening of steel structures and bridges [1].

The research presented in this thesis is focused on shear strengthening of steel web girder using CFRP strengthening system. In order to allow for an increase of the total load-carrying capacity of the strengthened steel bridge girder, the shear capacity of the member should be increased along with its flexural capacity.

Shear strength of steel girder is determined by the capacity of the web plate. The steel web plate subjected to shear results in two tensile and compressive stress components as schematically shown in Figure 1-1. Ultimate strength of the web plate is either due to elastic buckling (in case of slender web) or yielding of the material (in case of compact or non-compact web). The capacity of the web plate, and hence the shear strength of the steel girder, can be enhanced by reducing the state of stress in the web plate. The elastic buckling of slender web plates is directly related to level of the principal compressive stresses. Strengthening of

web plates using Fiber-Reinforced Polymer (FRP) materials could help reduce the stress level in the web, and potentially increase the shear capacity at which the elastic bucking or material yielding occurs.

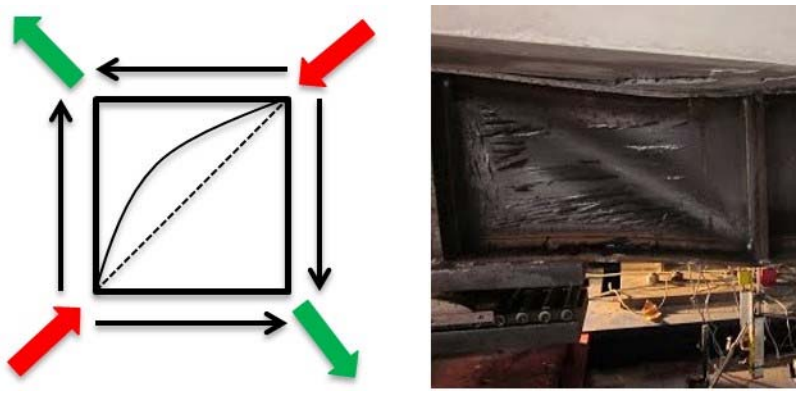

Figure 1-1: Shear Buckling Phenomenon [2]

Performance of CFRP materials in tension is well documented and is clearly understood. However, their behavior in compression is still very controversial and is still prohibited by many design guidelines. Therefore, for evaluating the efficiency of CFRP materials for enhancing shear strength of steel girders, their behavior in compression and their ability to undergo large deformations associated with buckling has to be assessed. Accordingly, the research program presented in this study will investigate the performance of CFRP material in compression followed by investigating the effectiveness of the proposed strengthening system to increase the shear capacity using specimens subjected to direct shear loading.

1.2 RESEARCH OBJECTIVE

The main objective of the research is to investigate the use of the CFRP strands to enhance the shear strength of steel bridge girders. Reducing the stresses in the web, could potentially lead

to a higher shear capacity of the girder. The stresses in the web have to be less than the stress level at which buckling occurs and/or the yield strength in order to allow for higher shear resistance. CFRP strands will be externally bonded to the web of the steel girder to reduce the induced compressive and tensile stresses in the web by contributing to the load-carrying mechanism of the forces in the web. Hence, the girder can carry higher shear loads before reaching its ultimate limit state.

The specific objectives of this research can be outlined as follows:

1) Determine the performance of small-diameter CFRP strands subjected to large deformations associated with web buckling.
2) Evaluate the effectiveness of the small-diameter CFRP strands for shear strengthening of steel girders.
3) Assess the performance of the different types of small-diameter CFRP strands including HM, IM, and LM and identify the most effective material stiffness, reinforcement ratio, orientation and configuration suitable for shear strengthening.
4) Develop analytical model to study different parameters not considered in the experimental program.
5) Develop design guideline for shear strengthening of steel girders.

1.3 RESEARCH SCOPE

The research consists of a comprehensive experimental program complemented by finite element modeling to study other parameters not considered in the experimental study. Rational

approach will be introduced based on the experimental and the analytical studies to introduce design guideline for the use of CFRP strands for shear strengthening of steel girders.

The proposed experimental and analytical program consisted of two phases. The first phase studied the effectiveness of the small-diameter CFRP strands in increasing the uniaxial compressive capacity of steel plates. Phase I included studies of steel plates with different slenderness ratio (h/t). The selected ratios covered a wide spectrum of compact, non-compact, and slender webs of typical steel bridge girders. With three types of CFRP strands, i.e. HM, IM, and LM, the experimental research identifies the most effective type of CFRP strands for enhancing the buckling load of steel plates. The effect of using low-modulus polyurea putty on the de-bonding capacity of the CFRP strands was also investigated. Furthermore, the effectiveness of using different reinforcement ratio of CFRP materials was also investigated experimentally and analytically by applying layers of small-diameter CFRP strands.

The second phase examined the pure shear testing of plates strengthened by selected CFRP strands to simulate typical steel bridge girders. Final selection of the strand type was based on the results of the phase I. The effect of using different fiber orientation and reinforcement ratio of CFRP strands were investigated in this phase of research. The analytical studies evaluated effects of strengthening system using wide range of slenderness ratio and three CFRP strengthening materials including HM, IM, and LM small-diameter strands.

This thesis is organized in six chapters. In the first chapter of the thesis the problem is presented and the objectives of the research are introduced. The second chapter of the thesis summarizes research background conducted on use of FRP strengthening system over compressive and

shear strengthening of steel structures. The third chapter describes the experimental program designed to investigate the objectives including the fabrication of the test specimens, the test setups, and instrumentation used. The material properties of the steel and CFRP strands used in this experimental program are reported based on the tested material coupons. Chapter three describes the strengthening techniques used in the experimental program. Chapter four describes the analytical phase of the research program using nonlinear finite element, FE, analysis to model and calibrate the behavior of the steel plates strengthened with CFRP strands subjected to uniaxial compressive and shear forces. The fifth chapter describes the use of the developed FE model is to study the effect of different parameters which were not considered in experimental program. The final chapter summarize the research findings of the program and recommends future works.

2 LITERATURE REVIEW

Fiber-Reinforced Polymer (FRP) materials were developed primarily for aerospace and defense industries [3] and are widely used in many industries today, including aeronautic, marine, automotive and electrical engineering. With the continuing cost reduction in FRP materials and the growing need for new materials to renovate civil infrastructures, FRP materials are now finding wider acceptance among civil engineers [4]. Although, use of FRP in civil engineering has a slow pace of growth, the civil engineering industry benefits applications of FRP in different fields such as structural, geotechnical and transportation [5-10].

Structures built by the traditional engineering materials such as reinforced and prestressed concrete, steel and masonry, suffer from variety of damages which reduce the service time of the structures. Structures with significant problems are those exposed to load increase, marine environments, de-icing salts, aggressive industrial environments and to a lesser extent those which are exposed to normal weather conditions. From an economic point of view it is generally more realistic to repair and strengthen, if possible, rather than to demolish the structures [11-15]. Traditional strengthening techniques including welding or bolting steel plates or sections to the existing structure could lead to increase of dead load, high construction cost, require high labor intensity, cause interruptions to traffic flow for bridges, and become prone to corrosion and fatigue. Therefore, use of FRP strengthening systems have revealed many advantages to be an excellent alternative material due to its high strength-to-weight

ratios, corrosion resistance, and ease of construction in comparison to the use of steel strengthening materials [16].

Use of FRP materials for strengthening of concrete structures and bridges has gained wide acceptance worldwide, due to its appealing benefits [17, 18]. There is also a growing demand for strengthening steel structures and bridges due to increase of load demand and/or possible reduction of the load-carrying capacity due to deterioration. Use of externally bonded FRP materials for strengthening steel structures did not progress similar to its use for concrete structures due to the low elastic modulus of the FRP material relative to steel. However, the recent production of high-modulus Carbon FRP (CFRP) laminates with an elastic modulus similar to or higher than that of steel offers a promising alternative for externally bonded strengthening system for steel structures [19, 20].

FRP is a composite material consist of a fibers made from carbon, glass, basalt or aramid embedded in a resin matrix [21]. Different orientations of fibers can be used to most efficiently follow the stress distribution of the structure. An important issue in strengthening of structures using FRP composite sheets/plates is to design against different failure modes [22]. Due to the uncertainties and the sudden nature of debonding failure experienced between FRP sheets/plates and steel surfaces, numerous studies were conducted experimentally and analytically to investigate the bond behavior [23-31]. Understanding the bond mechanism of the CFRP to steel typically started by testing flexural strengthening of steel beams. Followed by realizing the bond behavior, many researches have explored the use of externally bonded, high-modulus CFRP materials for flexural strengthening of steel members and have shown

significant increase in flexural capacity and stiffness [32-38]. However, to increase the total load-carrying capacity of the strengthened member, the shear capacity should also be increased along with its flexural capacity. There are very few researches investigated the shear strengthening of steel structures using externally bonded CFRP materials. The following sections are mainly focusing on the published information on this topic to emphasize the need for more studies on this subject.

2.1 STRENGTHENING OF COMPRESSIVE MEMBERS

The shear strength of steel beams is controlled by the capacity of the web plate. Failure of the web plate due to elastic buckling or yielding of the material depends on the slenderness ratio of the web. The elastic buckling of slender web plates is directly related to level of the principal compressive stresses induced within the high shear zone(s) of the beam. Strengthening of web plates using CFRP materials has the potential to reduce the stress level in the web, and consequently increase the shear-carrying capacity of the web. Therefore, to evaluate the efficiency of the CFRP materials for enhancing the shear strength of steel beams, their behavior in resisting the principal compressive stresses and their ability to undergo large deformations associated with buckling should be determined. Several studies have been reported on the use of CFRP laminates to increase the compressive resistance of steel members. Steel members under compression often fail in local or global buckling depending on the cross section and slenderness values. The presence of FRP can delay, eliminate, or reduce the buckling/collapse, leading to a higher load carrying capacity [21].

2.1.1 Column Strengthening

Shaat & Fam (2006) [39] investigated the behavior of axially loaded short and long-columns wrapped with both longitudinal and transverse CFRP sheets as shown in Figure 2-1. 27 short-column and five long-column HSS specimens were tested. The effect of CFRP sheet orientation in the longitudinal and transverse directions was studied for short-columns. For long-columns, CFRP sheets were oriented in the longitudinal direction only. A maximum strength gain of 18% was achieved for short columns with two transverse CFRP layers. For long columns, the maximum strength gain of 23% was achieved with three longitudinal CFRP layers applied on four sides. Strength gain in long-columns was highly dependent on the column's imperfection. Test results showed that debonding of CFRP sheets occurred for both short and long columns. Short-column specimens experienced debonding between steel and CFRP layers when local buckling occurred. Failure of strengthened long-column specimens was due to local buckling associated with combined debonding and crushing of the CFRP sheets.

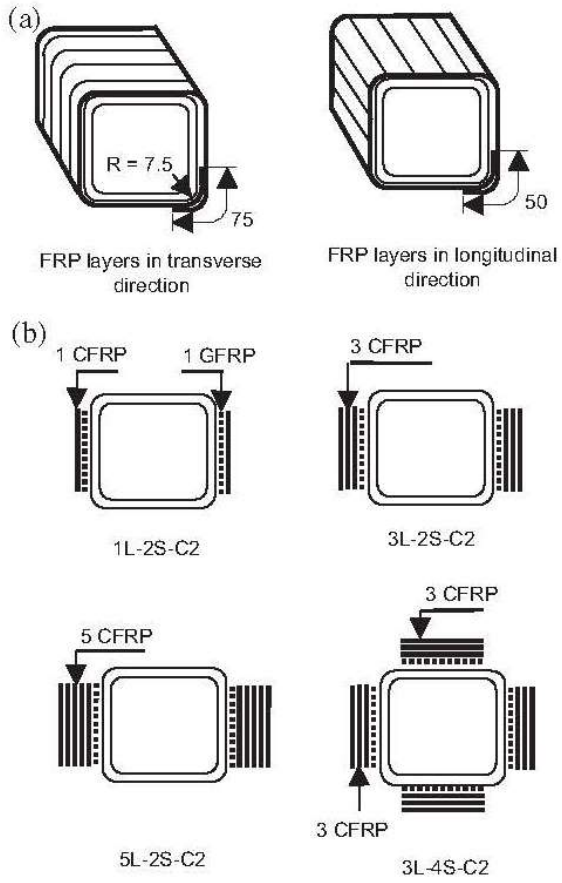

Figure 2-1: Details of FRP retrofit configurations, a) short-columns, b) long-columns [39]

Silvestre et al. (2008) [40] reported the results of an experimental and numerical investigation on the nonlinear behavior and load-carrying capacity of CFRP strengthened cold-formed steel lipped channel columns. A total of 19 short and long fixed-ended lipped channel columns were tested. The columns were strengthened with CFRP bonded at different outer surface locations and having the fibers oriented either longitudinally or transversally. Results concluded that the presence of the single layer of CFRP may increase the load-carrying capacity by up to 15%, for the short columns, and 20%, for the long columns. All column failures were due to local plate buckling mode interaction as illustrated in Figure 2-2. Then, the excessive column wall

deformations due to the buckling effects also causes CFRP debonding, which invariably occurs after the ultimate load is reached.

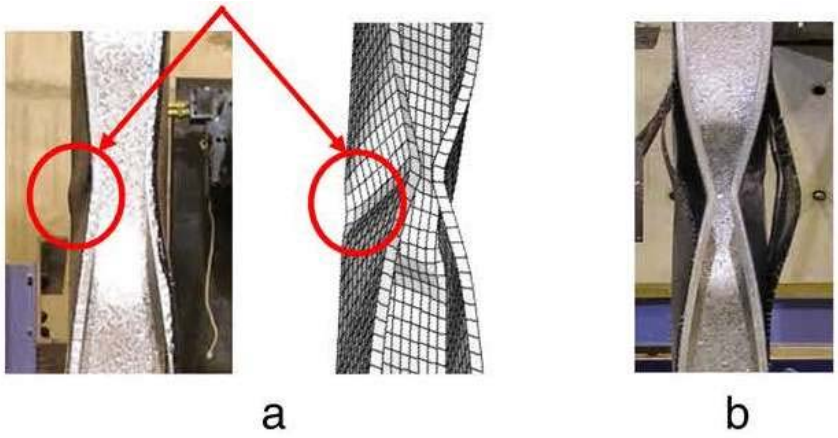

Figure 2-2: Debonding of the CFRP sheets, a) initial (near the yielded line), b) total [40]

Shaat & Fam (2009) [41] presented the results of an experimental investigation into the behavior of slender steel columns strengthened with high-modulus CFRP plates under uniaxial compression loads. Eighteen slender hollow structural section square column specimens, were concentrically loaded to failure. The effectiveness of CFRP was evaluated for different slenderness ratios. The maximum increases in ultimate load ranged from 6 to 71% and axial stiffness ranged from 10 to 17%, respectively, depending on slenderness ratio. Effectiveness of the strengthening system was reduced by reduction of the slenderness ratio. CFRP failure was observed to be due to debonding or crushing of the material prior to or after overall buckling of the column, depending on the column slenderness ratio.

Harries et al. (2009) [42] performed experimental research on improving global and local buckling behavior of steel compressive member using FRP materials. Concentric axial compressive tests were carried out on short and long WT column sections. Results indicated

that the effectiveness of adding FRP is negligible on the elastic buckling behavior of long sections which are typically used as structural bracings. The FRP retrofit is however able to affect local behavior. Improvement in load-carrying capacity is proportional to the increase in effective radius of gyration affected by the presence of the FRP. Test observations confirmed occurrence of failure due to debonding at the post-peak behavior.

2.1.2 Web Strengthening Subjected to End Bearing

The web crippling of the thin-walled steel members is often observed at loading or reaction points where concentrated forces exists. Web crippling consists of two failure modes: web buckling and web yielding. CFRP strengthening system can be a proper alternative to increase web crippling capacity of cold-formed and aluminum rectangular hollow sections (RHS), light steel beams (LSB), channels and I-section beams [21].

The web-crippling behavior of rectangular hollow sections (RHS) strengthened with CFRP sheets and plates was investigated by Zhao et al. (2006) [43]. Several types of strengthening technique, as illustrated in Figure 2-3, were investigated to improve the web crippling behavior of cold-formed RHS. It was found that the CFRP strengthening significantly increases the web crippling capacity especially for those with large web slenderness ratio. The failure mode observed from the strengthened specimens were either CFRP delamination accompanied by either web buckling or web yielding.

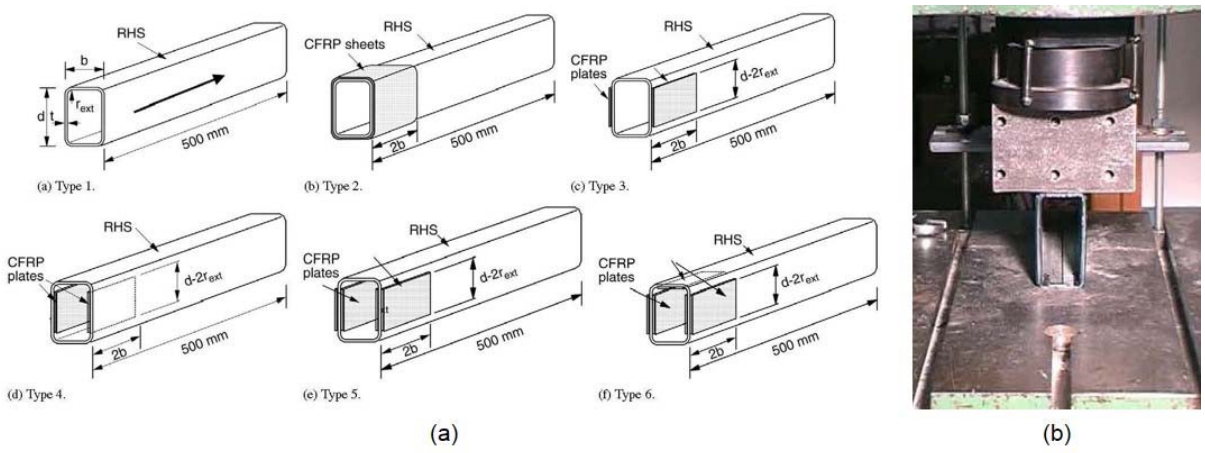

Figure 2-3: a) Different types of CFRP strengthening technique, b) Test setup [43]

The web-buckling of light-steel beams (LSB) strengthened with FRP systems was explored by Zhao & Al-Mahaidi (2009) [44]. A series of laboratory tests were conducted using three types of strengthening methods such as applying CFRP plates on the outer side or inner side or both sides of the web. Seven LSB sizes were chosen for each strengthening method. Test results demonstrated increase in the web-buckling capacity, especially by bonding CFRP plates on the both side of the web and for specimens with high depth-to-thickness ratios. Also, 50% reduction in effective length factor for CFRP strengthened LSB was captured compared to bare LSB. This behavior indicates imposed restraint on the strengthened system. Furthermore, CFRP debonding was captured as the failure mode of the test specimens strengthened by three different methods as shown in Figure 2-4.

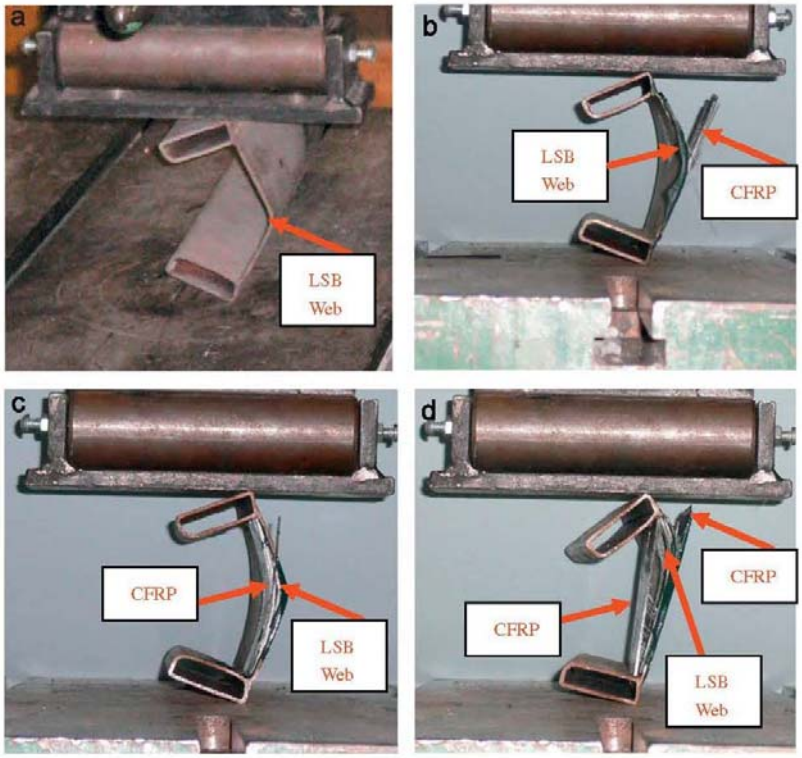

Figure 2-4: Failure modes, a) bare LSB (reference test), b) Method 1: CFRP on outer side, c) Method 2: CFRP on inner side, d) Method 3: CFRP on both sides [44]

Behavior of CFRP strengthened steel I-section under end bearing loads was examined by Zhao (2009) [45]. A series of laboratory tests were conducted adopting several types of strengthening configurations such as applying CFRP on the web or on the web and flanges. As results confirmed, more increase in web buckling capacity is achieved for slender steel web. As shown in Figure 2-5, due to large deformation, bonding behavior of the strengthened specimen with CFRP attached on the web and flanges was more acceptable compared to the strengthened specimen with attached CFRP on the web only.

Figure 2-5: Typical failure mode for I-section; a) Control , b) CFRP on web, c) CFRP on web and flange

Aguilera & Fam (2013) [46] studied the effectiveness of externally bonded FRP plates to strengthen rectangular hollow steel section T-Joints representing beam-column connections or joints in truss girders. Thin webs of HSS sections were subjected to transverse loading, thereby increasing their bearing load capacity. Twelve T-joints HSS chords, welded to HSS braces were tested under brace axial compression. GFRP plates of different configurations, with and without edge tapering, and high-modulus CFRP plates of equivalent stiffness, were adhesively bonded to the webs of the chord near the brace. Figure 2-6 shows test specimen, FRP installation and test setup of T-joints under brace axial compressive load. Results showed that increasing the slenderness ratio (h/t) from 34 to 65, resulted in strength gain increased from 9% to 38% and from 27% to 53% when narrow and wide GFRP plates were used, respectively. The total width of the FRP plates was shown to have a significant effect on the strengthening system as well. Very wide FRP plates changed failure modes from local buckling to shear failure near supports for members with slenderness ratio of 65 and also changed failure modes from local buckling to plate delamination in members with slenderness ratio of 34.

Figure 2-6: a) Test specimens and FRP installation, b) Test setup of T-joints under axial compression [46]

2.2 STRENGTHENING OF MEMBERS SUBJECTED TO SHEAR

In addition to increasing a bridge girder's flexural capacity, the girder's shear capacity should also be increased to match the girder's increased flexural capacity. Along with research done on thin walled sections, very limited number of research have been reported on increasing the shear capacity of an existing steel girders.

Patnaik et al. (2008) [47] published results of experimental and analytical program focused on shear strengthening of steel built-up I-beams. Three beams were specially designed to fail in shear. Two were strengthened by bonded CFRP to the webs, while, one was kept as an un-strengthened control specimen. Figure 2-7 shows typical elevation of the strengthened and control shear specimens. Test results of shear strengthening confirmed effectiveness of shear strengthening application by increasing the shear capacity of the steel beam up to 26%. Typical shear failure mode of the CFRP strengthened specimen is shown in Figure 2-8 and some part of CFRP sheet was peeled off from the steel substrate. The failure load of the control beam caused elastic buckling; however, inelastic buckling was the failure mode of strengthened beam. Failure of all the three beams occurred gradually, similar to ductile failure.

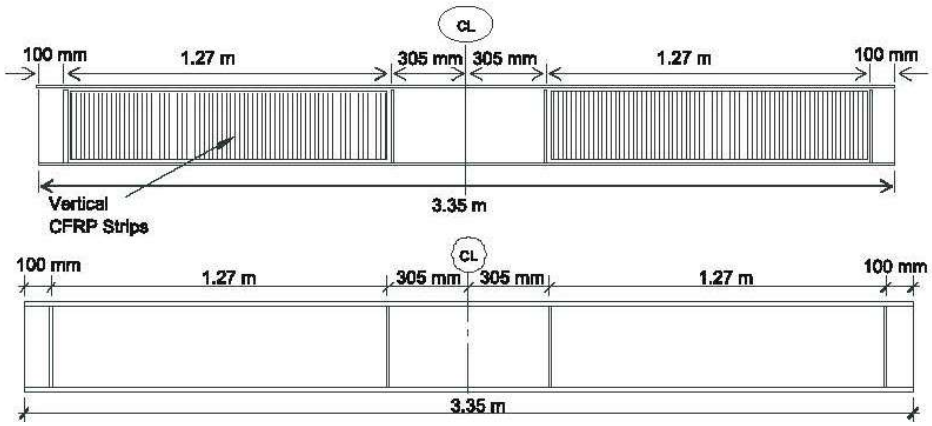

Figure 2-7: Typical elevation of the shear test beams [47]

Figure 2-8: Typical failure of shear failure beams [47]

Okeil et al. [48-50] improved the lateral stiffness of buckling-prone steel by bonding pultruded GFRP sections as shown in Figure 2-9. I-shaped steel beams were specially designed to fail in shear buckling and were tested to explore the feasibility of the proposed technique. Thin-walled steel plates were bonded by GFRP T-shaped in an orientation that contribute to the lateral stiffness of the plate web more than the in-plane strength as is the common practice in

most FRP strengthening cases. The strengthened specimen experienced shear buckling in 56% higher load compared with control un-strengthened specimen. However, common with most FRP strengthening techniques, the behavior of the strengthened specimen was more brittle compared with control specimen. Failure mode of the control specimens were due to web shear buckling. The strengthened specimens were intact until the beams failed by debonding of the GFRP stiffener followed by immediate web buckling. debounding occurred due to initiation of epoxy failure followed by cracking noises. Most of the epoxy cracks were not visible as they were under the GFRP stiffener with only a few cracks that could be seen at the edges. The study on using T-shaped GFRP stiffeners for shear strengthening of steel I-beams was continued by Babaizadeh (2012) [51] conducting analytical parametric studies. Results of FE analysis showed that strengthening steel beams with different flange width can result in increase of shear capacity up to 66% for square shear zones and up to 36% for rectangular shear zone. Furthermore, results indicated that GFRP stiffeners are more effective than steel stiffener in terms of enhancing the shear capacity of the strengthened steel beam. However the failure of the CFRP stiffened beams are less ductile compared with unstiffened or steel stiffened beams.

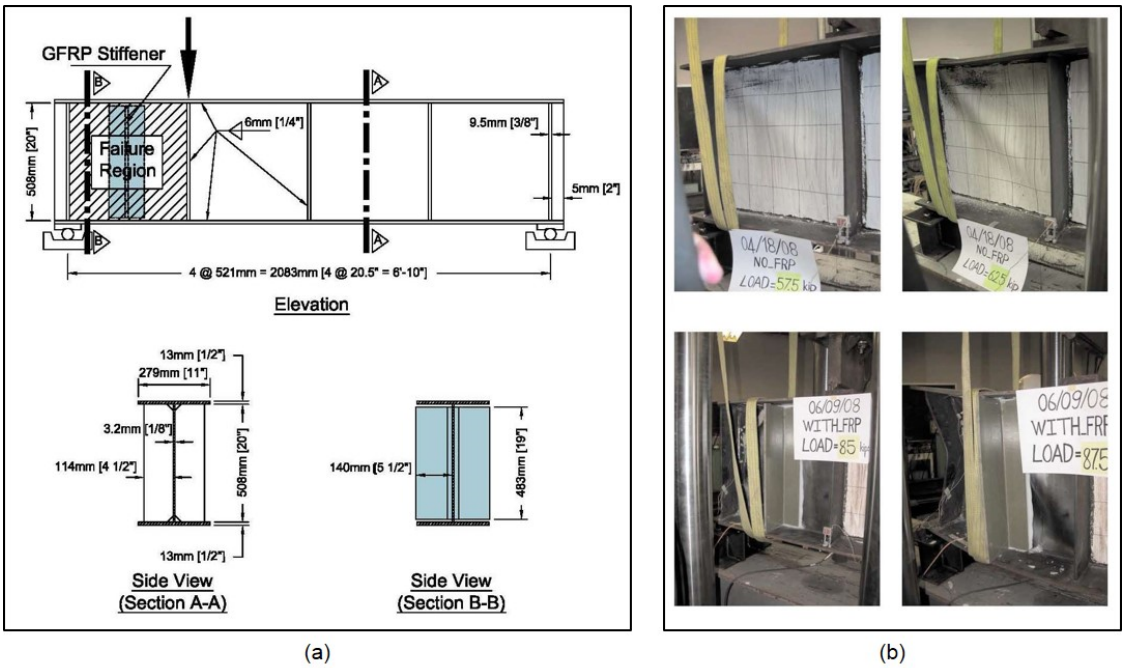

Figure 2-9: a) Dimensions of beam specimens, b) Failure of beam specimens

To examine the effectiveness of CFRP strengthening system, application of CFRP strips as shear reinforcement was investigated by Narmashiri et al. (2010) [52]. Strengthening specimens were developed by applying CFRP on one or both faces of the steel web, and using different values of CFRP area on the web. Five steel I-section beams were tested as shown in Figure 2-10. Two beams were strengthened on both sides of web with the CFRP ratios of 0.72 and 0.48. Two beams were strengthened on one side of web with the CFRP ratios of 0.72 and 0.48. Last beam was kept as un-strengthened control to be used for comparison.

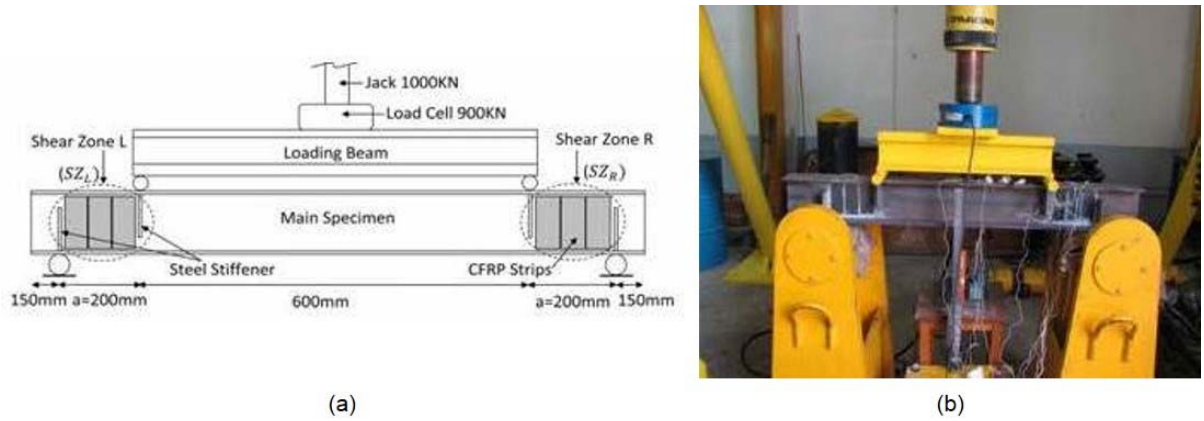

Figure 2-10: a) General specification of the specimen, b) Setup of the experimental test

Results clearly showed that externally bonded CFRP could increase the shear capacity of the steel strengthened I-beam up to 51%. Furthermore, both CFRP ratios for both sides of web had the same level of increase in shear capacity. Two failure modes including longitudinal delaminating of the CFRP strips and CFRP debonding of the strips were observed experimentally.

3 EXPERIMENTAL PROGRAM

The proposed experimental program consists of two phases. The first phase was designed to determine the effectiveness of the small-diameter CFRP strengthening system on the compressive strength and buckling capacity of steel plates. The second phase examines the effectiveness of the same strengthening system on increasing the shear capacity of the steel web girders. This chapter documents the testing, test results, and discussion of results obtained from material testing, uniaxial compressive strengthening tests (phase I) and shear strengthening tests (phase II).

3.1 MATERIAL PROPERTIES

3.1.1 Tensile Characteristics of the Selected Steel

High-Strength Low-Alloy Grade 50 steel (345 MPa (50 kips)) designated by ASTM A572 was selected for all test plates included in the experimental program. Tensile coupons were prepared and tested according to ASTM A370 using 200 kip (900 kN) capacity universal MTS Testing machine as shown in Figure 3-1. Elongations of the coupons were measured by a 51 mm (2 in.) extensometer and the applied load was measured directly by the machine load cell. The nominal dimensions of the steel tensile specimens are shown in Figure 3-2. However, the actual cross-section of each specimen was measured using a digital caliper with an accuracy of 0.01 mm (0.0004 in.) along the gage length and the average cross-sectional area was used.

All the plates were provided from the same heat patch of the tested plate to ensure accurate prediction of the material of the tested steel plates.

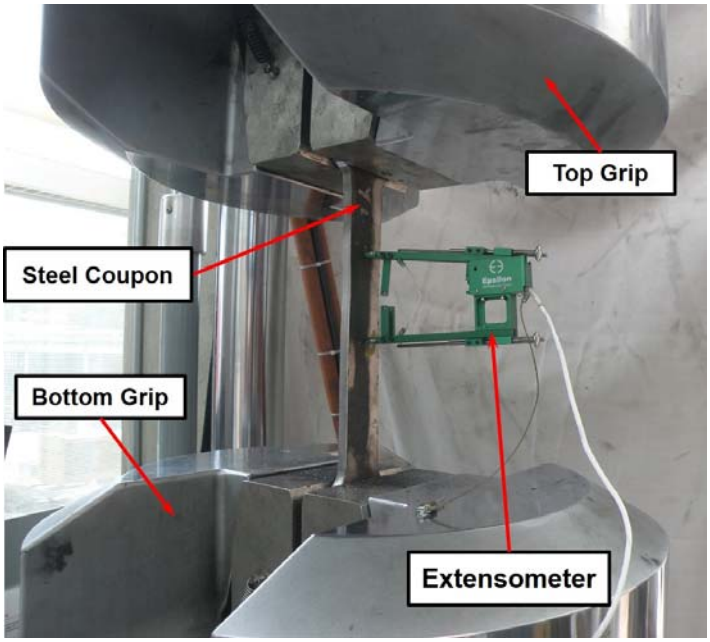

Figure 3-1: Testing steel tensile coupon using the universal MTS testing machine

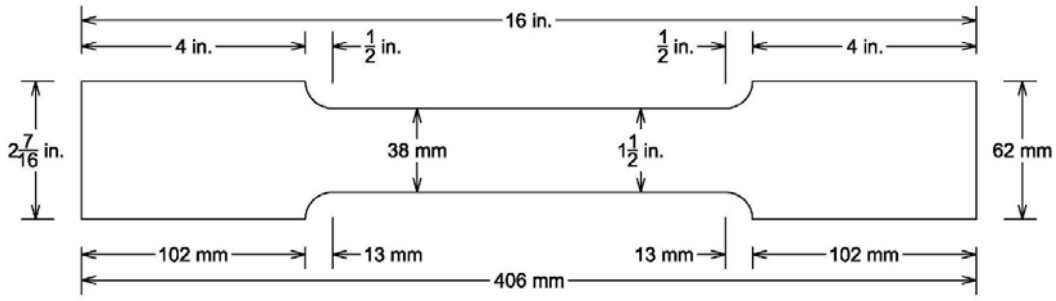

Figure 3-2: Dimensions of ASTM A370 steel tensile specimen

A total of 18 coupons were tested including nine coupons for each phase of the experimental program. Phase I tested three coupons out of each thickness of 8 mm (5/16 in.), 10 mm (3/8 in.) and 13 mm (1/2 in.). Phase II included nine coupons out of the three sets of the test specimens. Typical stress-strain curves for the steel specimens obtained from steel tensile

coupons for phase I and phase II are shown in Figure 3-3 and Figure 3-4, respectively. The yield strength, modulus of elasticity, and the corresponding yield strain are given in Table 3-1 and Table 3-2 for the three different specimens of in phase I and II, respectively.

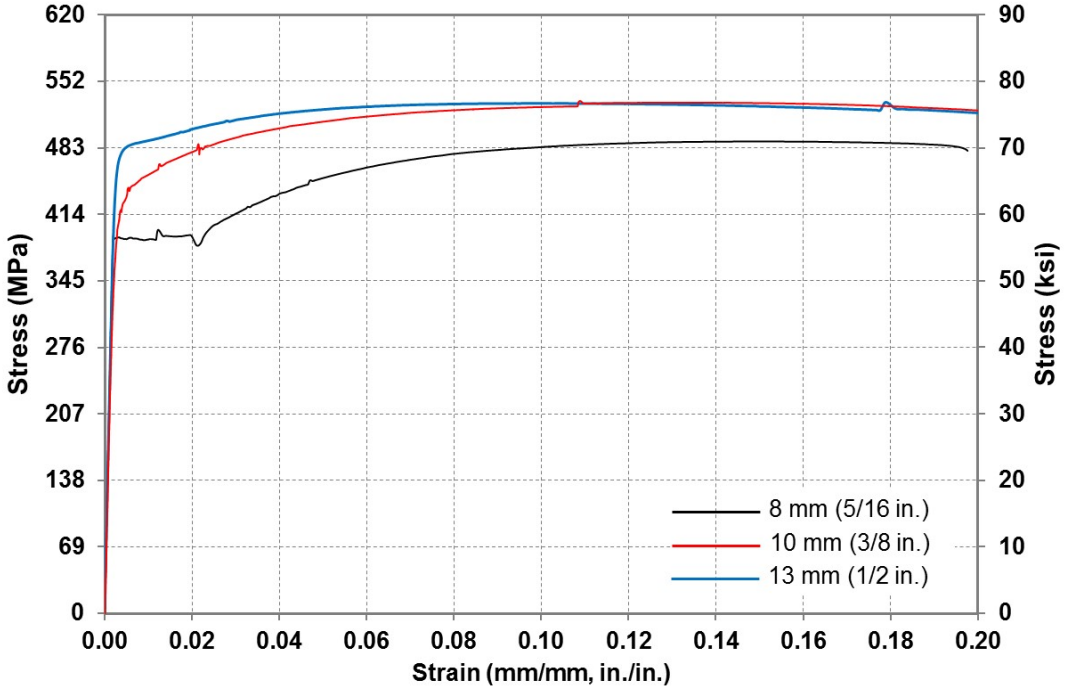

Figure 3-3: Typical stress-strain behavior of steel coupons tested in phase I

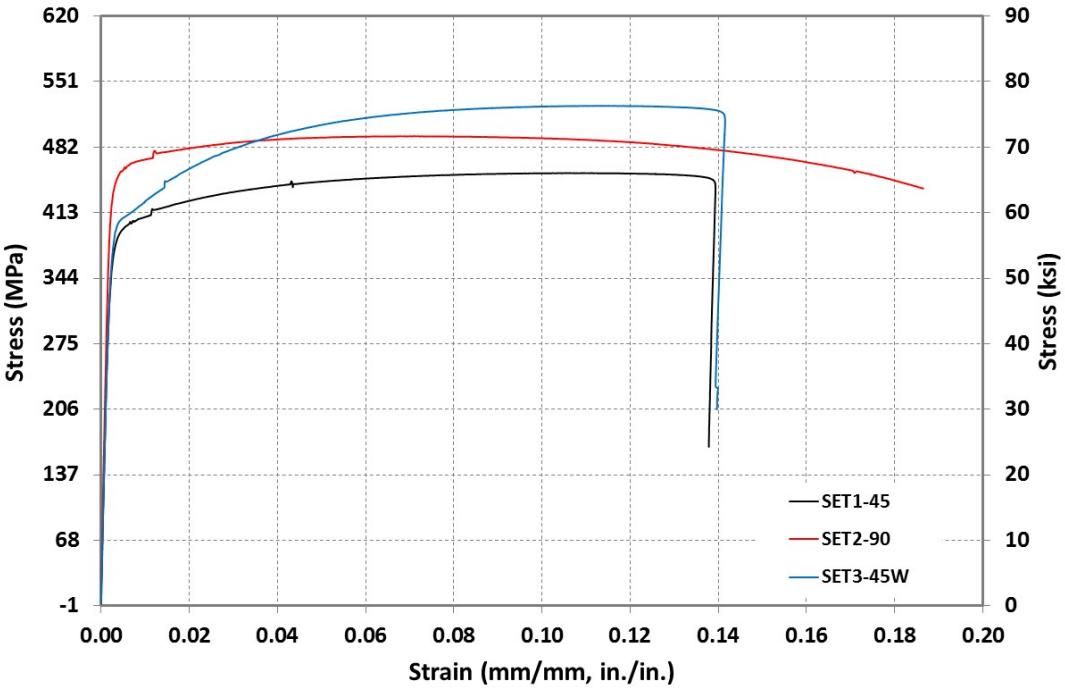

Figure 3-4: Typical stress-strain behavior of steel coupons tested in phase II

Table 3-1: Summary of measured tensile characteristics of steel tested in phase I

Nominal Thickness	Specimen	Yield Strength		Modulus of Elasticity		Yield Strain
mm (in.)		MPa	ksi	MPa	ksi	mm/mm
13 (1/2)	No. 1	435.9	63.226	204,133	29,607	0.00214
	No. 2	424.5	61.563	200,968	29,148	0.00211
	No. 3	467.4	67.786	177,705	25,774	0.00263
	AVG	**442.6**	**64.192**	**194,269**	**28,176**	**0.00229**
10 (3/8)	No. 1	482.3	69.785	204,644	29,680	0.00235
	No. 2	435.8	63.210	197328	28,620	0.00221
	No. 3	442.3	64.153	197804	28,689	0.00224
	AVG	**453.5**	**65.716**	**199,925**	**28,996**	**0.00227**
8 (5/16)	No. 1	387.8	55.680	205,250	29,768	0.00199
	No. 2	390.7	56.670	196,576	28,510	0.00201
	No. 3	396.5	57.512	194,156	28,160	0.00207
	AVG	**391.7**	**56.621**	**198,661**	**28,813**	**0.00202**

Table 3-2: Summary of measured tensile characteristics of steel tested in phase II

Nominal Thickness	Set #	Specimen	Yield Strength		Modulus of Elasticity		Yield Strain
mm (in.)			MPa	ksi	MPa	ksi	mm/mm
5 (3/16)	1	No. 1	390.0	56.57	194,012	28,139	0.002
		No. 2	400.3	58.07	199,231	28,896	0.00201
		No. 3	399.4	57.92	193,743	28,100	0.00205
		AVG	**396.6**	**57.519**	**195,662**	**28,378**	**0.00202**
	2	No. 1	453.8	65.81	218,426	31,680	0.00206
		No. 2	489.9	71.06	202,989	29,441	0.0023
		No. 3	462.3	67.05	188,482	27,337	0.00246
		AVG	**468.7**	**67.972**	**203,299**	**29,486**	**0.00227**
	3	No. 1	404.1	58.61	195,329	28,330	0.00207
		No. 2	414.8	60.16	189,909	27,544	0.00218
		No. 3	411.5	59.68	187,965	27,262	0.00218
		AVG	**410.1**	**59.485**	**191,068**	**27,712**	**0.00214**

Results measured from tensile coupons of phase I show that the 8 mm (5/16 in.) thick specimens exhibited a yield plateau with a well-defined yield point, while the 10 mm (3/8 in.) and 13 mm (1/2 in.) thick specimens did not have a well-defined yield point. According to the

stress-strain behavior, the 8 mm (5/16 in.) plates were Grade 50 (345 MPa), while the 10 mm (3/8 in.) and 13 mm (1/2 in.) plates were Grade 65 (450 MPa). Similarly, the yield strength of the tensile coupons of phase II was determined using the 0.2 percent offset method, since results obtained from steel did not exhibit well-defined yield point. Therefore, set #1 and #3 plates were Grade 50 (345 MPa), while set #2 plates were Grade 65 (450 MPa). Despite that Grade 50 (345 MPa) steel was orders for all plates, It is common in the U.S. that Grade 65 (450 MPa) is commercialized as dual grade steel.

3.1.2 CFRP Tensile Characteristics

The tensile characteristics of the three types of CFRP strands including High-Modulus (HM), Intermediate-Modulus (IM), and Low-Modulus (LM) were determined. Two sets of tests were carried out to clarify the characteristics of CFRP materials. First set attempted to capture the typical stress-strain curves utilizing the individual fiber strand. In the second set, coupons cut from the CFRP witness panels were tested to define the properties of the composite materials. Tensile specimens were prepared in accordance with ASTM D3039 and Test Method L2 of ACI 440.3R-04 and were tested in uniaxial tension using 20 kip (90 kN) universal testing machine.

3.1.2.1 *Individual Strand Tensile Tests*

To obtain the tensile properties of the small-diameter CFRP strands, different testing methods were applied using aluminum tabs or emery cloth along with different number of CFRP strands. Consequently, using aluminum tabs accompanied by individual CFRP strand could

reach to the most reliable results. Therefore, three tensile coupons were prepared from each type of CFRP materials. Each coupon included only one individual strand at the gage area as shown in Figure 3-5. The total length of the tensile coupons was 304 mm (12 in.) with a gage length of 152 mm (6 in.) and a gripping length of 76 mm (3 in.) on each end. Width of the aluminum tabs was 25 mm (1 in.).

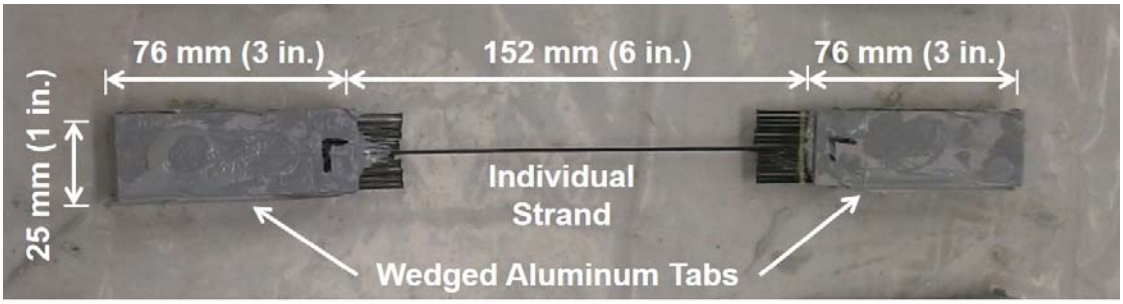

Figure 3-5: Plan view of tensile coupons made by individual CFRP strands

The tensile coupons were prepared by cutting from the CFRP strand sheets using 18 individual strands to meet the required dimensions. Aluminum tabs were cut to 76 mm (3 in.) long and were chamfered to form a wedge with an angle of approximately 30 degrees. The sharp edge of the tabs was rounded to prevent it from pinching the CFRP strands. The aluminum tabs were bonded to the CFRP strands using the epoxy and were left for curing of seven days before testing by the universal testing machine. 25 mm (1 in.) from edge of the tabs, 17 strands were cut and one strand was remained. This helps to minimize the stress concentration applied on an individual strand at the tab edge. Otherwise, high stress concentration on an individual strand leads to premature failure at the edges of the tabs prior to reaching the ultimate strain capacity of the material.

The average cross-sectional area of the CFRP strands was determined by volume displacement test. Fifteen individual strands were randomly extracted from the sheets and were cut to an approximate length of 305 mm (12 in.) as shown in Figure 3-6. The exact length of each strand was measured using a digital caliper with an accuracy of 0.01 mm (0.0004 in.). After measuring the length of the strands, their volume was determined by volume displacement of water using a calibrated burette as shown in Figure 3-7. The measured length and cross-sectional area of the individual strands of each CFRP type are given in Table 3-3.

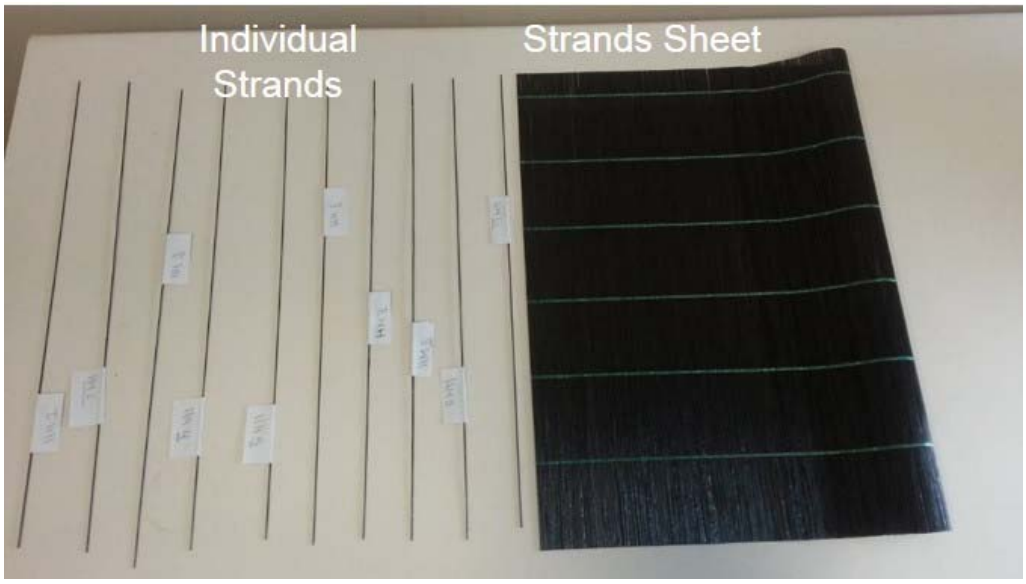

Figure 3-6: Individual strands uses for determining average cross-sectional area

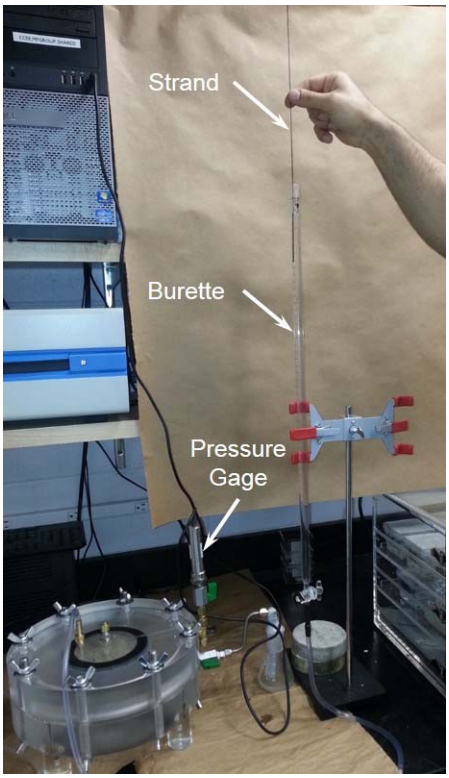

Figure 3-7: Determination of volume of individual strands

Table 3-3: Average measured cross-sectional area of individual CFRP strands

Strand Type	Measured Area	
	mm^2	$in.^2$
High-Modulus (HM)	1.14344	0.00177
Intermediate-Modulus (IM)	1.24194	0.00192
Low-Modulus (LM)	1.00881	0.00156

Due to difficulty of attaching the extensometer to an individual strand, the elongations of the coupons were measured by the use of OptotrakCertus® motion capturing system. Each coupon had two InfraRed Emitting Diodes (IREDs) attached to the individual strand. IREDs were inserted into the plastic caps and were glued to the strand. Figure 3-8 shows testing of the CFRP strand using the 20 kip (90 kN) universal testing machine.

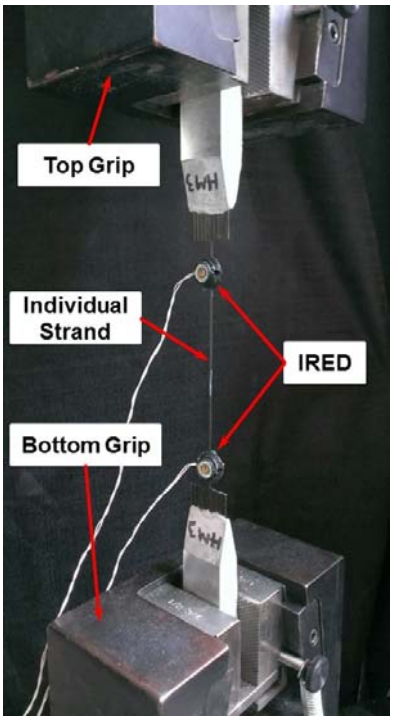

Figure 3-8: Testing the CFRP strand tensile coupon using the universal testing machine

Typical stress-strain curves for the three types of CFRP strands, i.e. HM, IM, and LM are shown in Figure 3-9. In addition, the modulus of elasticity, tensile strength, and the corresponding rupture strain are given in Table 3-4 for the three different coupons of each CFRP type.

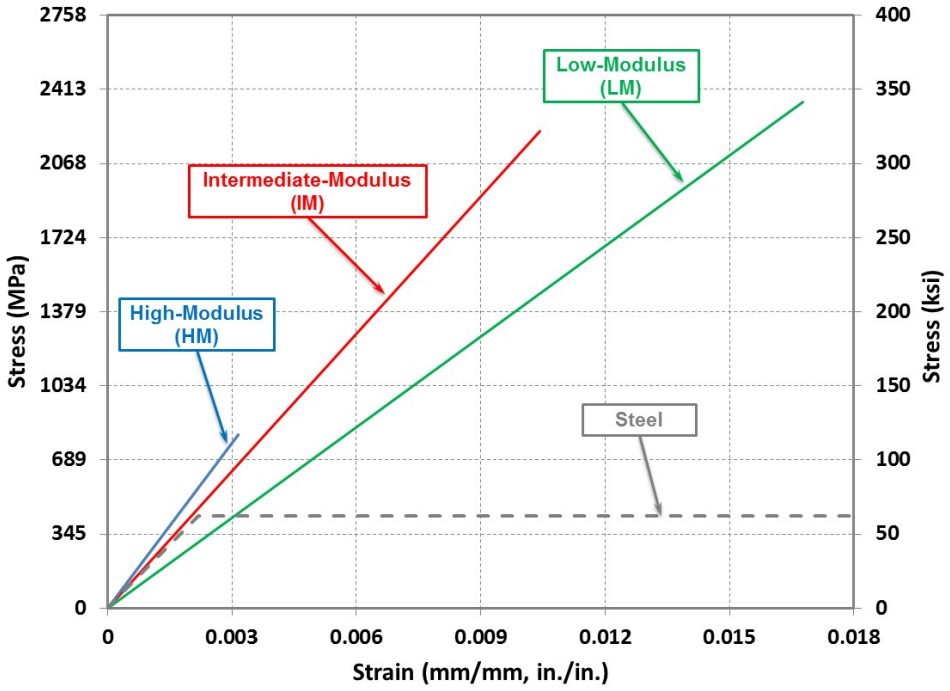

Figure 3-9: Typical tensile stress-strain behavior of CFRP strands

Table 3-4: Summary of measured tensile characteristics of CFRP strands

CFRP Type	Specimen	Modulus of Elasticity		Tensile Strength		Rupture Strain	
		MPa	ksi	MPa	ksi	mm/mm	%
High-Modulus (HM)	HM#1	258,765	37,531	775.71	112.51	0.00300	0.300
	HM#2	255,136	37,004	835.62	121.20	0.00328	0.328
	HM#3	252,602	36,637	807.22	117.08	0.00320	0.320
	AVG	**255,501**	**37,057**	**806.18**	**116.93**	**0.00316**	**0.316**
Intermediate-Modulus (IM)	IM#1	211,910	30,735	2,272.58	329.61	0.01063	1.063
	IM#2	212,041	30,754	2,305.18	334.34	0.01074	1.074
	IM#3	212,365	30,801	2,082.75	302.08	0.00993	0.993
	AVG	**212,106**	**30,763**	**2,220.17**	**322.01**	**0.01044**	**1.044**
Low-Modulus (LM)	LM#1	140,646	20,399	2,343.21	339.85	0.01657	1.657
	LM#2	138,571	20,098	2,343.21	339.85	0.01675	1.675
	LM#3	140,067	20,315	2,337.82	339.07	0.01651	1.651
	AVG	**139,761**	**20,271**	**2,341.41**	**339.59**	**0.01661**	**1.661**

3.1.2.2 ***Witness Panel Tensile Tests***

Witness panels were fabricated by applying the same materials used for strengthening the steel plates, under the same environmental conditions found to strengthen the test plates. The CFRP strand sheets were cut to the required square sheets using scissors. Simultaneous to the plate strengthening application, the epoxy (FP-E9S) was applied to the CFRP square sheets and left to spend seven days of curing. Then, the witness panels were cut to three specimens of 305 mm (12 in.) long and 25 mm (1 in.) wide using band-saw. Similar to the individual strand coupons, aluminum tabs were cut to the 76 mm (3 in.) long and were chamfered to form a wedge with an angle of approximately 30 degrees. The sharp edge of the tabs was rounded to prevent it from pinching the CFRP strands. The aluminum tabs were bonded to the witness panel specimen using the epoxy (FP-E9S). Both ends of the witness panel specimen with length of 76 mm (3 in.) were roughened using sand papers to ensure better bonding. The coupons then were left for curing for seven days before testing in the universal testing machine as shown in Figure 3-10.

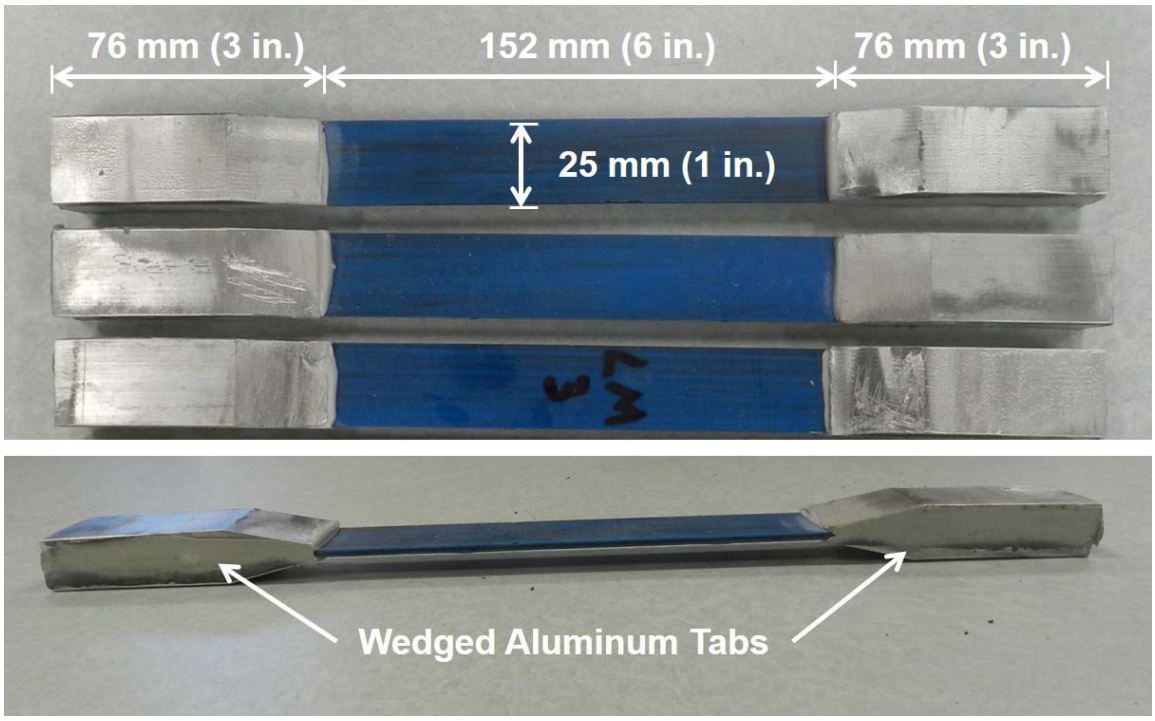

Figure 3-10: Plan and elevation view for tensile witness panel coupons of CFRP strands

The elongations of the witness panel coupons were measured using a 51 mm (2 in.) extensometer and the applied load was measured directly by the machine. The actual cross-section of each coupon was measured using a digital caliper with an accuracy of 0.01 mm (0.0004 in.) along the gage length and the average cross-sectional area was used to calculate stress. Figure 3-11 shows testing of the witness panel coupon using the 20 kip (90 kN) universal testing machine.

Typical stress-strain curves for the three types of witness panel coupons, i.e. HM, IM, and LM are shown in Figure 3-12. In addition, the modulus of elasticity, tensile strength, and the corresponding rupture strain are given in Table 3-5 for the three different coupons of each CFRP type.

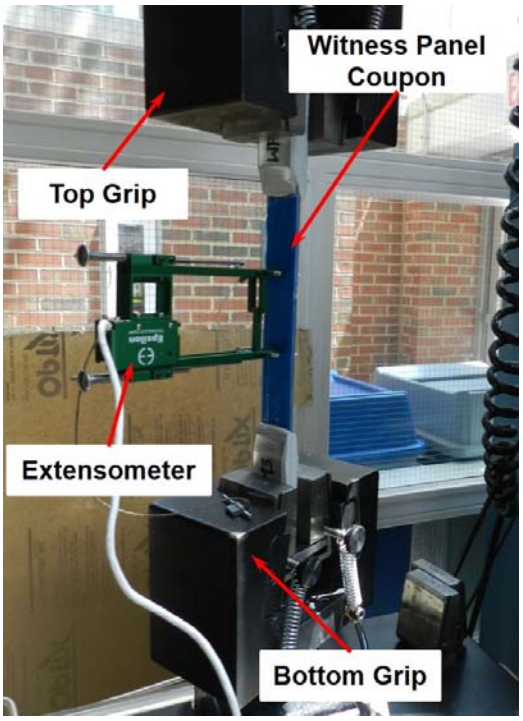

Figure 3-11: Tensile testing of witness panel coupon using the universal testing machine

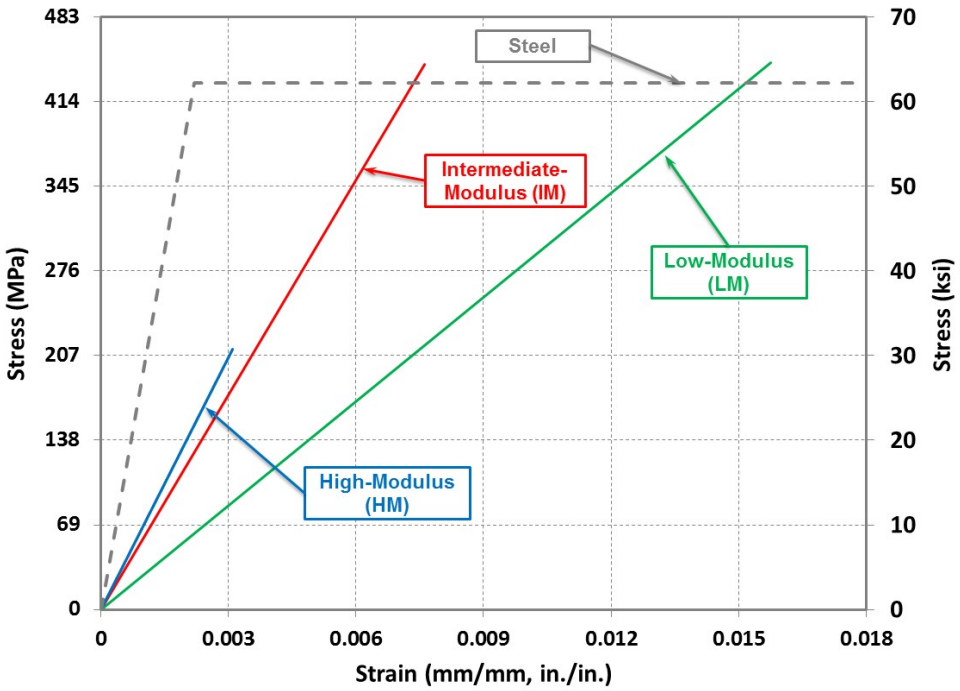

Figure 3-12: Typical tensile stress-strain behavior of CFRP witness panel coupons

Table 3-5: Summary of measured tensile characteristics of CFRPwitness panel coupons

CFRP Type	Specimen	Modulus of Elasticity		Tensile Strength		Rupture Strain	
		MPa	ksi	MPa	ksi	mm/mm	%
High-Modulus (HM)	TWP-HM#1	62,837	9,114	233	33.73	0.00370	0.370
	TWP-HM#2	72,713	10,546	189	27.40	0.00263	0.263
	TWP-HM#3	72,092	10,456	214	30.98	0.00294	0.294
	AVG	**69,214**	**10,039**	**211.69**	**30.70**	**0.00309**	**0.309**
Intermediate-Modulus (IM)	TWP-IM#1	56,314	8,168	482	69.84	0.00856	0.856
	TWP-IM#2	56,334	8,171	429	62.27	0.00764	0.764
	TWP-IM#3	65,626	9,518	421	61.01	0.00666	0.666
	AVG	**59,425**	**8,619**	**443.85**	**64.37**	**0.00762**	**0.762**
Low-Modulus (LM)	TWP-LM#1	26,517	3,846	384	55.72	0.01449	1.449
	TWP-LM#2	34,555	5,012	446	64.73	0.01531	1.531
	TWP-LM#3	32,662	4,737	505	73.29	0.01747	1.747
	AVG	**31,245**	**4,532**	**445.26**	**64.58**	**0.01576**	**1.576**

3.1.3 Compressive Characteristics of CFRP

The compressive characteristics of the three types of CFRP strands including High-Modulus (HM), Intermediate-Modulus (IM), and Low-Modulus (LM) were determined. Coupons cut from the CFRP witness panels were tested to define the properties of the composite materials. Compressive specimens were prepared in accordance with ASTM D6641 and were tested in uniaxial compression using 200 kip (900 kN) universal testing machine.

3.1.3.1 *Witness Panel Compressive Tests*

Similar procedure used to prepare the witness panel tensile coupons was applied to build compressive coupons. A total of ten witness panel coupons were cut into 140 mm (5.5 in.) long and 25 mm (1 in.) wide using band-saw. The CFRP strands of nine coupons, including three coupons out of each material type, were positioned in longitudinal direction parallel to the compressive applied load. However, only one coupon prepared by IM CFRP strand had transverse direction of strands relative to the compressive applied load. Un-tabbed coupon as shown in Figure 3-13, were used by means of 13 mm (0.5 in.) gauge length and were tested.

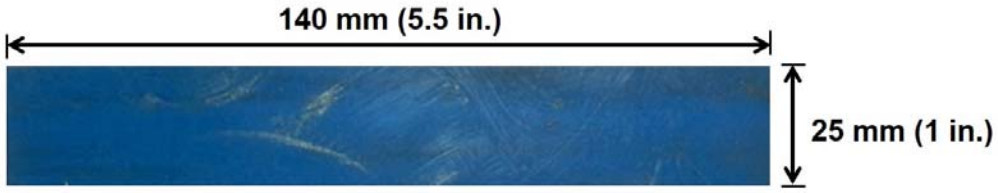

Figure 3-13: Plan view of compressive witness panel coupons of CFRP strands

Elongations of the witness panel coupons were measured using a tee rosette strain gauges and the applied load was measured directly by the machine. The tee rosette strain gage is an arrangement of two closely positioned gage grids, separately oriented perpendicularly. Two strain gauges were attached to both faces of each coupon at mid-height to measure the strains along vertical and horizontal directions. Strain measurements were resulted in compressive elastic modulus of the coupons as well as Poisson's ratio. The actual cross-section of each coupon was measured using a digital caliper with an accuracy of 0.01 mm (0.0004 in.) along the gage length and the average cross-sectional area was used to calculate stress. Figure 3-14 shows testing of the witness panel coupon using the 200 kip (900 kN) universal testing machine.

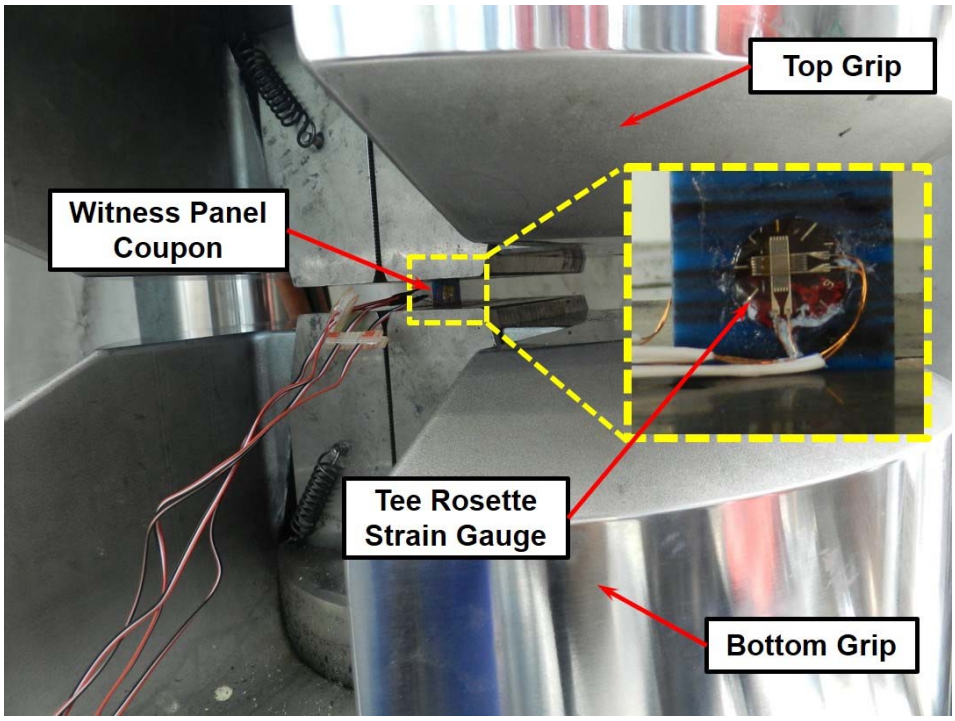

Figure 3-14: Compressive testing of witness panel coupon using the universal testing machine

The overall behavior measured from a sample witness panel coupon is shown in Figure 3-15. The governing failure mode of all coupons was global buckling of the gauge length. The average value of the measured strains at both faces were used to determine the properties of the specimens. Typical stress-strain curves for the three types of witness panel coupons, i.e. HM, IM, and LM having CFRP strand positioned longitudinally are shown in Figure 3-16. In addition, the modulus of elasticity, tensile strength, and the Poisson's ratio are given in Table 3-6 for the three different coupons of each CFRP type. Moreover, Table 3-7 shows the properties of the coupon having IM CFRP strands positioned perpendicular to the direction of applied load.

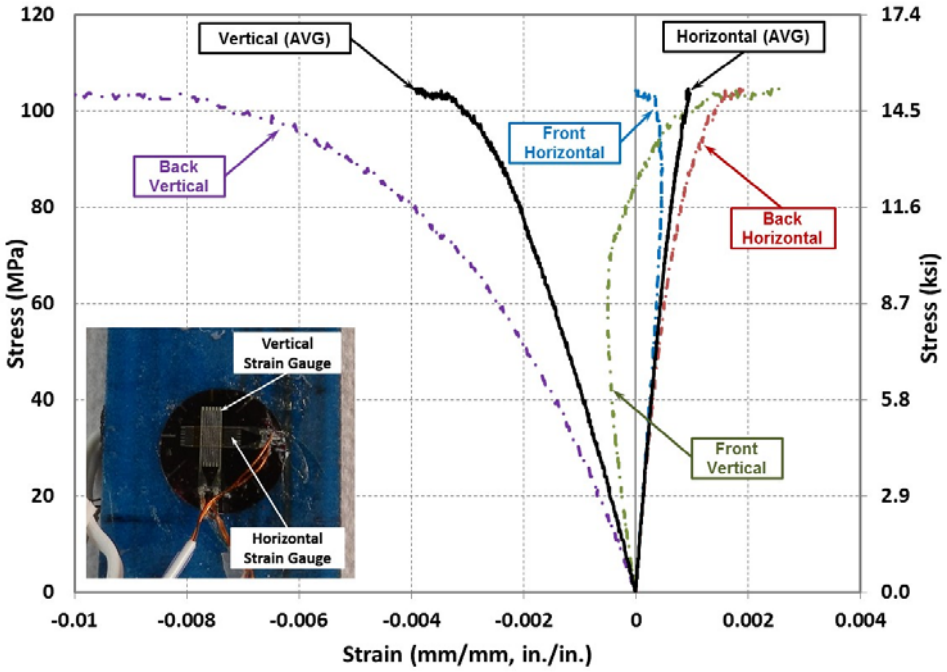

Figure 3-15: Stress-strain curve of CFRP witness panel coupon CWPL-IM#1

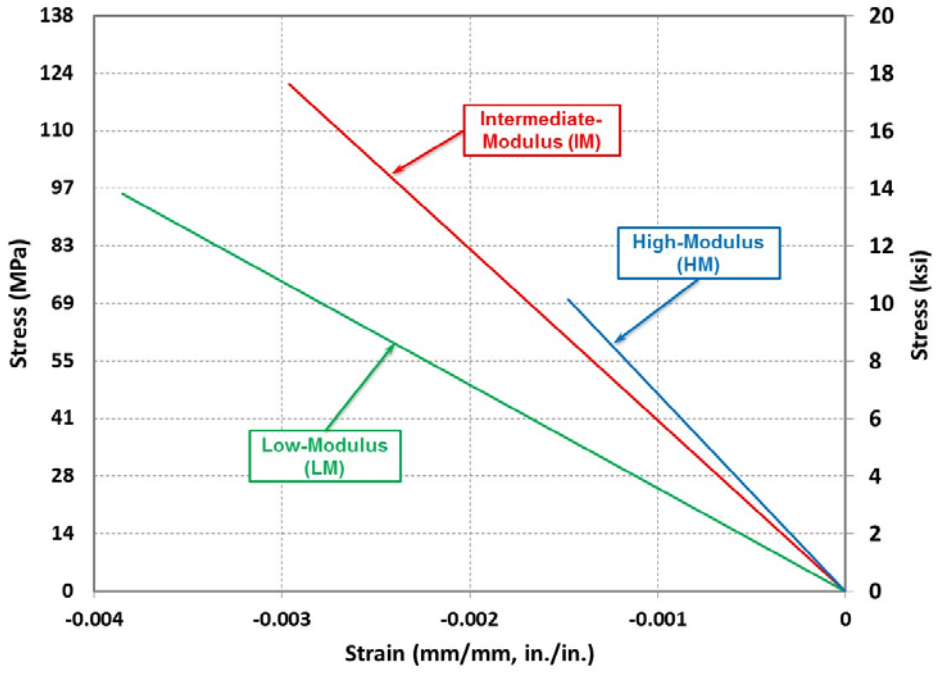

Figure 3-16: Typical compressive stress-strain behavior of longitudinally positioned CFRP witness panel coupons

Table 3-6: Summary of measured compressive characteristics of longitudinally positioned CFRP witness panel coupons

CFRP Type	Specimen	Modulus of Elasticity		Compressive Strength		Poisson's Ratio
		MPa	ksi	MPa	ksi	
High-Modulus (HM)	CWPL-HM#1	42,913	6,224	71.15	10.32	0.307
	CWPL-HM#2	53,152	7,709	69.02	10.01	0.246
	CWPL-HM#3	46,009	6,673	69.50	10.08	0.270
	AVG	**47,358**	**6,869**	**69.89**	**10.14**	**0.274**
Intermediate-Modulus (IM)	CWPL-IM#1	38,411	5,571	104.66	15.18	0.296
	CWPL-IM#2	45,595	6,613	132.72	19.25	0.323
	CWPL-IM#3	38,955	5,650	126.93	18.41	0.321
	AVG	**40,987**	**5,945**	**121.44**	**17.61**	**0.313**
Low-Modulus (LM)	CWPL-LM#1	25,062	3,635	91.01	13.20	0.353
	CWPL-LM#2	23,642	3,429	93.49	13.56	0.321
	CWPL-LM#3	25,593	3,712	101.35	14.70	0.330
	AVG	**24,766**	**3,592**	**95.29**	**13.82**	**0.335**

Table 3-7: Summary of measured compressive characteristics of transversely positioned CFRP witness panel coupons

CFRP Type	Specimen	Modulus of Elasticity		Compressive Strength		Poisson's Ratio
		MPa	ksi	MPa	ksi	
Intermediate-Modulus (IM)	CWPT-IM#1	3,296	478	49.37	7.16	0.051

3.2 UNIAXIAL COMPRESSIVE STRENGTHENING (PHASE I)

3.2.1 Test Setup & Instrumentation

3.2.1.1 *Test Setup*

A special test setup was designed to allow the application of concentric uniaxial compressive forces to the steel plates schematically shown in Figure 3-17 [53]. The test setup was used to be a self-reacting A-frame. The test plates were welded at both ends to high-strength steel tubes (referred to as sleeves hereafter), with an inner diameter of 152 mm (6 in.) and thickness of 13 mm (1/2 in.). Two high-strength, chrome-painted steel pins were greased and inserted inside the sleeves. The sleeves were able to freely rotate on the two pins due to the minimal friction forces between the pins and the sleeves, and thus providing boundary conditions virtually resembling hinged-hinged end conditions. The pins were loaded by two 40-mm (1-5/8 in.) diameter high-strength steel pre-stressing bars (referred to as HS bars) and two hydraulic jacks. The load was transferred from the pins to the sleeves by bearing and then from the sleeves to the test plate by the weld. The hydraulic jacks were simultaneously connected to the same hydraulic pump to ensure equal load in both bars, hence subjected the test plate to uniform stresses. The entire fixture of the pins with the sleeves and the test plates were maintained in vertical position by means of the supporting A-frame. The supporting A-frame was tied down to the laboratory strong floor at four locations to ensure the stability of the frame during testing. The specimen was hanged over the test setup prior to testing to remove any pre-compression on the plate. Figure 3-18 shows an elevation and side views of the test setup and illustrates the

different components of the setup. Metal Inert Gas (MIG) welding was used to weld the test plates to the sleeves. The welding process was performed in stich configured welds on opposite sides of the plate over an extended period of time, while allowing cooling between weld lines to avoid excessive thermal stresses resulting from the welding arcs. Figure 3-19 depicts the welding process that was followed during the experimental program.

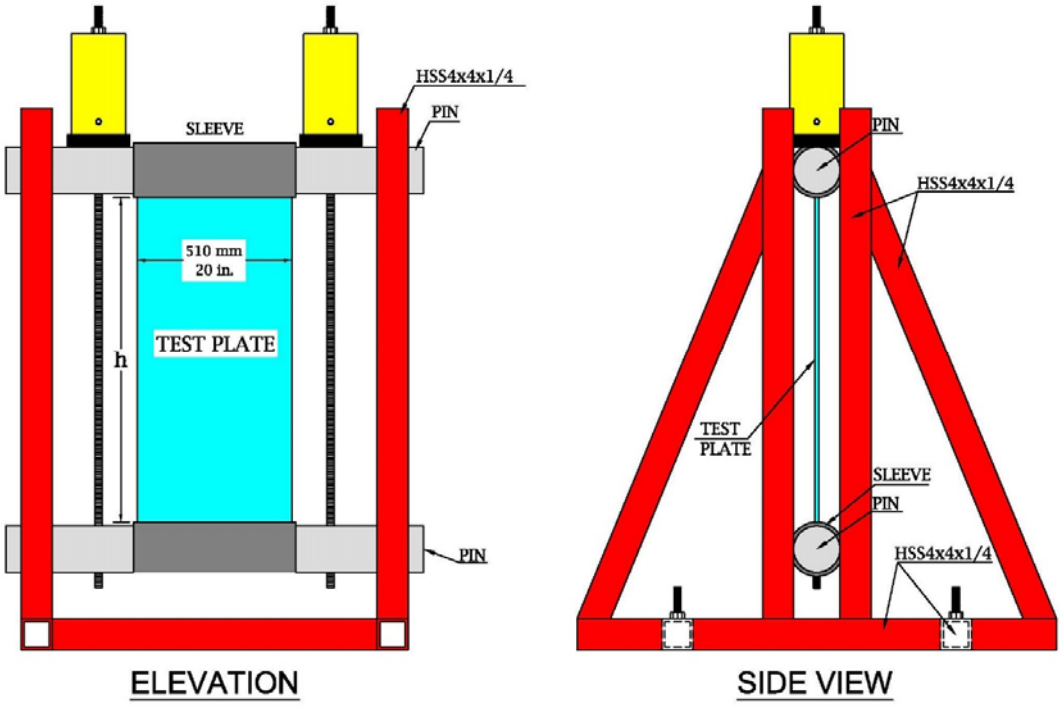

Figure 3-17: Schematic of test setup for uniaxial compressive testing of plates

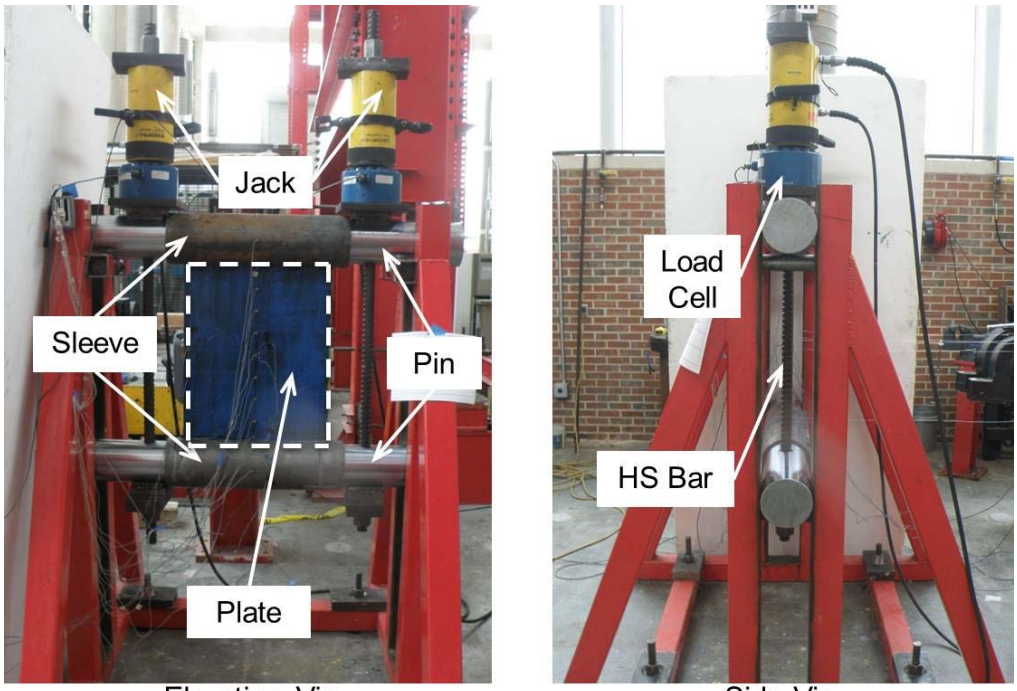

Figure 3-18: Test setup for uniaxial compressive testing of plates

Figure 3-19: Welding of Test Specimens

3.2.1.2 ***Instrumentation***

Different types of instrumentation were used. Load was applied using two hydraulic jacks connected simultaneously to the same pump to ensure equal load in both jacks. The applied load was measured using calibrated load cells mounted on each high-strength pre-stressing bar under the hydraulic jack as shown in Figure 3-20.

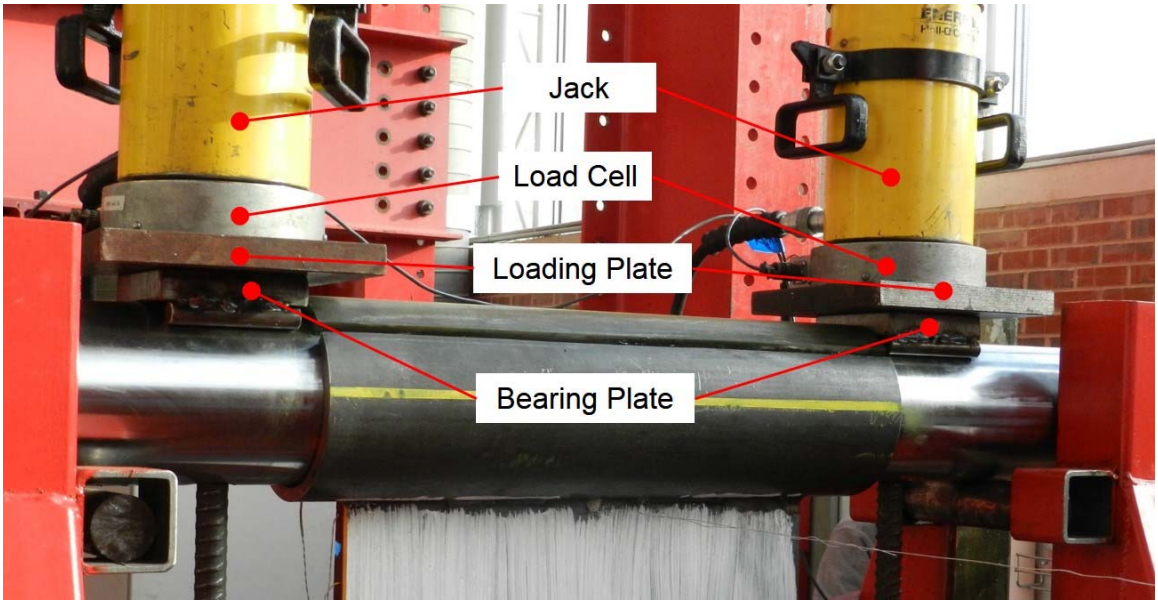

Figure 3-20: Positions of load cells in test setup

Strains in the test plates were measured using electrical resistance strain gages with a gage length of 5 mm (3/16 in.). Four strain gages were attached to both faces of the test plates at mid-height, one in the middle and one at the side of the plate as shown in Figure 3-21. A total of eight strain gauges were attached to strengthened specimens at mid-height. Four strain gauges were attached to the base steel before application of the strengthening system. The remaining four strain gauges were attached to the outer surface of the CFRP strand sheets after curing of the epoxy resin. For specimens with two layers of CFRP strands, strain gauges were

only applied to the outer-most layer of CFRP strands. Figure 3-22 shows a schematic sketch of the cross-section view and the location of the strain gauges applied to the strengthened test plate at mid-height.

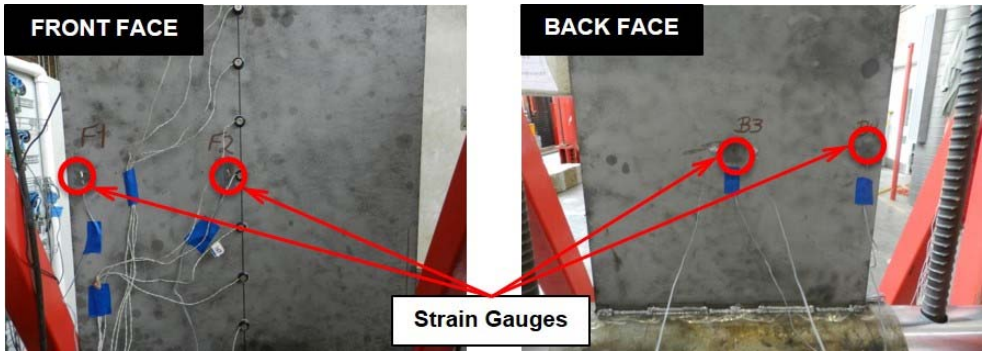

Figure 3-21: Electrical resistance strain gages attached to test plates

Figure 3-22: Location of strain gauges at mid-height cross-section of strengthened test plates

Lateral deformations along the vertical centerline of the plate at top and bottom ends, and mid-height were measured using linear string potentiometers as shown in Figure 3-23. Four string potentiometers were used, where one potentiometer was attached to the top end, one to the bottom end, and two at the mid-height of the plate. The spatial (3-D) deformation of the test plate during loading was monitored and measured using a 3-D OptotrakCertus® motion capturing system. The motion capturing system creates a three-dimensional (3-D) coordinate system by the use of InfraRed Emitting Diodes (IRED) attached to the specimen at points of interest. Any subsequent movement of the IREDs is captured by a camera system in reference

to the established coordinate. An origin for the coordinate system is established by the user at any arbitrary point. The Optotrak 3-D system has an accuracy of 0.1 mm (0.004 in.) and resolution of 0.01 mm (0.0004 in.). The IREDs were attached to the front faces of the test plates over their entire heights along their centerlines and were spaced vertically at 75 mm (3 in.). One IRED was also attached to each sleeve to monitor their movement, and hence their rotation. Figure 3-24 shows the IREDs attached to the plate "IB-48-5/16-HM-U". All instruments were connected to an electronic data acquisition system. Data was continuously monitored and recorded at a sample rate of 10 Hz.

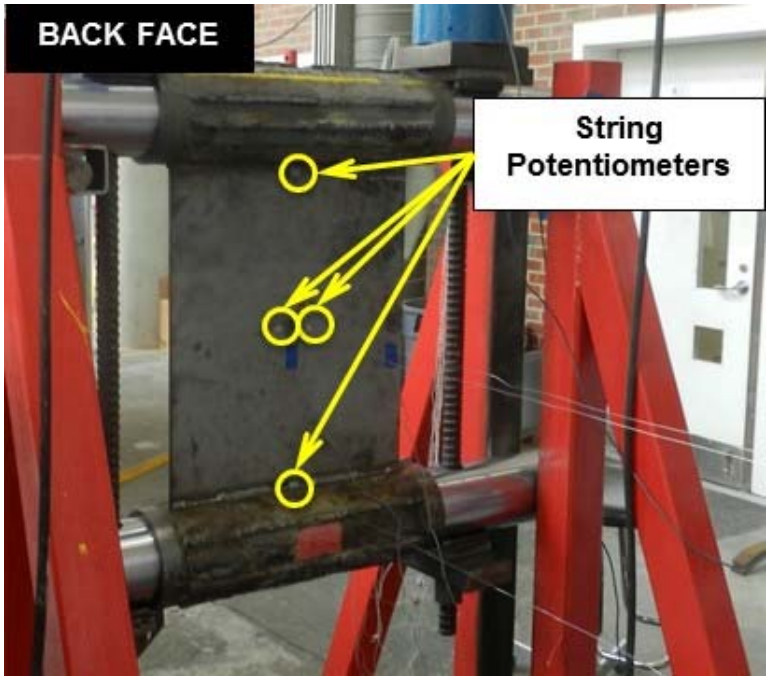

Figure 3-23: String potentiometers attached to the back face of test plates

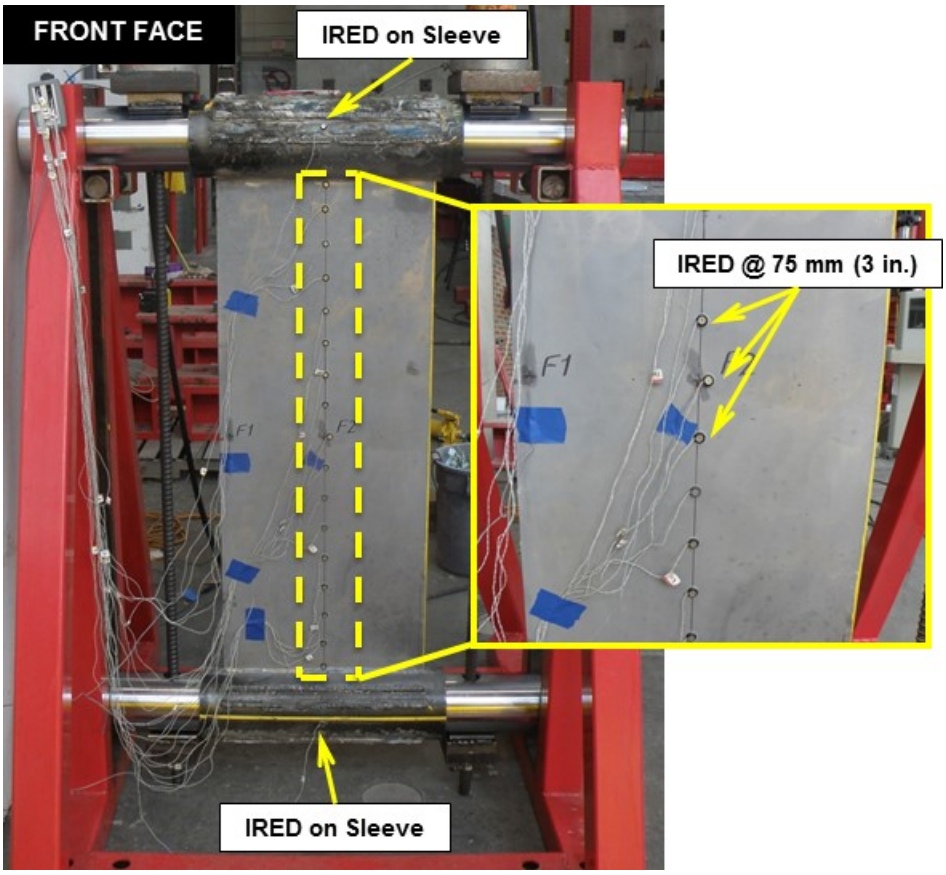

Figure 3-24: IREDs attached the front face of test plate and vertically spaced at 75 mm (3 in.)

3.2.2 Test Matrix

A total of 14 plates were tested to investigate the effect of slenderness ratio (height-to-thickness) ranged from 48 to 154 under uniaxial compressive load. The small slenderness ratios were selected to represent stocky webs of hot-rolled steel beams, while the large ratios are typically used for built-up bridge girders. Eight plates were strengthened with High-Modulus (HM) CFRP strands and six plates without strengthening were used as control specimens. The test matrix is given in Table 3-9. All test plates are 510 mm (20 in.) wide. For all strengthened plates, one layer of High-Modulus (HM) CFRP strands was externally bonded to each side of

the plates. The length of the CFRP strands was 13 mm (½ in.) shorter than the height (h) of the plate to avoid touching the weld of the test plate and the sleeves. The fibers were oriented vertically in the same direction of the applied load. Two of the strengthened plates did not have polyurea putty to investigate its effect on the bonding and buckling capacity of the strengthening system. The specimen designation is self-descriptive. For example, specimen IA-24-3/8-S-P means that the specimen is from Phase I-A, is 610 mm (24 in.) tall, 10 mm (3/8 in.) thick, and is strengthened with putty.

Table 3-8: Test matrix of phase I-A (Effect of slenderness ratio)

Plate Designation	h		t		h/t	Strengthening	Polyurea Putty
	mm	in.	mm	in.			
IA-24-1/2-U	610	24	13	1/2	48	NO	NO
IA-24-1/2-S-P						YES	YES
IA-24-3/8-U			10	3/8	64	NO	NO
IA-24-3/8-S-P						YES	YES
IA-24-5/16-U			8	5/16	77	NO	NO
IA-24-5/16-S-P						YES	YES
IA-24-5/16-S						YES	NO
IA-48-1/2-U	1220	48	13	1/2	96	NO	NO
IA-48-1/2-S-P						YES	YES
IA-48-3/8-U			10	3/8	128	NO	NO
IA-48-3/8-S-P						YES	YES
IA-48-5/16-U			8	5/16	154	NO	NO
IA-48-5/16-S-P						YES	YES
IA-48-5/16-S						YES	NO

Additional 18 tests were conducted to examine the effect of elastic modulus and reinforcement ratio of CFRP strands. Three different elastic moduli were investigated: High-Modulus (HM),

Intermediate-Modulus (IM) and Low-Modulus (LM). Effect of reinforcement ratio was studied using one and two layers of the CFRP strands for selected specimens. Only two slenderness ratios of 77 and 154 were included. Six plates were strengthened with one layer of either HM, IM, or LM CFRP strands on each face of the plate. In addition, six plates were strengthened with two layers of either HM, IM, or LM small-diameter CFRP strands on each face of the plate. The remaining six plates were not strengthened and used as control specimens. The test matrix of the specimens is given in Table 3-9. The specimen designation is similar to Phase I-A. Last letters show the strengthening condition. For the control plates, letter "U" is used. For the strengthened plate, number of layers at each face is followed by type of CFRP material. For example, specimen IB-24-5/16-2IM means that the specimen is from Phase I-B, is 610 mm (24 in.) tall, 8 mm (5/16 in.) thick, and is strengthened with two layers of IM CFRP material.

Table 3-9: Test matrix of phase I-B (Effect of elastic modulus and reinforcement ratio)

Plate Designation	h	t	h/t	Fiber Type	Number of Layers
	mm (in.)	mm (in.)			
IB-24-5/16-LM-U	610 (24)	8 (5/16)	77	NO (CONTROL)	0
IB-24-5/16-1LM				LM	1
IB-24-5/16-2LM				LM	2
IB-24-5/16-IM-U				NO (CONTROL)	0
IB-24-5/16-1IM				IM	1
IB-24-5/16-2IM				IM	2
IB-24-5/16-HM-U				NO (CONTROL)	0
IB-24-5/16-1HM				HM	1
IB-24-5/16-2HM				HM	2
IB-48-5/16-LM-U	1220 (48)	8 (5/16)	154	NO (CONTROL)	0
IB-48-5/16-1LM				LM	1
IB-48-5/16-2LM				LM	2
IB-48-5/16-IM-U				NO (CONTROL)	0
IB-48-5/16-1IM				IM	1
IB-48-5/16-2IM				IM	2
IB-48-5/16-HM-U				NO (CONTROL)	0
IB-48-5/16-1HM				HM	1
IB-48-5/16-2HM				HM	2

3.2.3 Application of the Strengthening System

Application of the CFRP strands followed the procedures recommended by the producer of the CFRP material, which is detailed and illustrated as follows.

3.2.3.1 *Surface Preparation*

The steel plates were sandblasted prior to the commencement of the application process. After the completion of sandblasting, the plates were cleaned using pressurized air to remove any grit or dust on the plates. Immediately after the completion of sandblasting and cleaning, the steel plates were moved inside the laboratory under controlled environment and were sealed until the time of application of the strengthening system. The strain gages were attached the steel on the same day of strengthening before the application of the primer resin as shown in Figure 3-25.

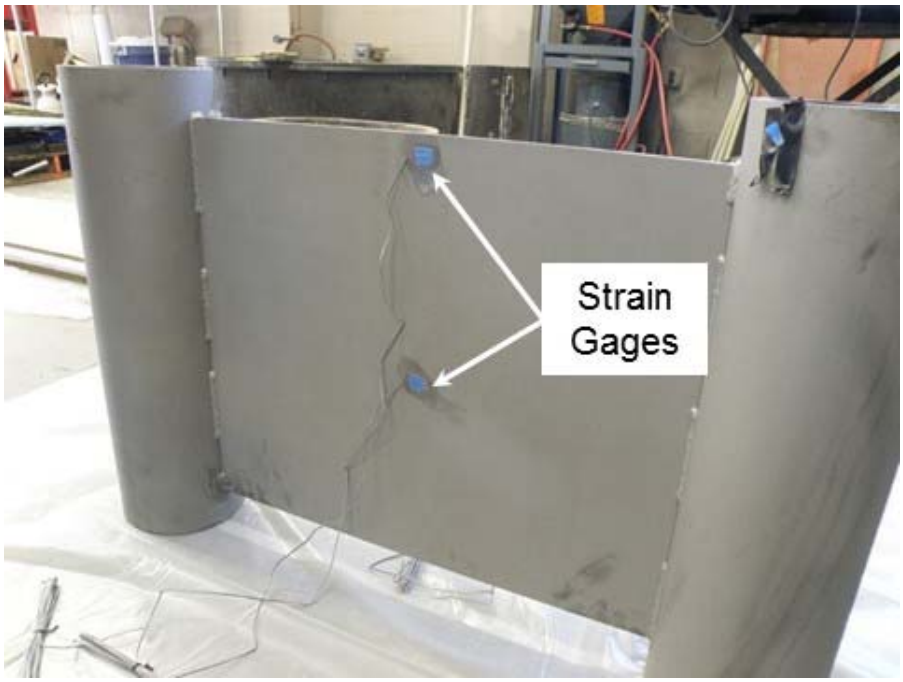

Figure 3-25: Sandblasted steel plate prior to application of strengthening system

3.2.3.2 ***Application of the Primer***

The primer resin (FP-UL1) was applied to the steel plates after sandblasting and cleaning. The resin and the hardener were mixed by weight using a ratio of 1:1 as recommended. A calibrated digital balance measuring to the nearest 0.1 gm was used for weighing the resin and the hardener. The two components were mixed for at least 2 minutes using an electrical mixer until a uniform mixture was obtained. A rich layer of the primer mixture was applied using a hand roller as shown in Figure 3-26.

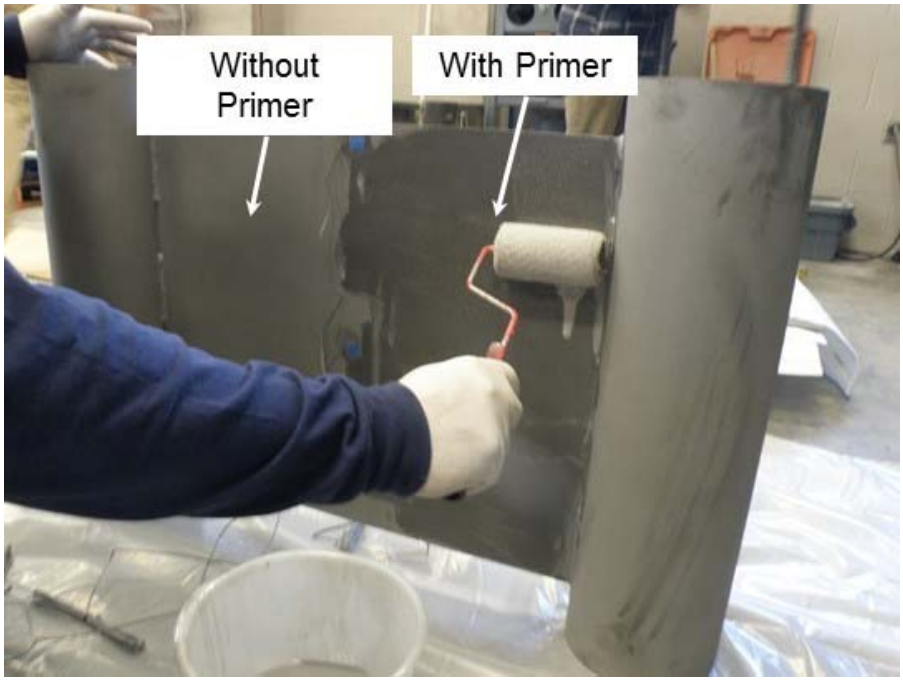

Figure 3-26: Application of primer resin using hand roller

3.2.3.3 ***Application of the Polyurea Putty***

The polyurea putty (FP-UL1) layer, was applied to the steel plates after at least two hours from the application of the primer resin. The resin and the hardener were mixed by weight using a ratio of 3:1 as recommended. A calibrated digital balance measuring to the nearest 0.1 gm was

used for weighing the resin and the hardener. The two components were mixed for at least 2 minutes using an electrical mixer until a uniform mixture was obtained. A rich layer of the putty mixture was applied using spatulas. Figure 3-27 shows a steel plate after the application of the polyurea putty layer.

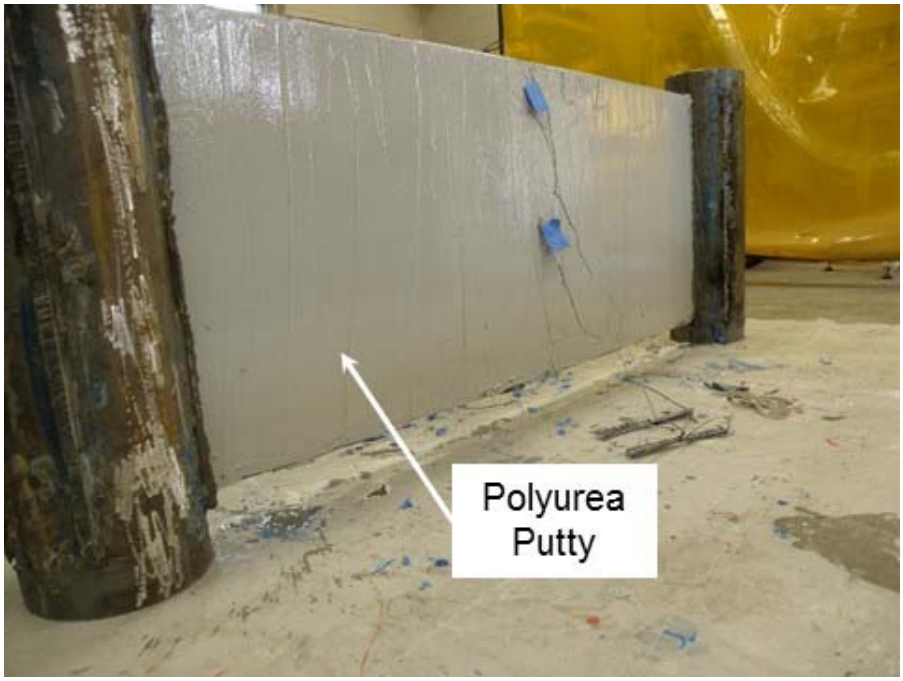

Figure 3-27: Polyurea putty applied to steel plate

3.2.3.4 ***Application of CFRP Strands***

The CFRP strand sheets were carefully cut to the required lengths using scissors as shown in Figure 3-28. Epoxy (FP-E9S) was applied after at least six hours from the application of the polyurea putty layer. The resin and the hardener were mixed by weight using a ratio of 4:1 as recommended. A calibrated digital balance measuring to the nearest 0.1 gm was used for weighing the resin and the hardener. The two components were mixed for at least 2 minutes using an electrical mixer until a uniform mixture was obtained as shown in Figure 3-29. A

thick layer of the epoxy was applied using spatulas as shown in Figure 3-30. The application of epoxy was carried out while the steel plate was laid horizontally. After applying the epoxy layer, the cut CFRP sheets were attached the steel plate. The strain gauge wires were passed through the strands as shown in Figure 3-31. Spatulas were used to press on the CFRP sheets until the excessive epoxy was squeezed out between the strands as shown in Figure 3-32 to ensure the elimination of any air pocket. A second layer of epoxy was applied on the top of the CFRP sheets. The strengthened plates were left for at least seven days to cure before they were tested.

Figure 3-28: Cutting of CFRP strands sheets using scissors

Figure 3-29: Mixing of epoxy

Figure 3-30: Application of epoxy using spatulas

Figure 3-31: Passing strain gauge wires through the CFRP sheet

Figure 3-32: Attaching the CFRP sheet

3.2.3.5 ***Application of Multiple Layers of CFRP Strands***

The first phase of the experimental program consists of two sub-phases. The focus for second sub-phase (I-B) was to determine the effect of multiple layers of the CFRP strands on the uniaxial compressive behavior of the specimens. Therefore, in order to apply the second layer of CFRP strands, the pre-existing layer CFRP strengthening was sanded down using a 125 grit sanding sponge as demonstrated in Figure 3-33 below. Once the surface had been sanded, compressed air was used to remove residue present from the sanding process. Then the surface was wiped cleaned with acetone to ensure it was free of unwanted residue. Upon reaching a desired surface, the second layer of CFRP strands was applied identical to the process just described.

Figure 3-33: Sanding the surface prior to preparation of second layer

3.2.4 Pilot Tests

3.2.4.1 *Pilot Plate Specimens*

Three pilot plate specimens, without strengthening, were tested to verify the efficiency of the designed test setup and develop proper preparation procedures. The pilot plates were selected as the plates with largest and smallest slenderness ratios, h/t = 154 and 48, respectively as shown in Table 3-10. Two duplicate plates of the same slenderness ratio of 154 were tested for further validation. Figure 3-34 shows the pilot plate "IA-48-5/16/P-a" before testing.

Table 3-10: Test matrix of pilot plates

Plate Designation	h		t		h/t	Strengthening
	mm	in.	mm	in.		
IA-24-1/2-P	610	24	13	1/2	48	NO
IA-48-5/16-P-a	1220	48	8	5/16	154	NO
IA-48-5/16-P-b	1220	48	8	5/16	154	NO

Figure 3-34: Pilot plate "IA-48-5/16-P-a" before testing

3.2.4.2 *Results and Discussion of Pilot tests*

Load-Strain Behavior

The measured applied load versus the measured longitudinal strain of the steel at mid-height in the direction of the applied load of the three test plates is shown in Figure 3-35, Figure 3-36, and Figure 3-37, respectively. Five strain gages were used on each side of the pilot plate "IA-24-1/2-P", while four strain gages were used on each side of the pilot plates "IA-48-5/16-P-a and -b". All strain gages were equally spaced across the width of the plate. In addition, Figure 3-38, Figure 3-39, and Figure 3-40 show the distribution of the measured longitudinal strain at mid-height of the plates across their widths at different load levels. It was aimed to investigate even distribution of the strains due to the uniform applied compression on plate.

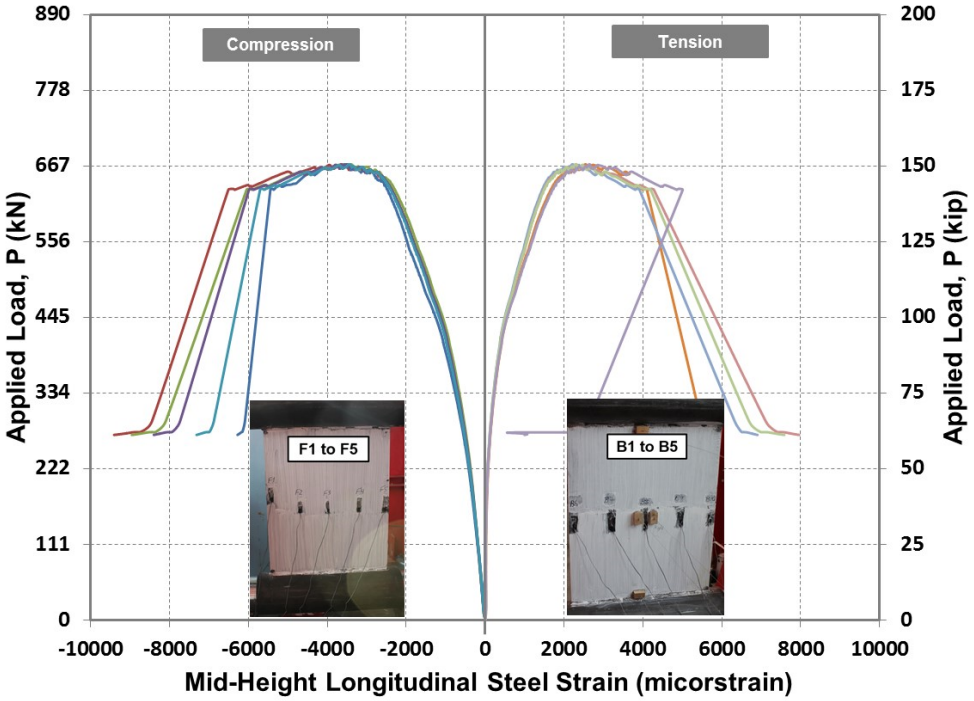

Figure 3-35: Applied load vs. longitudinal steel strain at mid-height of pilot plate IA-24-1/2-P (h/t=48)

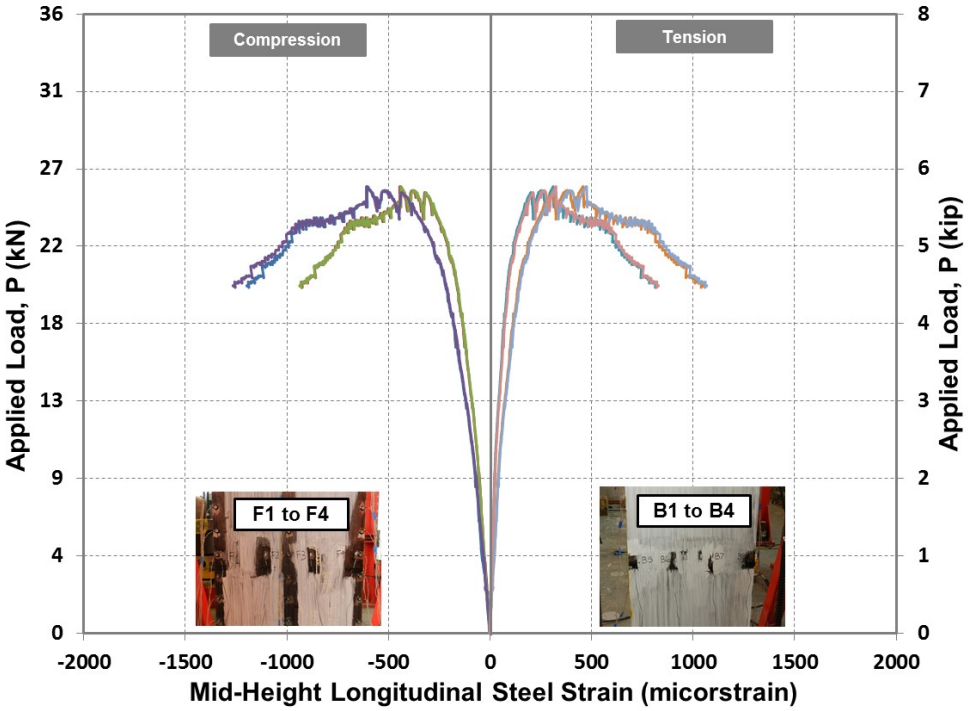

Figure 3-36: Applied load vs. longitudinal steel strain at mid-height of plate IA-48-5/16-P-a (h/t=154)

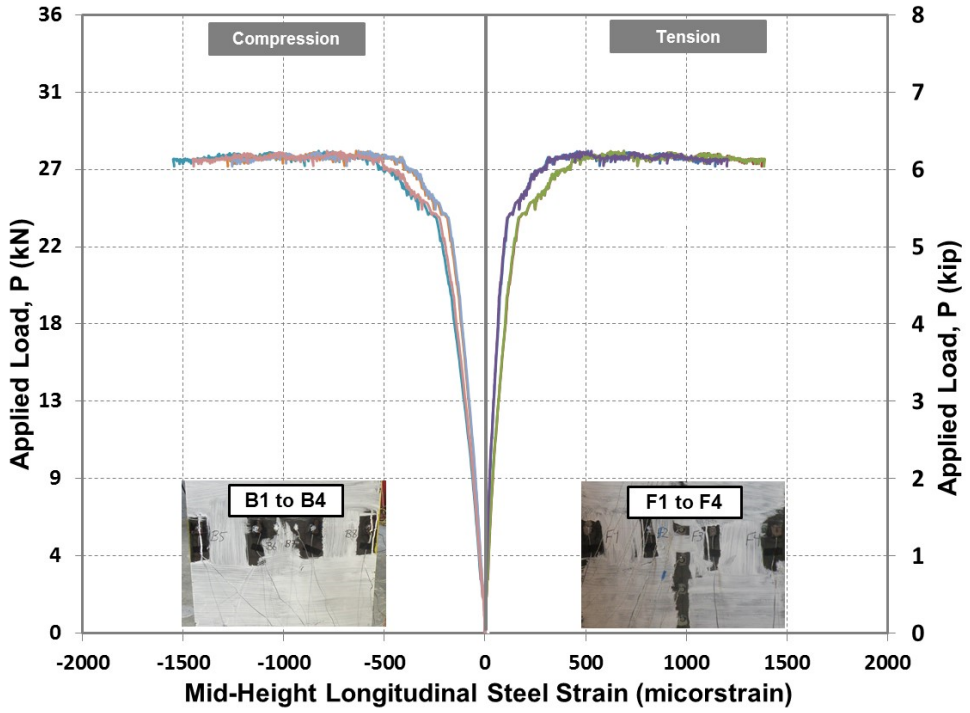

Figure 3-37: Applied load vs. longitudinal steel strain at mid-height of plate IA-48-5/16-P-b (h/t=154)

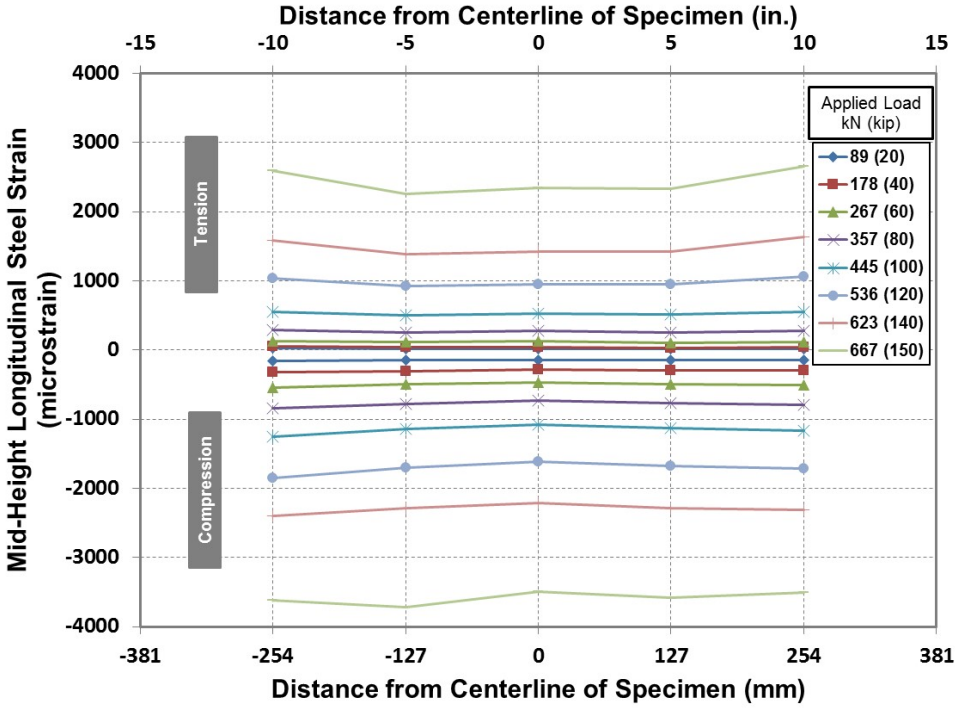

Figure 3-38: Longitudinal strain distribution across the width of the pilot plate IA-24-1/2-P (h/t=48)

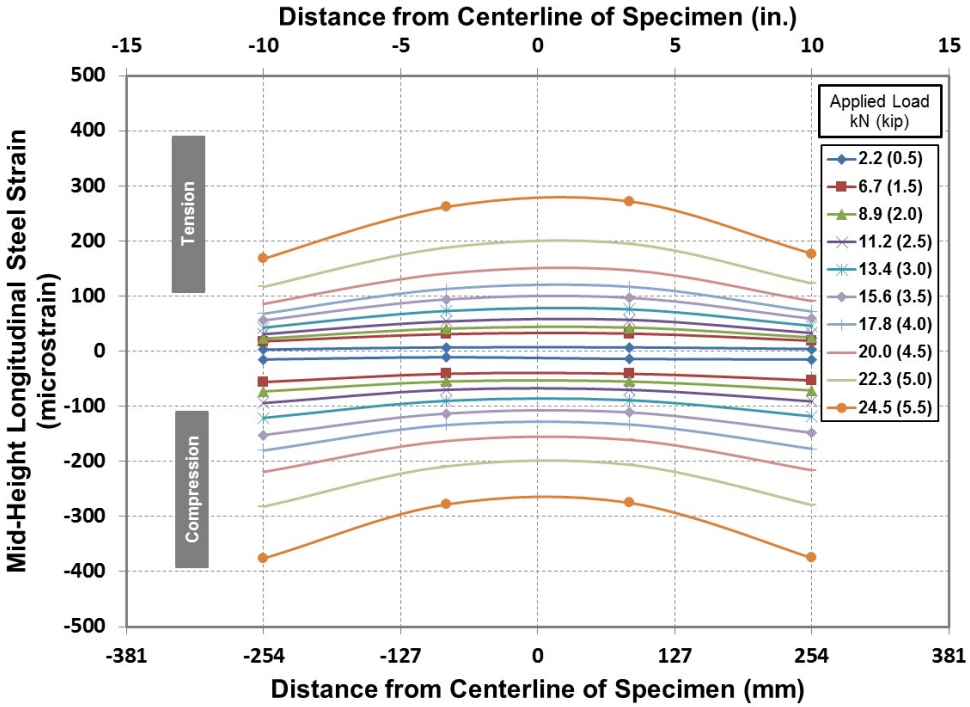

Figure 3-39: Longitudinal strain distribution across the width of the pilot plate IA-48-5/16-P-a (h/t=154)

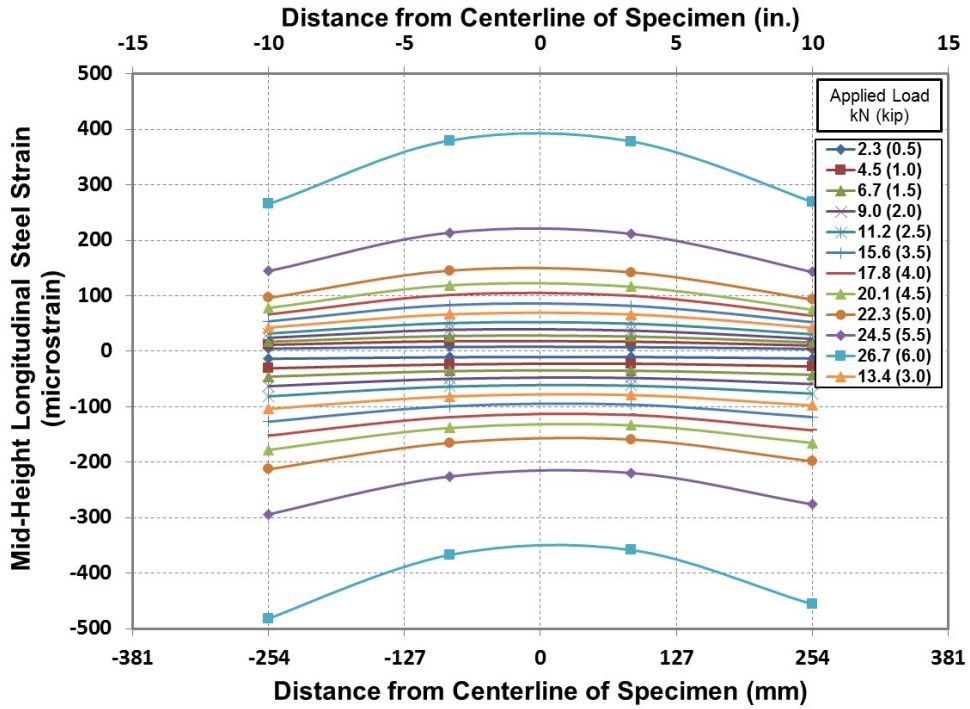

Figure 3-40: Longitudinal strain distribution across the width of the pilot plate IA-48-5/16-P-b (h/t=154)

It is evident from the measured strain results that the test setup was able to distribute the applied load uniformly across the width of the test plate. Therefore, using two strain gauges attached to each face of the plate, one in the middle and one at the side of the plate were considered for the main tests. Further, the test results clearly demonstrated that the measured compressive strains were higher than the tensile strains. This behavior is attributed to the combined stresses from axial loading and second order effect moments from the increase in the lateral deformation of the plate.

Load-Deformation Behavior

The measured total applied load versus the lateral deformation of the plate measured using string potentiometers are graphically presented in Figure 3-41, Figure 3-42, and Figure 3-43 for the three pilot test plates. The shown deformations are measured at the top and bottom ends of the plates, and at mid-height. The measured lateral deformation of the plate at the top and bottom ends is attributed to the rotation of the two sleeves as illustrated in Figure 3-44. The lateral deformation of the test plate at mid-height with respect to its ends, which is referred to as net lateral deformation versus the applied axial load is shown in Figure 3-45, Figure 3-46, and Figure 3-47 for three pilot test plates. The net lateral deformation was obtained by subtracting the average value of the measured top and bottom deformations from the measured mid-height deformation.

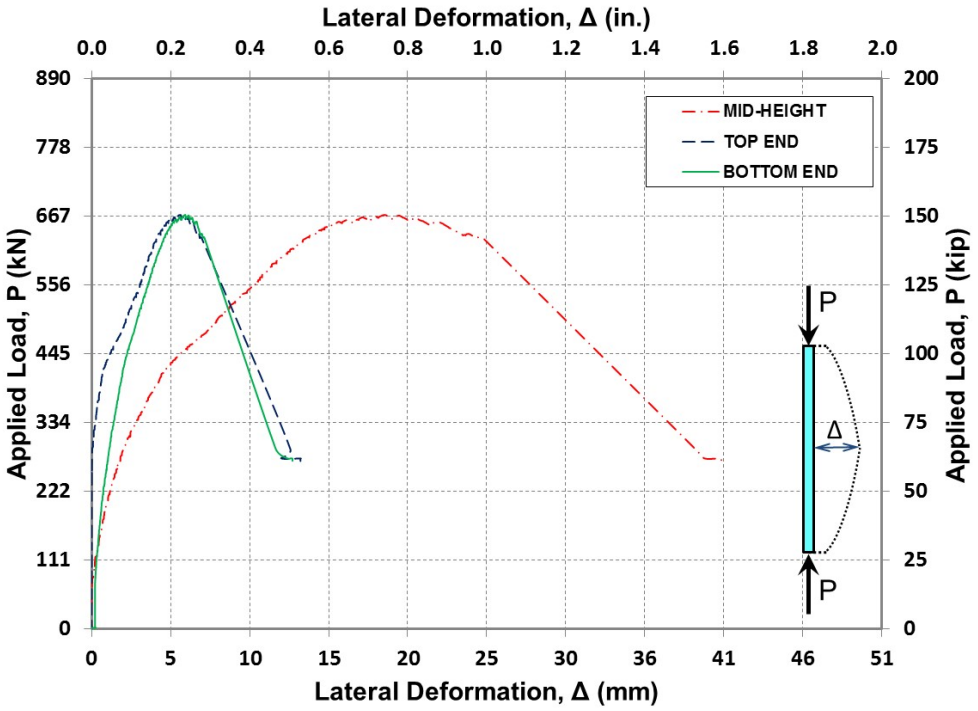

Figure 3-41: Applied load vs. mid-height lateral deformation of plate IA-24-1/2-P (h/t=48)

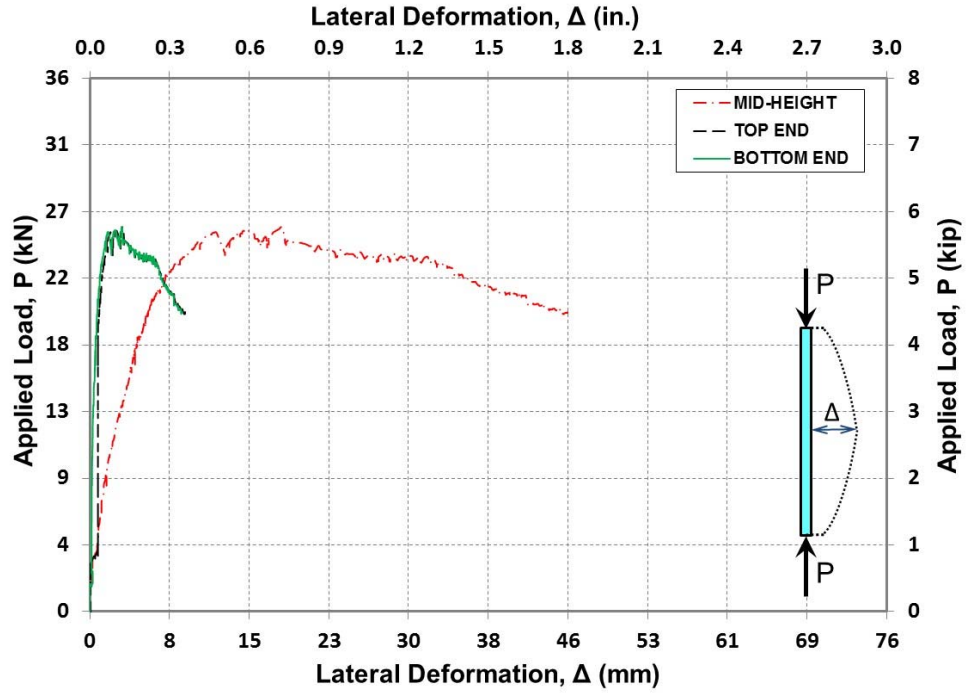

Figure 3-42: Applied load vs. mid-height lateral deformation of plate IA-48-5/16-P-a (h/t=154)

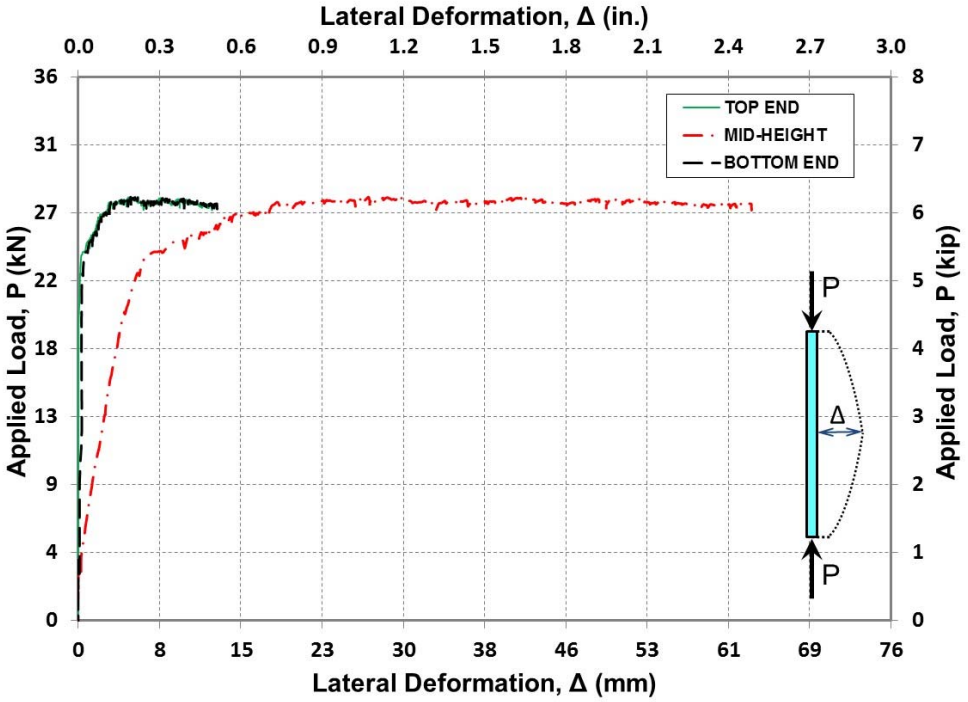

Figure 3-43: Applied load vs. lateral deformation of plate IA-48-5/16-P-b (h/t=154)

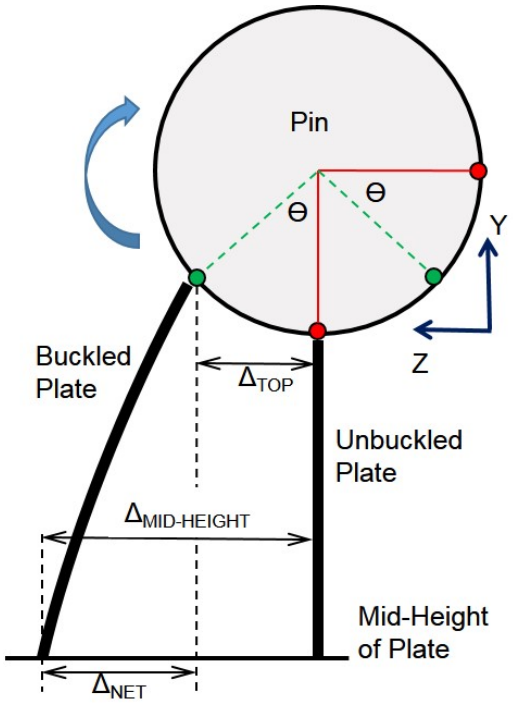

Figure 3-44: Depiction of the effect of the sleeves rotation on the deformation of the plate

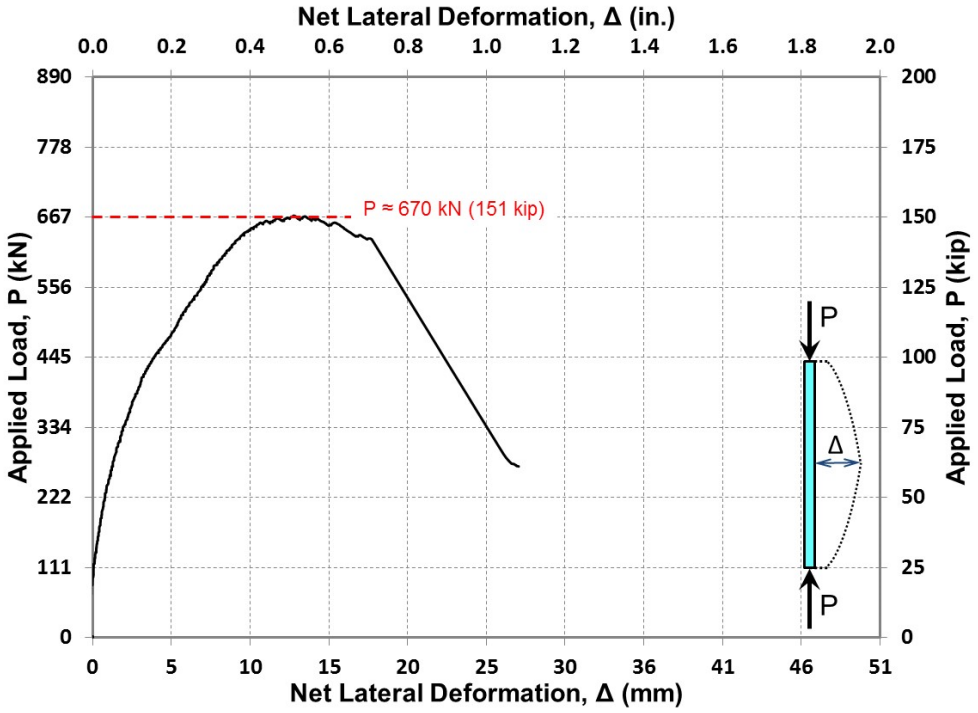

Figure 3-45: Applied load vs. net lateral deformation at mid-height of plate IA-24-1/2-P

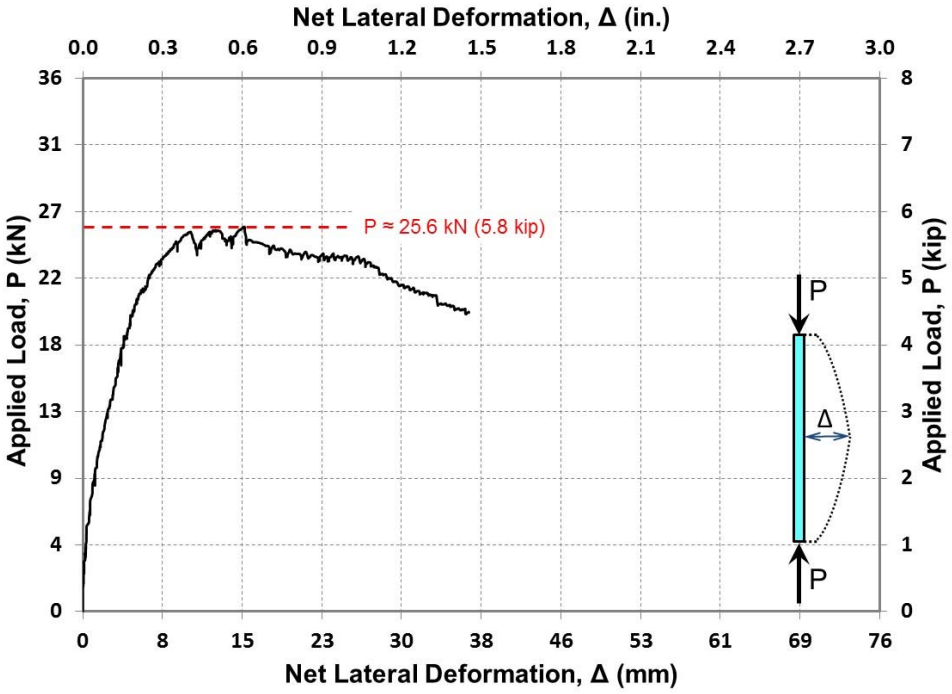

Figure 3-46: Applied load vs. net lateral deformation at mid-height of plate IA-48-5/16-P-a

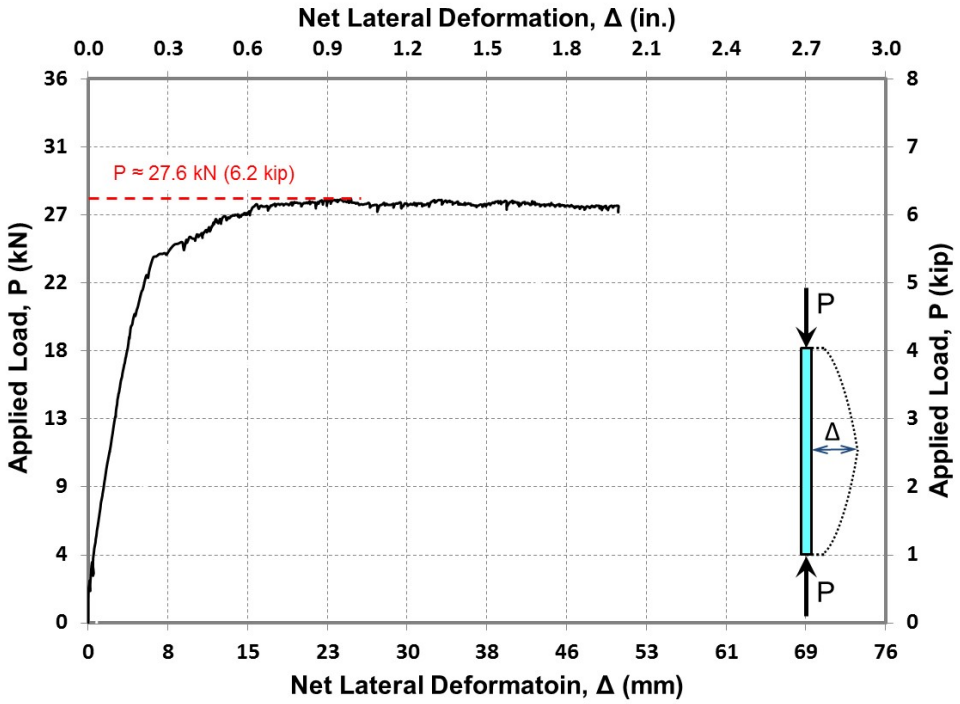

Figure 3-47: Applied load vs. net lateral deformation at mid-height of plate IA-48-5/16-P-b

The load-deformation behavior of the three pilot plates shows that the axial stiffness of the plates remarkably changed due to increase of the P-δ effect. It should be noted that the initial stiffness of the plate is attributed to the imperfection in the plates, which was noticed in the three pilot plates. The excessive imperfection in the pilot plates can be correlated to the manufacturing process.

Rotation of Sleeves

In order to ensure that the designed test setup will simulate pin-ended boundary conditions for the steel plates, the rotation of the sleeves were monitored using the Optotrak system. One IRED was attached to each sleeve at its centerline as shown in Figure 3-24. Using the measured vertical displacement (Y) and lateral displacement (Z) of the IRED attached to the sleeve, the

angle of rotation (Θ) of the top and bottom sleeves were computed as follows. Figure 3-48 shows the measured angle of rotation of the top and bottom sleeves of pilot plate "IA-48-5/16-P-b" throughout load application.

$$\theta\ (rad) = \frac{\sqrt{(\Delta Z)^2 + (\Delta Y)^2}}{r}$$

Where, r is the outer radius of sleeve and is equal to 89 mm (3.50 in.).

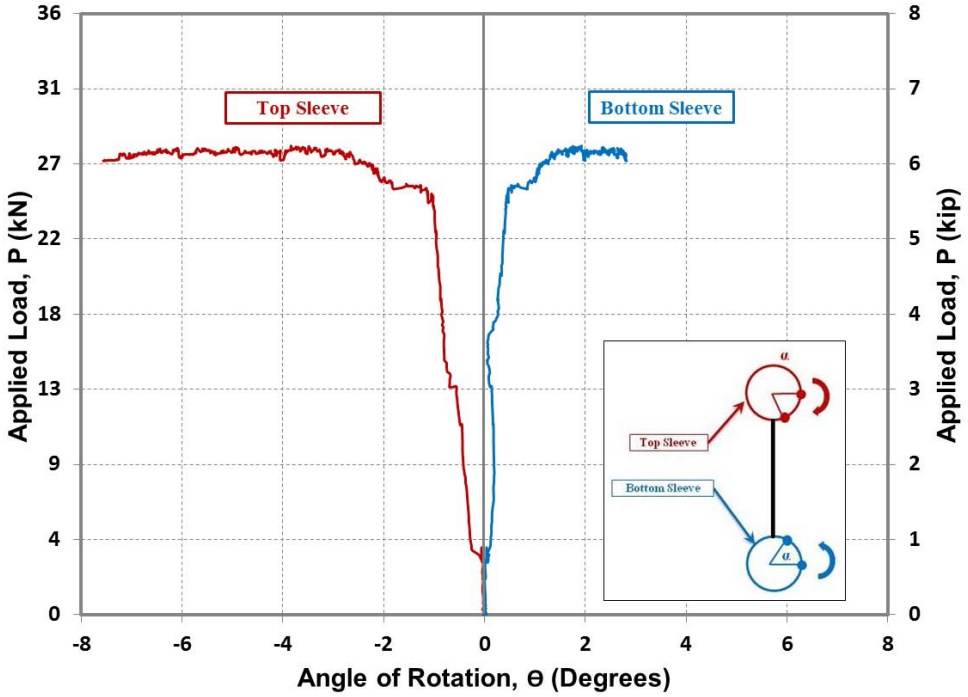

Figure 3-48: Measured angle of rotation of sleeves of pilot plate "IA-48-5/16-P-b"

In addition, the rotation of the sleeve was visually monitored by painting a marking line on the top sleeve and fixing a thread to the frame. Figure 3-49 and Figure 3-50 show the top sleeve of test plate "IA-48-5/16-P-a" with the paint and fixed lines before and after testing, respectively. It is evident that the painted line was displaced with respect to the fixed line, indicating rotation of the sleeve.

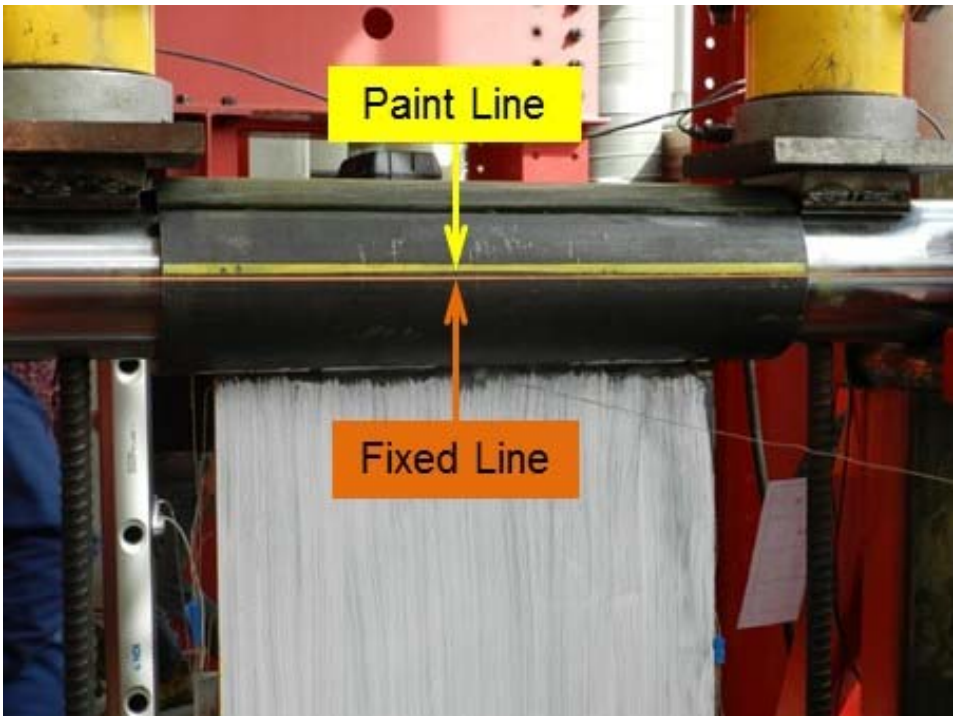

Figure 3-49: Top sleeve of pilot plate "IA-48-5/16-P-a" before testing

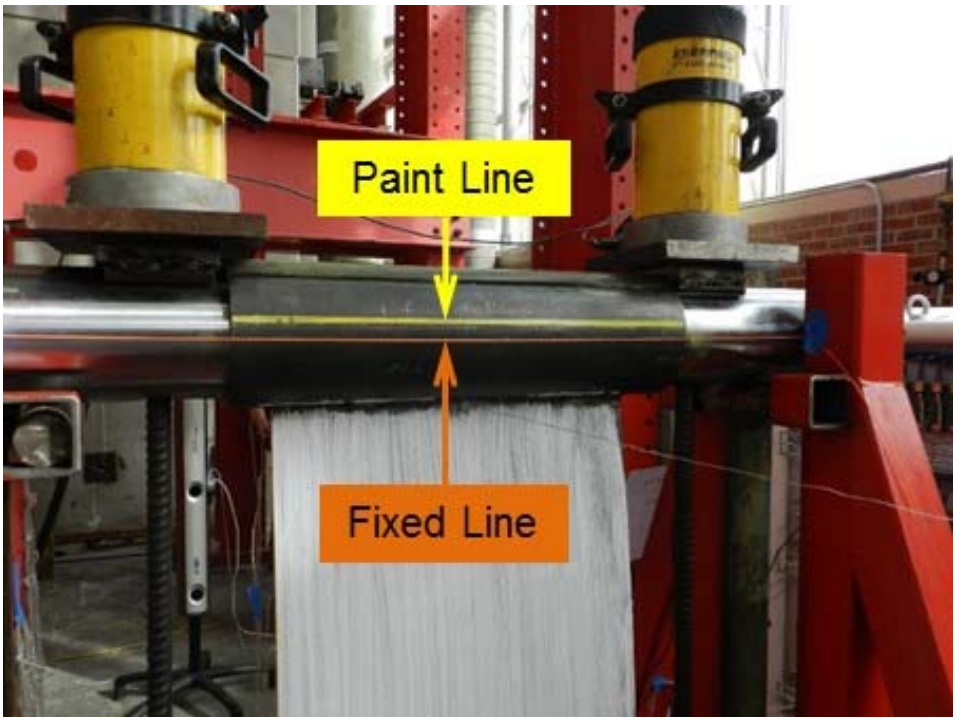

Figure 3-50: Top sleeve of pilot plate "IA-48-5/16-P-a" after testing

3.2.5 Test Results and Discussion of Phase I-A

3.2.5.1 *Buckling Definition*

In general, plate compressive elements are separated into two categories. First, stiffened elements which are supported along two edges parallel to the direction of compressive stresses. Second, unstiffened elements which are supported along one edge and free on the other edge parallel to direction of compressive stresses. If longitudinal edges parallel to the direction of the compressive stresses are unrestrained and free to move, there will be equal deflection across the center of the section just as in the case of a column. Therefore, due to have two unrestrained and free edges along to the direction of the compressive applied load, the total behavior is expected to be similar to column behavior and all the columns buckling equations may be implemented.

Due to imperfection of the plate, it deforms before reaching the theoretical buckling load (P_b) of the perfect plate. Therefore, buckling is not expected to be sudden; rather it is a gradual process until an ultimate load is reached. In this case, P_b of the perfect structure is replaced by an ultimate load which is very close to P_b. Despite not being equal in value, the ultimate load is defined as the buckling load. Figure 3-51 shows the axial and lateral deformation of a perfect and imperfect plate with 2 free edges in direction of applied load acting as a column.

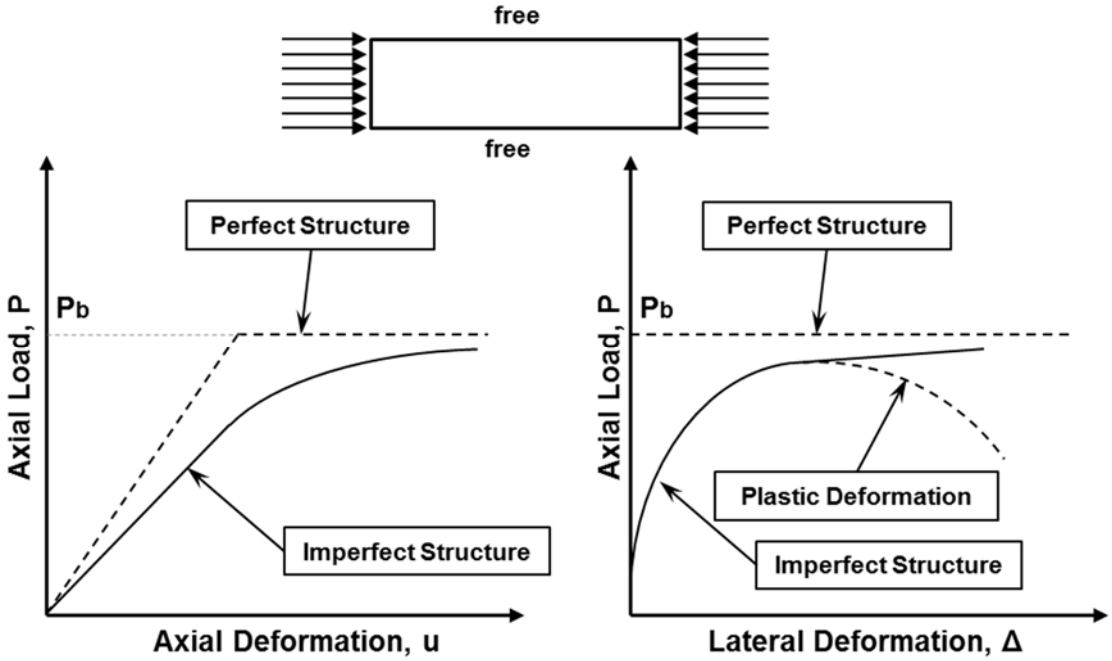

Figure 3-51: Typical behavior of steel column with and without imperfection [13]

3.2.5.2 ***Imperfections***

Steel plates are typically not usually perfectly flat, but have small initial imperfections. The initial imperfections in our test specimen can be results of different reasons. First, rapid and uneven cooling of steel after rolling which results in residual stresses and can induce deformation [54]. Welding the plate to the sleeves at both ends also induced residual stresses at the edges of the plate. Eccentricities are another type of imperfections imposed on the test specimen due to errors conducted by keeping the plate at the centerline of the both sleeves. Moreover, application of the CFRP strengthening system could be another reason to induce initial imperfections. Since the application is not a machined process, there is no guarantee to keep the thickness of the strengthening layers perfectly constant. This process might result in

unsymmetrical sections. The Optotrak system was used to capture out-of-straightness imperfections. Values of maximum imperfections are given in Table 3-11 for the specimens tested in Phase I-A. Regardless to the height and thickness of the plates, values of imperfections are within a limited range. Measured initial imperfections with respect to its ends are also shown in Figure 3-52 and Figure 3-53 for plates tested in Phase I-A having height of 610 mm (24 in.) and 1220 mm (48 in.), respectively. Results indicate that values of imperfection are not identical for the test specimens. However, they follow somehow a curved shape by having maximum deformation nearby mid-height. It is worth noting that these measured results are presented only from the front face of the steel plates and there is no data for the other side.

Table 3-11: Measured imperfection values obtained from Phase I-A

Specimen ID	Strengthening Layer	Measured Imperfection Value, δ	
		(in.)	(mm)
IA-24-1/2-U	0	0.02	0.5
IA-24-3/8-U		*	*
IA-24-5/16-U		*	*
IA-48-1/2-U		0.08	1.9
IA-48-3/8-U		0.09	2.2
IA-48-5/16-U		0.05	1.4
IA-24-1/2-S-P	1	0.05	1.4
IA-24-3/8-S-P		0.03	0.8
IA-24-5/16-S-P		0.05	1.3
IA-24-5/16-S		0.06	1.6
IA-48-1/2-S-P		0.07	1.7
IA-48-3/8-S-P		0.13	3.2
IA-48-5/16-S-P		*	*
IA-48-5/16-S		0.07	1.8
AVG		**0.06**	**1.6**

*No value was recorded by optotrack system.

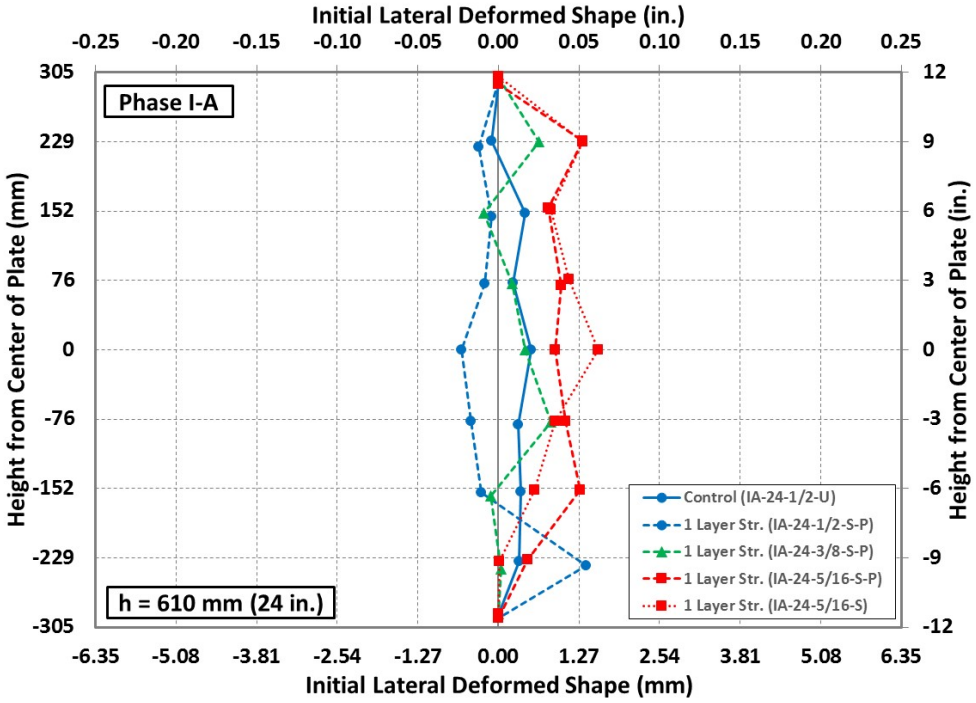

Figure 3-52: Measured initial imperfection of the specimens at Phase I-A (h = 610mm (24in.))

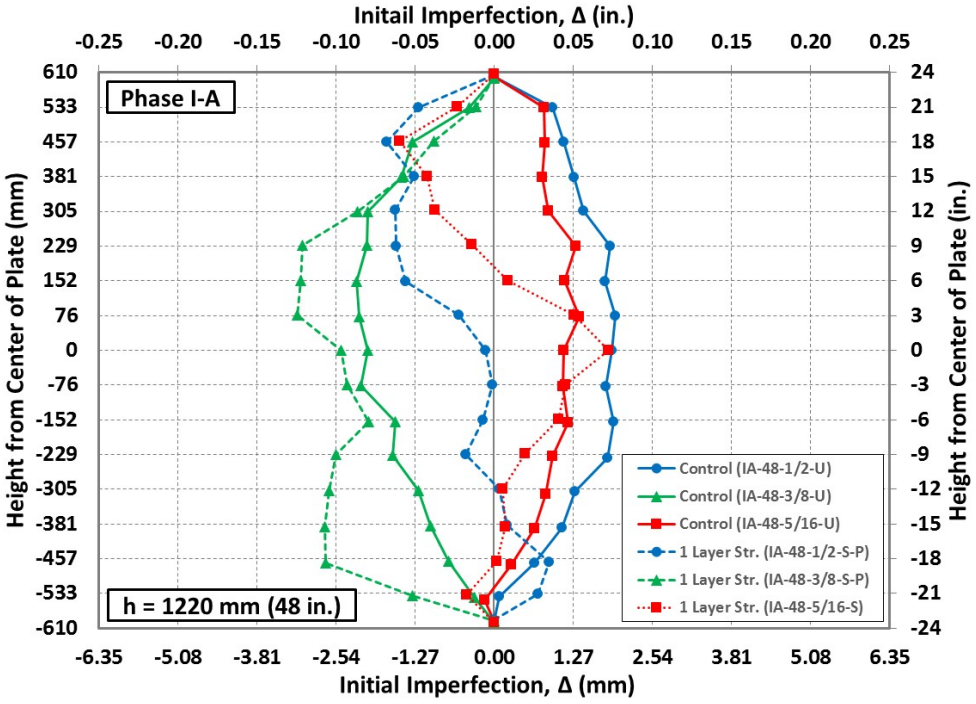

Figure 3-53: Measured initial imperfection of the specimens at Phase I-A (h = 1220mm (48in.))

3.2.5.3 ***Buckling Load***

The Buckling load of strengthened plates was compared to the buckling load of un-strengthened control plates. The measured test results from Phase I-A are given in Table 3-12. The increase in the measured buckling load indicates that bonding of HM CFRP strands to the steel plates increased its buckling capacity up to 61 percent. Test results indicate also that the effectiveness of the CFRP strands in increasing the buckling load of steel plates is dependent on the slenderness ratio of the steel plate. Enhancement of the buckling load was more pronounced for steel plates with high slenderness ratio. The discrepancy in the percentage increase is due to the different in the plate imperfection observed for the test plates.

Table 3-12: Test results summary of test plates in Phase I-A

Plate Designation	h/t	Buckling Load		
		kN	kip	Increase (%)
IA-24-1/2-U	48	645	145	-
IA-24-1/2-S-P		787	177	22
IA-24-3/8-U	64	374	84	-
IA-24-3/8-S-P		430	97	15
IA-24-5/16-U	77	210	47	-
IA-24-5/16-S-P		295	66	40
IA-24-5/16-S		325	73	55
IA-48-1/2-U	96	112	25	-
IA-48-1/2-S-P		176	39	56
IA-48-3/8-U	128	62	14	-
IA-48-3/8-S-P		89	20	43
IA-48-5/16-U	154	58	13	-
IA-48-5/16-S-P		76	17	31
IA-48-5/16-S		93	21	61

3.2.5.4 ***Measured Strain***

The average measured longitudinal strain versus the measured applied axial load are shown in Figure 3-54 through Figure 3-61 for the plates with slenderness ratio of 48 to 154, respectively.

For each specimen, steel strain of the strengthened plate is compared with the steel strain of the un-strengthened control plate. Since the strain was virtually constant across the width of the plate, as confirmed in the pilot test plates, the reported strain values are the average of the strain gages attached on each face of the plate.

Test results show that at the initial lading, both faces of the plate are under compressive strains. Increasing the load combined the effect of the axial and bending stresses and induced tensile strains to one face of steel plate. In general for each of the plates, as the applied load increases, the longitudinal strain values gradually increase until the buckling load is reached. Upon reaching the buckling load, the longitudinal strain values begin to increase more rapidly coinciding with a decrease in load carrying capacity of the plate. Also, strain measurements show that all test plates (strengthened and control) lost their load carrying capacity at a steel strain value less than the yielding strain measured from tensile coupons. This indicates that the plate experienced elastic buckling. Results indicated that externally bonded CFRP strands contributed to the load carrying capacity by reducing the strains of the steel plate at the same load level which is contributed to an increase in plate buckling load.

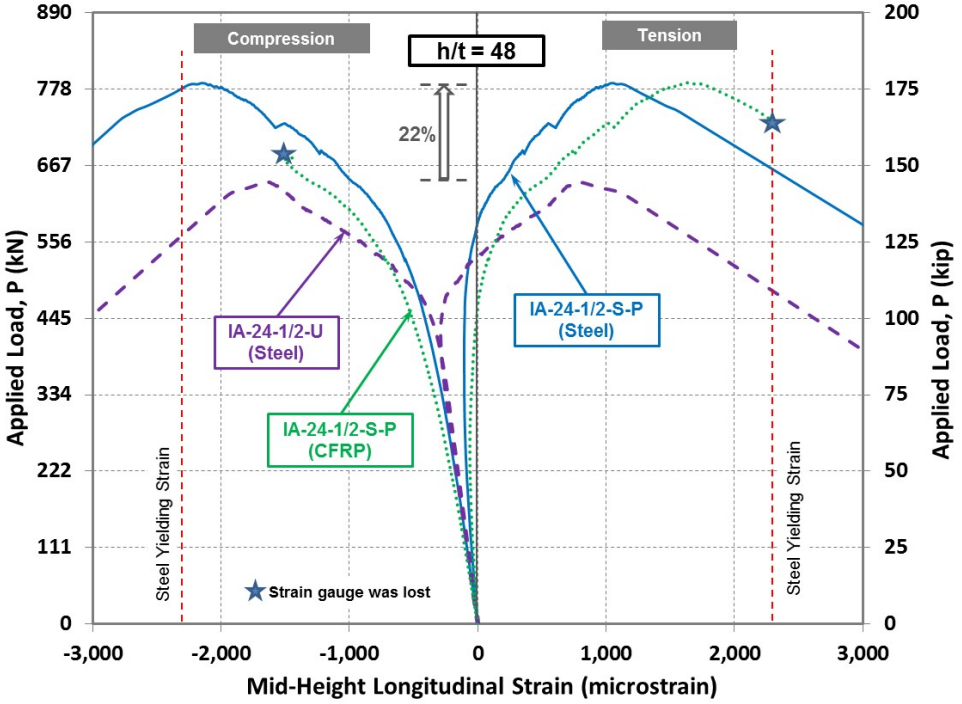

Figure 3-54: Applied load vs. longitudinal strain at mid-height of plates IA-24-1/2

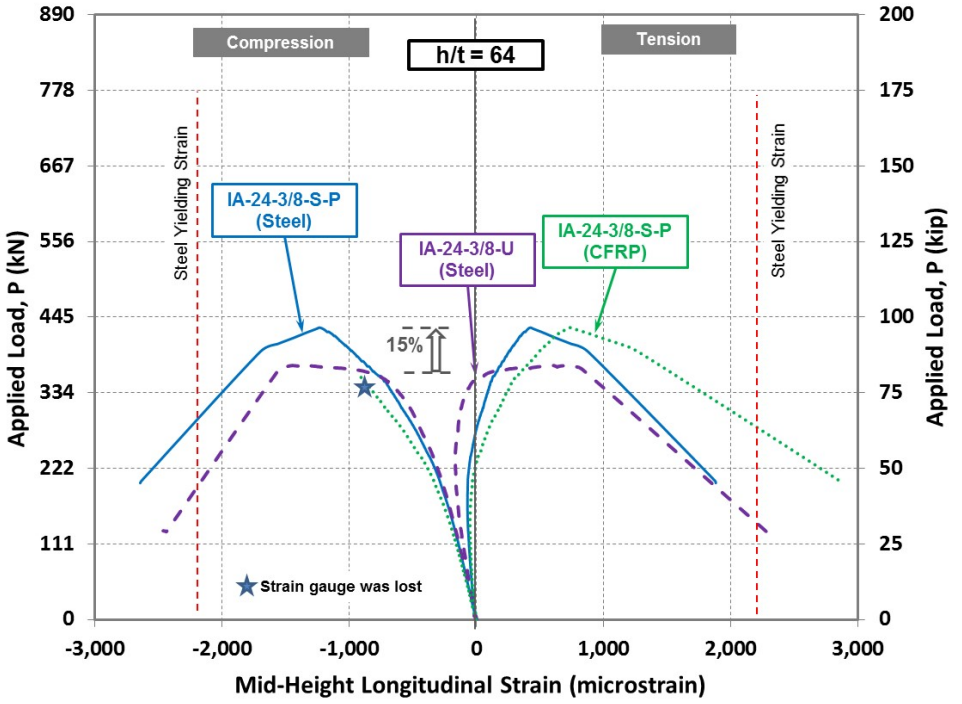

Figure 3-55: Applied load vs. longitudinal strain at mid-height of plates IA-24-3/8

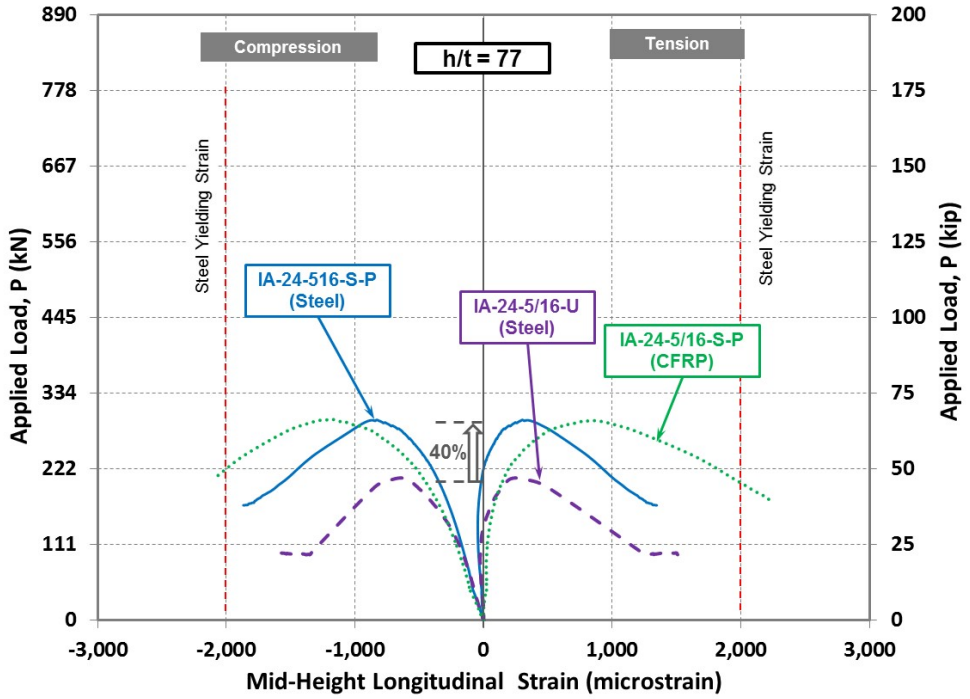

Figure 3-56: Applied load vs. longitudinal strain at mid-height of plates IA-24-5/16 (with putty)

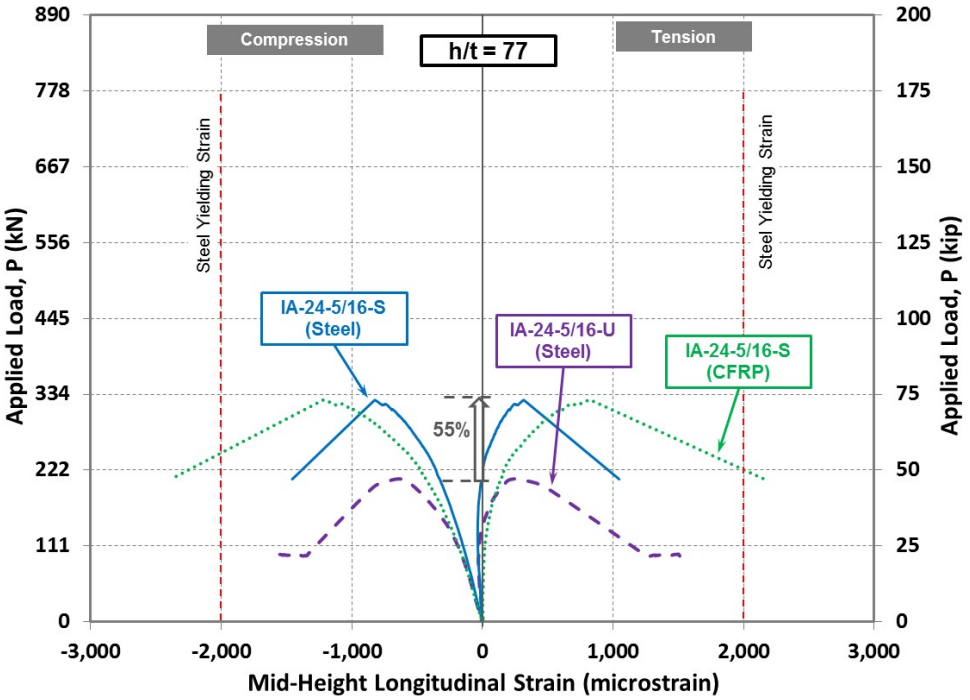

Figure 3-57: Applied load vs. longitudinal strain at mid-height of plates IA-24-5/16 (without putty)

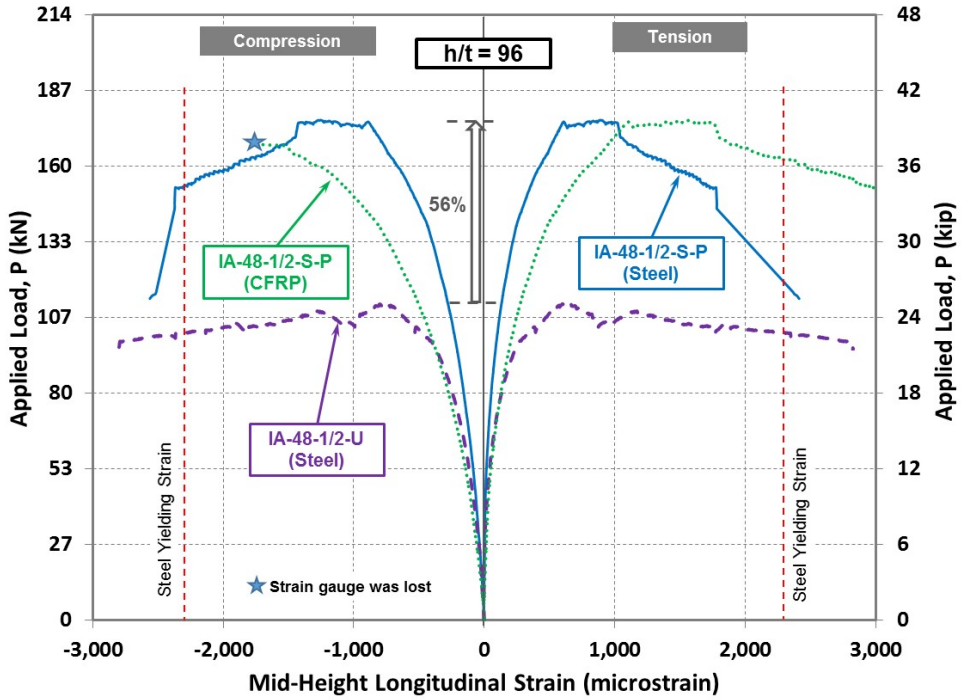

Figure 3-58: Applied load vs. longitudinal strain at mid-height of plates IA-48-1/2

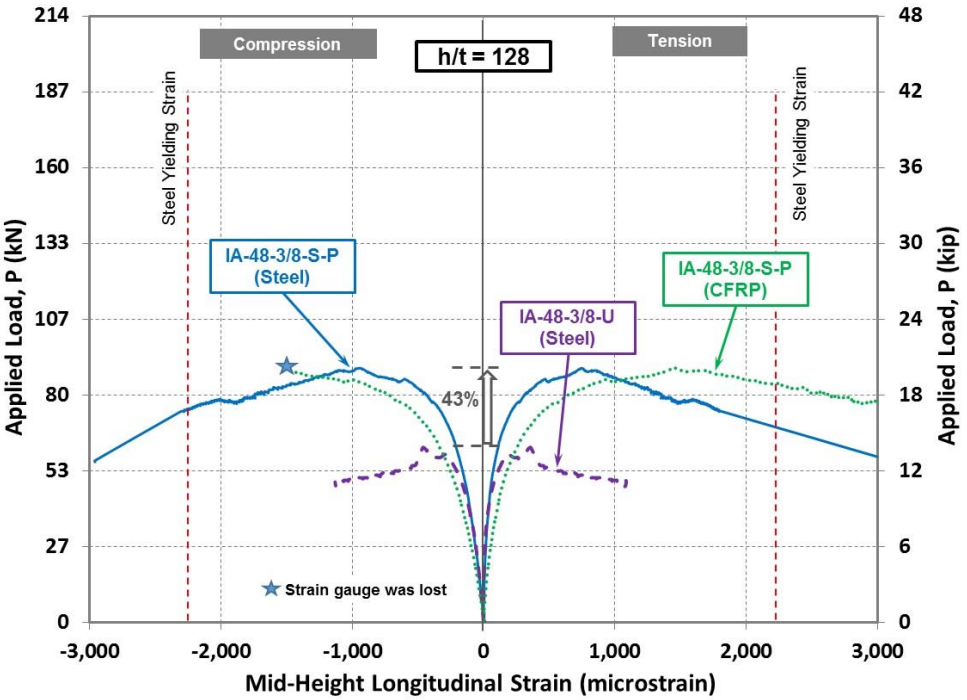

Figure 3-59: Applied load vs. longitudinal strain at mid-height of plates IA-48-3/8

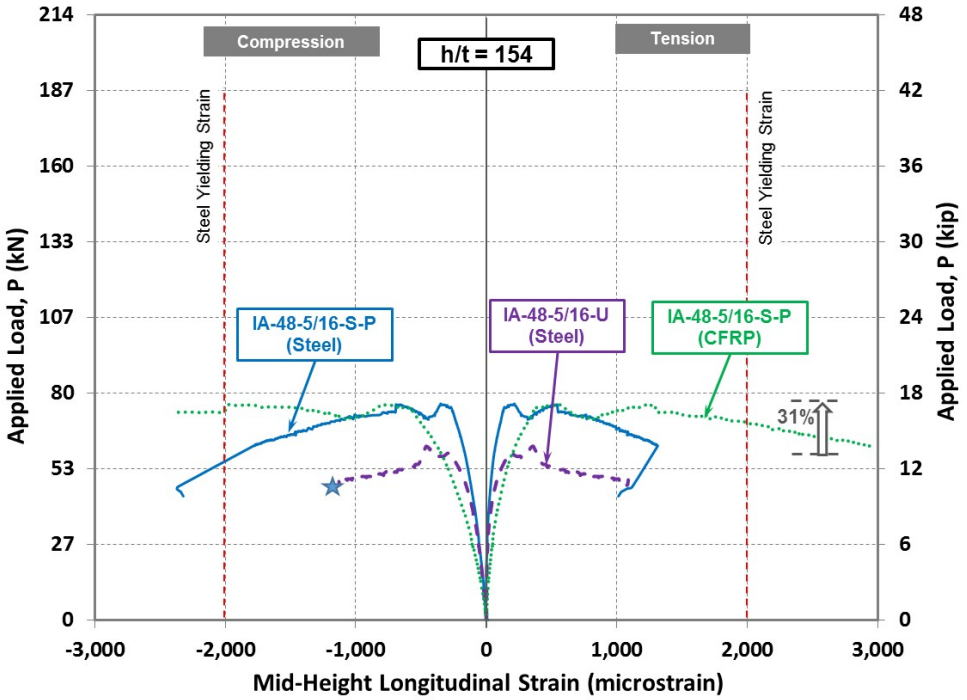

Figure 3-60: Applied load vs. longitudinal strain at mid-height of plates IA-48-5/16 (with putty)

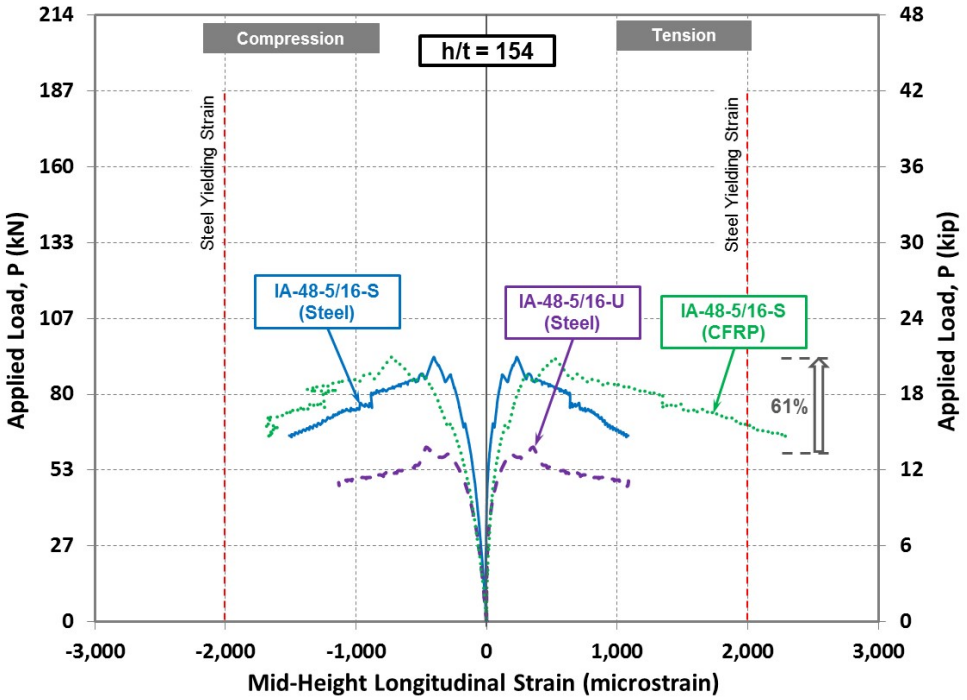

Figure 3-61: Applied load vs. longitudinal strain at mid-height of plates IA-48-5/16 (without putty)

3.2.5.5 ***Load-Deformation Behavior***

The measured applied load versus the measured net lateral deformation of the test plates with slenderness ratio of 48 through 154 is graphically presented in Figure 3-62 through Figure 3-67. Also, a summary of the applied load versus the net lateral deformation for plates with height of 610 mm (24 in.) and 1220 mm (48 in.) is shown in Figure 3-68 and Figure 3-69, respectively.

The load deformation behavior of the plates reveals that external bonding of High-Modulus (HM) CFRP strands to the steel plates increased their buckling load carrying capacity. The figures show in general that by applying an axial compressive load, the lateral deformation gradually increase until the onset of the buckling occurred. Ultimate failure of the all test plates (control and strengthened) was due to the loss of their lateral stability followed by large deformation, where the plates experienced elastic buckling without yielding of the steel material. Although it appears that there is a reduction in stiffness of the strengthened plates which can be attributed to either the inconsistency of thickness of the strengthening layers at both sides of the plate observed from witness panels or the eccentricity imposed at both ends of the plate. Thus, adding more of an eccentricity that leads to an initial increase of bending effects.

Test results indicate that use of polyurea putty has no significant effect on the efficiency of the CFRP strands strengthening system. Elimination of polyurea putty layer may minimize the imperfection of the plate and may slightly increase the plate buckling capacity.

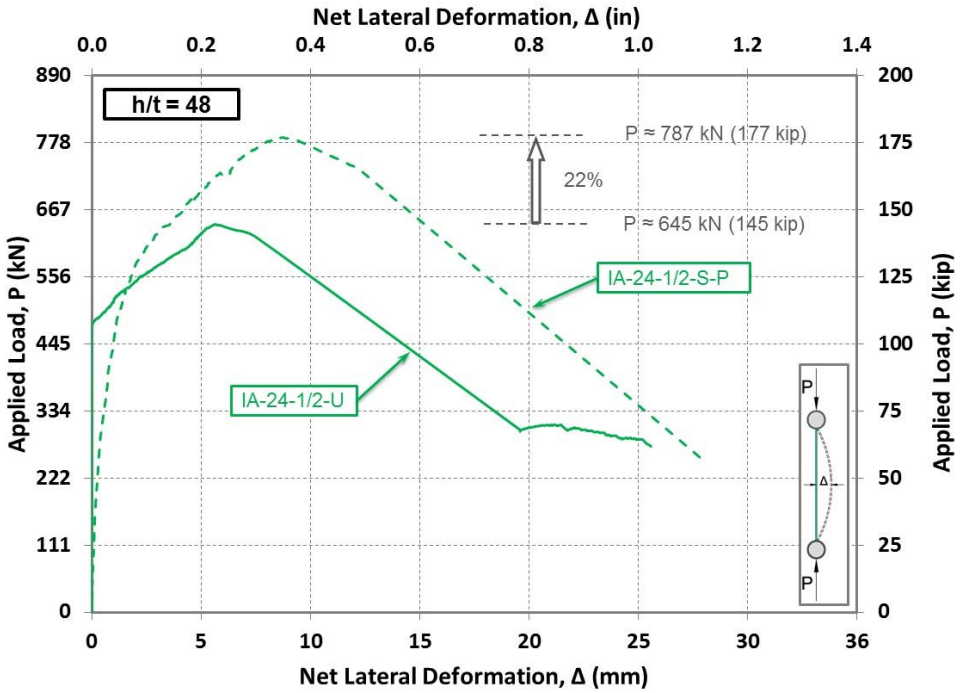

Figure 3-62: Applied load vs. mid-height net lateral deformation of plates IA-24-1/2 (h/t=48)

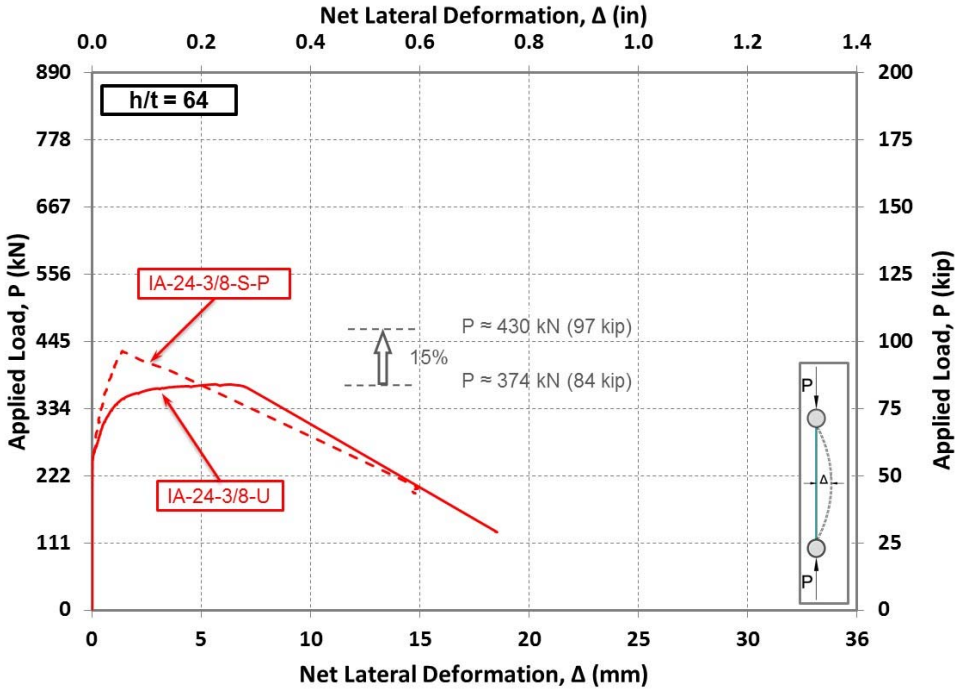

Figure 3-63: Applied load vs. mid-height net lateral deformation of plates IA-24-3/8 (h/t=64)

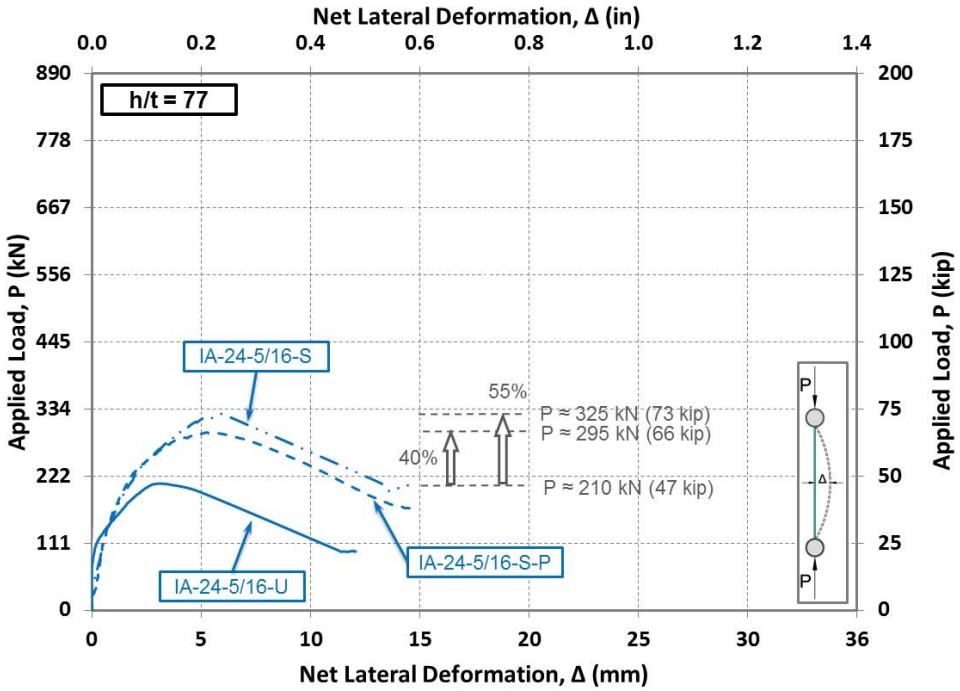

Figure 3-64: Applied load vs. mid-height net lateral deformation of plates IA-24-5/16 (h/t=77)

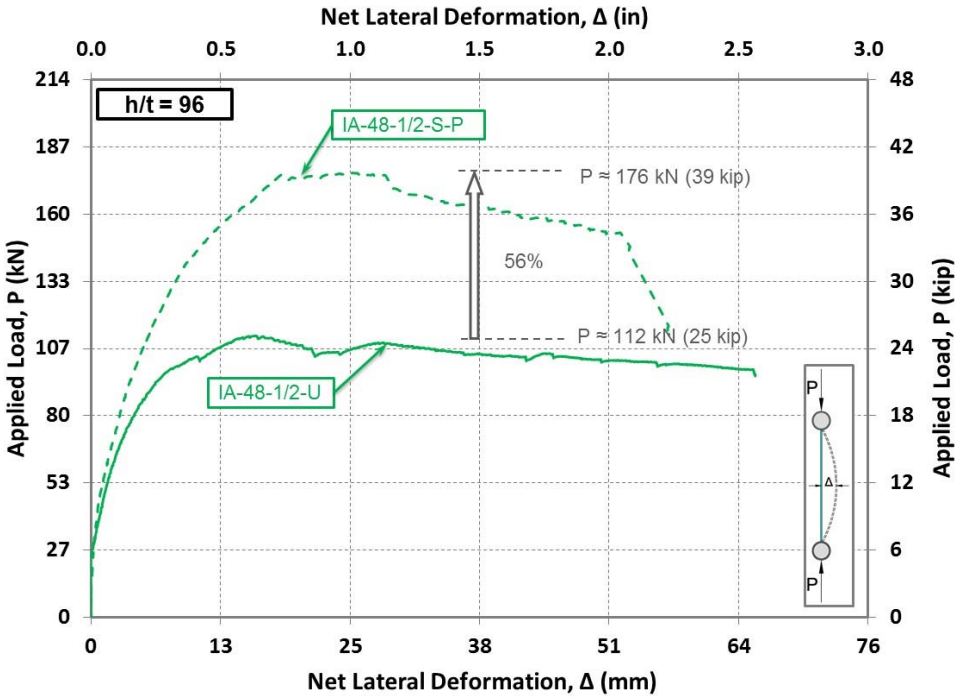

Figure 3-65: Applied load vs. mid-height net lateral deformation of plates IA-48-1/2 (h/t=96)

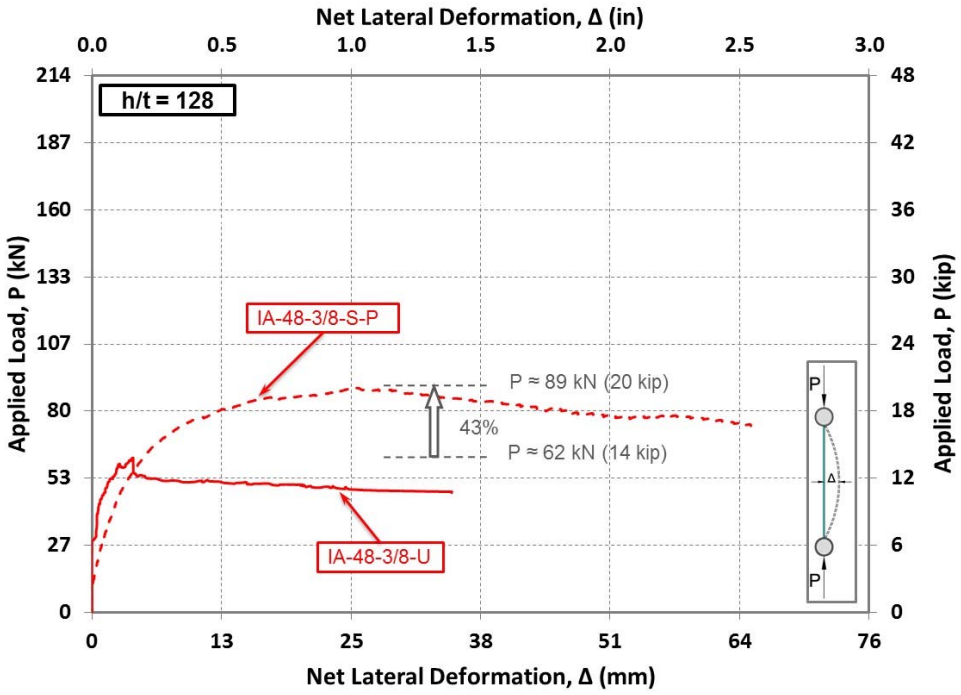

Figure 3-66: Applied load vs. mid-height net lateral deformation of plates IA-48-3/8 (h/t=128)

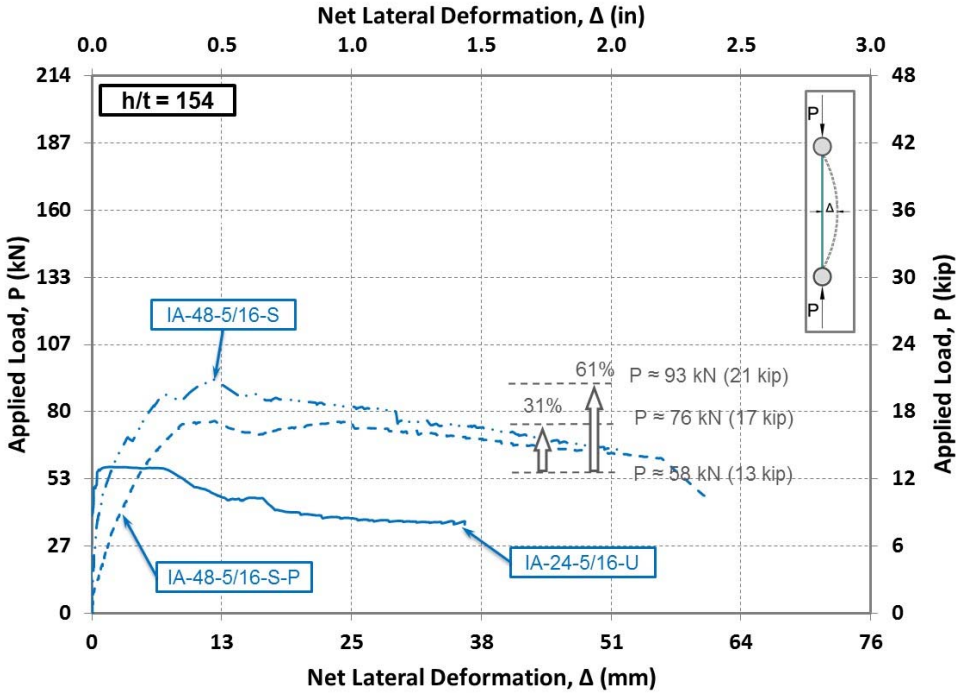

Figure 3-67: Applied load vs. mid-height net lateral deformation of plates IA-48-5/16 (h/t=154)

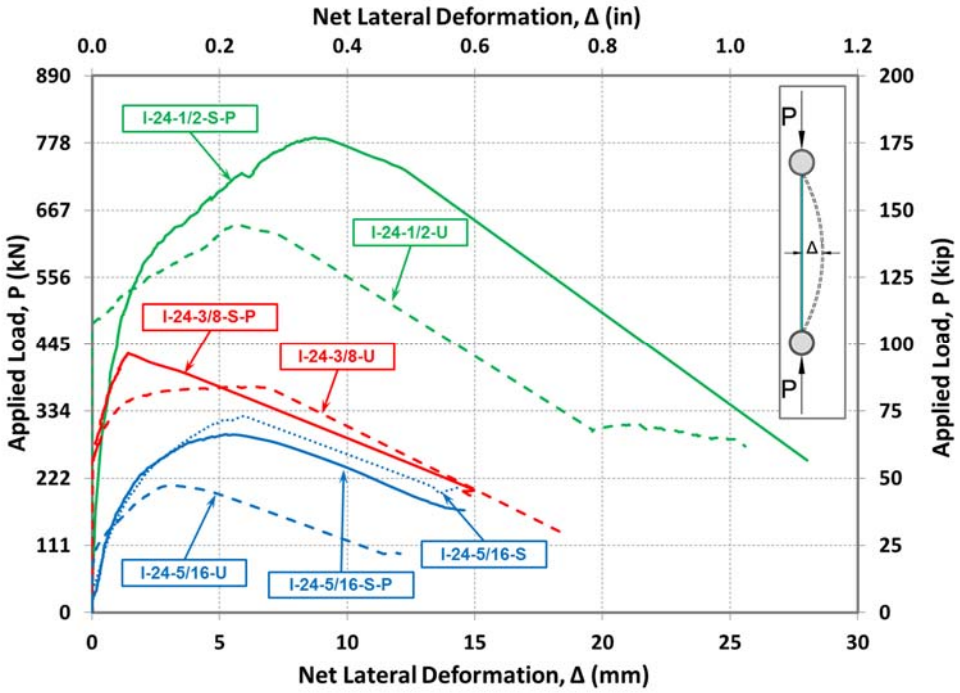

Figure 3-68: Applied load vs. mid-height net lateral deformation of plates with 610 mm (24 in.) height

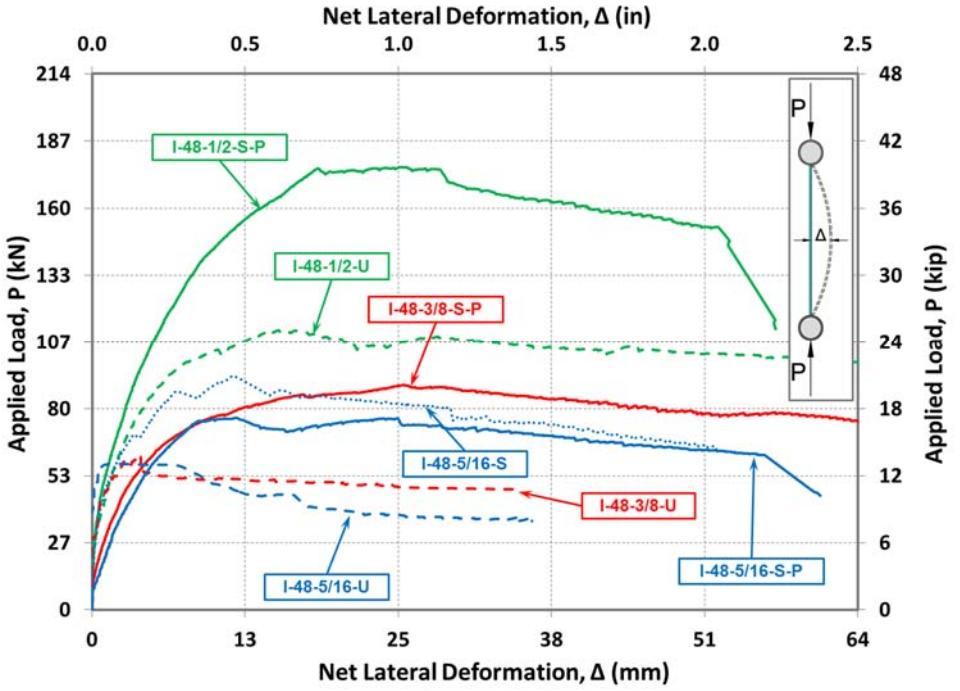

Figure 3-69: Applied load vs. mid-height net lateral deformation of plates with 1220 mm (48 in.) height

3.2.5.6 ***Measured Sleeve Rotation***

The measured sleeve rotations versus the applied load are shown in Figure 3-70 through Figure 3-75. The sleeve rotations of test plates IA-24-1/2-U, IA-24-3/8-U, and IA-24-5/15-U were not recorded. The comparison between the sleeves rotations of the un-strengthened control and their strengthened counterparts indicates that the plates were virtually subjected to the same end conditions. Thus the variation of the end conditions on the measured loads was minimal.

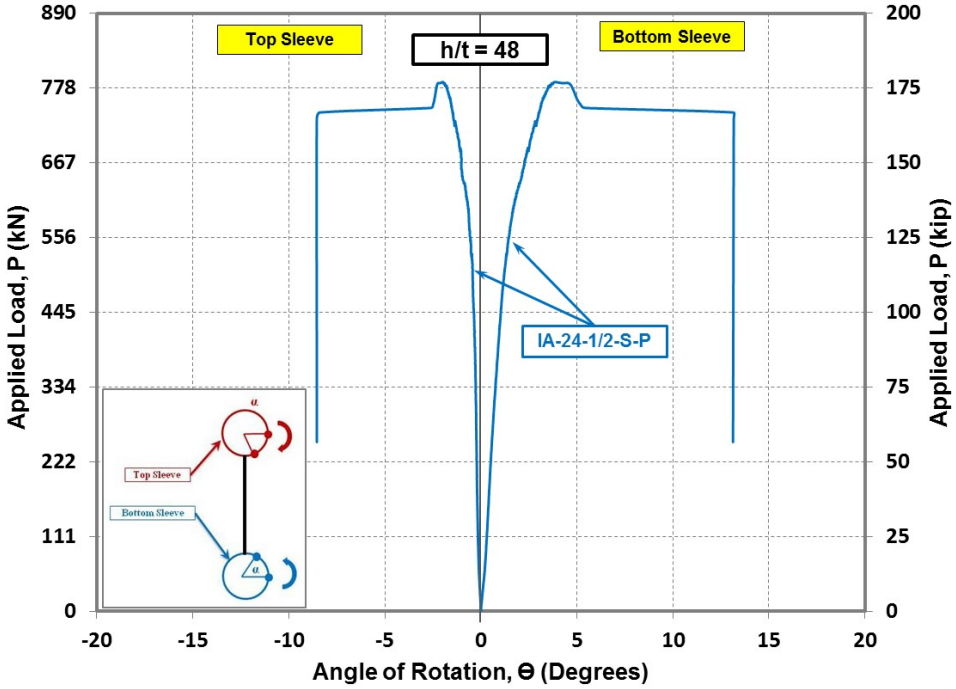

Figure 3-70: Applied load vs. rotation of sleeves of plates IA-24-1/2 (h/t=48)

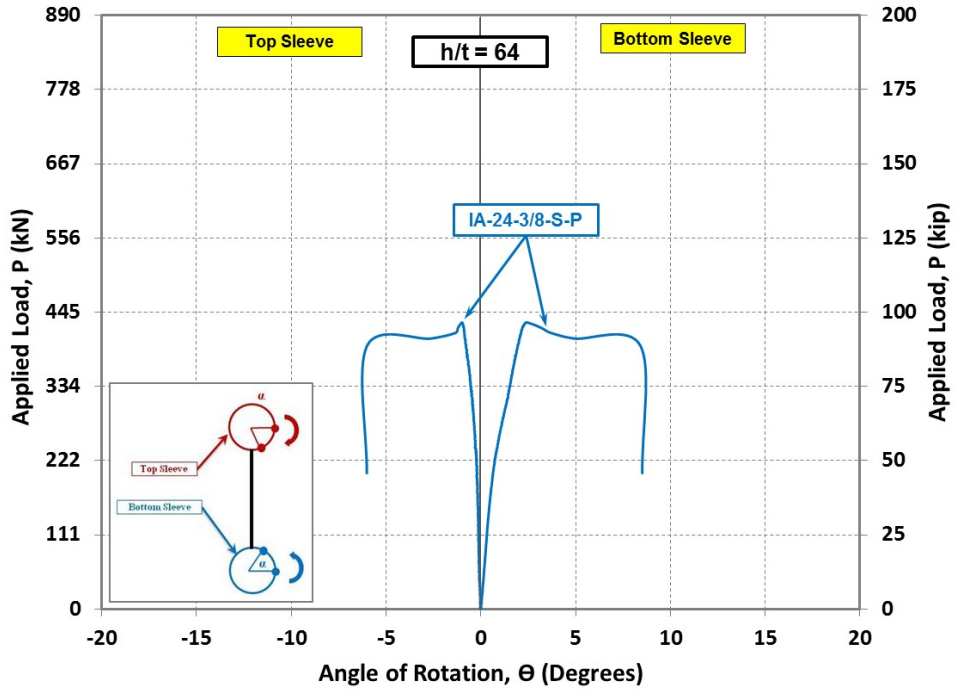

Figure 3-71: Applied load vs. rotation of sleeves of plates IA-24-3/8 (h/t=64)

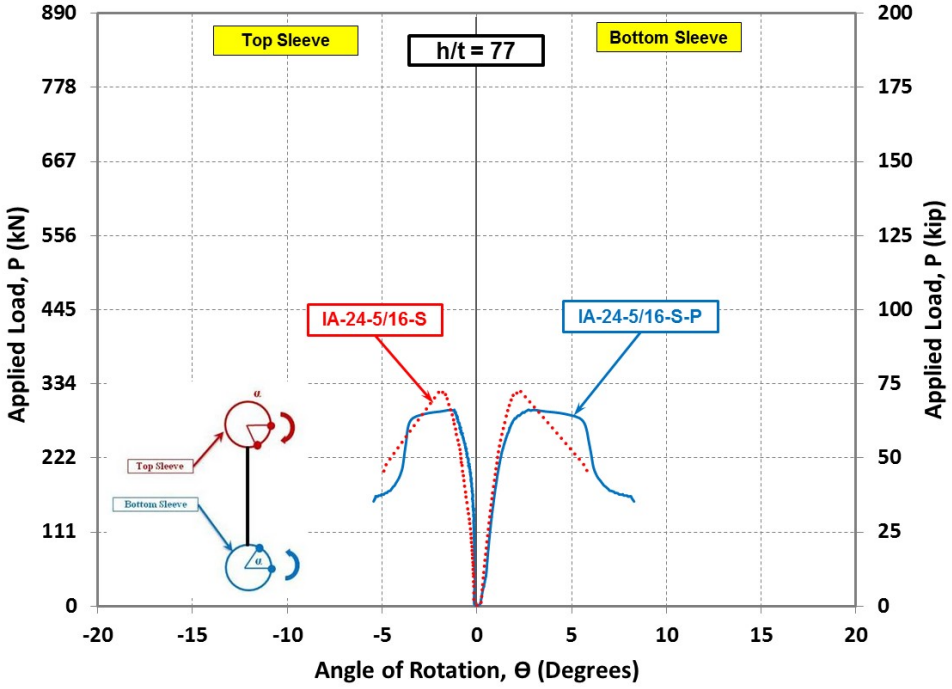

Figure 3-72: Applied load vs. rotation of sleeves of plates IA-24-5/16 (h/t=77)

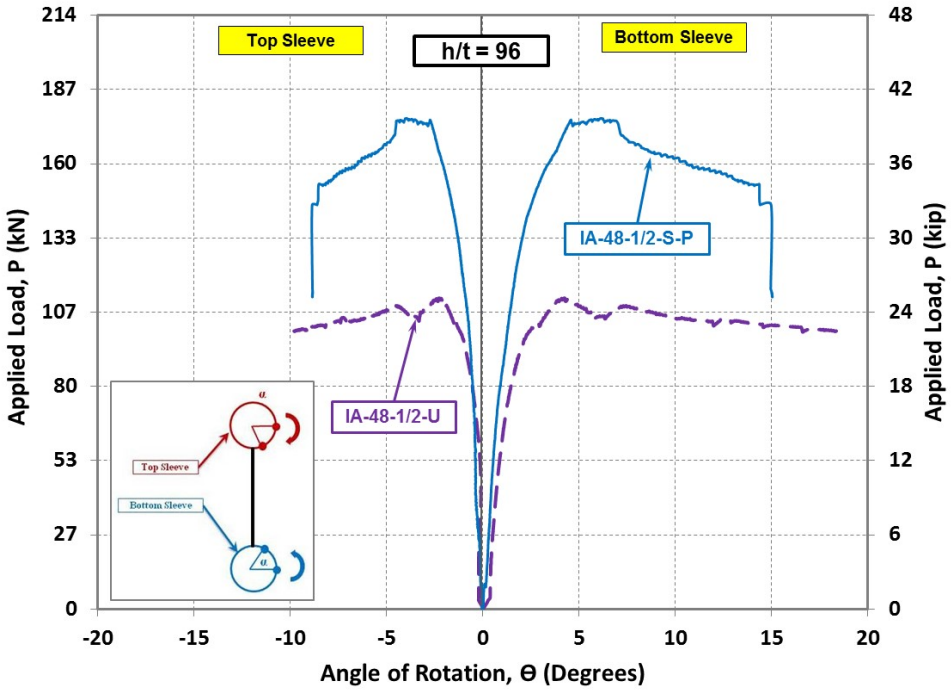

Figure 3-73: Applied load vs. rotation of sleeves of plates IA-48-1/2 (h/t=96)

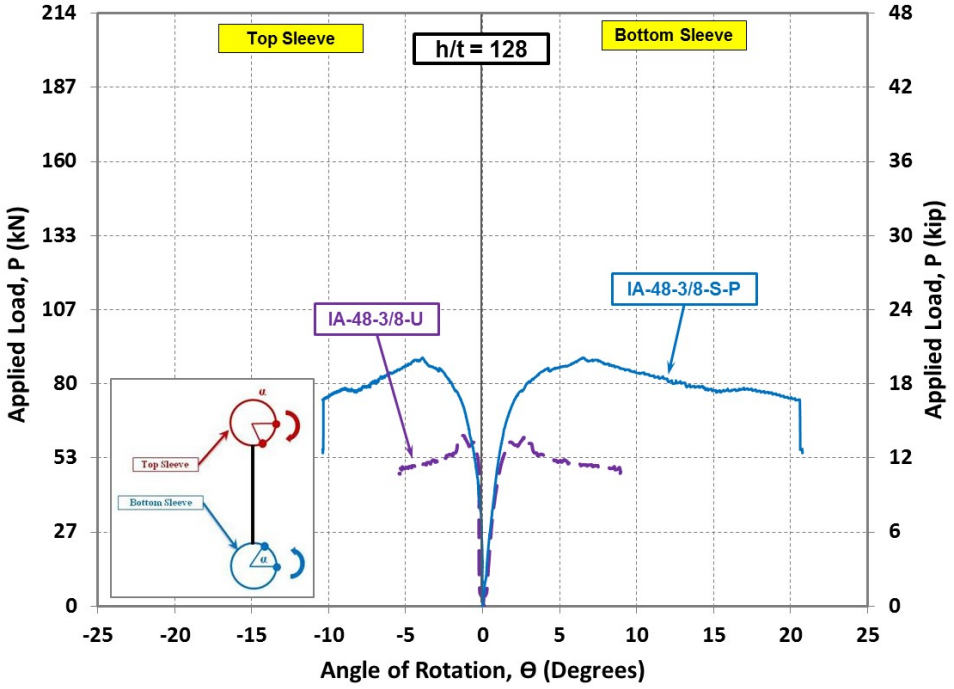

Figure 3-74: Applied load vs. rotation of sleeves of plates IA-48-3/8 (h/t=128)

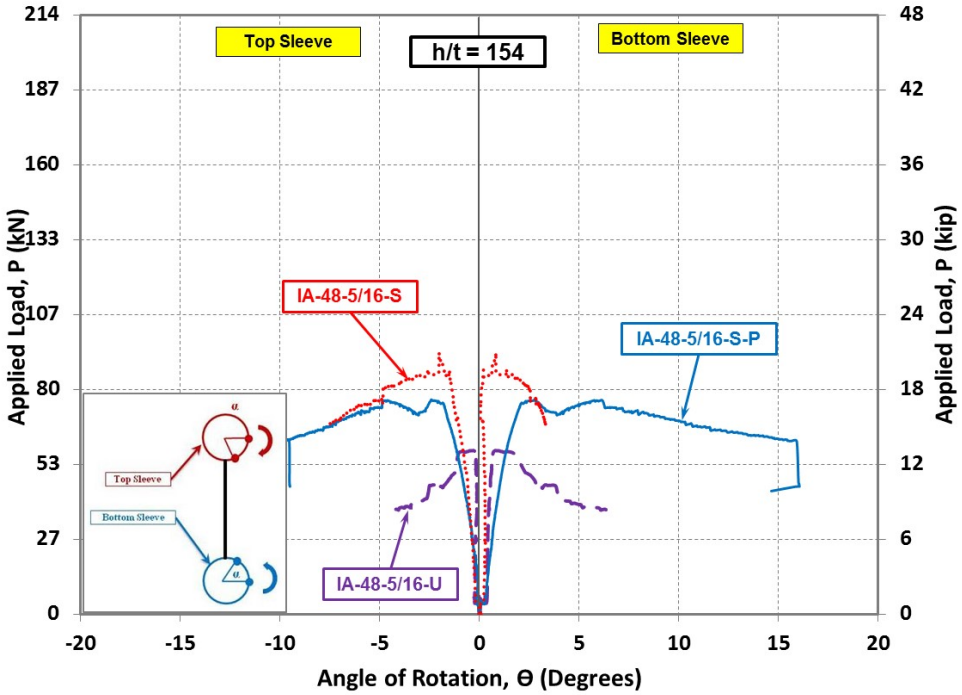

Figure 3-75: Applied load vs. rotation of sleeves of plates IA-48-5/16 (h/t=154)

3.2.5.7 ***Failure of the Strengthening System***

The measured lateral deformed shape versus the measured applied load for the strengthened plates of 24 in. height and 48 in. height are shown in Figure 3-76 and Figure 3-77, respectively. The lateral deformed shapes are plotted in three different load steps using recorded data from the Optotrak system. The behavior was selected at the load levels corresponding to apparent change in lateral stiffness of load-deflection relationships, i.e., prior to buckling load, at the onset of buckling load, and after buckling and loss of load-carrying capacity where the lateral deformation is significantly large compared to that of the buckling load stage.

Plate IA-24-1/2-S-P (h/t=48) and IA-48-1/2-S-P (h/t=96), shown in Figure 3-76 and Figure 3-77, experienced rupture of HM CFRP strands on the tension face after the buckling occurred. Among eight strengthened plates, four of them had rupture after the buckling load and none of them experienced any debonding, as given in Table 3-13. Therefore, CFRP rupture did not lead the system to fail; rather, the failure was due to loss of stability of the system. Figure 3-78 and Figure 3-79 represent a sample of plates that with rupture and without rupture of HM CFRP strands due to plate instability, respectively.

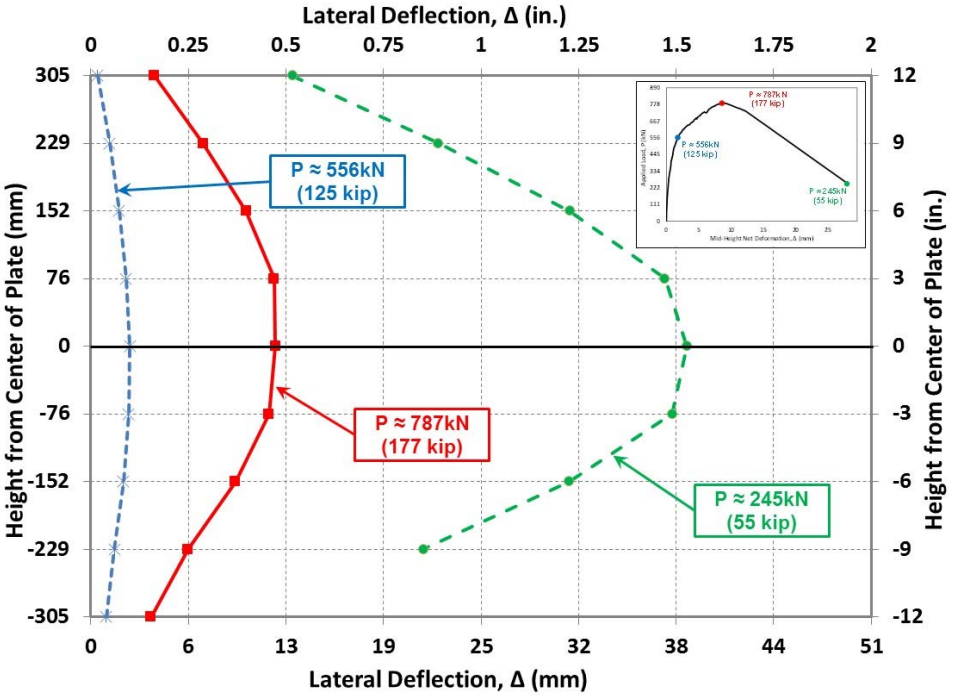

Figure 3-76: Height from center of plate vs. lateral deformation of plate IA-24-1/2-S-P (h/t=48)

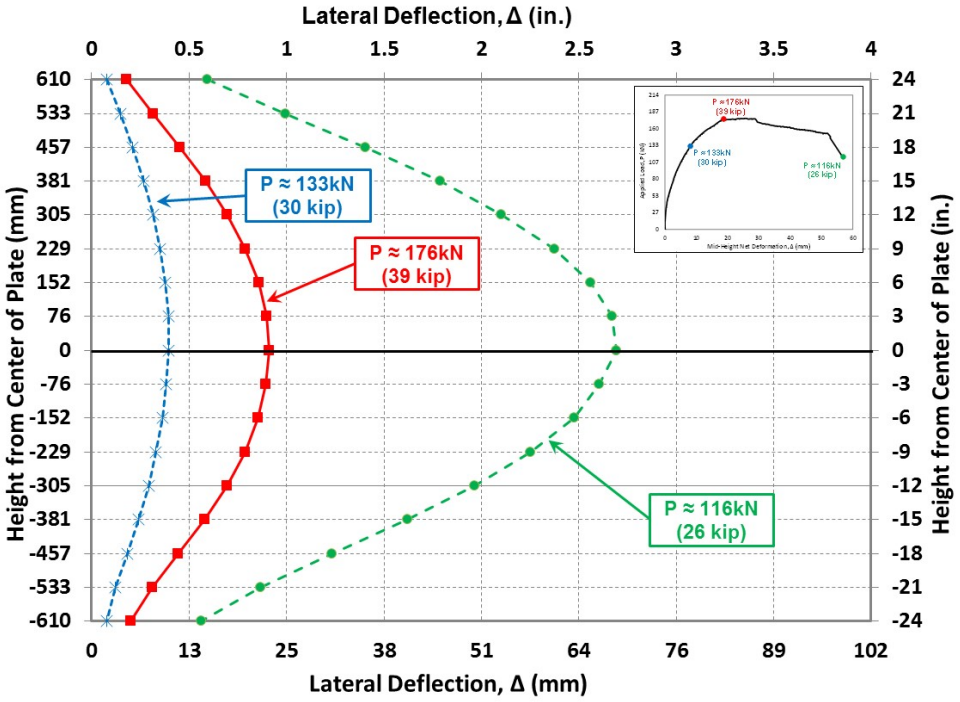

Figure 3-77: Height from center of plate vs. lateral deformation of plate IA-48-1/2-S-P (h/t=96)

Table 3-13: Failure modes of CFRP sheets of strengthened plates

Plate Designation	CFRP Rupture due to Plate Instability	CFRP Debonding
IA-24-1/2-S-P	YES	NO
IA-24-3/8-S-P	NO	NO
IA-24-5/16-S-P	NO	NO
IA-24-5/16-S	NO	NO
IA-48-1/2-S-P	YES	NO
IA-48-3/8-S-P	YES	NO
IA-48-5/16-S-P	YES	NO
IA-48-5/16-S	NO	NO

IA-24-1/2-S-P (h/t=48)

IA-48-1/2-S-P (h/t=96)

Figure 3-78: Rupture of CFRP due to the large deformation (plate instability) after buckling

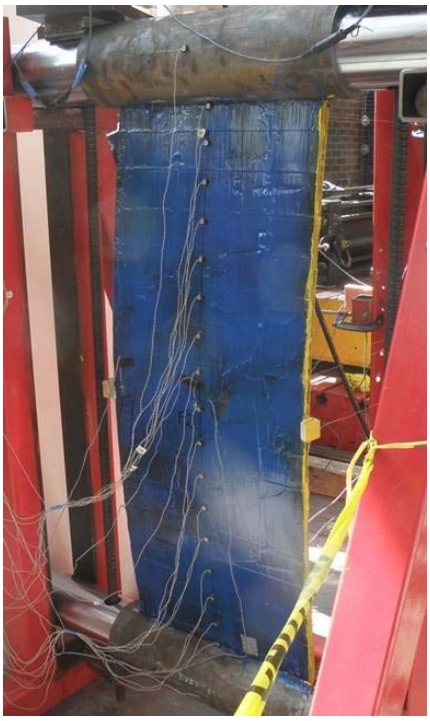

Figure 3-79: Undamaged CFRP sheet at instability of the plateIA-48-5/16-S (h/t=154)

3.2.6 Test Results and Discussion of Phase I-B

Phase I-B tested two slenderness ratio of 77 and 154 to examine the effectiveness of three types of CFRP materials, LM, IM, and HM as well as the effectiveness of reinforcement ratio. Based on the experience gained from phase I-A, to avoid effect of imperfection on test results control specimens were considered to be strengthened with one layer of CFRP strands and two layers of CFRP strands. This was able to be performed due to the fact that both of the selected slenderness ratios would fail by elastic buckling, rather than inelastic buckling. This behavior was observed and confirmed in phase I-A. Therefore, yielding of the plate at the buckling load was not of concern for the selected slenderness ratios.

To avoid yielding of the control plates and strengthened plates due to the sudden large lateral deformation, the applied loads were stopped before onset of plateau. The plateau shows no more increase in load carrying capacity coinciding with an increase in longitudinal strains and lateral deformations.

3.2.6.1 ***Imperfections***

Using recorded data from the Optotrak system, out-of-straightness imperfections were captured and values are given in Table 3-14 for the specimens tested in Phase I-B. Similar to the results of Phase I-A, Regardless to the height and thickness of the plates, values of imperfections are within a limited range. Measured initial imperfections with respect to its ends are also shown in Figure 3-80 and Figure 3-81 having height of 610 mm (24 in.) and 1220 mm (48 in.), respectively.

Table 3-14: Measured imperfection values obtained from Phase I-B

Specimen ID	Strengthening Layer	Measured Imperfection Value, δ	
		(in.)	(mm)
IB-24-5/16-LM-U	0	0.04	0.9
IB-24-5/16-IM-U		0.04	1.1
IB-24-5/16-HM-U		0.05	1.2
IB-48-5/16-LM-U		0.10	2.5
IB-48-5/16-IM-U		0.07	1.8
IB-48-5/16-HM-U		0.09	2.4
IB-24-5/16-1LM	1	0.04	0.9
IB-24-5/16-1IM		0.03	0.8
IB-24-5/16-1HM		0.12	2.9
IB-48-5/16-1LM		0.08	2.1
IB-48-5/16-1IM		0.10	2.5
IB-48-5/16-1HM		0.07	1.8
IB-24-5/16-2LM	2	0.07	1.7
IB-24-5/16-2IM		0.10	2.4
IB-24-5/16-2HM		0.08	2.0
IB-48-5/16-2LM		0.07	1.9
IB-48-5/16-2IM		0.14	3.7
IB-48-5/16-2HM		0.09	2.3
AVG		**0.08**	**1.9**

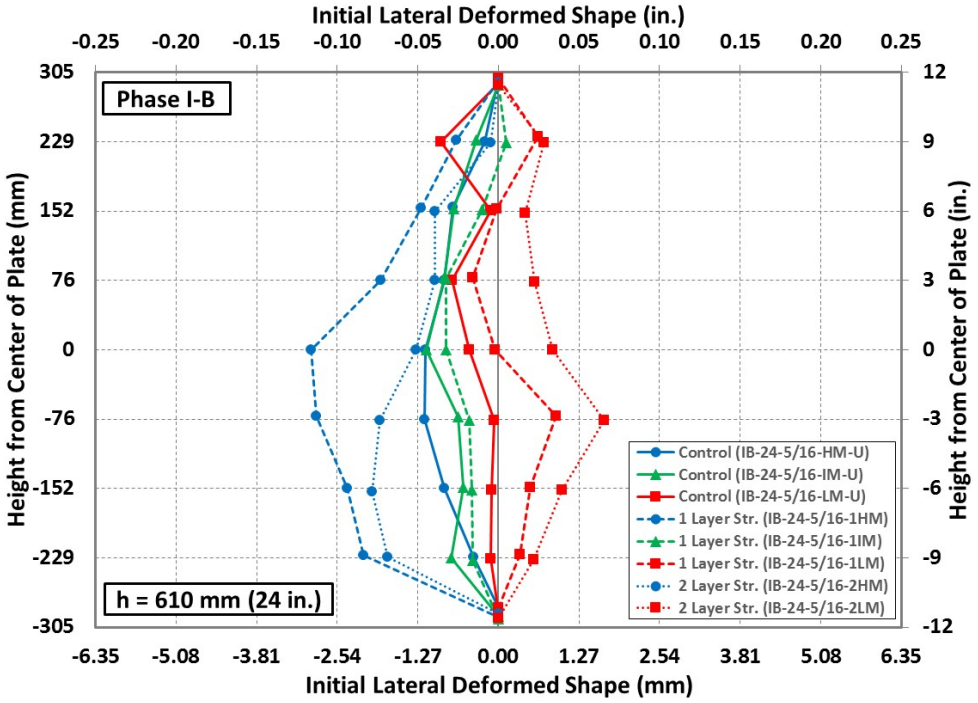

Figure 3-80: Measured initial imperfection of the specimens at Phase I-B (h = 610mm (24in.))

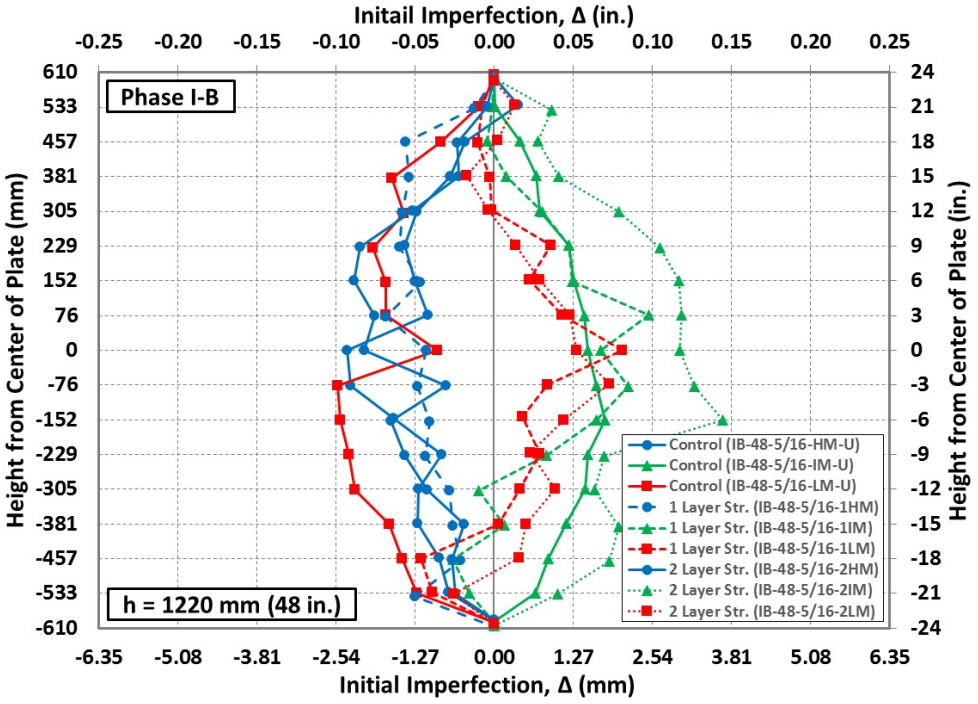

Figure 3-81: Measured initial imperfection of the specimens at Phase I-B (h = 1220mm (48in.))

3.2.6.2 ***Buckling Load***

Test results of the specimens tested in phase I-B are given in Table 3-15. Results show that different types of CFRP materials increased the buckling capacity of the steel plates. The maximum increase in buckling load for plates strengthened with one layer of CFRP was up to 117% and for plates strengthened with two layers of CFRP was up to 358%.

Table 3-15: Test results summary of specimens in Phase I-B

Plate Designation	h/t	Buckling Load		
		kN	kip	Increase (%)
IB-24-5/16-LM-U	77	228	51	-
IB-24-5/16-1LM		282	63	24
IB-24-5/16-2LM		362	81	59
IB-24-5/16-IM-U		233	52	-
IB-24-5/16-1IM		314	71	35
IB-24-5/16-2IM		392	88	68
IB-24-5/16-HM-U		240	54	-
IB-24-5/16-1HM		343	77	43
IB-24-5/16-2HM		458	103	90
IB-48-5/16-LM-U	154	44	10	-
IB-48-5/16-1LM		75	17	71
IB-48-5/16-2LM		94	21	115
IB-48-5/16-IM-U		52	12	-
IB-48-5/16-1IM		89	20	71
IB-48-5/16-2IM		144	32	178
IB-48-5/16-HM-U		36	8	-
IB-48-5/16-1HM		78	18	117
IB-48-5/16-2HM		165	37	358

3.2.6.3 ***Measured Strain***

The average measured longitudinal strains at steel versus the measured applied load are shown in Figure 3-82 through Figure 3-84 for specimens with a slenderness ratio of 77. These figures contain results obtained from control plates, plates strengthened with one layer of CFRP, and two layers of CFRP. For specimens with a slenderness ratio of 154, the average measured longitudinal strains at steel versus the applied load are shown in Figure 3-85 through Figure 3-87. Due to loss of strain gauges attached to the steel surface of the strengthened plates with two layers of CFRP, only results measured from control specimens and specimens strengthened with one layer of CFRP are presented. Due to loss of strain gauges attached to the plates with slenderness ratio of 154 and strengthened with two layers of CFRP strands, the measured strain of the CFRP is used.

In general, for each of the specimens, as the applied load increases, the longitudinal strain values gradually increase until the buckling load is reached. After the buckling load is reached, there is a reduction in load carrying capacity, coinciding with a rapid increase in longitudinal strain. Furthermore, the longitudinal strain values at the level of the steel at the buckling load were well within the material's linear elastic range. That being said, the buckling loads were determined to be the loss of stability of the specimen, rather than a material limit/failure. The buckling loads are designated by dashed lines, and the buckling load values are given in each plot for each particular specimen. Furthermore, the increase in buckling load from the control case is given as well. It is worth noting that measured compression strains were higher than

the tension strains in all test plates, which is attributed to the combined effect of the axial and bending stresses.

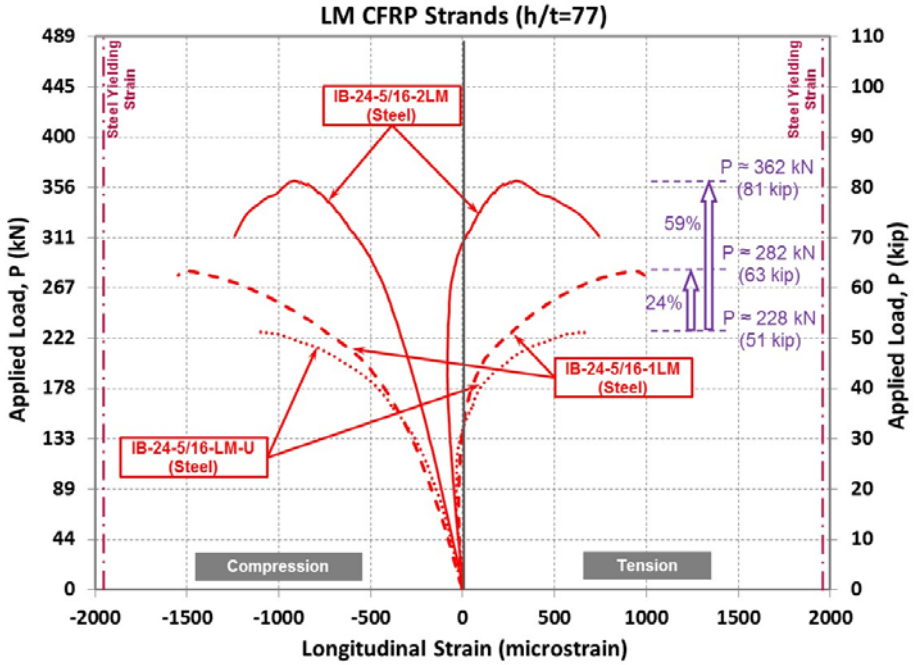

Figure 3-82: Applied load vs. longitudinal steel strain at mid-height of plates with h/t=77 and strengthened by LM CFRP strands

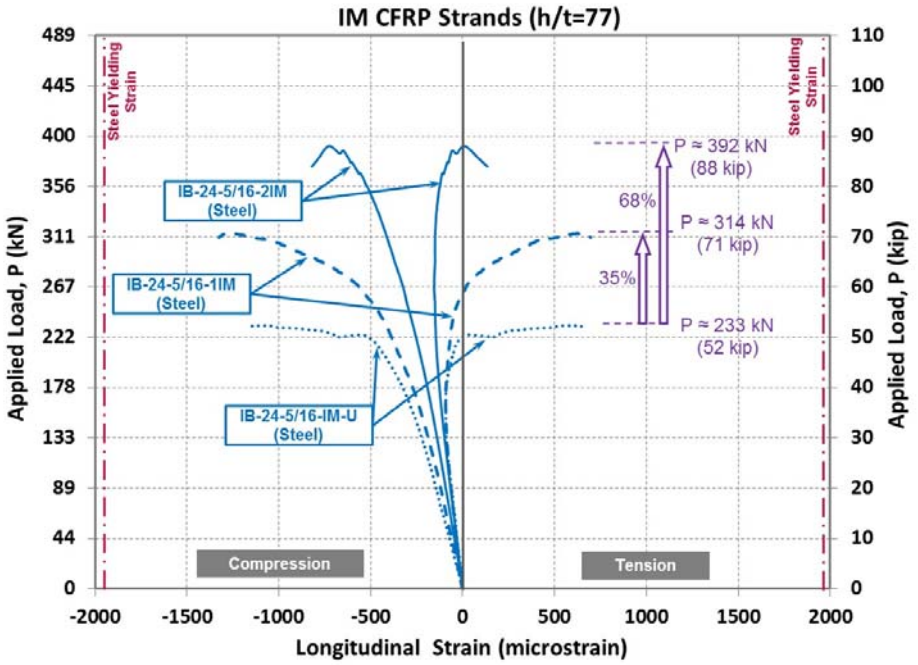

Figure 3-83: Applied load vs. longitudinal steel strain at mid-height of plates with h/t=77 and strengthened by IM CFRP strands

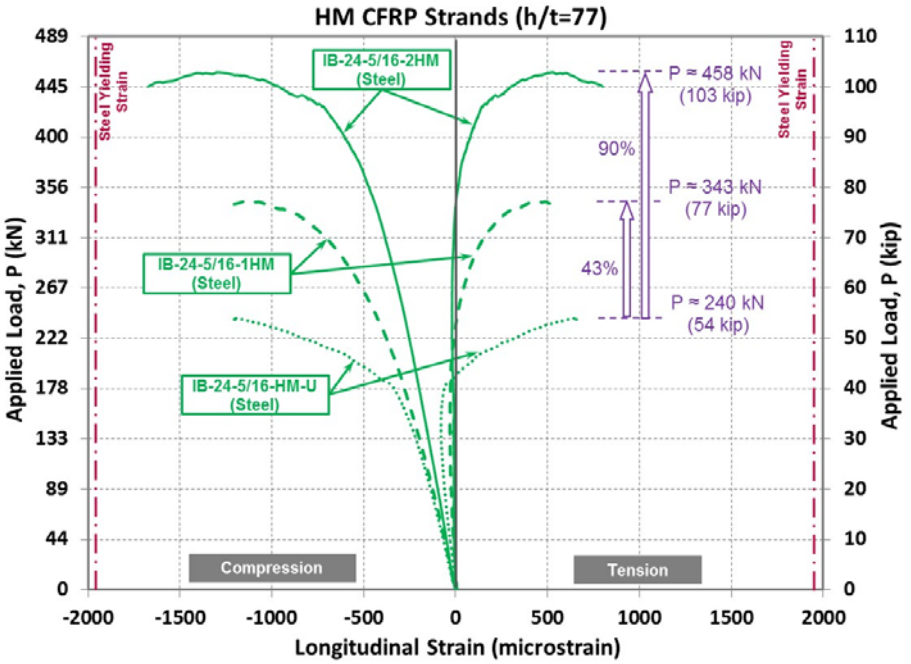

Figure 3-84: Applied load vs. longitudinal steel strain at mid-height of plates with h/t=77 and strengthened by HM CFRP strands

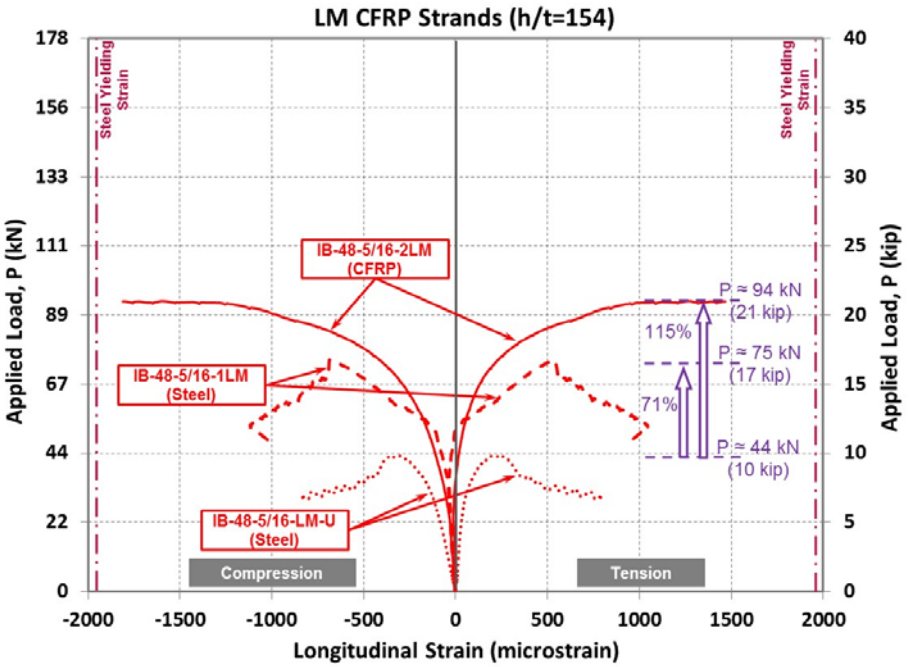

Figure 3-85: Applied load vs. longitudinal steel strain at mid-height of plates with h/t=154 and strengthened by LM CFRP strands

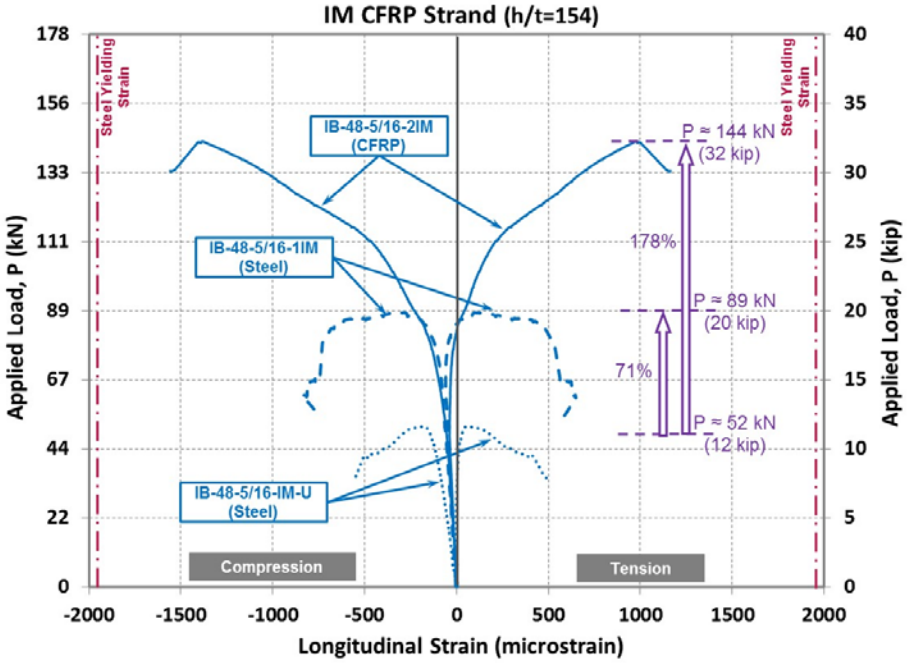

Figure 3-86: Applied load vs. longitudinal steel strain at mid-height of plates with h/t=154 and strengthened by IM CFRP strands

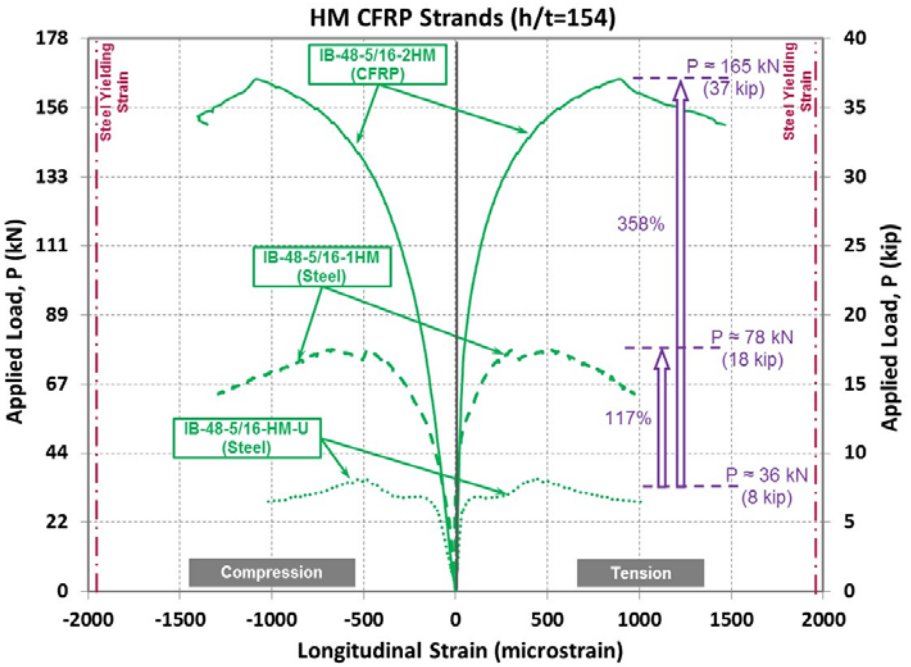

Figure 3-87: Applied load vs. longitudinal steel strain at mid-height of plates with h/t=154 and strengthened by HM CFRP strands

3.2.6.4 ***Load-Deformation Behavior***

The measured net lateral deformation versus the measured applied axial load is graphically presented in Figure 3-88 through Figure 3-93 for test plates with slenderness ratio of 77 and 154. The net lateral deformation was obtained by subtracting the average value of the measured top and bottom deformations from the measured mid-height deformation.

The load-deformation behavior of the plates reveals that external bonding of CFRP strands to the steel plates increased their buckling load carrying capacity. The plots display the increase of buckling load and generally increase of stiffness for each additional layer of CFRP strengthening. However, due to application of inconsistent strengthening layers at both faces of few plates, there is very small sign of increase in initial stiffness from control plate to the plate strengthened with one layer of CFRP. Moreover, in overall, ductility of the strengthened system drops by increasing layers of the CFRP strands. This observation is mainly due to an increase in total stiffness of the system tends to have lower deformation until reaching the buckling load. The solid arrows at the end of data sets indicate that if load were to continue to be applied, the lateral deformation would continue to increase; thus, the system has lost lateral stability.

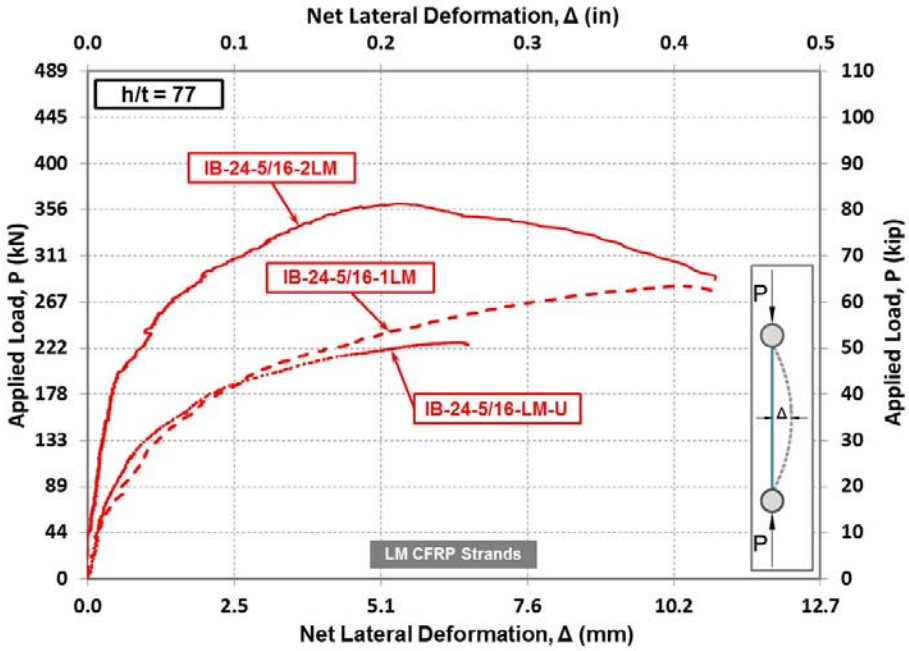

Figure 3-88: Applied load vs. net lateral deformation at mid-height of plates with h/t=77 and strengthened by LM CFRP strands

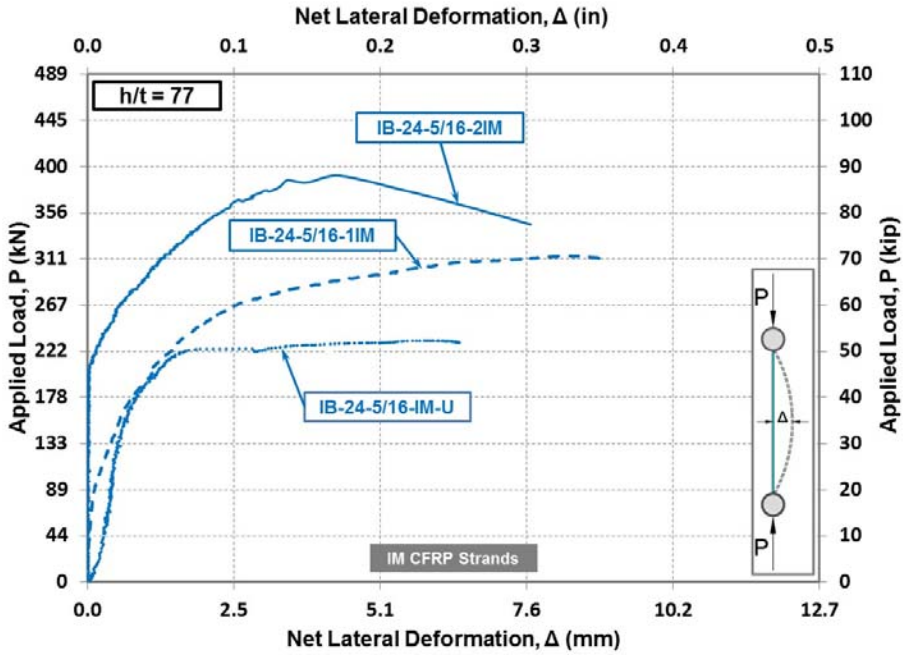

Figure 3-89: Applied load vs. net lateral deformation at mid-height of plates with h/t=77 and strengthened by IM CFRP strands

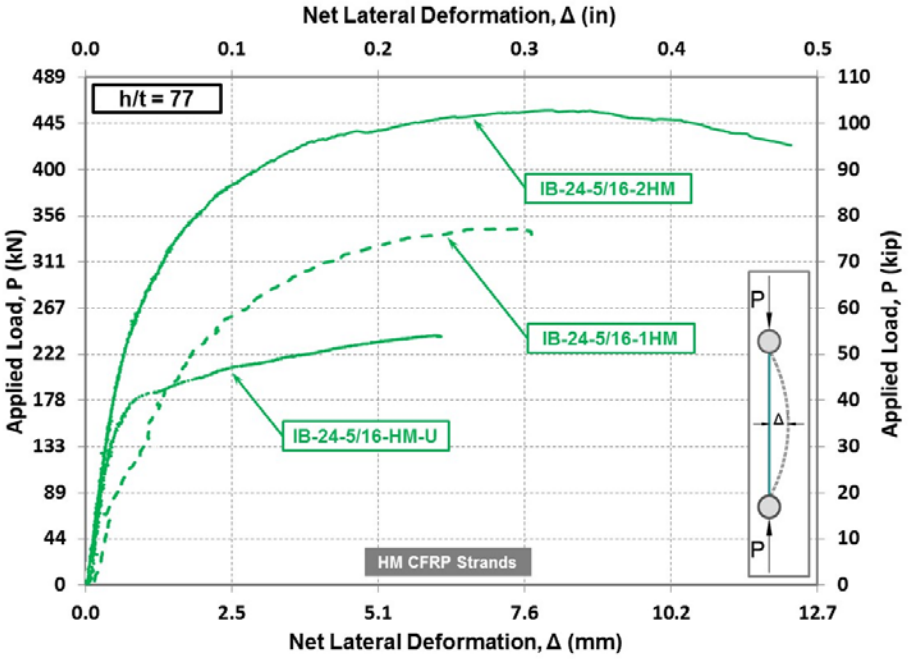

Figure 3-90: Applied load vs. net lateral deformation at mid-height of plates with h/t=77 and strengthened by HM CFRP strands

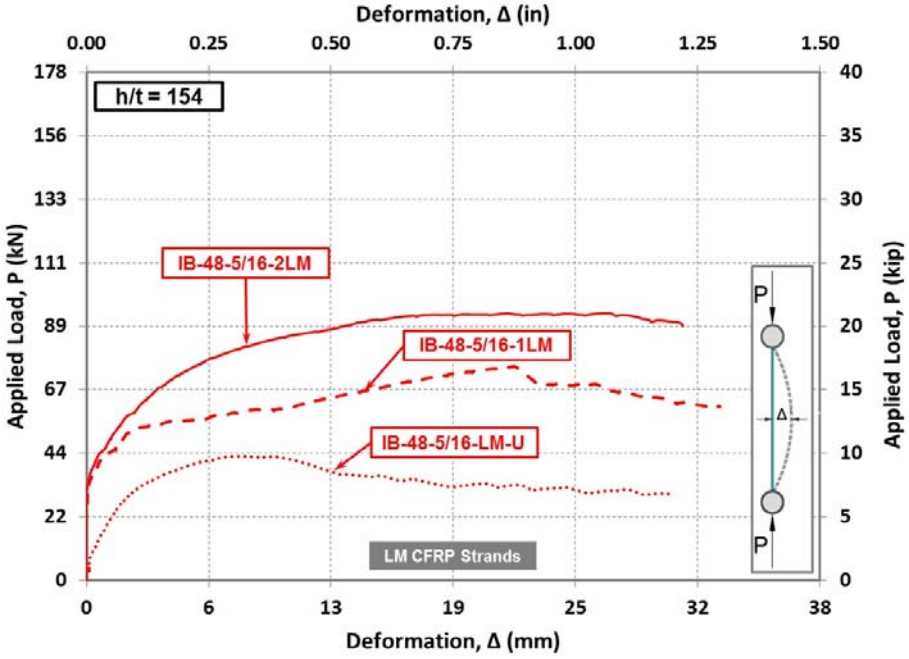

Figure 3-91: Applied load vs. net lateral deformation at mid-height of plates with h/t=154 and strengthened by LM CFRP strands

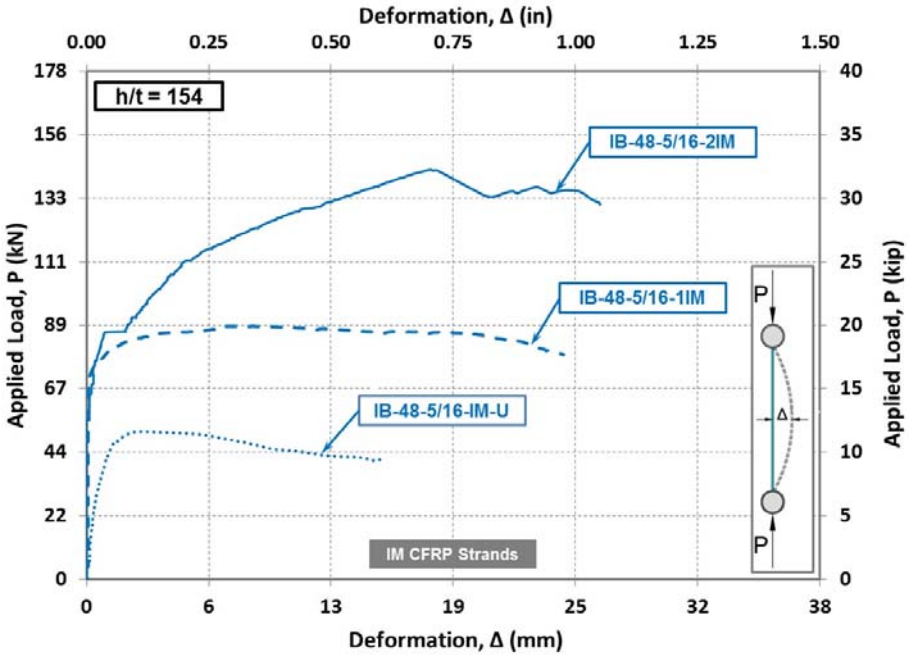

Figure 3-92: Applied load vs. net lateral deformation at mid-height of plates with h/t=154 and strengthened by IM CFRP strands

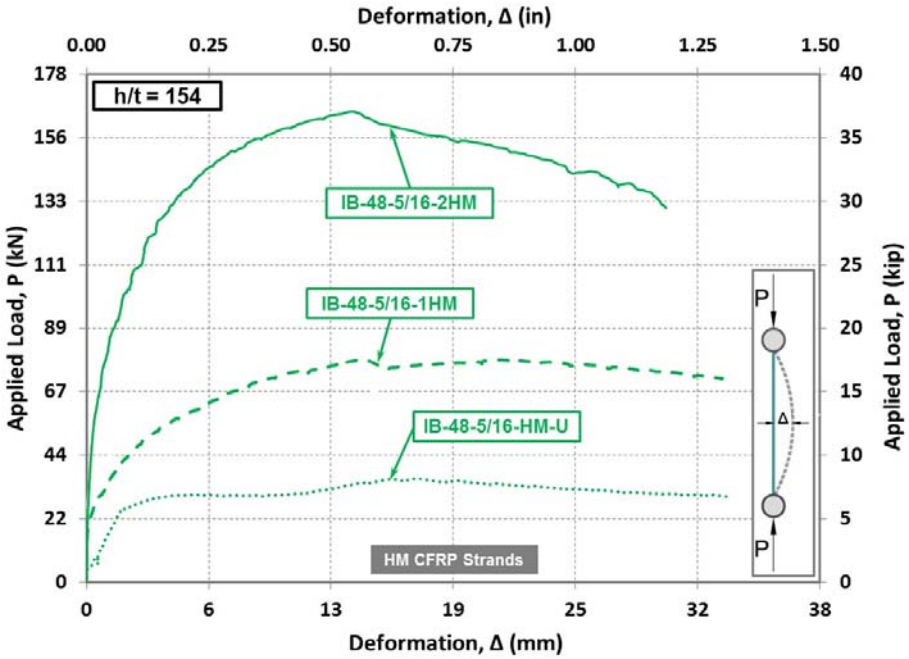

Figure 3-93: Applied load vs. net lateral deformation at mid-height of plates with h/t=154 and strengthened by HM CFRP strands

3.2.6.5 ***General Observations***

The increase in the buckling load with an increase of elastic modulus of the CFRP strengthening system as well as increase in reinforcement ratio is shown in Figure 3-94 for slenderness ratios 77 and 154. The trend indicates that increasing the elastic modulus of the CFRP strands attributes to higher buckling capacity since the ultimate capacity is not governed by the rupture strength of the CFRP strands. Furthermore, the effect of the CFRP strengthening system is more announced with an increase in slenderness ratio. This behavior can be attributed to the higher CFRP to steel plate stiffness ratio for the higher slenderness plates compared to the lower ones.

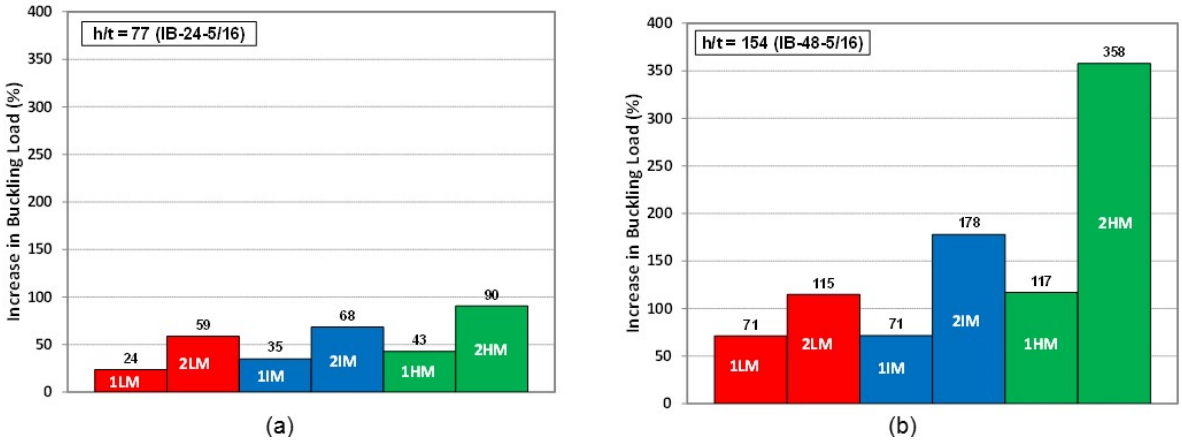

Figure 3-94: Buckling load percentage increase of plates strengthened with one and two layers of HM, IM, and LM CFRP strands, a) h/t = 77, b) h/t = 154

3.2.6.6 ***Failure of the Strengthening System***

As realized in phase I-A, it is also confirmed in phase I-B that the plate lateral deformation at the final load is much larger compared to that of the buckling load stage. Furthermore, there

was no indication of CFRP failure due to de-bonding or rupture prior to the buckling load stage.

3.3 SHEAR STRENGTHENING (PHASE II)

The research in the second phase examined the effectiveness of the proposed small-diameter CFRP strands for shear strengthening of steel web girders. The parameters which were considered are the fiber orientations and number of layers of the CFRP strands [55, 56].

3.3.1 Test Setup & Instrumentation

3.3.1.1 *Test Setup*

To simulate pure shear stresses acting on steel plate, the square plate specimen is rotated 45 degree and clamped to a heavy steel frame which is subjected to tensile load on diagonally opposite corners as schematically shown in Figure 3-95(a). Through this geometry, the applied tensile load to the steel frame induces equivalent shear forces along the edges of the steel test plate as shown in Figure 3-95(b) through the uniformly distributed pre-stressed bolts. The shear forces along the edges of the specimen induced compressive stresses perpendicular to the direction of the applied tensile load and tensile stresses parallel to direction of the applied tensile load.

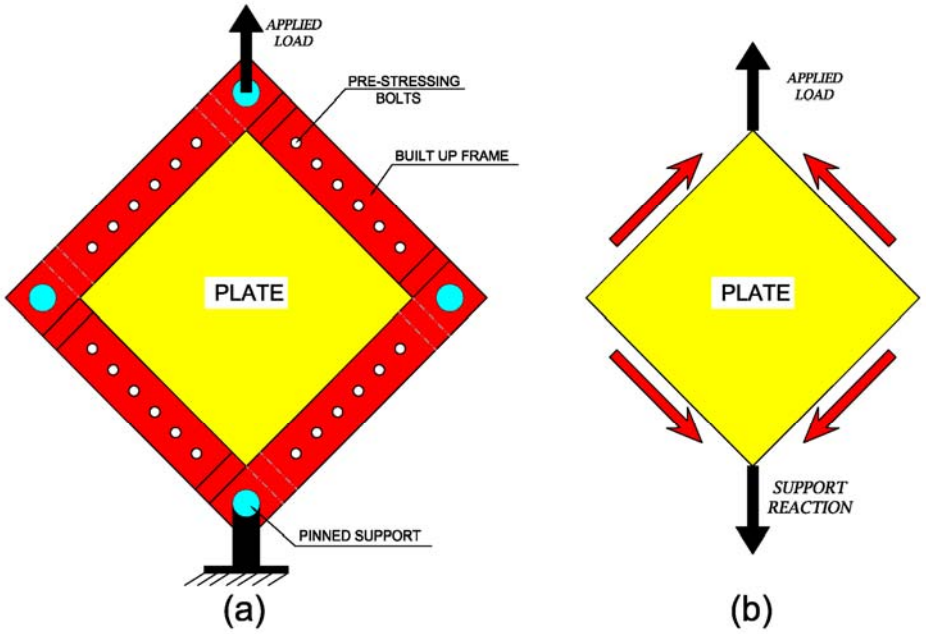

Figure 3-95: State of forces acting on the test plate

The steel plate specimen is pre-stressed to the articulated built-up steel frames through series of 40 mm (1-1/2 in.) diameter high-strength (HS) bolts as shown in Figure 3-96. Twenty four HS bolts were torqued using 1500 kN.mm (1100 lb.ft) impact wrench. Induced stresses are transferred to the test plate through friction-type connection provided by the bolts. An exposed test plate has a dimensions of 910x910x5 mm (36x36x3/16 in.) resulting in slenderness ratio (h/t) of 192. The steel frames were specially designed to fail the test plate without permanent deformation on the frame. Therefore, the frame is made up by four very stiff steel plate legs, each consist of stiff short and long plates having dimensions of 760x200x25 mm (30x8x1 in.) and 1320x200x25 mm (52x8x1 in.), respectively. Each two legs are connected at the corners using high-strength steel pins with a diameter of 100 mm (4 in.) to allow rotation. To avoid

bearing of the test plate on the pins at the corners, plate holes are machined having diameter of 127 mm (5 in.) which are larger than the pin diameter of diameter as 25 mm (1 in.).

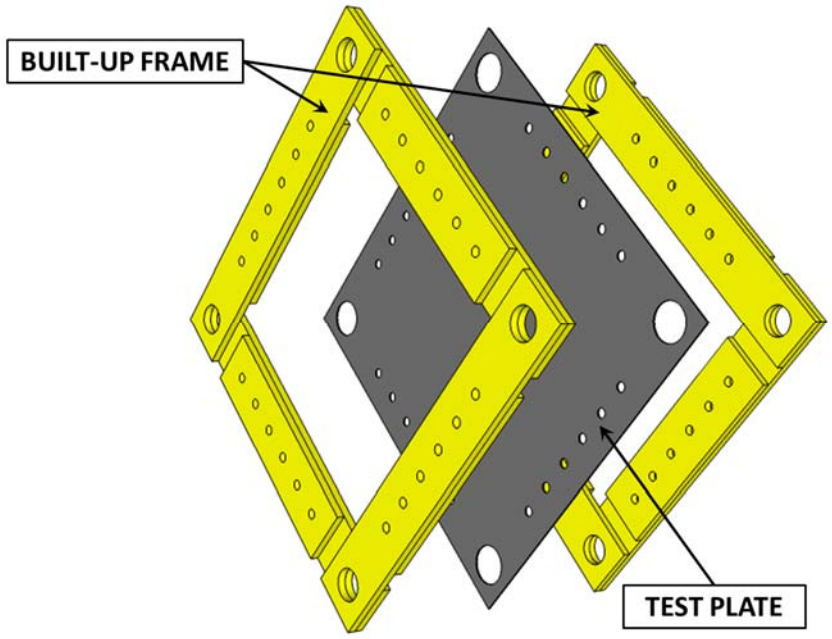

Figure 3-96: Schematic 3D view and positions of the test plate and frames

Two 2000 kN (440 kip) capacity hydraulic actuators were used to apply the tensile load to the steel frame. The two hydraulic actuators were connected to the same controller to ensure equal loads from each actuator. Two highly stiffened spreader beams were especially designed to transfer the tensile load to the shear frame. The bottom spreader beam is pre-stressed to the strong floor using high strength bars, pedestals and bearing plates to provide reaction equal to the applied load. Schematic sketch and view of the test setup are shown in Figure 3-97 and Figure 3-98, respectively.

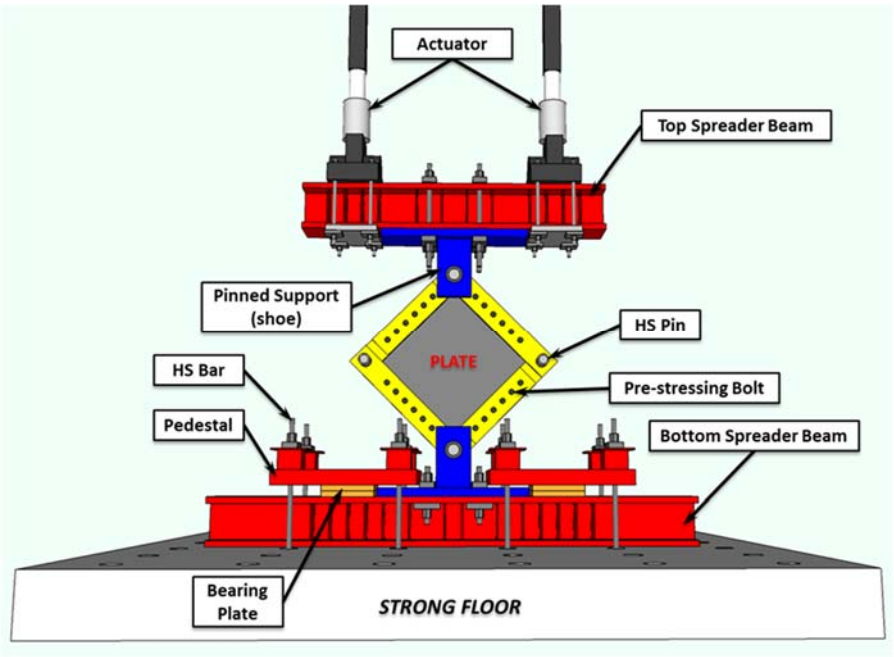

Figure 3-97: Schematic view of pure shear test setup

Figure 3-98: View of pure shear test setup

3.3.1.2 ***Instrumentation***

The instrumentations used to measure behavior of the specimens are shown in Figure 3-99. Vertical and horizontal strains at mid-point were measured using electrical resistance strain gages with a gage length of 5 mm (3/16 in.). Four Strain gages are attached to both faces of the control plate, with two strain gauges on each face. Two vertical strain gauges were attached in direction of diagonal tensile load and two horizontal strain gauges were attached in direction of the compressive component. A total of eight strain gauges were attached to the strengthened specimens at mid-point. Four strain gauges were attached to the base steel and the remaining four strain gauges were attached on the outer surface of the CFRP strand sheets. The overall out-of-plane lateral deformation of the steel plates was measured using five linear string potentiometers. OptotrakCertus® motion capturing system was also used. The motion capturing system measures a three-dimensional (3-D) coordinate system by the use of Infrared Emitting Diodes (IRED) attached to the specimen at points of interest. The IREDs were attached to the front face of the test specimens along with the vertical and horizontal centerlines and were spaced at 75 mm (3 in.). All instrumentations were connected to an electronic data acquisition system.

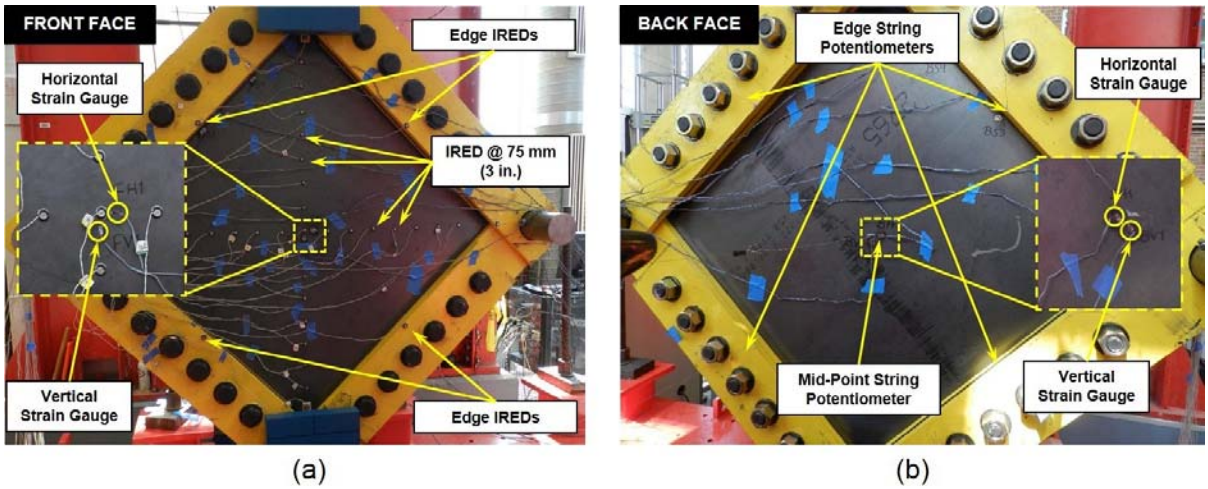

(a) (b)

Figure 3-99: Specimen instrumentations, a) IREDs and strain gauges attached on the front face of test plate, b) string potentiometers and strain gauges attached to the back face

3.3.2 Test Matrix

A total of nine square steel plates included in this phase are given in Table 3-16. The CFRP strands are externally bonded at an angle of 45°, 90°, and ±45° relative to the applied tensile load using one and two layers of the HM CFRP strands on each side of the plate. The following nomenclature was adopted to distinguish the various cases. The first letter of specimen ID represents phase number. The second and third numbers specify the length and thickness of the plate, respectively. The forth number is the set number. The fifth number represents angle of the orientation relative to the applied tensile load. Last letters show the strengthening condition. For the control plates, letter "C" is used. For the strengthened plate, number of layers at each face is followed by type of CFRP material. Figure 3-100shows configuration of each specimen including orientation of HM CFRP strands. A layer of the low-modulus polyurea putty was used between the steel plate and the CFRP strands for all strengthened specimens. The control specimen was used as strengthened specimen with one layer and subsequently two

layers of HM CFRP strands to eliminate the effect of plate initial imperfections. The percentage increase of the shear capacity from each test is used to determine the effectiveness of the proposed strengthening configurations.

Table 3-16: Shear strengthening test matrix

Plate Designation	Set #	Height mm (in.)	Thickness mm (in.)	h/t	Fiber Orientation	No. of Layers
II-36-3/16-1-45-C	1	915 (36)	5 (3/16)	192	NO	NO
II-36-3/16-1-45-1HM					45º	1
II-36-3/16-1-45-2HM					45º	2
II-36-3/16-2-90-C	2				NO	NO
II-36-3/16-2-90-1HM					90º	1
II-36-3/16-2-90-2HM					90º	2
II-36-3/16-3-45W-C	3				NO	NO
II-36-3/16-3-45W-1HM					45º	1
II-36-3/16-3-45W-2HM					±45º	2

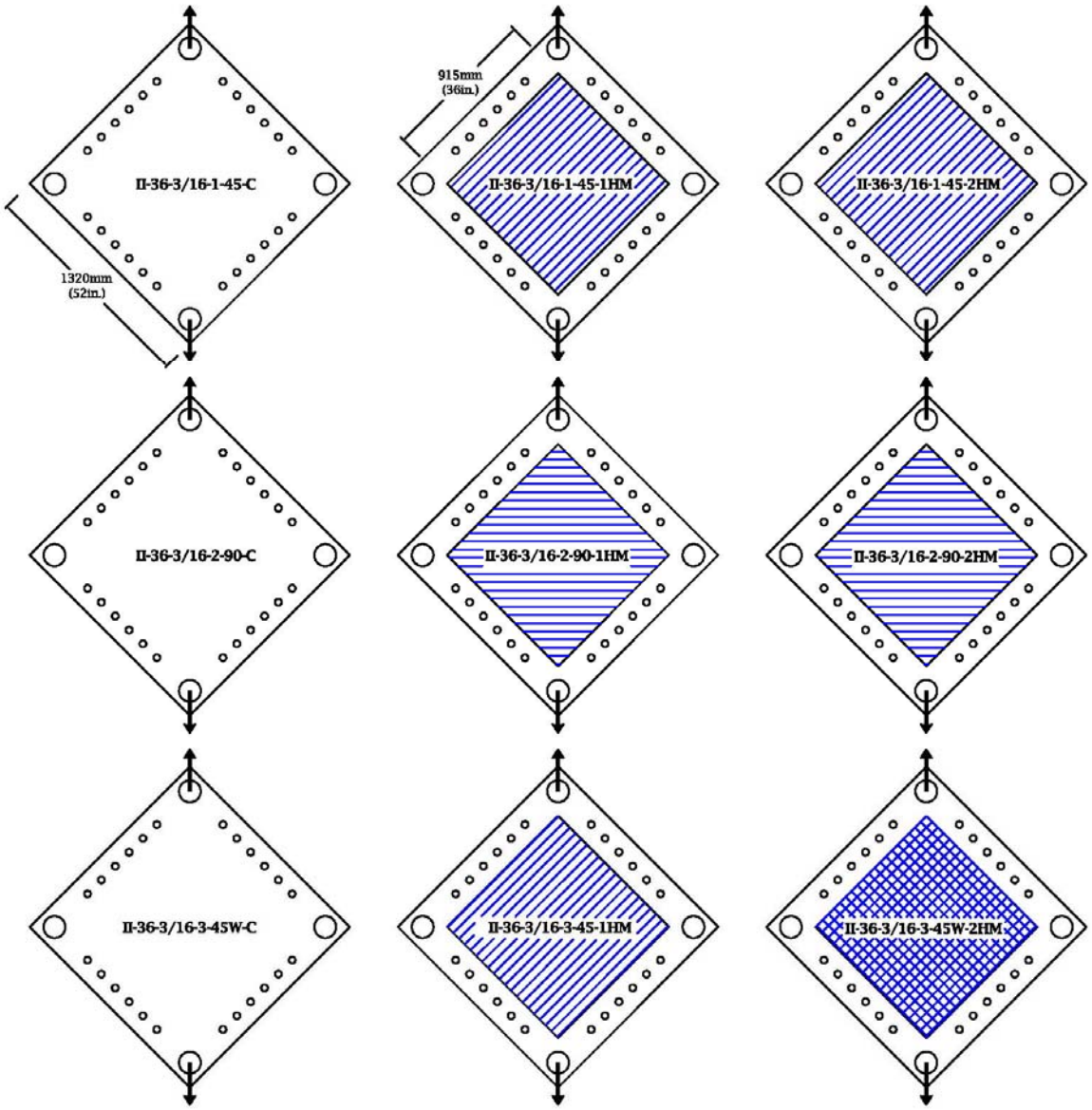

Figure 3-100: Schematic sketch of shear strengthening test matrix

3.3.3 Application of the Strengthening System for Phase II

Application of the CFRP strands provided by Nippon Steel & Sumikin Materials, Co. Ltd. followed the identical procedures as described in Phase I, which is detailed and illustrated as follows.

3.3.3.1 *Surface Preparation and Application of Primer Resin*

The steel plates were sandblasted prior to the commencement of the application process. After the completion of sandblasting, the plates were cleaned using pressurized air to remove any grit or dust on the plates. The strain gages were attached to the steel on the same day of strengthening before the application of the primer resin. The application process was conducted face by face and the steel plate was kept horizontally on two saw horses. The primer resin (FP-UL1) was applied to the steel plates after sandblasting and cleaning. The resin and the hardener were mixed by using weight ratio of 1:1 as recommended. A rich layer of the primer mixture was applied using a hand roller as shown in Figure 3-101.

Figure 3-101: Application of primer resin on Sandblasted steel plate

3.3.3.2 ***Application of Polyurea Putty***

The polyurea putty (FP-UL1) layer, was applied to the steel plates within two hours from the application of the primer resin at both faces. The resin and the hardener were mixed by weight using a ratio of 3:1 as recommended. The two components were mixed for at least 2 minutes using an electrical mixer until a uniform mixture was obtained. A rich layer of the putty mixture was applied using spatulas. Figure 3-102 shows a steel plate after the application of the polyurea putty layer.

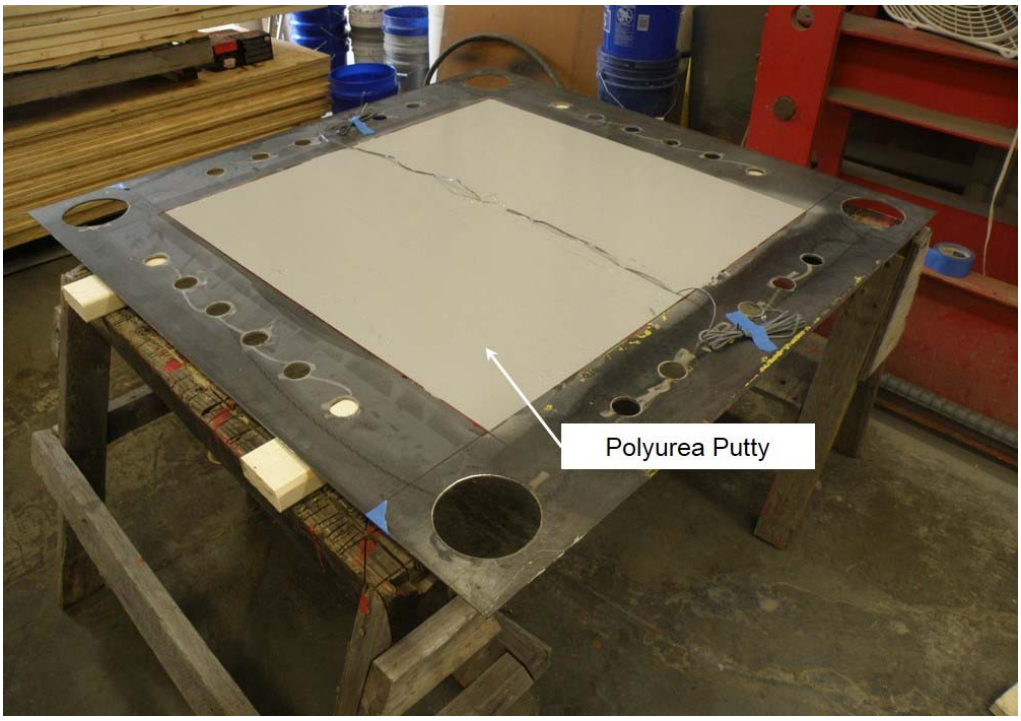

Figure 3-102: Polyurea putty applied to steel plate

3.3.3.3 ***Application of CFRP Strands***

The epoxy (FP-E9S) was applied after at least six hours from the application of the polyurea putty layer on both faces. The resin and the hardener were mixed by weight using a ratio of 4:1 as recommended. The two components were mixed for at least 2 minutes using an electrical mixer until a uniform mixture was obtained. A thick layer of the epoxy was applied using spatulas. The application of epoxy was carried out while the steel plate was laid horizontally. After applying the epoxy layer, the cut CFRP sheets were attached the steel plate matching the proper orientation in each case. The strain gauge wires were passed through the CFRP strands. Spatulas were used to press on the CFRP sheets until the excessive epoxy was squeezed out between the strands to ensure the elimination of any air pocket. A second layer of epoxy was

applied on the top of the CFRP sheets. The strengthened plates as shown in Figure 3-103 were left for at least seven days to cure before they were tested.

It is worth noting that the CFRP strand sheets were carefully cut to the required lengths and orientation using scissors. To have CFRP strands externally bonded at an angle of 45^{o} relative to applied tensile load, they were cut perpendicularly relative to the strands longitudinal direction. However, to have CFRP strands externally bonded at an angle of 90^{o} relative to applied tensile load, they were cut in 45^{o} relative to the strands longitudinal direction as shown in Figure 3-104. Therefore, cutting the CFRP strands manufactured in rectangular sheets of 3050x510 mm (120x20 in.) in 45^{o} relative to the strands longitudinal direction leaves a lot of wastes out of CFRP strands.

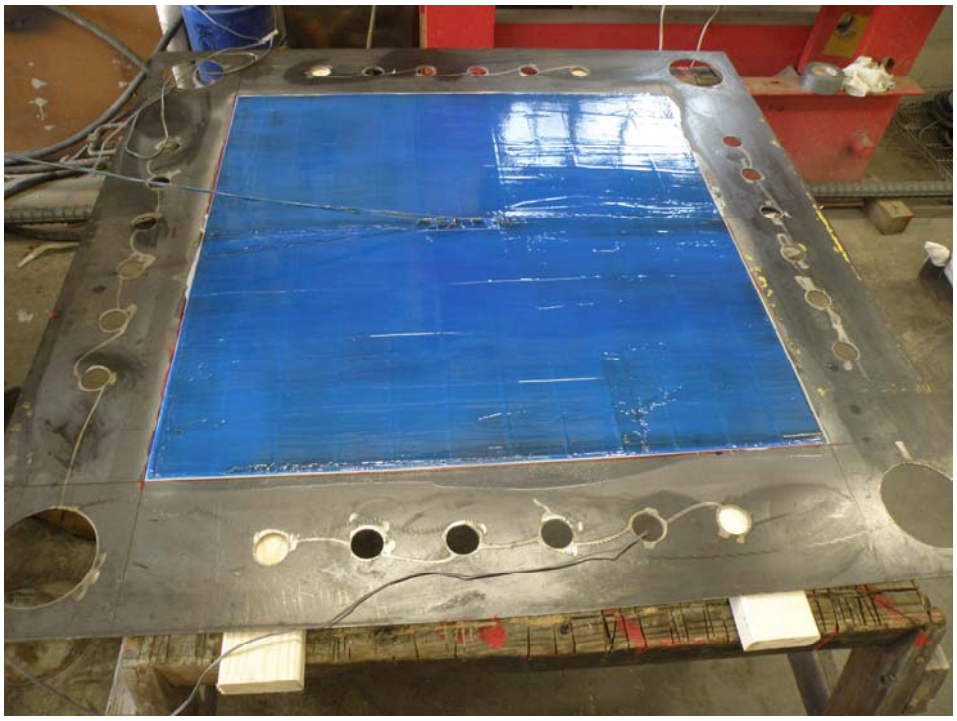

Figure 3-103: CFRP strands applied to steel plate

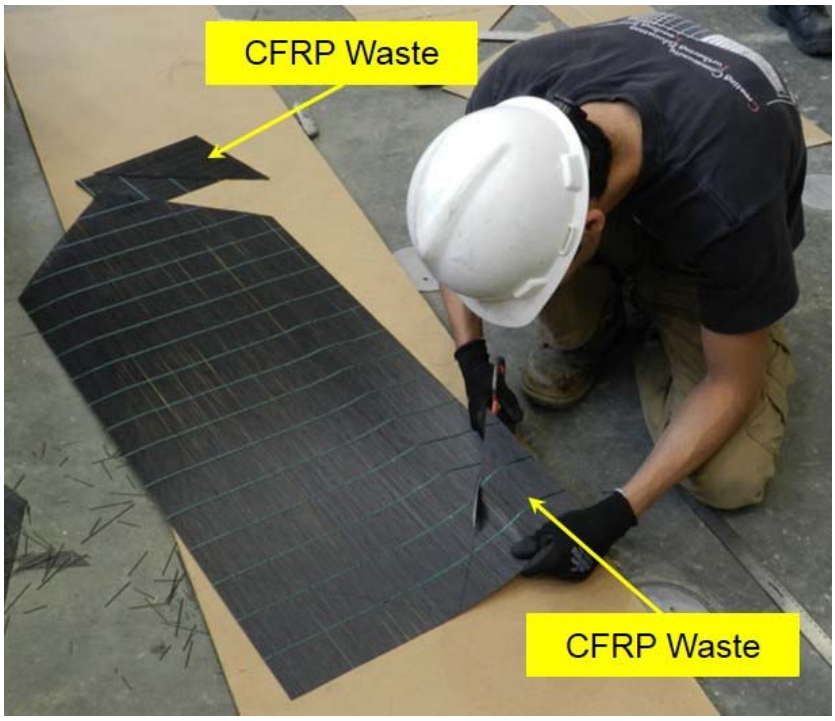

Figure 3-104: Waste of CFRP strands due to cut in 45^{o} relative to the strands longitudinal direction

3.3.3.4 ***Application of Multiple Layers of CFRP Strands***

Similar to Phase I-B, in order to apply the second layer of CFRP strands, the pre-existing layer CFRP strengthening was sanded down using a 125 grit sanding sponge as demonstrated in Figure 3-105 below. Once the surface had been sanded, compressed air was used to remove residue present from the sanding process. Then the surface was wiped cleaned with acetone to ensure it was free of unwanted residue. Upon reaching a desired surface, the second layer of CFRP strands was applied identical to the process just described.

Figure 3-105: Sanding the surface prior to preparation of second layer

3.3.4 Test Results and Discussion of Phase II

3.3.4.1 *Shear Buckling*

Figure 3-106 shows a flat plate simulating typical web of steel plate girder of large span bridge considering shear stresses distributed uniformly along the four edges. The stresses induce equivalent principal stresses in tension and compression as shown in Figure 3-106. Orientation of the tension and one compression are at 45 degree with respect to the shear stresses. These type of loading conditions induces buckling in the form of waves or wrinkles inclined at about 45 degree as shown in Figure 3-106 [57].

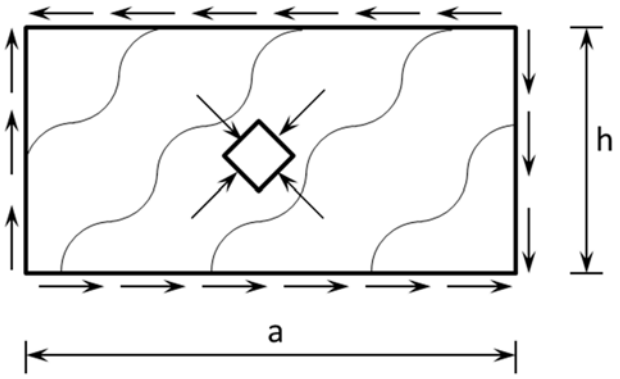

Figure 3-106: State of principle and shear stresses on the plate subjected to pure shear [57]

When a plate is initially imperfect and is not absolutely flat, it deflects before reaching the theoretical buckling load (P_b). Due to the plate imperfection the behavior shows a gradual increase of load with increasing in-plane or lateral deflections. The transition point between pre-buckling and post-buckling behavior vanishes as shown in Figure 3-107. Moreover, at loads far beyond buckling load (P_b) the curve may approach the curve for flat plate as shown in Figure 3-107 [58].

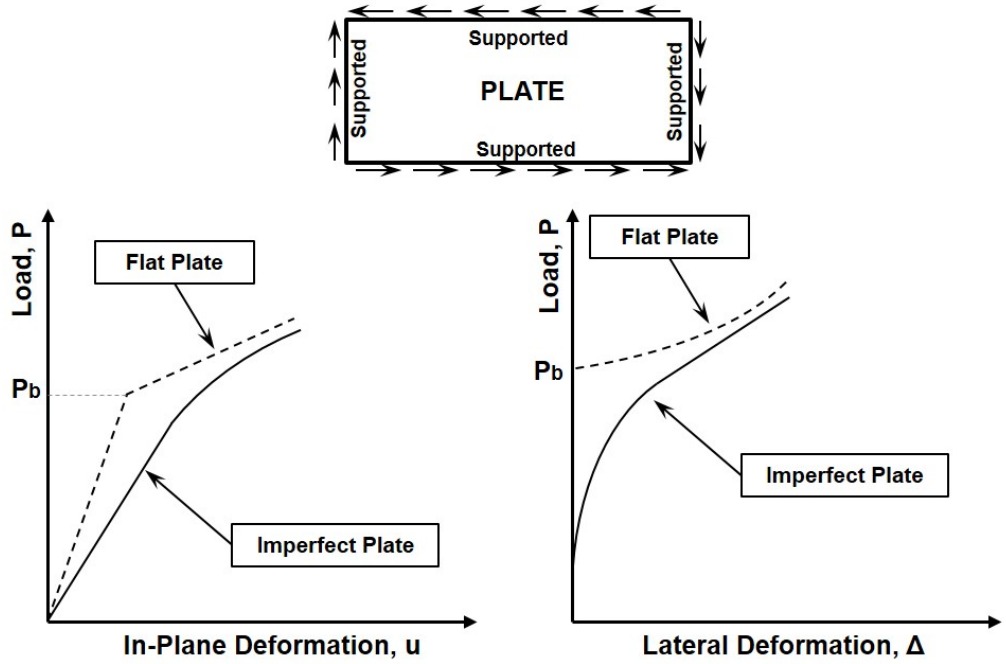

Figure 3-107: Typical behavior of steel plate under pure shear with and without imperfection [58]

3.3.4.2 ***Imperfections***

Using the recorded data from the Optotrak system, values of maximum imperfections are given in Table 3-17. Measured initial imperfections are also shown in Figure 3-108 and Figure 3-109 in the horizontal and vertical directions of the specimens tested in Phase II, respectively. Results indicate that values of imperfection are not identical for every specimen. However, the deformed shape follows somehow a curved shape by having maximum deformation nearby mid-point and flat tangents at the edges. Therefore, for the purpose of FE analysis, a simplified shape used by applying small horizontal pressure on the surface of test plate. This kind of imposed imperfection established curved shape with its apex at mid-height and flat tangent near the edges representing shape of the first buckling mode. The applied pressure induces a level of stress and strain that are account in the existing residual stresses.

Table 3-17: Measured imperfection values obtained from experiments

Specimen ID	Strengthening Layer	Measured Imperfection Value, δ	
		(in.)	(mm)
II-36-3/16-1-45-C	0	0.04	1.0
II-36-3/16-2-90-C		0.03	0.8
II-36-3/16-3-45W-C		0.03	0.8
II-36-3/16-1-45-1HM	1	0.04	1.0
II-36-3/16-2-90-1HM		0.17	4.4
II-36-3/16-3-45W-1HM		0.12	2.9
II-36-3/16-1-45-2HM	2	0.09	2.2
II-36-3/16-2-90-2HM		0.12	3.0
II-36-3/16-3-45W-2HM		0.24	6.1
AVG		**0.10**	**2.5**

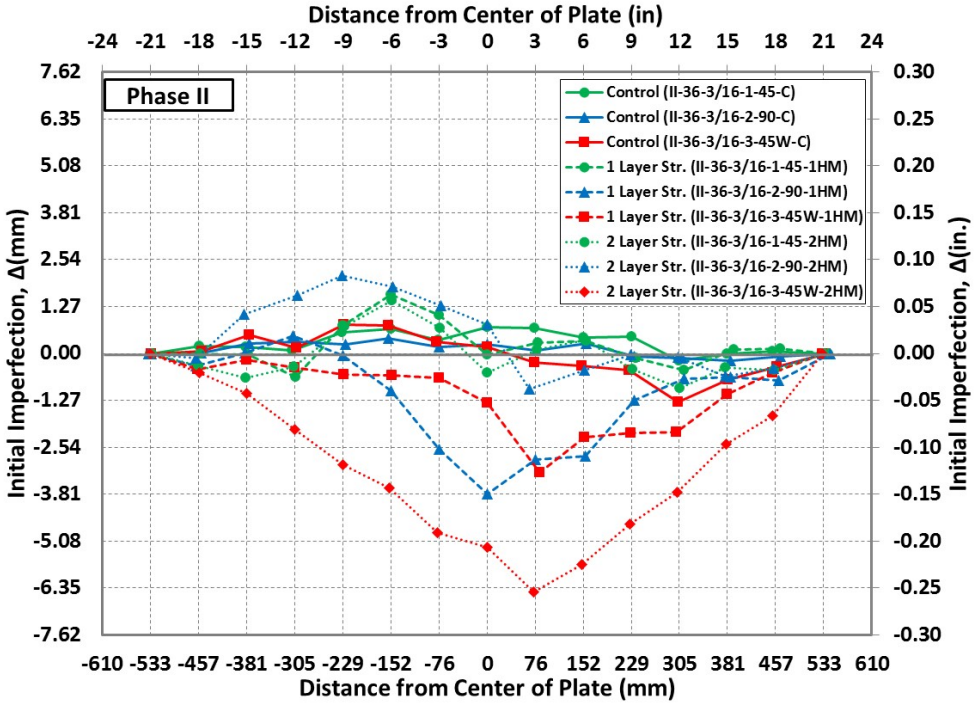

Figure 3-108: Measured initial imperfection of the specimens at horizontal direction (Phase II)

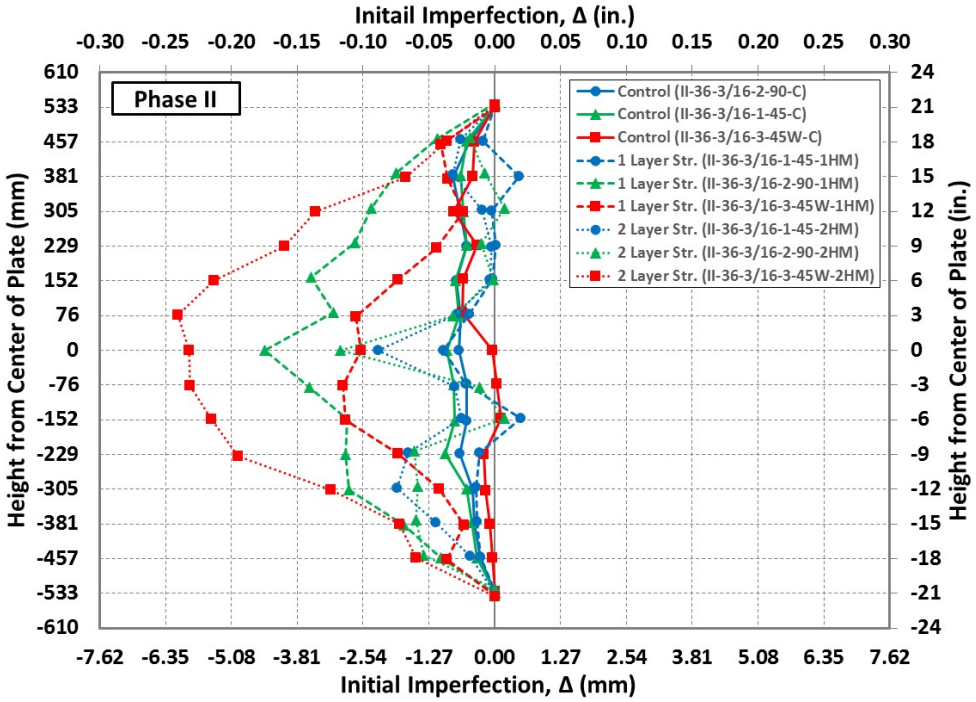

Figure 3-109: Measured initial imperfection of the specimens at vertical direction (Phase II)

3.3.4.3 ***Measured Principle Strain***

The total applied load versus measured horizontal and vertical strains at mid-point of the specimens are shown in Figure 3-110, Figure 3-111 and Figure 3-112, for the plates strengthened with CFRP strands with an angle of 45^{o}, 90^{o} and ±45^{o}, respectively. Each figure contains results of the control plate, plate strengthened with one layer and plate strengthened with two layers of HM CFRP strands. Due to loss of vertical strain gauge attached to the back face of strengthened plates with CFRP strands oriented with an angle of ±45^{o}, only measured results from front face of these specimens are presented.

Results confirm the effectiveness of the externally bonded CFRP small-diameter strands in increasing the shear capacity of the steel plate. As discussed above, since buckling was not observed, the shear capacity of the strengthened plates are compared to the control plates prior to the steel yielding. The strengthening system contributed to the load carrying capacity by highly reducing the horizontal strains at each load level which is resulted to an increase in shear capacity. However, the measured vertical strain reveals slight effect of the CFRP strands in tensile direction. Regarding to the reinforcement ratio, it is clear that increasing the number of layers of CFRP strands increases the shear capacity of the strengthened plate.

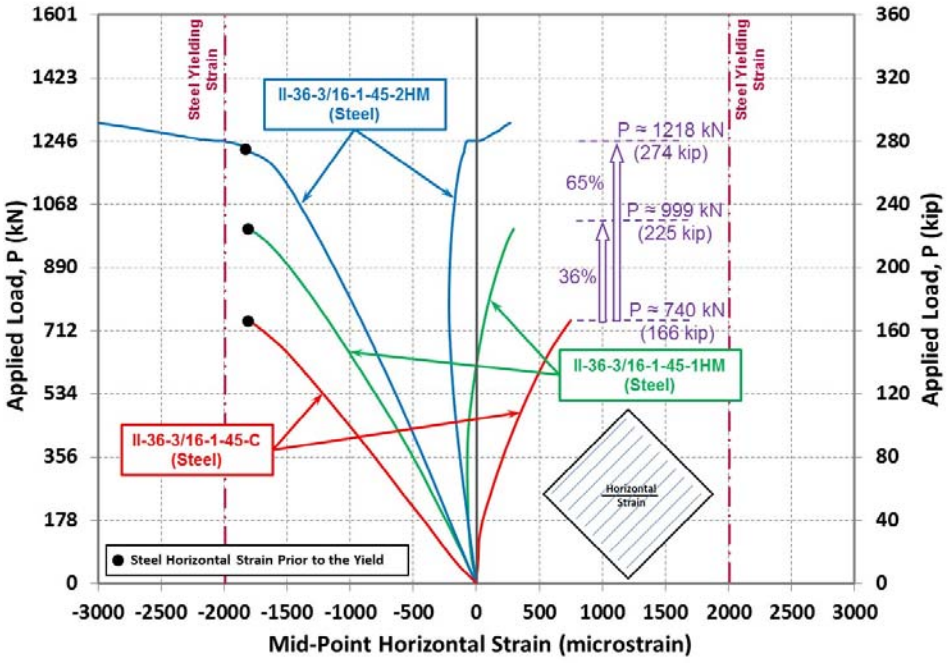

(a)

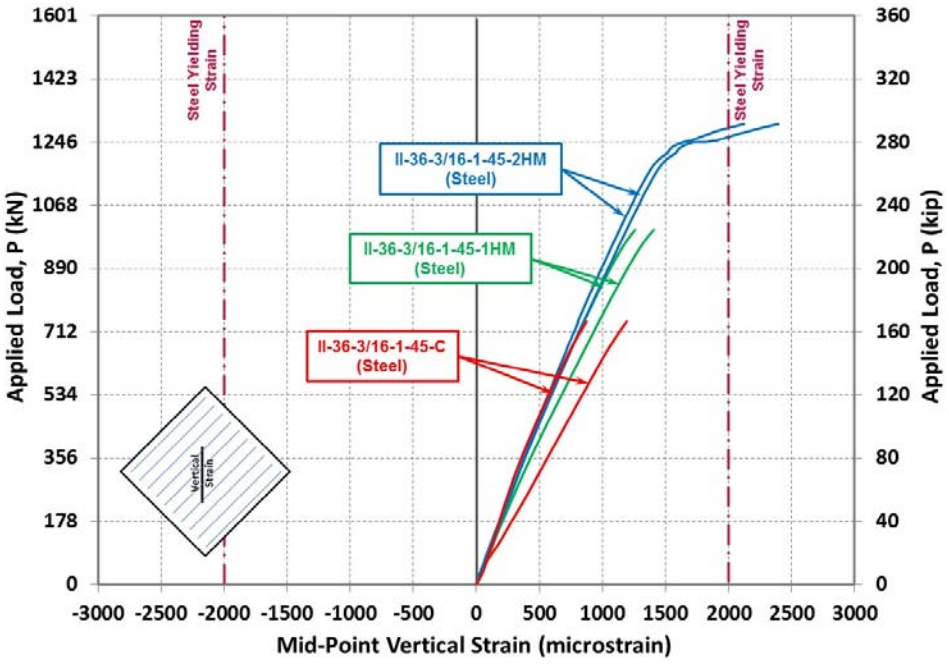

(b)

Figure 3-110: Applied load vs. principle steel strain of the plates (II-36-3/16-1-45) under pure shear, a) horizontal strain, b) vertical strain

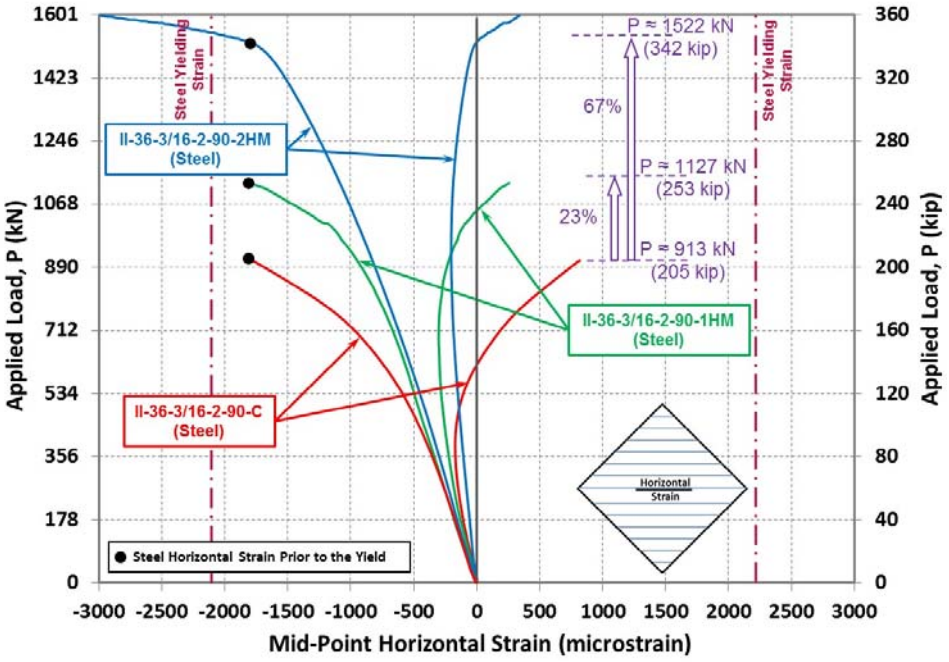

(a)

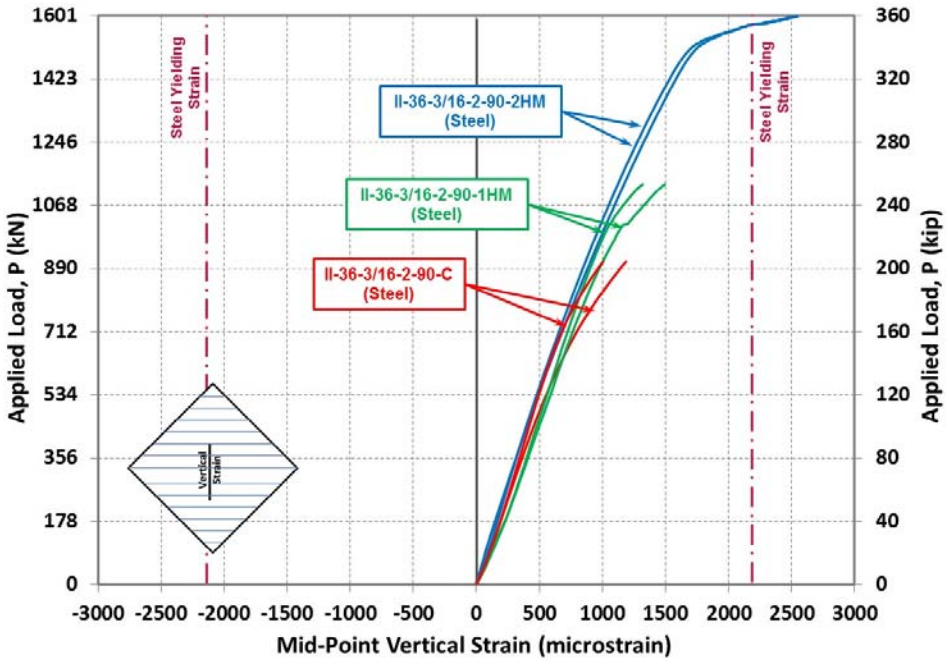

(b)

Figure 3-111: Applied load vs. principle steel strain of the plates (II-36-3/16-2-90) under pure shear, a) horizontal strain, b) vertical strain

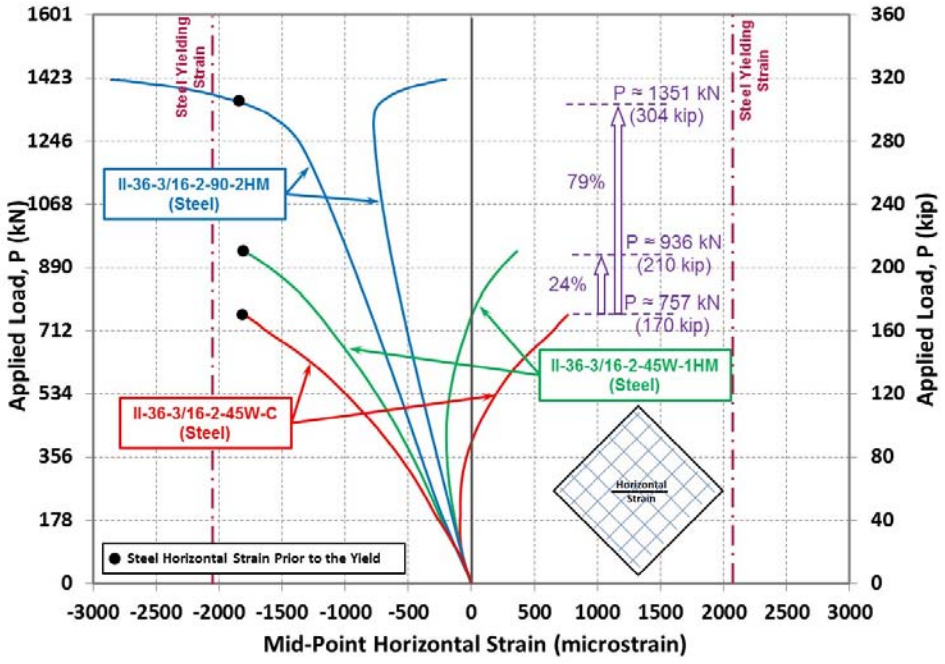

(a)

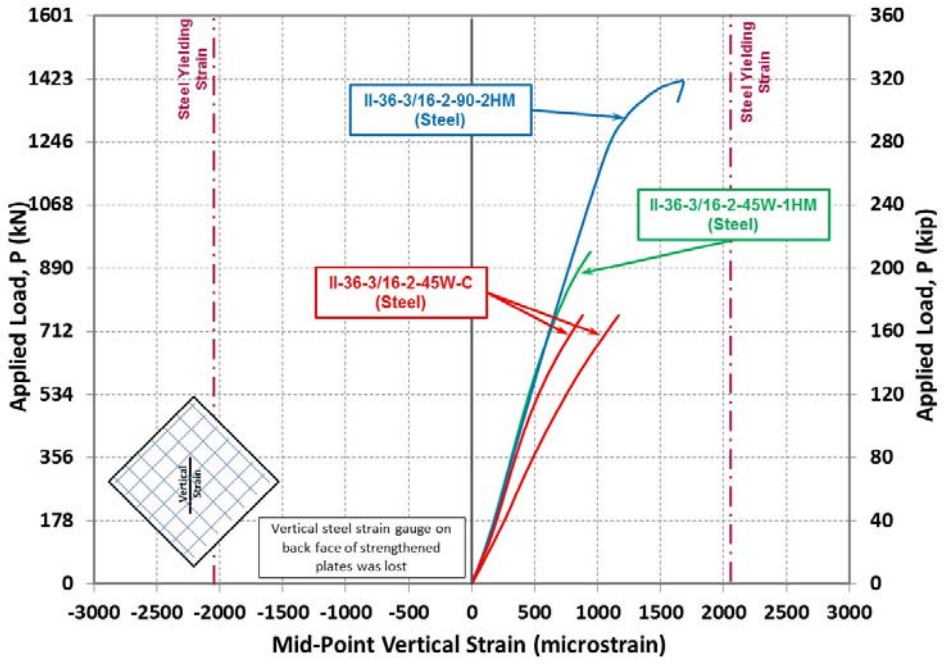

(b)

Figure 3-112: Applied load vs. principle steel strain of the plates (II-36-3/16-3-45W) under pure shear, a) horizontal strain, b) vertical strain

The increase in the shear capacity with an increase of reinforcement ratio for different CFRP strands orientations is shown in Table 3-18 and Figure 3-113. Results show that one layer and two layers of externally bonded HM CFRP strands can increase shear capacity of the strengthened plates up to 36 and 79 percent, respectively. The trend indicates that increasing the reinforcement ratio of the CFRP strands contributes to higher shear capacity since it is dependent to the stiffness of the specimen. Effect of the CFRP strengthening system is similar for plates strengthened with different configurations and selected reinforcement ratio. Because of the imperfections there was slight differences in the increase of the shear capacities.

Table 3-18: Shear capacity of the specimens in Phase II

Plate Designation	Shear Capacity (at steel horizontal strain prior to yield)		
	kN	**kip**	**Increase (%)**
II-36-3/16-1-45-C	740	166	-
II-36-3/16-1-45-1HM	999	225	36
II-36-3/16-1-45-2HM	1218	274	65
II-36-3/16-2-90-C	913	205	-
II-36-3/16-2-90-1HM	1127	253	23
II-36-3/16-2-90-2HM	1522	342	67
II-36-3/16-3-45W-C	757	170	-
II-36-3/16-3-45W-1HM	936	210	24
II-36-3/16-3-45W-2HM	1351	304	79

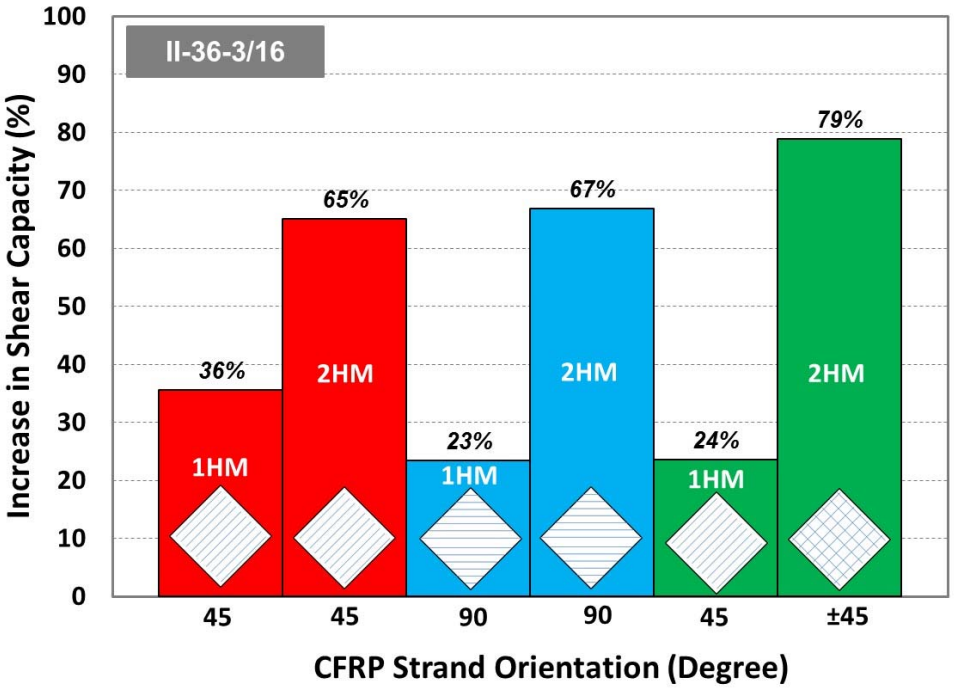

Figure 3-113: Shear capacity percentage increase of plates strengthened with one and two layers of HM CFRP strands

3.3.4.4 *Load - Lateral Deformation*

The lateral deformation of the test plate at mid-point with respect to its edges is referred to as net lateral deformation. The net lateral deformation versus the applied tensile load is graphically presented in Figure 3-114 through Figure 3-116 for the test plates strengthened with CFRP strands with an angle of 45°, 90° and ±45°, respectively. The measured lateral deformation of the plate at the edges is attributed to the lateral movement of the built-up frame. The net lateral deformation was obtained by subtracting the average value of the measured deformations on four edges of the frame from the measured mid-point deformation of the test plate.

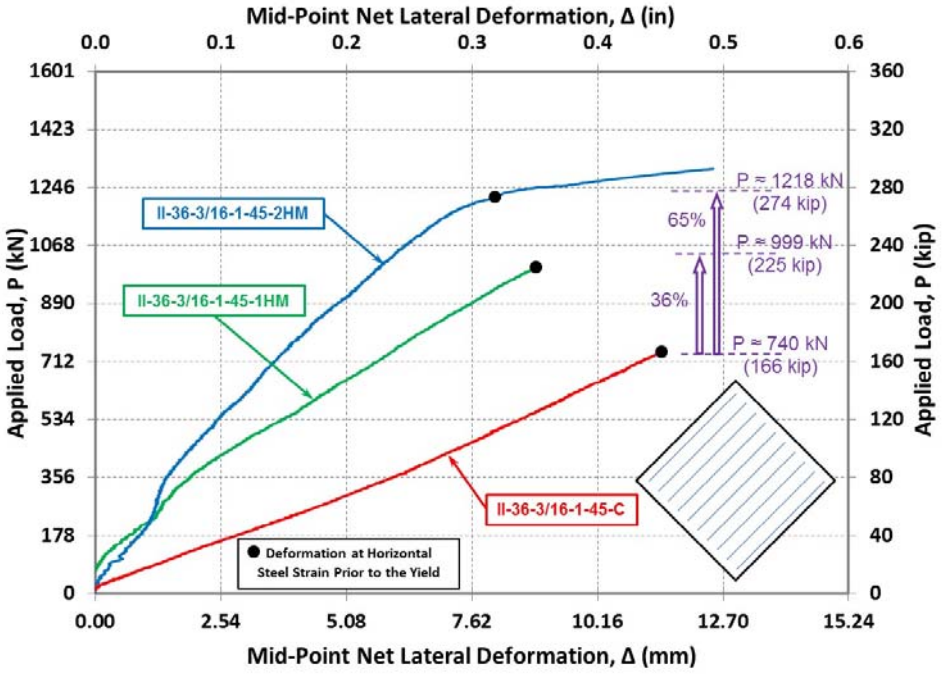

Figure 3-114: Applied load vs. net lateral deformation of the plates (II-36-3/16-1-45) under pure shear

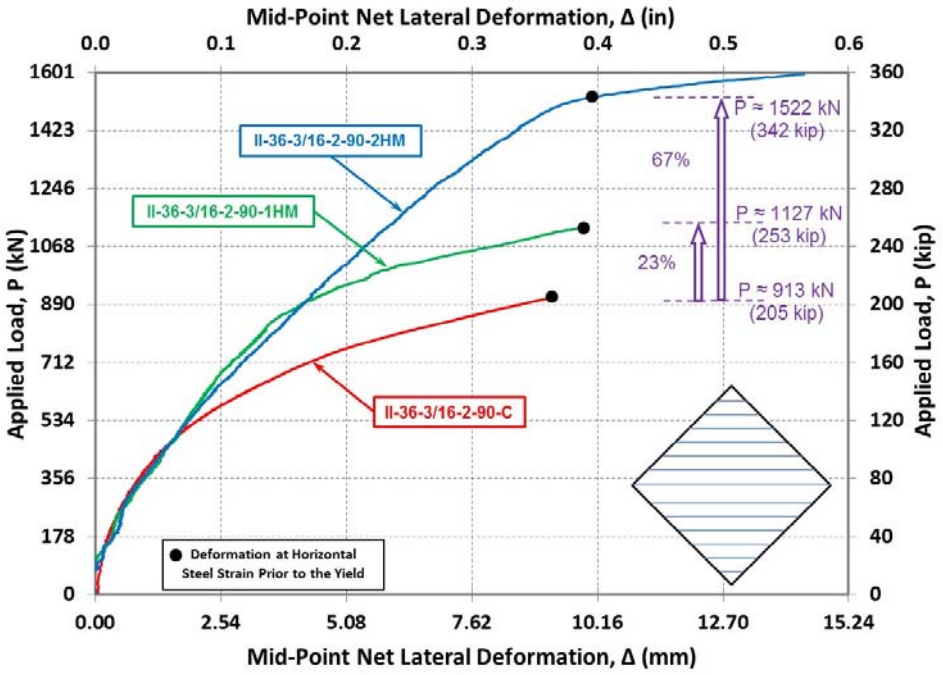

Figure 3-115: Applied load vs. net lateral deformation of the plates (II-36-3/16-2-90) under pure shear

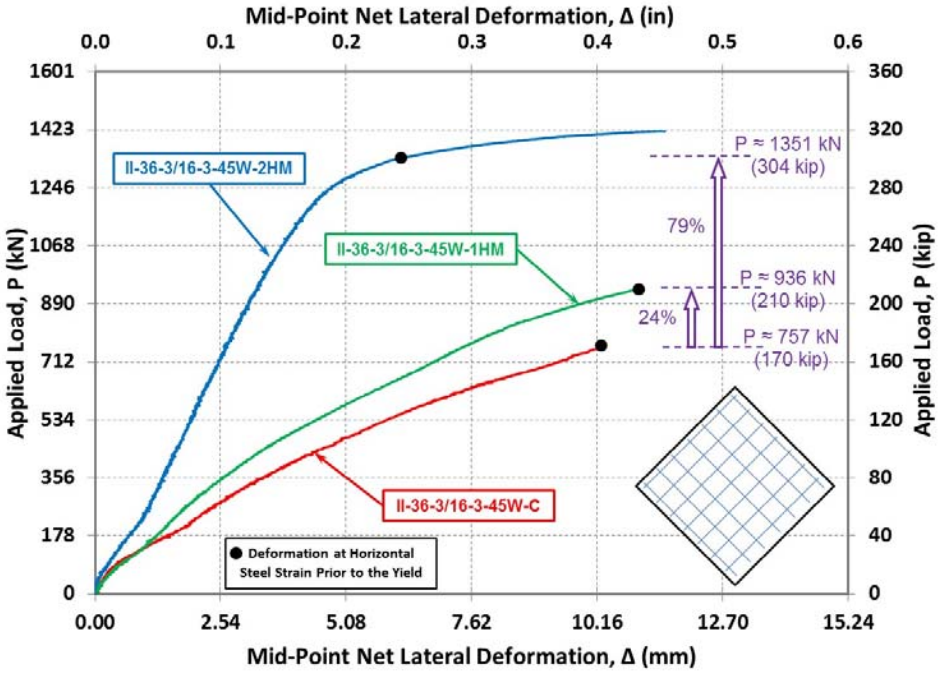

Figure 3-116: Applied load vs. net lateral deformation of the plates (II-36-3/16-2-45W) under pure shear

The increase in the shear stiffness with an increase of reinforcement ratio for different CFRP strand orientations is shown in Table 3-18 and Figure 3-117. The load-deformation behavior of the plates reveals that the strengthening system increased their lateral stiffness for each additional layer of CFRP strengthening. For the plates strengthened with one layer of CFRP strands increase in the lateral stiffness remain within the similar range. However, increase in the lateral stiffness of strengthened plate with two layers of CFRP strand is highly dependent on the fiber orientation of additional layer. The lateral stiffness was increased up to 350 percent for plate strengthened with two layers of CFRP strands with an angle of ±45^{o} relative to the applied load. Two layers of CFRP strands at an angle of ±45^{o} relative to applied load creates weaved configuration. This configuration efficiently decreases the effective length of the

CFRP strands in compression and results in increasing lateral stiffness of the strengthened plate.

Table 3-19: Lateral stiffness of the specimens in Phase II

Plate Designation	Lateral Stiffness		
	kN/mm	kip/in.	Increase (%)
II-36-3/16-1-45-C	63	357	-
II-36-3/16-1-45-1HM	91	522	46
II-36-3/16-1-45-2HM	143	815	128
II-36-3/16-2-90-C	62	356	-
II-36-3/16-2-90-1HM	85	488	37
II-36-3/16-2-90-2HM	141	807	127
II-36-3/16-3-45W-C	63	359	-
II-36-3/16-3-45W-1HM	75	429	19
II-36-3/16-3-45W-2HM	283	1615	350

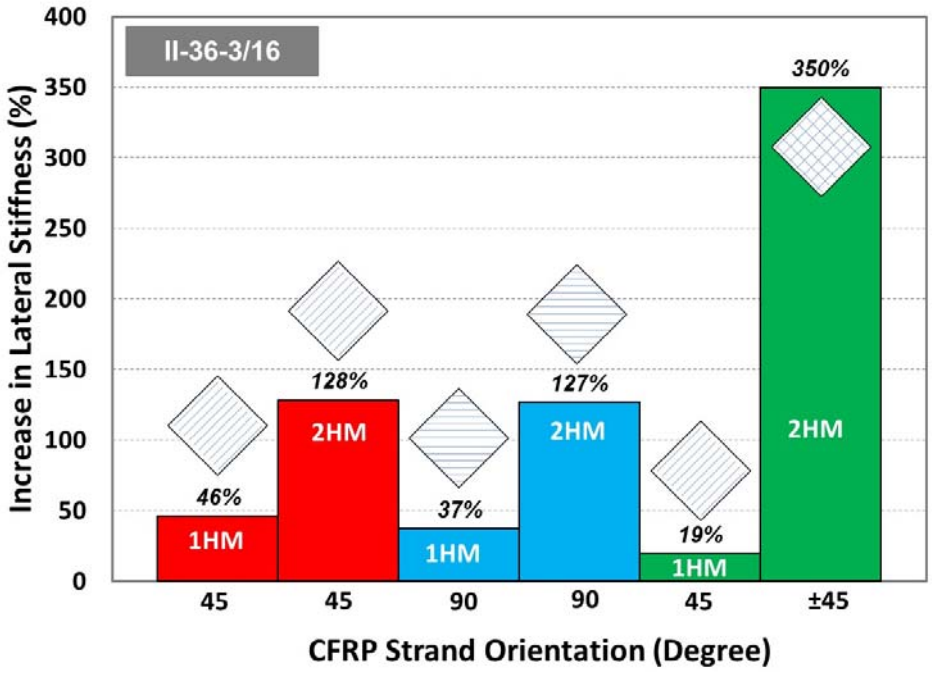

Figure 3-117: Increase of the lateral stiffness for the plates strengthened with one and two layers of HM CFRP strands

3.3.4.5 ***Deformed Shape***

The measured lateral deformed shape versus the applied load at both horizontal and vertical directions of the test plates are plotted in Figure 3-118 through Figure 3-123. The lateral deformed shapes are plotted at a similar load level for each set of tests using recorded data from the Optotrak system. For each set of tests, the selected load level was the ultimate applied load on the control test plate. Results of the strengthened test plate II-36-3/16-1-45-2HM were not shown due to loss of measured data.

Figures show maximum deformation occurred at the mid-point of the steel plate. Deformed shape was in general form of full wavelength cosine and half wavelength sine across the horizontal and vertical diagonal of the specimens, respectively. Deformed shapes confirm the clamping effects at the edges of the plates. Results obtained from each set of test plates indicate that at similar load level, lateral deformation decreased by increasing the reinforcement ratio of the CFRP strengthening system. Furthermore, adding more layers of the CFRP strands induces less distortion in plate deformed shape.

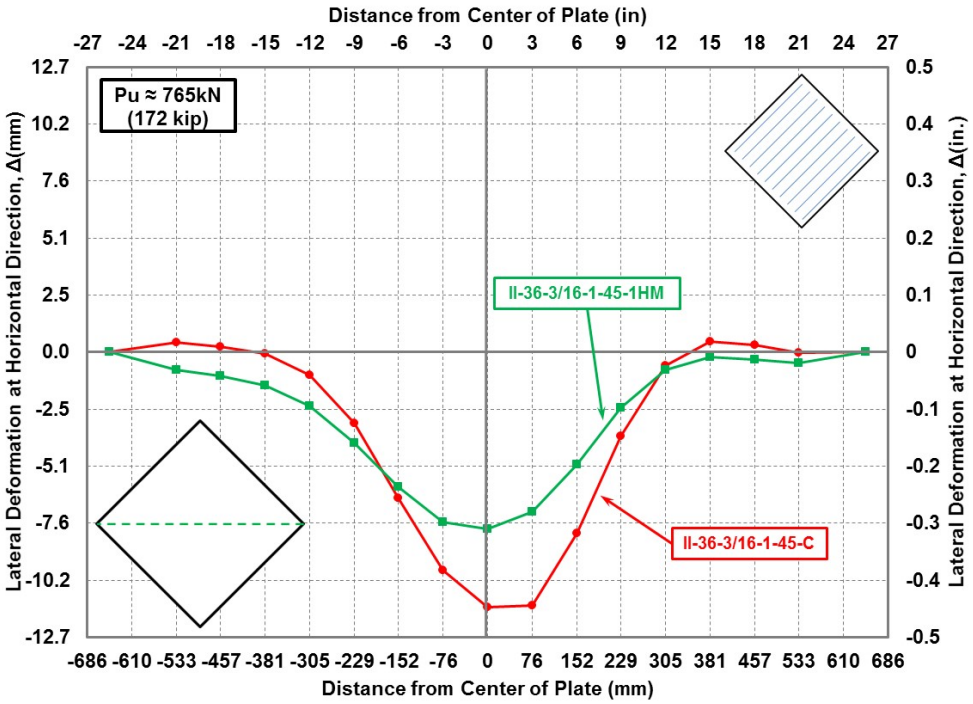

Figure 3-118: Lateral deformed shape of the plates (II-36-3/16-1-45) at horizontal direction

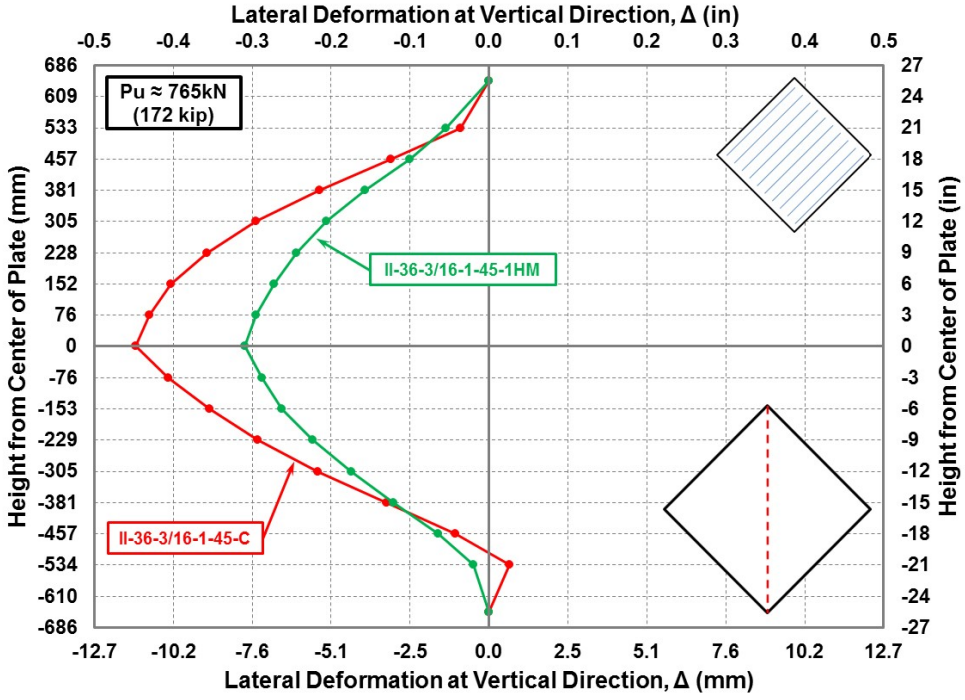

Figure 3-119: Lateral deformed shape of the plates (II-36-3/16-1-45) at vertical direction

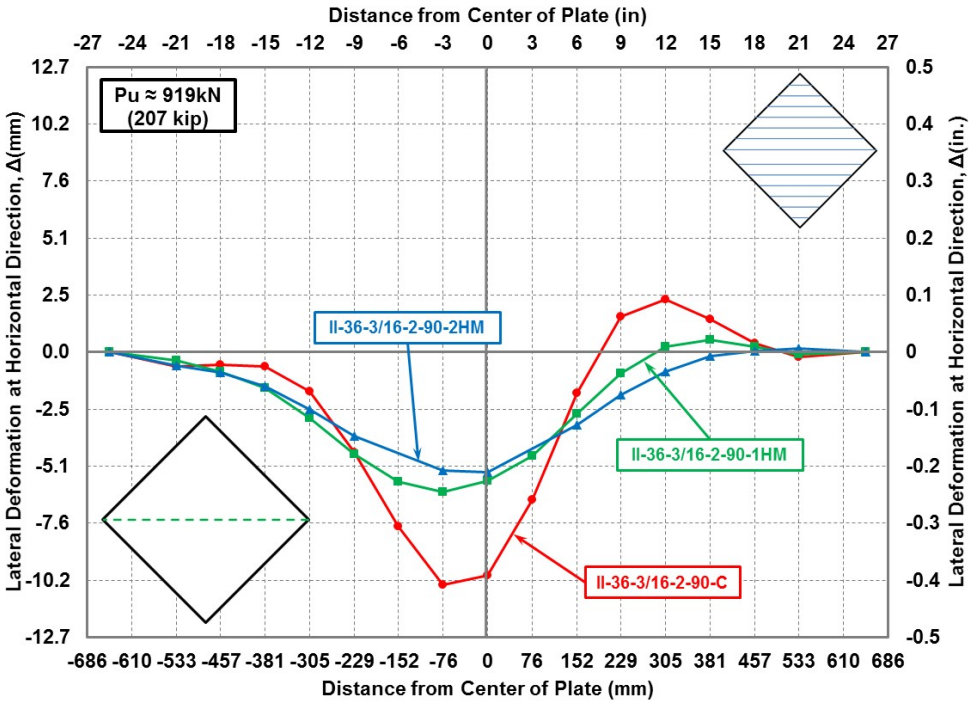

Figure 3-120: Lateral deformed shape of plates (II-36-3/16-2-90) at horizontal direction

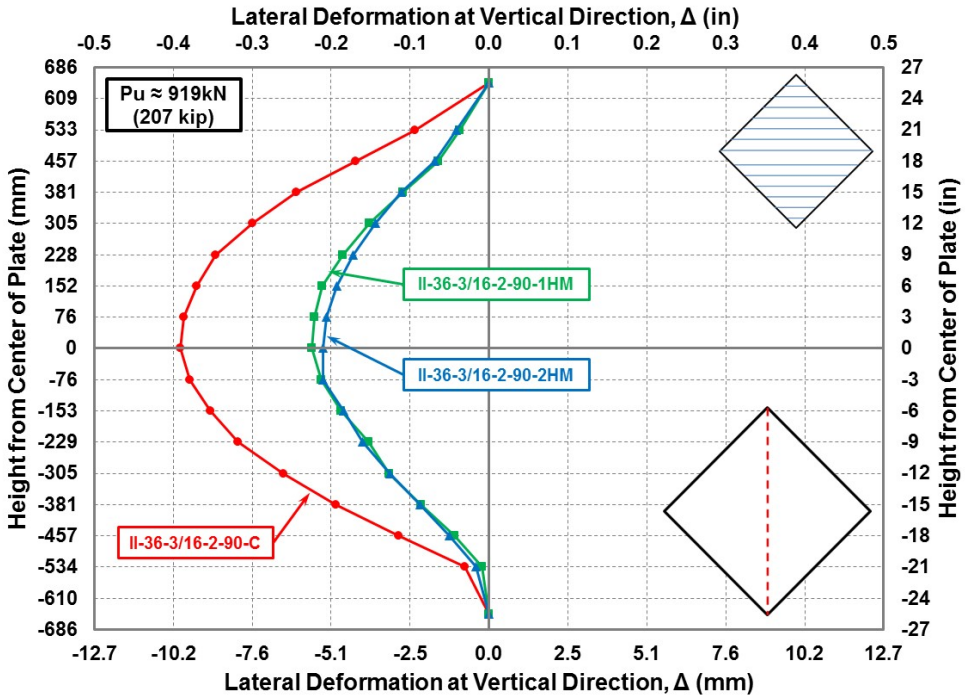

Figure 3-121: Lateral deformed shape of plates (II-36-3/16-2-90) at vertical direction

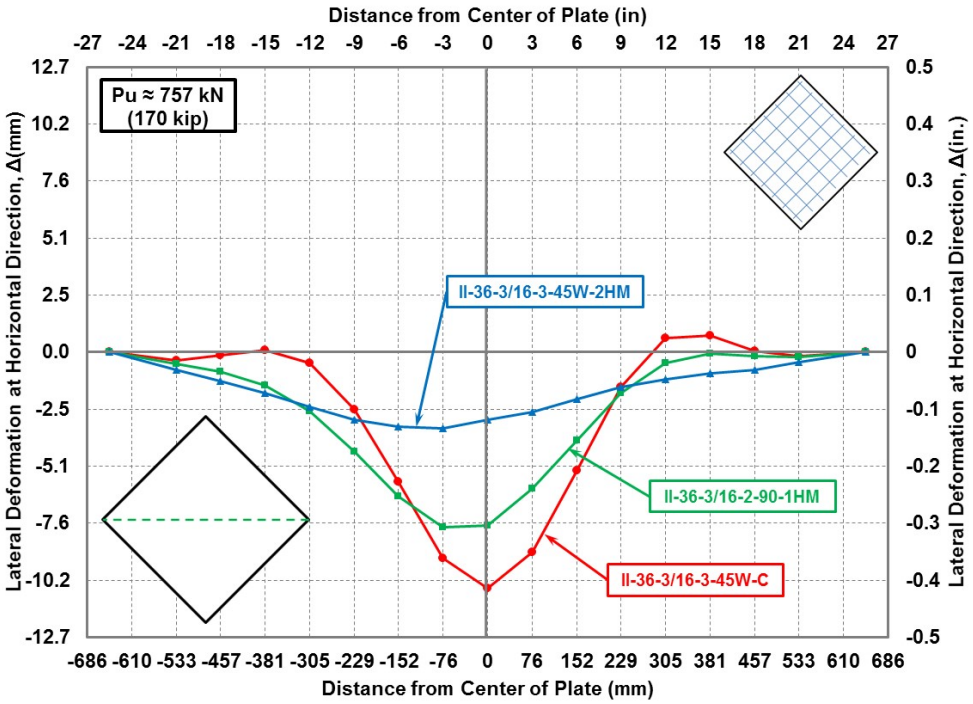

Figure 3-122: Lateral deformed shape of plates (II-36-3/16-3-45W) at horizontal direction

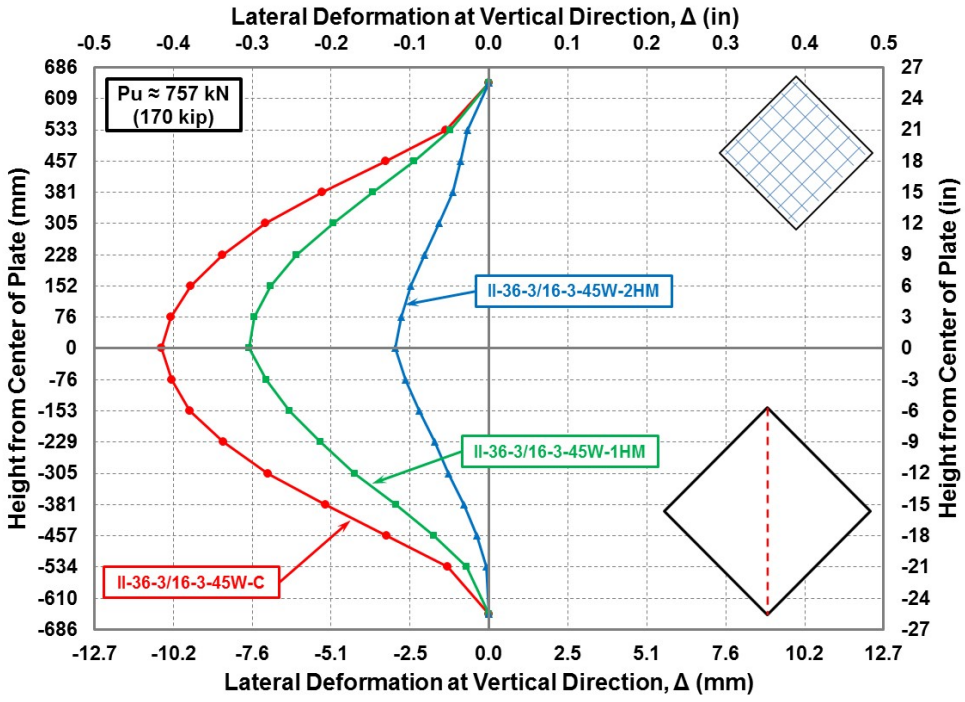

Figure 3-123: Lateral deformed shape of plates (II-36-3/16-3-45W) at vertical direction

3.3.4.6 ***Failure of the Strengthening System***

There was no indication of CFRP failure due to de-bonding or rupture up to the yielding of the plate.

4 MODEL ANALYSIS

The analytical phase of the research program was performed using nonlinear finite element, FE, analysis to model the behavior of the steel plates strengthened with CFRP strands subjected to uniaxial compressive and shear forces. For both cases, the FE models were calibrated with the experimental results. Calibration process resulted in building a confidence to use the developed FE models as a tool to study several parameters and for the development of the design guideline.

The nonlinear finite element analysis was based on the commercially available program ANSYS® Workbench (v16.1) [59] which was used to model overall behavior of the specimens. A typical simulation consists of setting up the model, solving for the model's response to the loads, and then examining the details of the response with a variety of tools. The finite element simulation consisted of nonlinear analysis performed on the control and strengthened plates with geometry of the test specimens, material constitutive relationship, and contacts definitions to accurately capture the observed experimental behaviors.

4.1 PHASE I: UNIAXIAL COMPRESSIVE LOADING

4.1.1 Finite Element Model

The following sections address various aspects of the finite element modeling including material properties, element type, layers definition, loading, boundary conditions, geometrical imperfections and mesh density. The control specimen IB-24-5/16-IM-U and strengthened

specimen with two layers of HM CFRP IB-48-5/16-2HM were selected as samples to be presented in details in the following sections.

4.1.1.1 ***Material Properties***

The steel constitutive relationship used in the FE model was full elastic-plastic stress-strain relationship as described in section 3.1.1. The idealized perfectly-plastic stress-strain relationship was used as an input to ANSYS Workbench and assigned to steel plate as given in Table 4-1. The steel material was defined using Bilinear Isotropic Hardening plasticity model. However since a very high strength steel was used for the pins and sleeves, these parts were simply modeled with Isotropic-Elastic steel material with Young's modulus 200 GPa (29000 ksi). The Poisson's ratio of the steel used was 0.3.

Mechanical properties of CFRP composite and polyurea putty used in the FE model are given in Table 4-2. Properties of CFRP composite material was based on testing witness panels. CFRP composite material is transversely isotropic material with respect to longitudinal direction. Transversely isotropic CFRP material has one axis of symmetry in the direction of fibers. The material properties in the transverse directions are usually identical [60]. Therefore, in ANSYS, the CFRP composites were defined as Orthotropic Elastic material using similar properties in the transverse direction. Pulyurea putty was also defined as Isotropic Elastic material based on the measured results reported by Okuyama et al. (2012) [61].

Table 4-1: Mechanical properties of steel considered in FE model

Specimen Thickness	Yield Strength		Modulus of Elasticity	
mm (in.)	MPa	ksi	MPa	ksi
13 (1/2)	442.6	64.192	194,269	28,176
10 (3/8)	453.5	65.716	199,925	28,996
8 (5/16)	391.7	56.621	198,661	28,813

Table 4-2: Mechanical properties of CFRP composite and putty considered in FE model

Property	Component		HM CFRP	IM CFRP	LM CFRP	Putty
Young's Modulus	E_x	MPa (ksi)	47,400 (6,869)	41,000 (5945)	24,800 (3,592)	76 (11)
	E_y, E_z		33,000 (4,784)	33,000 (4,784)	33,000 (4,784)	
Shear Modulus	G_{xy}		18,600 (2,696)	15,600 (2,264)	9,300 (1,345)	24,900 (3,612)
	G_{yz}, G_{xy}		15,700 (2,278)	15,700 (2,278)	15,700 (2,278)	
Poisson's Ratio	υ_{xy}		0.274	0.313	0.335	0.05
	υ_{yz}, υ_{xy}		0.05	0.05	0.05	

4.1.1.2 ***Selection of the Elements***

The steel plate, pins and sleeves were modeled using three-dimensional 8-node second order quadrilateral shell element (SHELL281). The element configuration is shown in Figure 4-1. Each node has 6 degree of freedoms: translations in the x, y, and z axes, and rotations about the x, y, and z-axes. This element is well-suited for linear, large rotation, and/or large strain nonlinear applications. The element accounts for effects of distributed pressures [62].

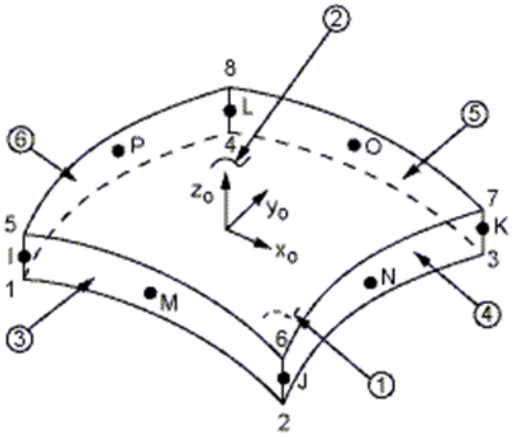

Figure 4-1: 3D 8-node SHELL281 element [62]

4.1.1.3 ***Layers Definition***

SHELL281 may be used for layered applications for modeling laminated composite shells or sandwich constructions. The accuracy in modeling composite shells is governed by the first order shear deformation theory [62]. Due to the observed perfect bond characteristics from the experimental program, the CFRP composite material and polyurea putty were modeled using layered section feature of ANSYS Workbench. For each layer, the thicknesses and angles are defined as shown in Figure 4-2 for specimen IB-48-5/16-2HM. The mid-layer was steel material having a thickness of 8 mm (5/16 in.). The polyurea putty layer was considered at each face of the steel plate with thickness of 1 mm (0.04 in.) as measured. The outer faces were assigned two layers of CFRP composites with thickness of 2.5 mm (0.1 in.) for each layer. Since, the orientation of the CFRP composite material was in direction of defined element local coordinate, the angle was set to zero.

Layered Section

Right click on the grid to add, modify and delete a row.

Layer 1 is on the bottom. Subsequent layers are added to the top, increasing in the +Z normal direction.

Layer	Material	Thickness (in)	Angle (°)
(+Z)			
7	HM CFRP X	0.1	0
6	HM CFRP X	0.1	0
5	PUTTY	0.04	0
4	Structural Steel	0.3125	0
3	PUTTY	0.04	0
2	HM CFRP X	0.1	0
1	HM CFRP X	0.1	0
(-Z)			

Figure 4-2: Defining multiple layers on SHELL281 (Plate IB-48-5/16-2HM)

4.1.1.4 *Loading and Boundary Conditions*

Boundary conditions were modeled to match the boundaries of the tested specimens as shown in Figure 4-3. The plate at both ends was modeled to be fully bonded to the sleeves since welded connections was used. The sleeves were allowed to rotate around the pins. However, results obtained from the linear buckling analysis indicated that this boundary condition cannot fully resembling hinged-hinged end condition due to the presence of friction acting between sleeve and pin surfaces. Therefore, frictional contacts were assigned at both ends between pins and sleeves. The two faces of the frictional contact surfaces are free to separate. When in contact, they may slide only when the contact shear stress exceeds a critical value. The critical value is determined by multiplying the normal stress and friction coefficient which was used as an input in the contact property [62]. Bottom pin is allowed to move upwards, however, the top pin was completely constraint from the translations. Pins were modeled as hollow pipes to decrease number of mesh elements and consequently reduce the time of analysis.

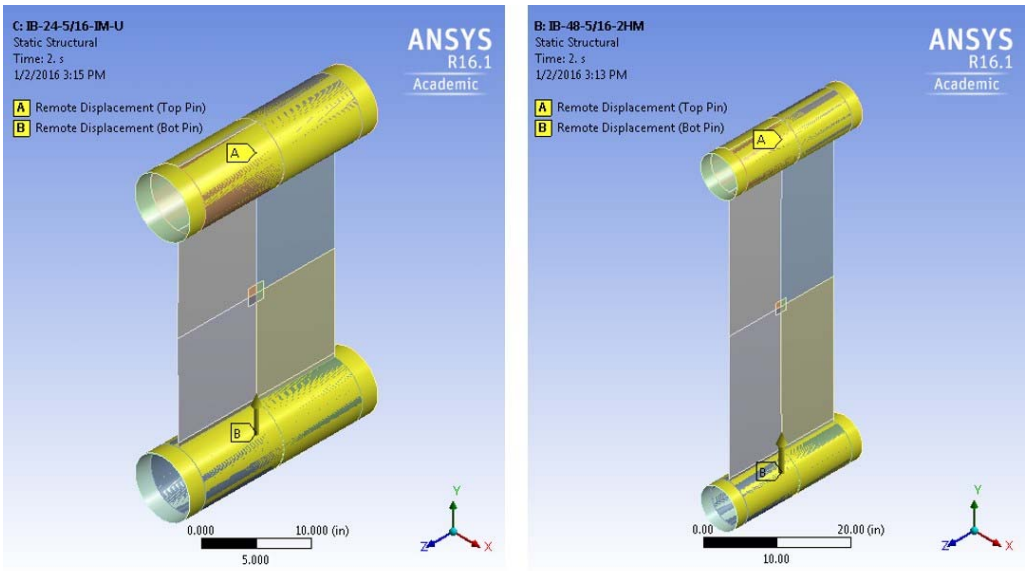

Figure 4-3: Finite element model and the Boundary conditions in ANSYS Workbench (v16.1) for specimen a) IB-24-5/16-IM-U, b) IB-48-5/16-2HM

4.1.1.5 *Geometric imperfections*

The initial geometric imperfections were defined by assuming a simplified shape. The effect of initial imperfection was assumed to follow a half wavelength sine curve with its apex at mid-height which is representing the first mode of buckling as shown in Figure 4-4.

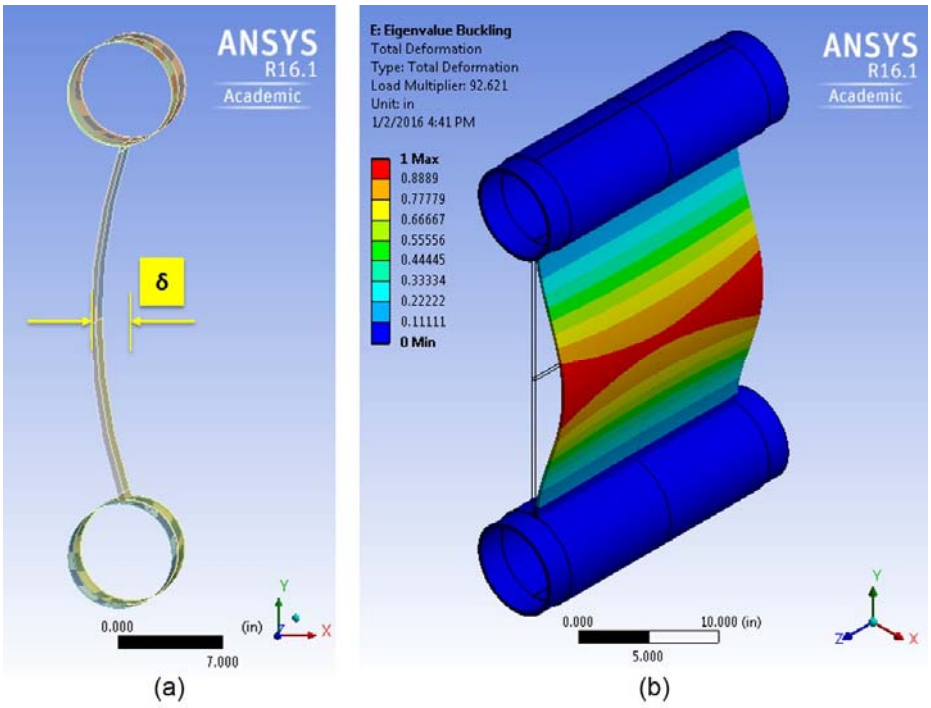

Figure 4-4: a) Assumed initial imperfection as a half wavelength sine curve, b) First mode of buckling of specimen IB-24-5/16-IM-U

4.1.1.6 ***Mesh Density***

The mesh configuration used for the analysis in this study is shown in Figure 4-5. To determine the effect of mesh size, a mesh sensitivity analysis was performed using three different mesh sizes. Figure 4-6and Figure 4-7illustrate the effect of mesh size on mid-height longitudinal strain and net lateral deformation of the control steel plate from the finite element analysis, respectively. Three different mesh sizes of 25x25 mm (1x1 in.), 13x13 mm (0.5x0.5 in.), and 6x6 mm (0.25x0.25 in.) were examined resulting in the total number of 7816, 29887, and 117759 elements, respectively. The figures show identical results, where no change in the behavior and buckling load is occurred by refining the mesh size. However, the computer run

time dramatically increased by refining the mesh size. Therefore mesh size of 25x25 mm (1x1 in.) was used for the further analyses.

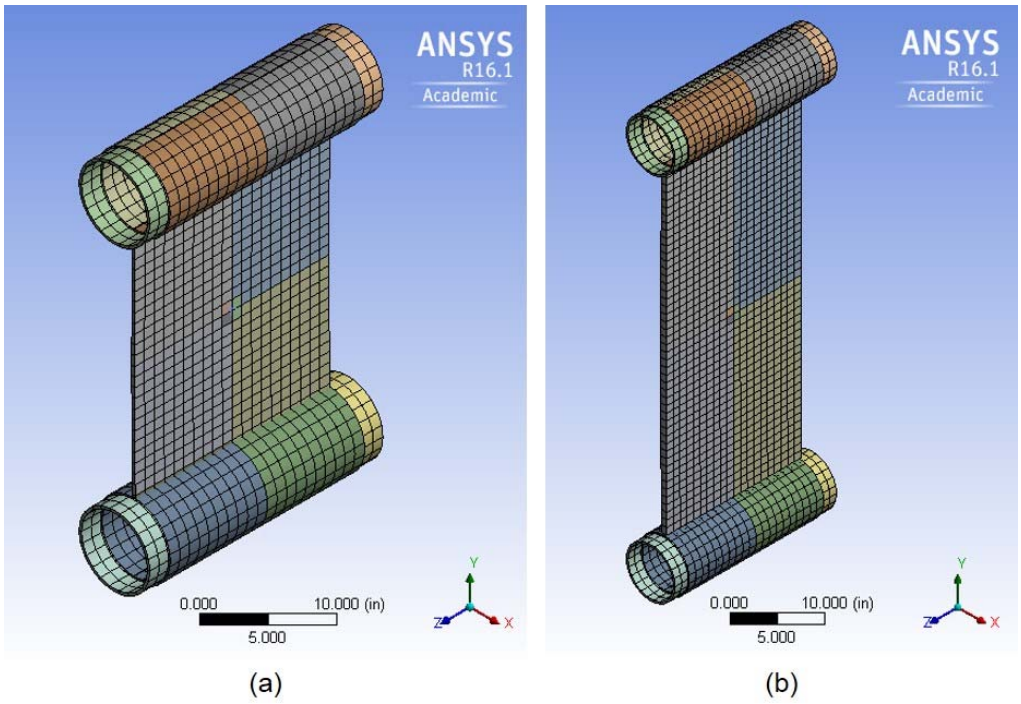

Figure 4-5: Mesh configuration (25x25 mm (1x1 in.)) used for specimen a) IB-24-5/16-IM-U, b) IB-48-5/16-2HM

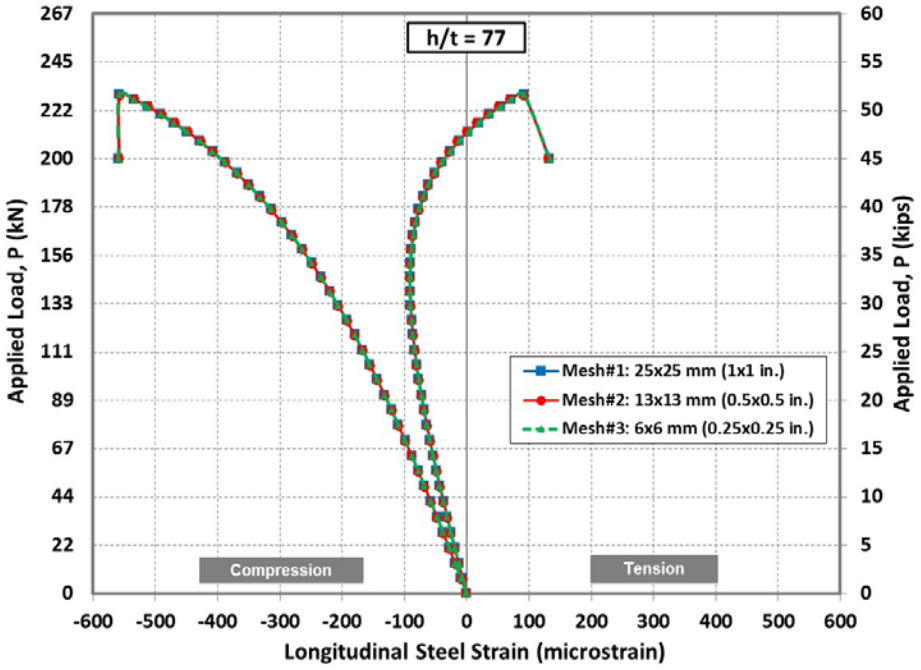

Figure 4-6: Applied load vs. longitudinal steel strain at mid-height of a control plate to show effect of mesh size on finite element results

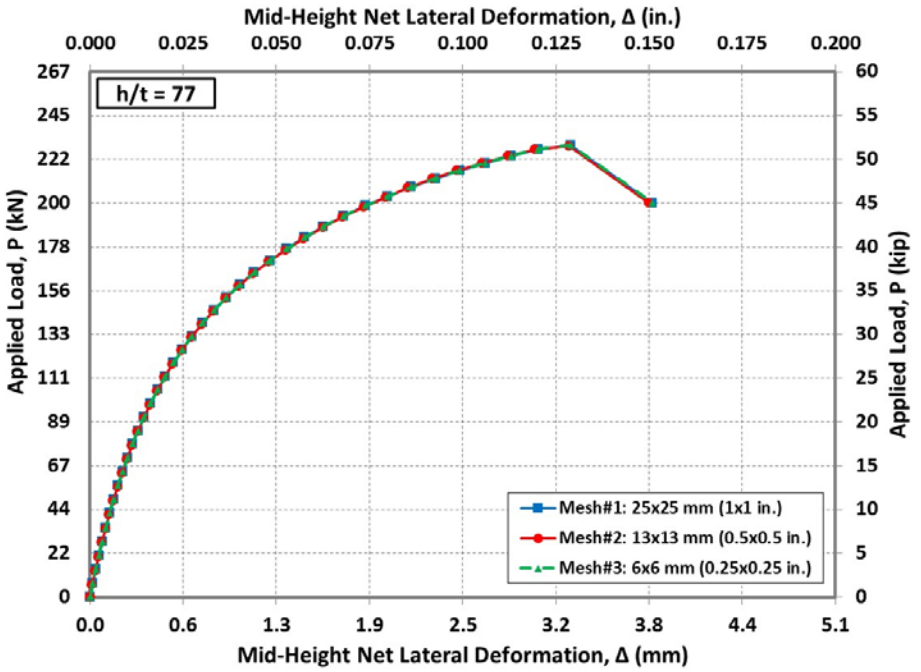

Figure 4-7: Applied load vs. net lateral deformation at mid-height of a control plate to show effect of mesh size on finite element results

4.1.1.7 *Analysis Technique*

The Newton-Raphson Method was implemented in ANSYS to converge the solution. The method is an iterative solution method used to determine the nonlinear response of a structure subjected to prescribed load or displacement increments up to failure. Displacement control method was used in this study, wherein the displacement was increased monotonically in a series of discrete steps. At each step, the Newton-Raphson method was applied until the model equations were satisfied within an acceptable convergence criteria. If the program was unable to converge within a specified number of iterations, the structure was deemed unstable, and the analysis was terminated. Penalty-based formulation was selected as contact algorithm and gauss integration points were used for surface-to-surface contact elements. Penalty-based formulation showed good convergence behavior by having few equilibrium iterations. This formulation penalizes the nodes which penetrate by attaching a stiff spring and stretching the spring by the penetration distance. Therefore, the penalty traction pushes back the nodes to reduce penetration. To count on the geometrical nonlinearities, large deflection analyses were considered.

4.1.2 Calibration of the FE Model

This chapter describes the process used to calibrate the finite element model to capture the overall behavior and buckling load of the CFRP strengthened steel plates. The calibration was carried out based on measured test results of the first phase of the experimental program. The two parameters that were calibrated are friction factor between pin and sleeve and the initial out-of-straightness imperfection of the steel plate at the mid-height of plates.

Prior to the calibration studies, the FE model was examined to ensure that it converges, captures the behavior, and produces similar measured responses. Figure 4-8 presents deformation of the two tested plates using the FE model at the onset of buckling. Maximum lateral deformation was detected at the mid-height of the plate as measured from the experimental program. Equivalent strain contour at the onset of buckling is also shown in Figure 4-9. Maximum strains are observed at mid-height of the plate similar to what captured from the experimental measurements.

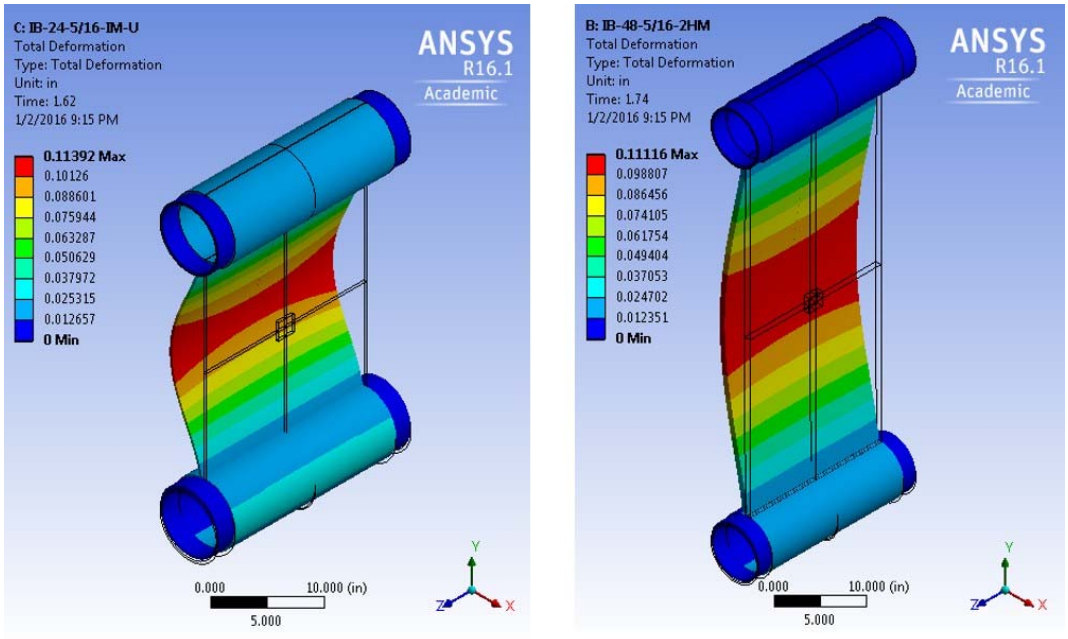

Figure 4-8: Total deformation at buckling of the specimens a) IB-24-5/16-IM-U, b) IB-48-5/16-2HM (Scale Factor: 10)

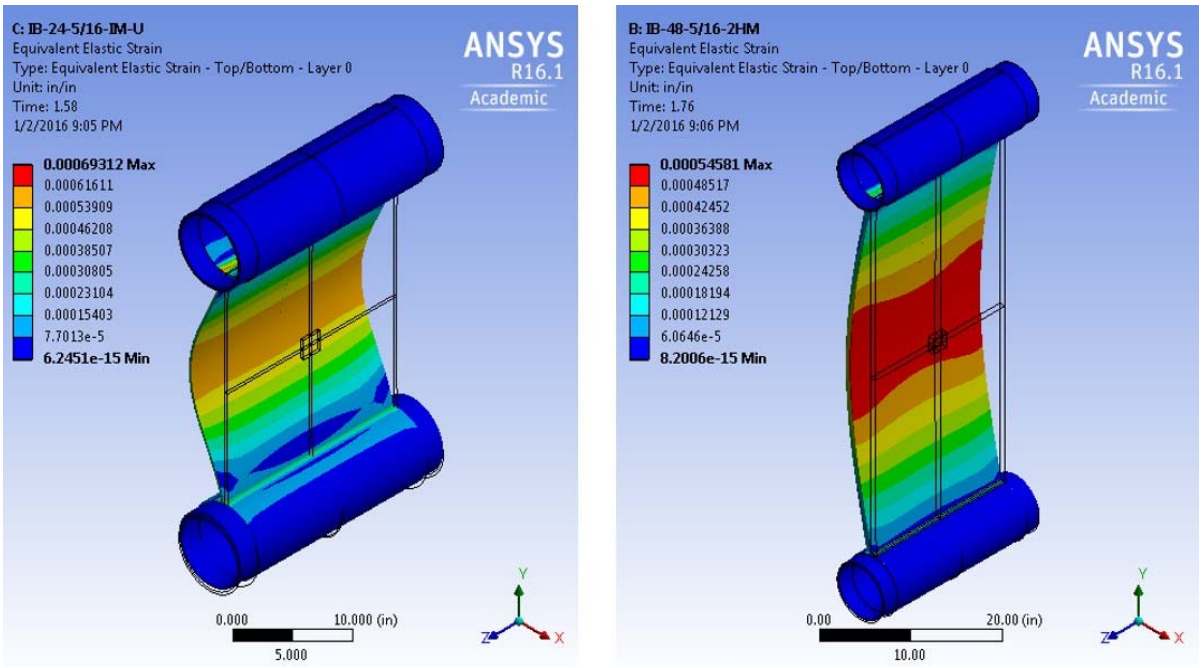

(a) (b)

Figure 4-9: a) Equivalent elastic steel strain at buckling for specimen IB-24-5/16-IM-U, b) Equivalent elastic CFRP strain at buckling for specimen IB-48-5/16-2HM (Scale Factor: 10)

Figure 4-8 and Figure 4-9 show the successful performance of the FE model to simulate the contact between the pins and the sleeves. Examining deformation of the bottom pin and the sleeve clearly confirms that the sleeve has rotated over the pin including the observed deformation and strain similar to experimental program. Since the pin did not rotate, the model did not show any deformation or strain.

4.1.2.1 *Friction Coefficient*

The coefficient of friction (μ) between two bodies usually varies between 0 for slippery surface and 1 for rough surface. In the experimental program, the friction develops between steel surfaces of pin and sleeve due to the sliding mechanism. Reasonable ranges of friction

coefficients are suggested for different materials [63]. Suggested friction coefficient used for greasy hard steel on hard steel is ranged from 0.025 to 0.12. The three friction coefficients determined from the calibrated process were 0.025, 0.075, and 0.12 using measured results of the three control specimens IB-24-5/16-HM-U, IB-24-5/16-IM-U, and IB-24-5/16-LM-U. The comparison between experimental results and numerical FE predictions for the three control specimens using friction factors of 0.025, 0.075, and 0.12 are presented in Figure 4-10 through Figure 4-12. The comparisons are presented for the longitudinal steel strain parallel to the applied load and the lateral deformation at mid-height of the steel plate. For each friction coefficient, results of FE are presented for three imperfection values. The comparison clearly indicates that friction factor of 0.025 provides the best agreement with measured data and match the stiffness and buckling load. Therefore, factor of 0.025 was selected as a calibrated friction factor for the rest of FE analyses. It is worth noting that the low friction factor obtained from the calibration process can be justified due to use of chromed-painted pins and use of grease for all the contact surfaces.

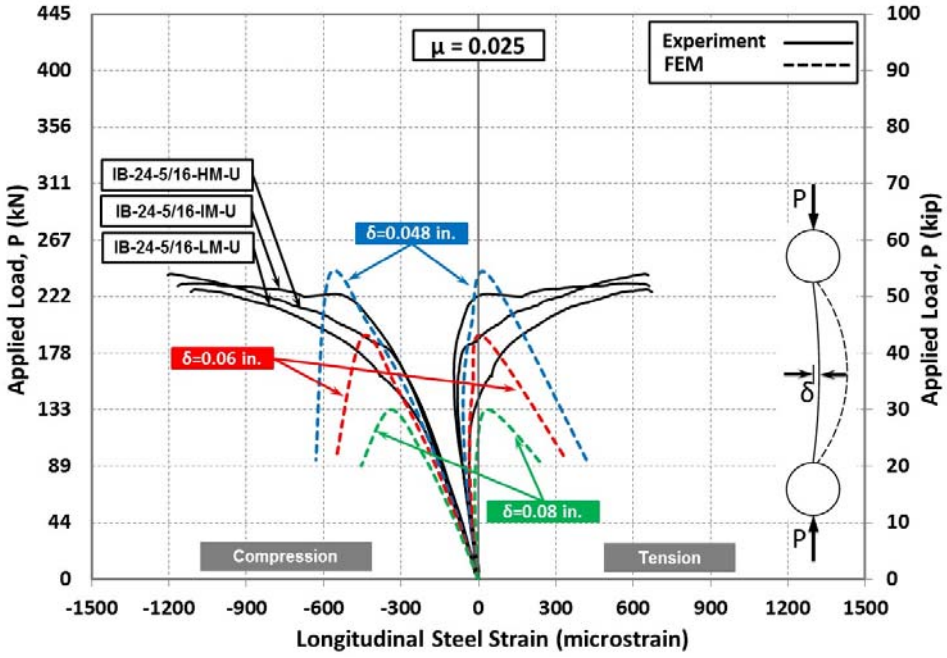

(a)

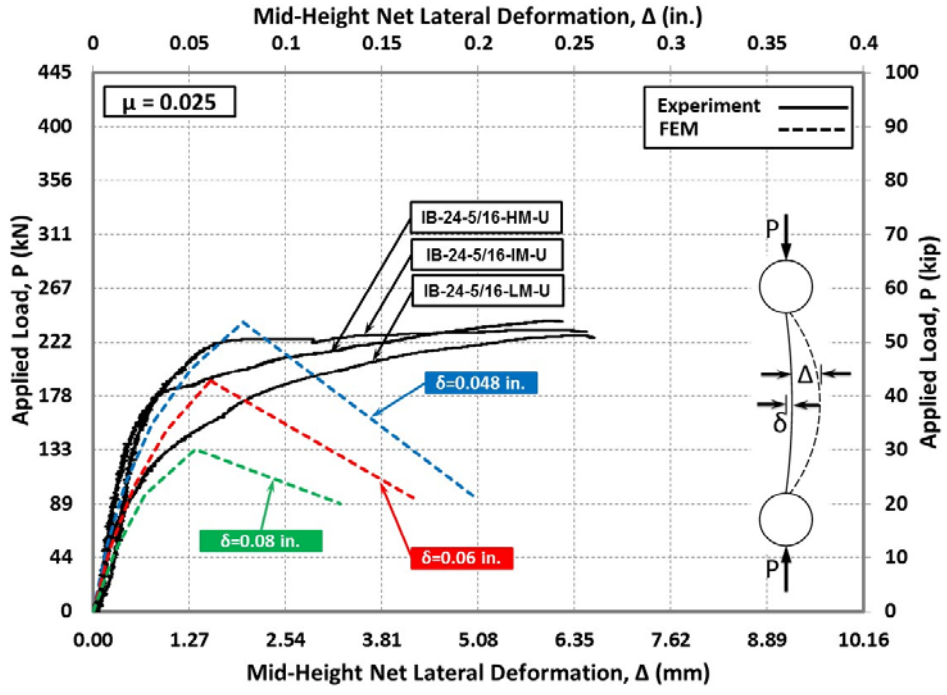

(b)

Figure 4-10: comparison between experimental results and FE prediction of control plates at mid-height using friction factor of 0.025; Applied load vs. a) net lateral deformation, b) longitudinal strain

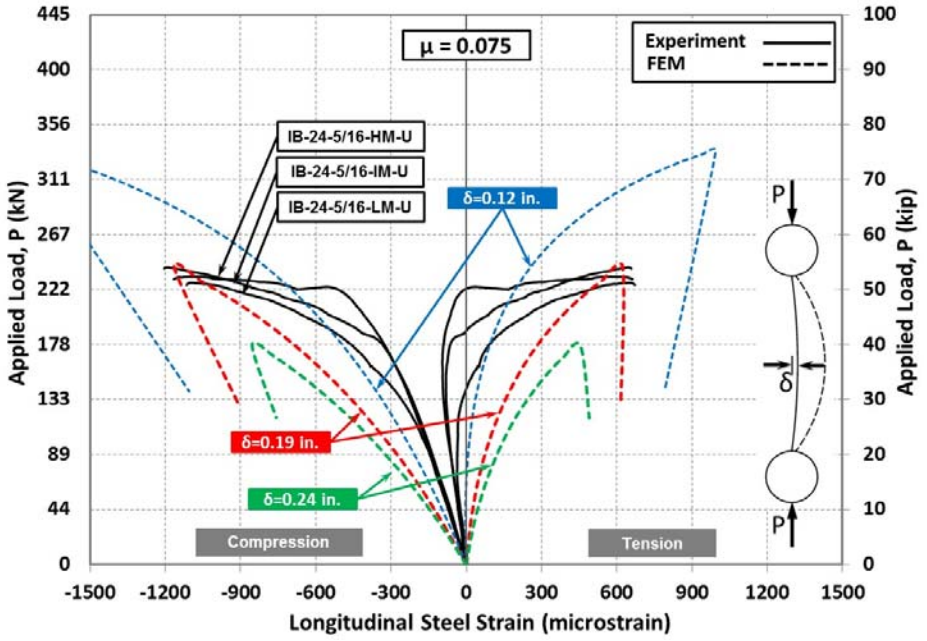

(a)

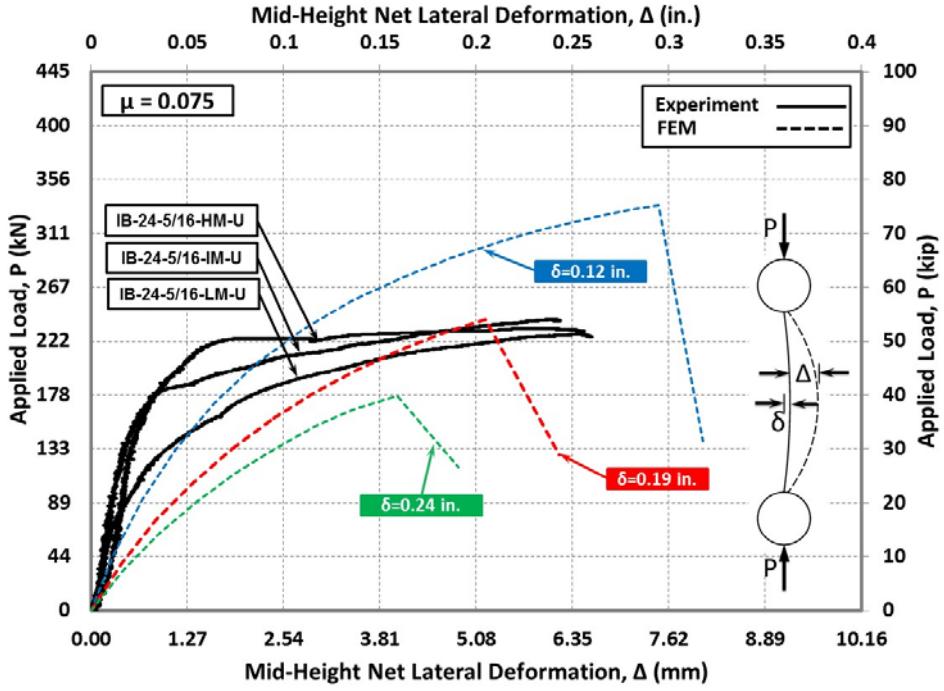

(b)

Figure 4-11: comparison between experimental results and FE prediction of control plates at mid-height using friction factor of 0.075; Applied load vs. a) net lateral deformation, b) longitudinal strain

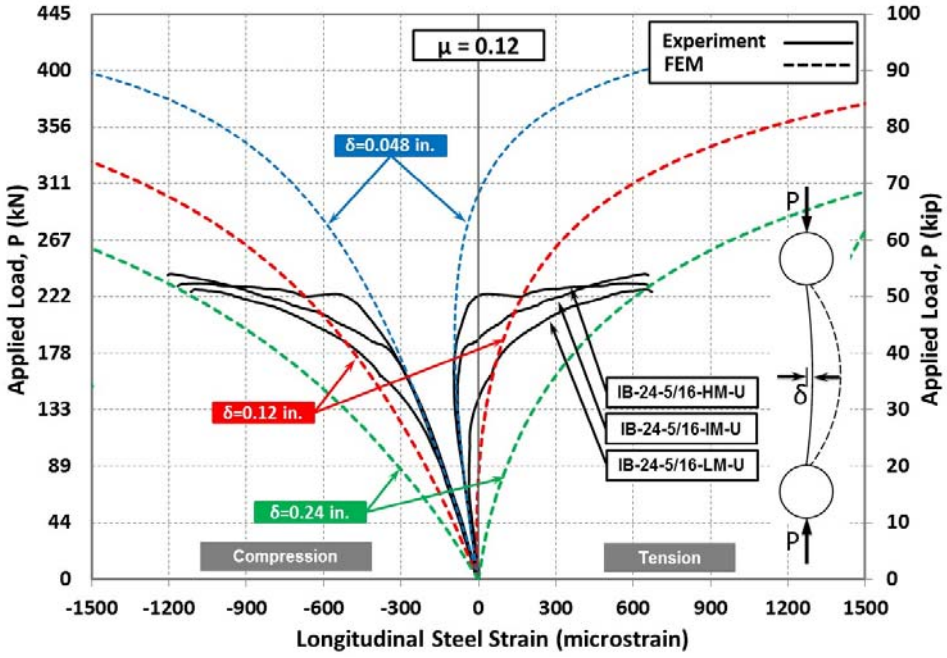

(a)

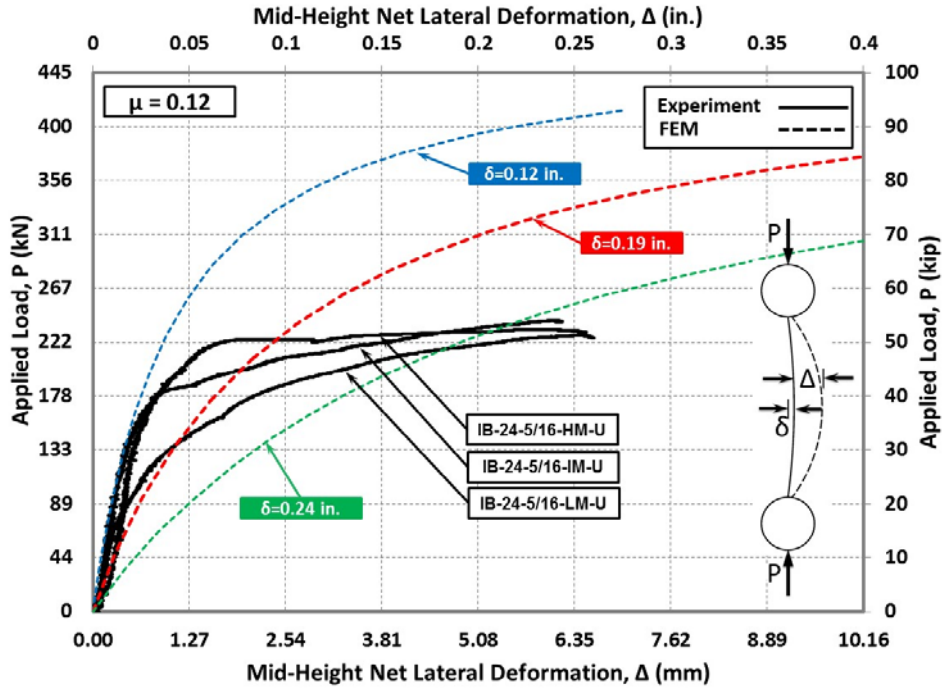

(b)

Figure 4-12: comparison between experimental results and FE prediction of control plates at mid-height using friction factor of 0.012; Applied load vs. a) net lateral deformation, b) longitudinal strain

4.1.2.2 ***Imperfection of the steel plate***

Using calibrated friction factor 0.025, all the specimens were modeled and imperfection values were evaluated by capturing the overall behavior and measured buckling loads. The imperfection values obtained from FE analyses are given in Table 4-3. Regardless to the height and thickness of the plates, the average initial deflection at mid-height were found 2 mm (0.08 in.) to the best estimation can be used for the analysis..

Table 4-3: Calibrated imperfection values obtained from FE analyses

Specimen ID	Strengthening Layer	FE Predicted Imperfection Value, δ	
		(in.)	(mm)
IA-24-1/2-U	0	0.08	1.9
IA-24-3/8-U		0.06	1.6
IA-24-5/16-U		0.07	1.8
IB-24-5/16-LM-U		0.06	1.6
IB-24-5/16-IM-U		0.06	1.6
IB-24-5/16-HM-U		0.06	1.5
IA-48-1/2-U		0.11	2.7
IA-48-3/8-U		0.10	2.5
IA-48-5/16-U		0.07	1.8
IB-48-5/16-LM-U		0.09	2.3
IB-48-5/16-IM-U		0.08	2.0
IB-48-5/16-HM-U		0.10	2.6
IA-24-1/2-S-P	1	0.08	2.1
IA-24-3/8-S-P		0.08	2.1
IA-24-5/16-S-P		0.08	2.0
IA-24-5/16-S		0.07	1.9
IB-24-5/16-1LM		0.07	1.8
IB-24-5/16-1IM		0.07	1.9
IB-24-5/16-1HM		0.07	1.8
IA-48-1/2-S-P		0.10	2.5
IA-48-3/8-S-P		0.11	2.7
IA-48-5/16-S-P		0.09	2.4
IA-48-5/16-S		0.07	1.8
IB-48-5/16-1LM		0.08	2.1
IB-48-5/16-1IM		0.08	2.0
IB-48-5/16-1HM		0.09	2.3
IB-24-5/16-2LM	2	0.08	2.1
IB-24-5/16-2IM		0.09	2.3
IB-24-5/16-2HM		0.08	2.1
IB-48-5/16-2LM		0.09	2.4
IB-48-5/16-2IM		0.08	2.0
IB-48-5/16-2HM		0.07	1.9
AVG		**0.08**	**2.1**

4.1.2.3 ***Accuracy of the FE Model***

The applied load versus predicted net lateral displacements and longitudinal steel strains of the steel plates are compared to the measured values for three specimens. Figure 4-13 through Figure 4-15 show the predicted responses versus the measured values for the control specimen IB-48-5/16-IM-U, the strengthened specimen with one layer of CFRP strands IB-24-5/16-1IM, and the strengthened specimen with two layer of CFRP strands IB-24-5/16-2LM, respectively. The comparison shows good agreement between the FE results and the measured data. The initial stiffness, the general trend of the curves, and buckling loads captured were within a good precision. The discrepancy in some cases may be attributed to the presence of possible eccentricities of the applied load and the different imperfections of tested plates from the assumption used.

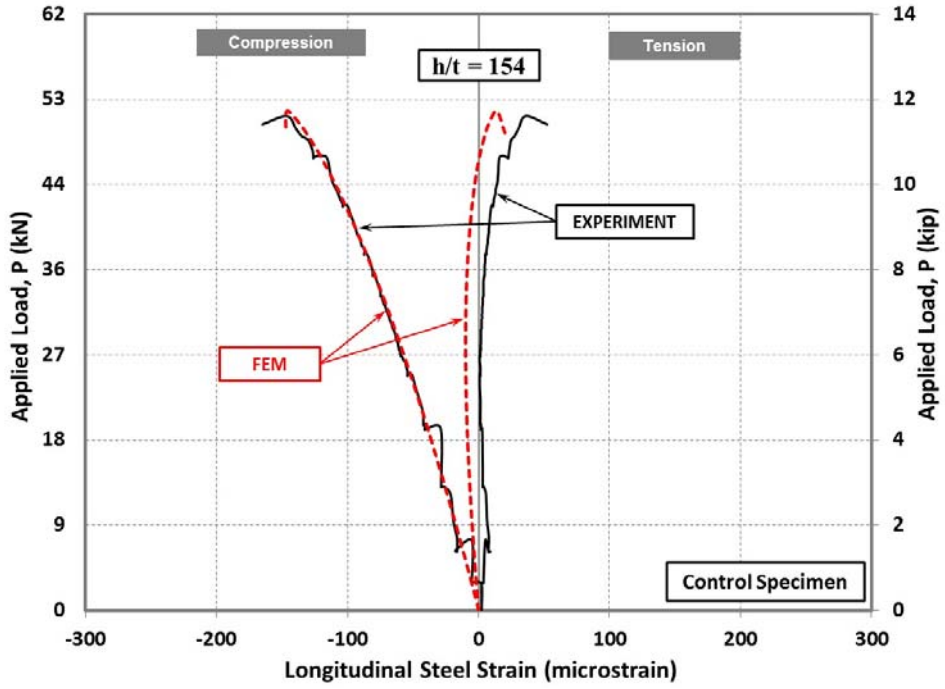

(a)

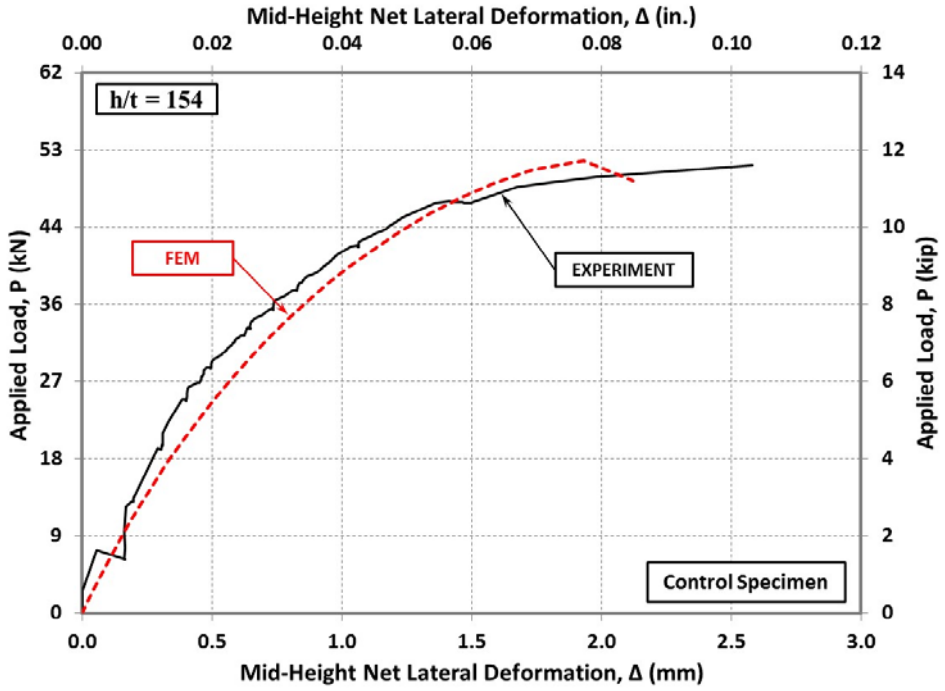

(b)

Figure 4-13: Comparison between experimental results and FE predictions of control specimen (IB-48-5/16-IM-U) at mid-height; applied load vs. a) longitudinal strain, b) net lateral deformation

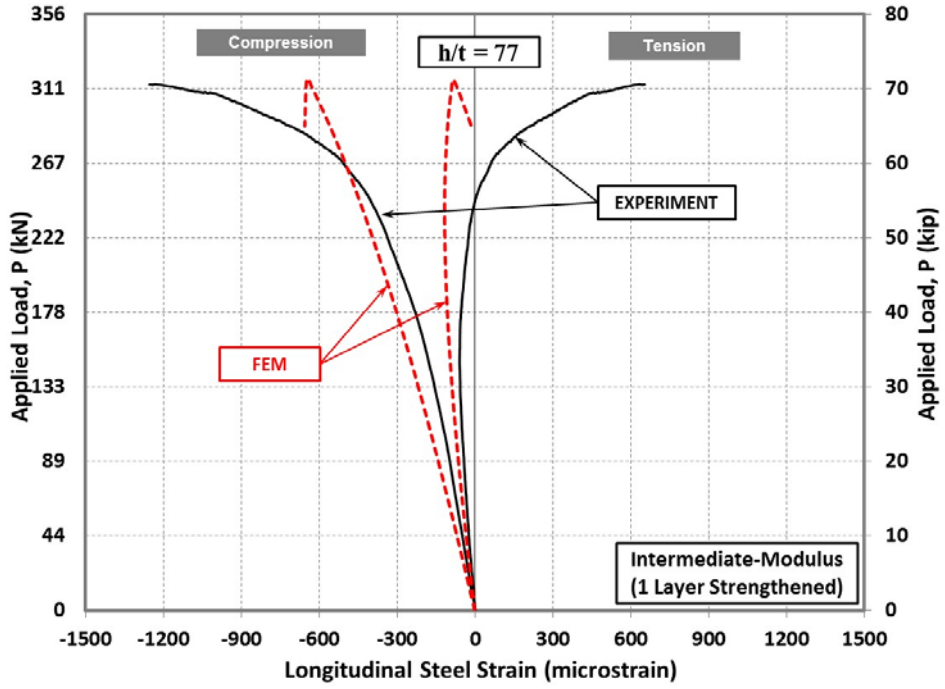

(a)

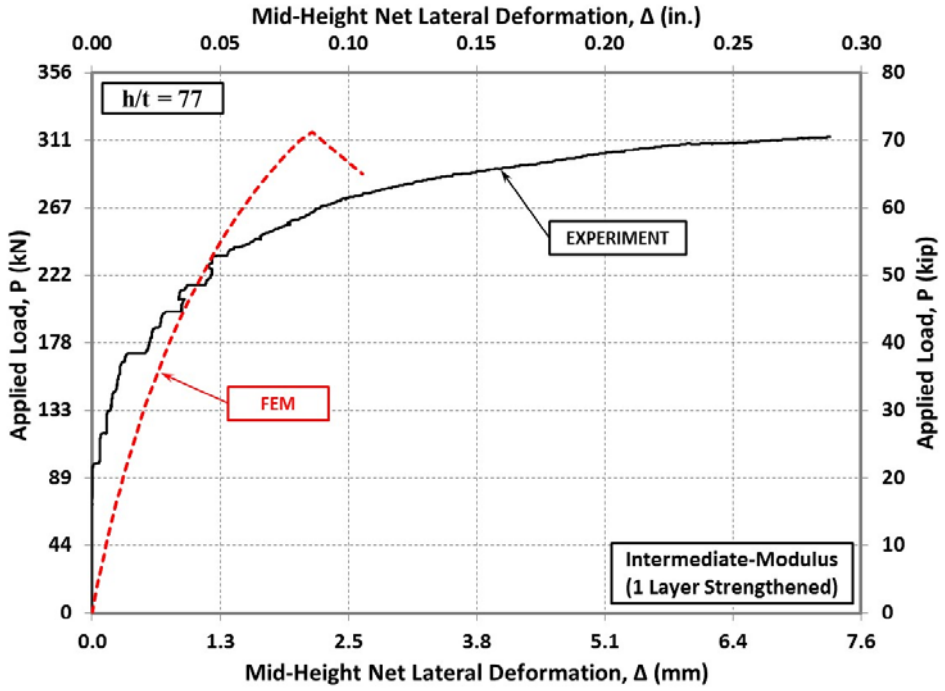

(b)

Figure 4-14: Comparison between experimental results and FE predictions of 1 layer strengthened specimen (IB-24-5/16-1IM) at mid-height; applied load vs. a) longitudinal strain, b) net lateral deformation

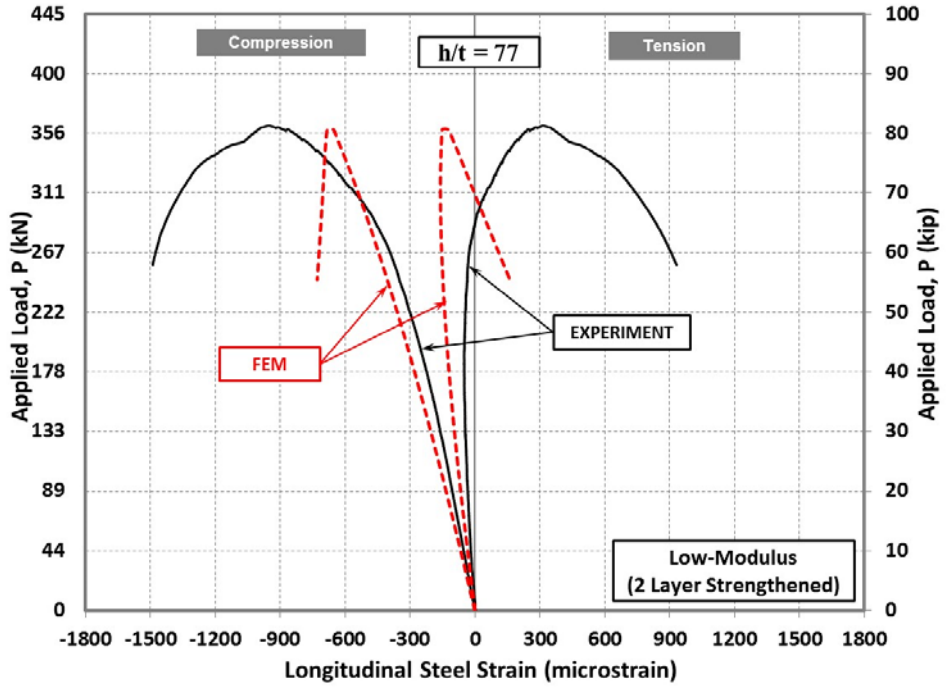

(a)

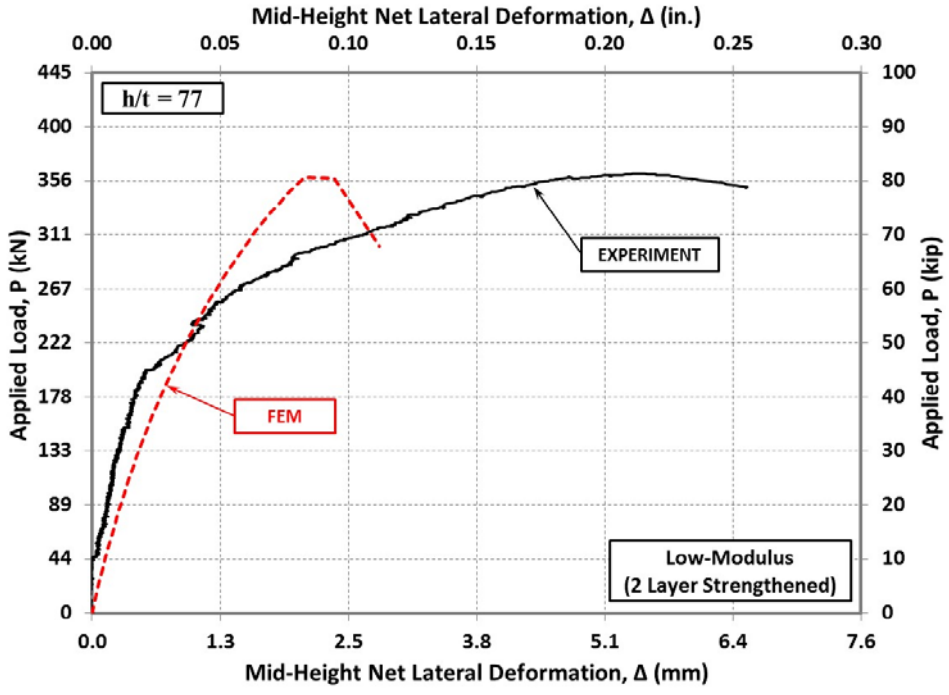

(b)

Figure 4-15: Comparison between experimental results and FE predictions of 2 layer strengthened specimen (IB-24-5/16-2LM) at mid-height; applied load vs. a) longitudinal strain, b) net lateral deformation

4.2 PHASE II: SHEAR STRENGTHENING

4.2.1 Finite Element Model

The following sections address various aspects of the FE model developed to capture the behavior of the control and strengthened steel plates subjected to pure shear. These aspects categorized as material properties, element type, loading, boundary conditions, geometrical imperfection and mesh density.

4.2.1.1 *Material Properties*

The material constitutive relationship of the three test sets used for the FE model was Bilinear Isotropic Hardening material with strain hardening values as given in Table 4-4. Due to use of high strength bolts, Isotropic-Elastic steel material with Young's modulus 200 GPa (29000 ksi) was used. Typical value of the specified Poisson's ratio of the steel was 0.3. Mechanical properties of CFRP composite and polyurea putty are given in Table 4-5. Compressive properties of CFRP composite material, measured from witness panels were used. CFRP composite material is transversely isotropic material with respect to the longitudinal direction. Therefore, in ANSYS, the CFRP composites were defined as Orthotropic Elasticity material using similar properties in transverse direction. Pulyurea putty was also defined as Isotropic Elastic material based on the measured results reported by Okuyama et al. (2012) [23].

Table 4-4: Mechanical properties of steel considered in FE model

Set#	Yield Strength		Modulus of Elasticity		Strain Hardening	
	MPa	ksi	MPa	ksi	MPa	ksi
1	396.6	57.519	195,662	28,378	400	57.52
2	468.7	67.972	203,299	29,486	470	67.97
3	410.1	59.485	191,068	27,712	410	59.49

Table 4-5: Mechanical properties of CFRP composite and putty considered in FE model

Property	Component		HM CFRP	IM CFRP	LM CFRP	Putty
Young's Modulus	E_x	MPa (ksi)	47,400 (6,869)	41,000 (5945)	24,800 (3,592)	76 (11)
	E_y, E_z		33,000 (4,784)	33,000 (4,784)	33,000 (4,784)	
Shear Modulus	G_{xy}		18,600 (2,696)	15,600 (2,264)	9,300 (1,345)	24,900 (3,612)
	G_{yz}, G_{xy}		15,700 (2,278)	15,700 (2,278)	15,700 (2,278)	
Poisson's Ratio	υ_{xy}		0.274	0.313	0.335	0.05
	υ_{yz}, υ_{xy}		0.05	0.05	0.05	

4.2.1.2 ***Elements Type***

3D 20-node second order structural solid element (SOLID186), shown in Figure 4-16, was used to model all steel plate, steel frame and bolts. SOLID186 is a higher order element that exhibit quadratic displacement behavior. Each node in 3D solid element has three translational degrees of freedom in x, y, and z directions. The element supports plasticity, stress stiffening, large deflection, and large strain capabilities. The element can be used to orient the material properties and stress/strain output [62]. SOLID elements were used for modeling the bolts and the nuts which simplifies defining the surfaces of the contacts elements.

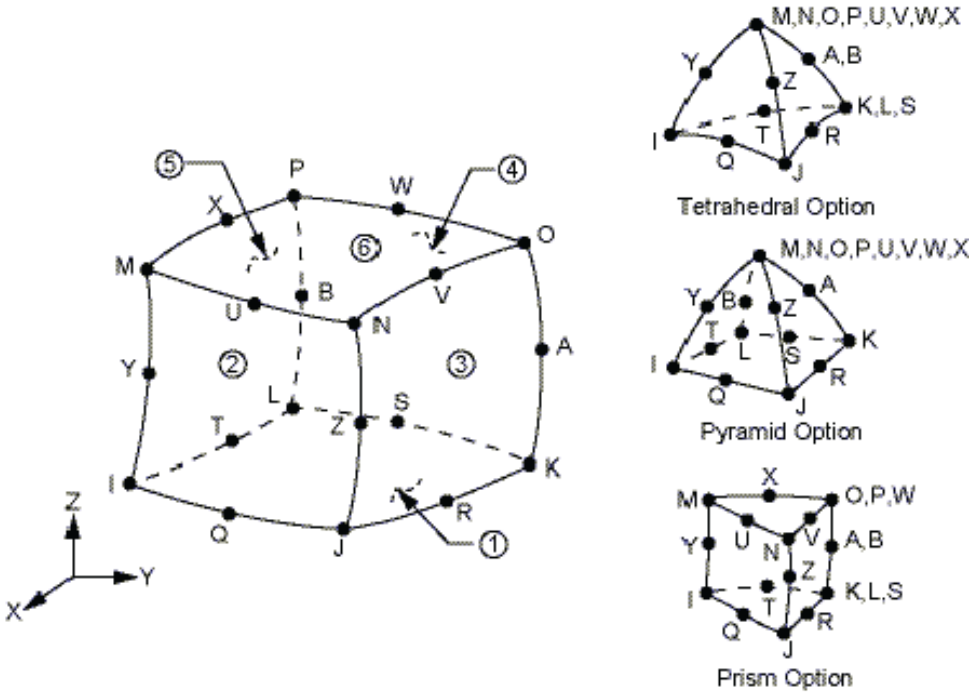

Figure 4-16: 3D 20-node SOLID186 element [62]

4.2.1.3 ***Loading and Boundary Conditions***

Boundary conditions used were compatible to the actual boundaries used in the experiments as shown in Figure 4-17. Bolts and nuts were modeled. Very large number of contact elements was used in the model. A frictional contact element with friction coefficient of 0.15 was used between all steel pieces that are in touch. The two faces of the frictional contact elements are free to separate; however, when they are in contact, they will slide when the shear stress between them exceeds a critical shear stress. Using frictional contact elements between bolts and test plate was used to simulate the edge bearing observed from the tests. Nuts were bonded to the bolts using bonded contact elements. Bonded contacts couple faces together in their tangential direction and normal direction. Since no sign of CFRP de-bonding was observed in the test, layers of CFRP material and test plate were coupled using bonded contact elements.

The top pin was given displacement upward. Bottom pin was assigned as a fixed support. Left and right pins were allowed to have in-plane translations. All the elements except the test plate and CFRP layers were restrained from any out-of-plane translations. To count on the geometrical nonlinearities, large deflection analyses were considered. The effect of bolts pre-tensioning was neglected due to observed bearing effects on the holes. The edge bearing showed that the shear stress between the frame legs and the test plates exceeded the critical value and sliding occurred at a certain load level.

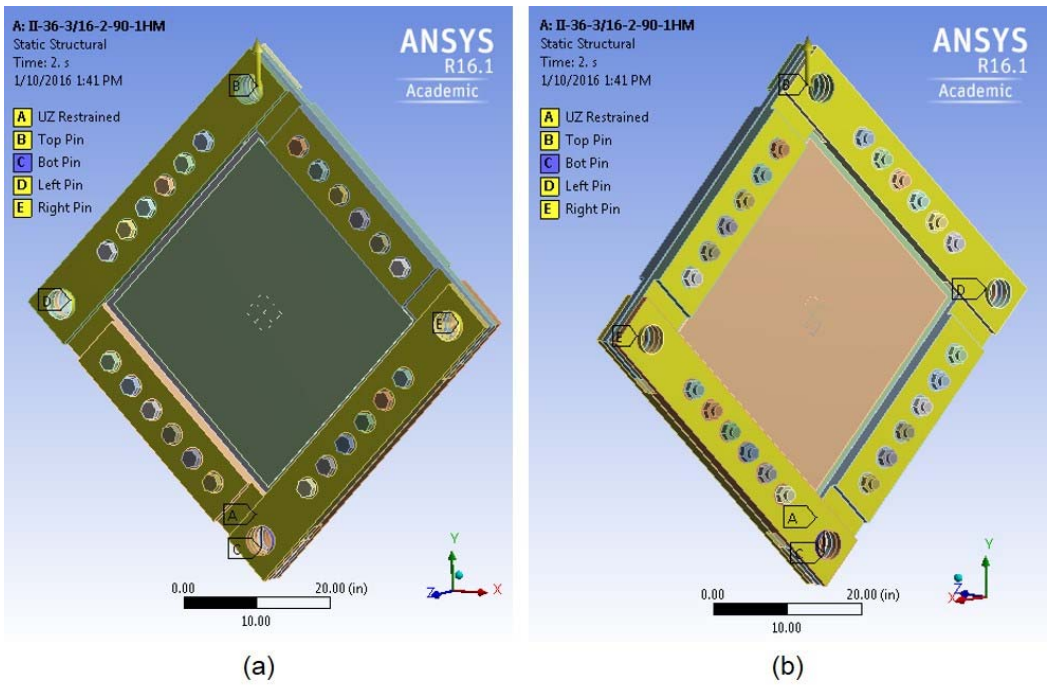

Figure 4-17: Finite element model and the boundary conditions at Phase II for specimen II-36-3/16-2-90-1HM, a) Front face, b) Back face

4.2.1.4 *Geometric imperfections*

Based on the measured initial imperfections, a simplified shape was assumed by applying small horizontal pressure on the surface of the test plate. The imperfection configuration was two-

way parabolic shape with an apex at mid-point and zero tangent near the edges of the frame as shown in Figure 4-18. The applied pressure induces a residual stress/strain to be considered in the analysis.

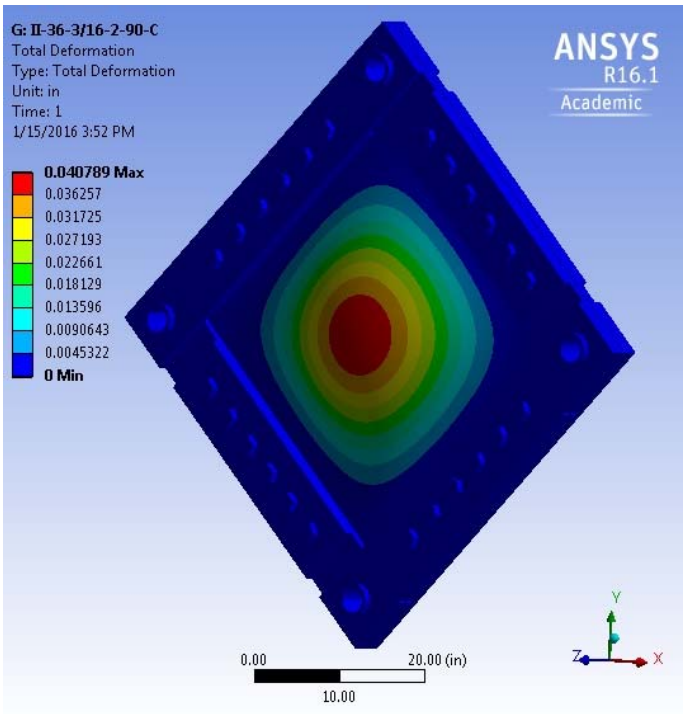

Figure 4-18: Assumed initial imperfection as a two-way parabolic curve, control specimen II-36-3/16-2-90-C

4.2.1.5 ***Mesh Density***

The mesh configuration used for the FE analysis is shown in Figure 4-19. Thickness of the test plate was modeled by two elements through the thickness. Mesh sensitivity analysis was performed using two different mesh sizes. The effect of mesh size on mid-point horizontal steel strain and net lateral deformation of plate strengthened with one layer of HM CFRP from FE analysis are shown in Figure 4-20 and Figure 4-21, respectively. Two different mesh sizes investigated was 25x25 mm (1x1 in.) and 13x13 mm (0.5x0.5 in.). The total number of

elements varied from 139,006 elements to 702,297 elements. The figures show almost identical results, where no change in the behavior is occurred by refining the mesh size. However, using small number of elements reduced dramatically the computation time for the analysis. Therefore mesh size of 25x25 mm (1x1 in.) was used in the remaining analyses.

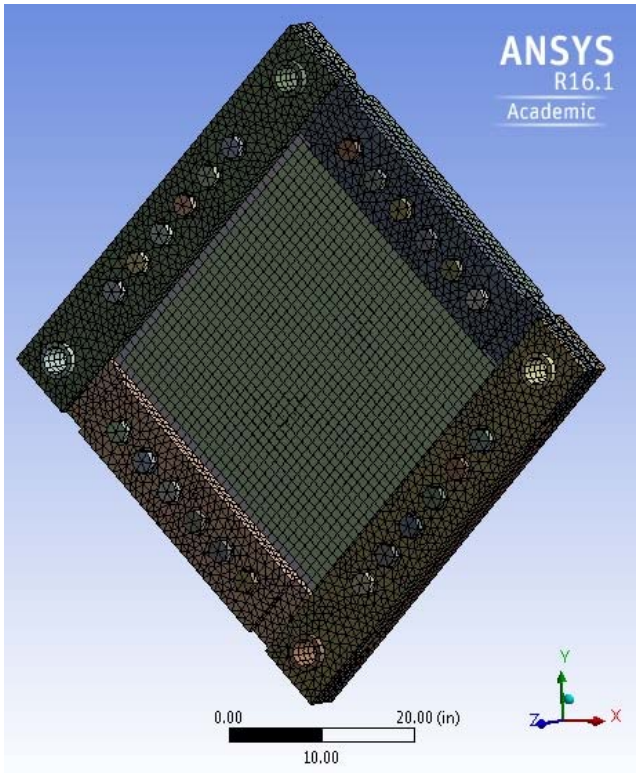

Figure 4-19: Mesh configuration used for specimen II-36-3/16-1-45-1HM (25x25 mm (1x1 in.))

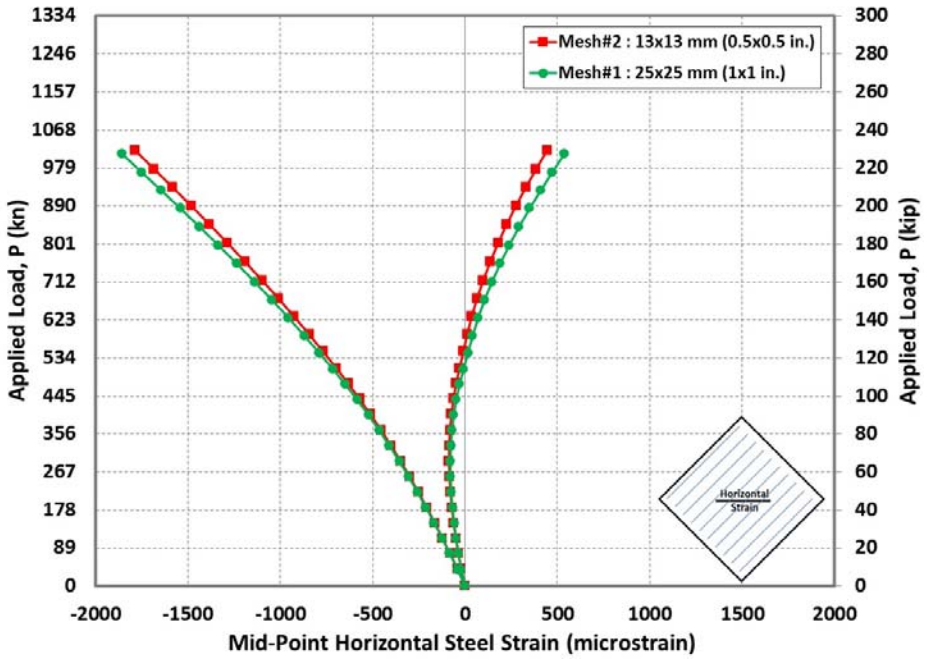

Figure 4-20: Applied load vs. horizontal steel strain at mid-point of a specimen II-36-3/16-1-45-1HM to show effect of mesh size on finite element results

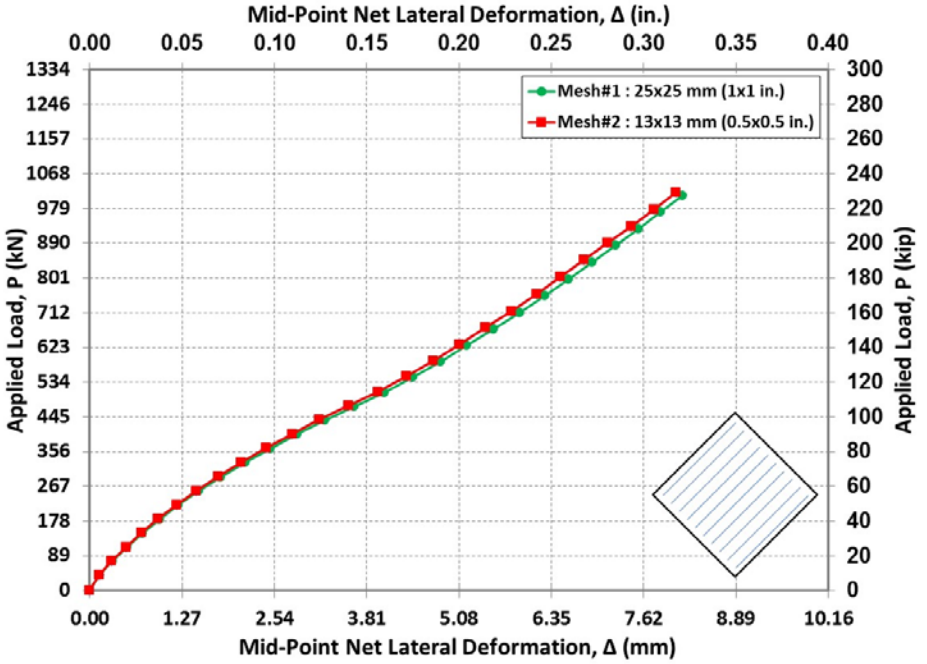

Figure 4-21: Applied load vs. net lateral deformation at mid-point of a specimen II-36-3/16-1-45-1HM to show effect of mesh size on finite element results

4.2.2 Calibration of the FE Model

Typical deformation of the test shear panel predicted by the FE model and the observed deformations are shown in Figure 4-22 (a) and (b), respectively. The two figures show successful simulation of the observed deformation. The equivalent elastic strain contours are plotted in Figure 4-23. Deformation of the outer frame acted in as a scissor and transferred the shear stresses to the plate. Maximum lateral deformation was detected at the mid-point of the plate. FE shows deformed a shape in the form of full wavelength cosine and half wavelength sine across the horizontal and vertical diagonal of the specimen, respectively, as observed from the test specimens.

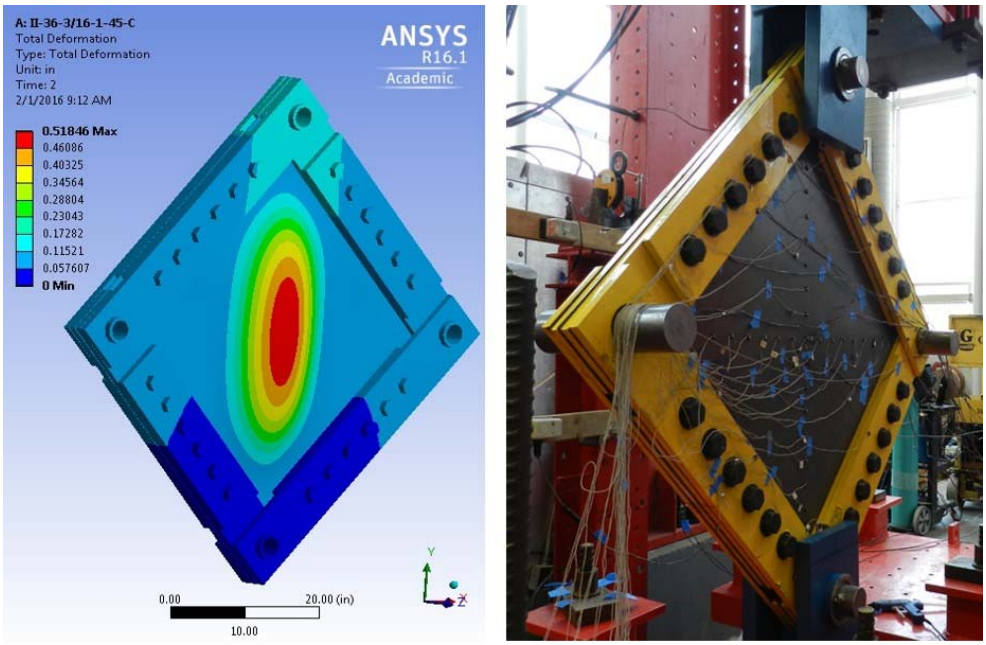

Figure 4-22: Total deformation of the specimen II-36-3/16-1-45-C, a) FE model, b) Experiment

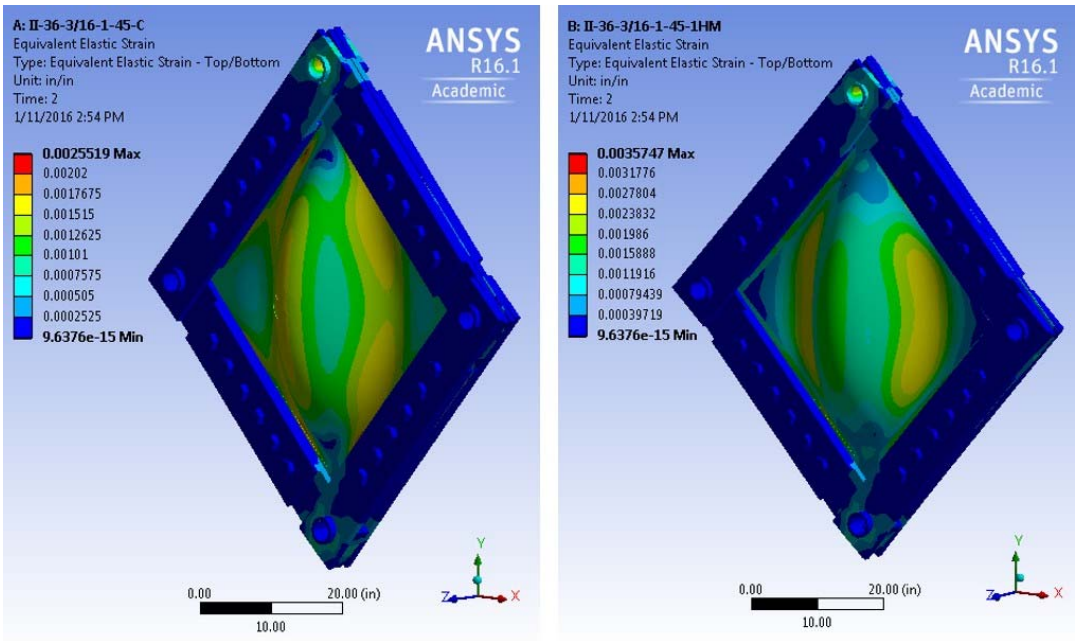

(a) (b)

Figure 4-23:a) Equivalent elastic steel strain for specimen II-36-3/16-1-45-C, b) Equivalent elastic CFRP strain for specimen II-36-3/16-1-45-1HM (Scale Factor: 20)

All tested specimens were modeled and the imperfection values were calibrated by comparing the overall behavior to the measured net lateral deformation and horizontal mid-point steel strain. Imperfection values resulted from FE analyses are given in Table 4-6. The imperfection values are scattered similar to what was observed from the measurement values.

Table 4-6: Predicted imperfection values obtained from FE analyses

Specimen ID	Strengthening Layer	Imperfection Value from Calibration, δ	
		(in.)	(mm)
II-36-3/16-1-45-C	0	0.05	1.2
II-36-3/16-2-90-C		0.04	1.0
II-36-3/16-3-45W-C		0.04	1.1
II-36-3/16-1-45-1HM	1	0.06	1.4
II-36-3/16-2-90-1HM		0.22	5.5
II-36-3/16-3-45W-1HM		0.17	4.2
II-36-3/16-1-45-2HM	2	0.14	3.6
II-36-3/16-2-90-2HM		0.15	3.9
II-36-3/16-3-45W-2HM		0.34	8.7
AVG		**0.13**	**3.4**

The full responses of load vs horizontal steel strains and net lateral deformation at mid-point, were predicted and compared to the experimental results. Initial models showed non-convergence agreement between the experimental measurements and FE predictions. Detailed investigation of the behavior indicated that some of the bolts were initially in bearing contacts with the plate and frame holes while other bolts were not in touch with holes walls. This behavior confirmed by the measured low lateral stiffness in comparison to the FE assuming no imperfection and bearing of all bolts. The high horizontal stresses are induced by initially contacted bolts which were located closer to the mid-height of the plate. As a result, mid-height bolts transferred the shear forces to the steel plate and induced high bending effects on the area

around mid-point. Therefore, the models assumed an initial bearing contacts for 12 bolts at mid-height and produced a small gap between the rest of the bolts and holes walls. Using this assumption provided a reasonable agreement between the FE results and measured data. FE predictions of all specimens were compared by measured data and are presented in Figure 4-24 through Figure 4-26 for the plates strengthened with CFRP strands with an angle of 45^{o}, 90^{o} and ±45^{o}, respectively. The general trend of the curves are captured and were in good agreement with the measured values. Similar to experimental tests, results of FE element confirm the effectiveness of the externally bonded CFRP strands in increasing the shear capacity of the steel plate. Also, strengthening system increased lateral and axial stiffness for each additional layer of CFRP strengthening. The FE results indicate close prediction of the percentage increases in the shear capacities compared to the measured data. However, discrepancy between the predictions and measurements can be attributed to imperfections of the tested plates which is different from the assumption used and inadequate bearing of the bolts to the holes. Consequently, FE model could build enough confidence to be used as a tool in the parametric studies with the assumed boundary conditions.

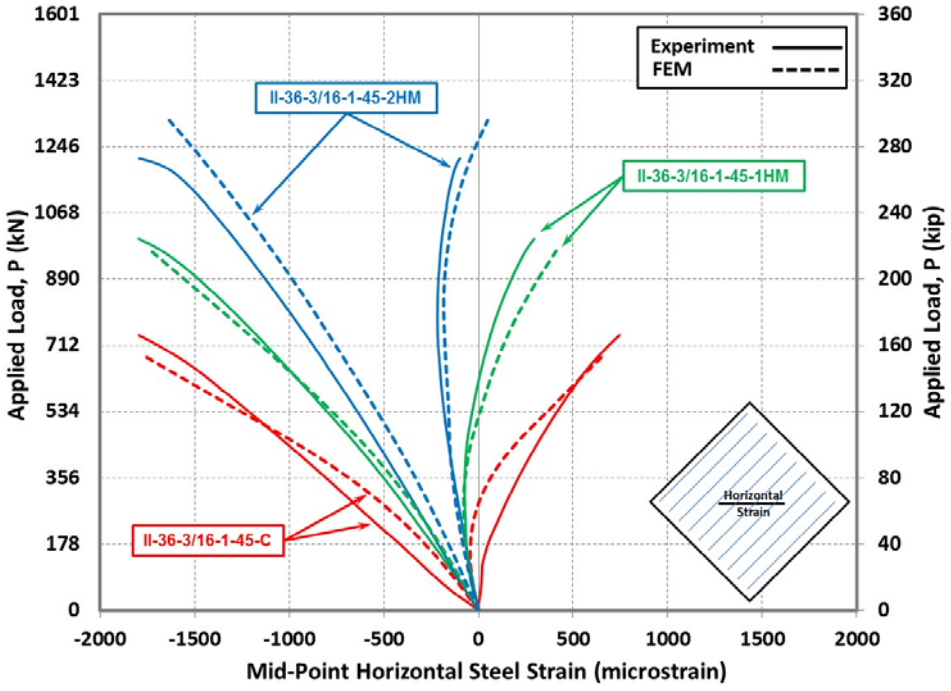

(a)

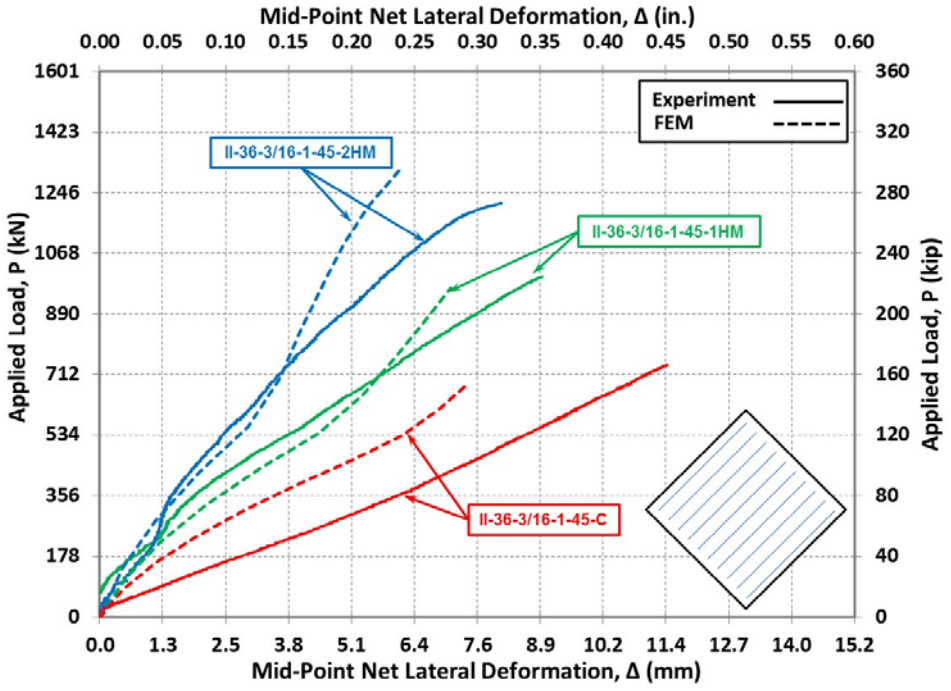

(b)

Figure 4-24: Comparison between experimental results and FE predictions at mid-point of set #1 specimens; applied load vs. a) horizontal steel strain, b)net lateral deformation

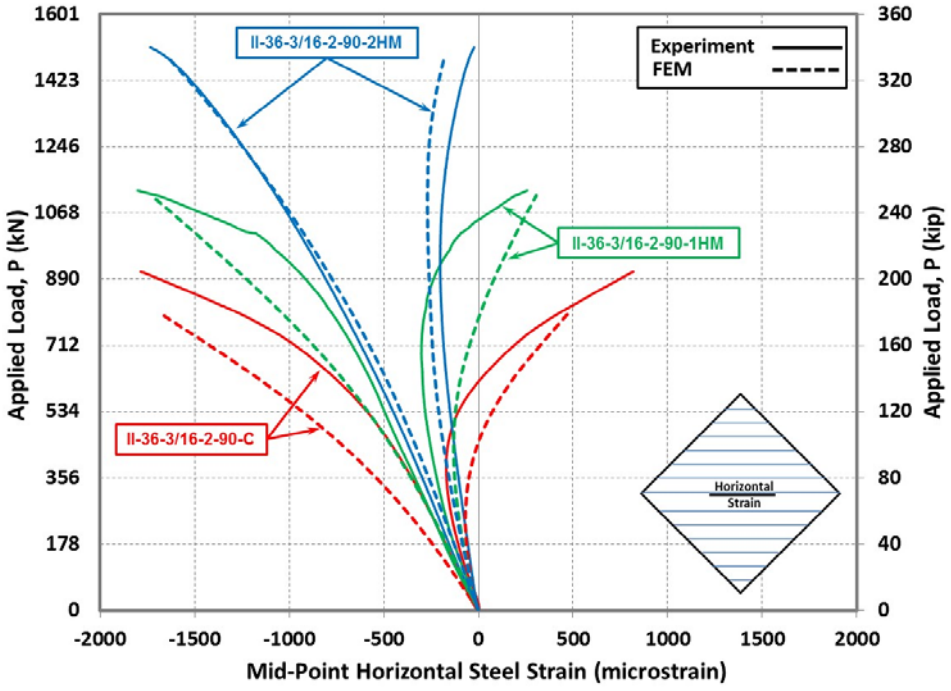

(a)

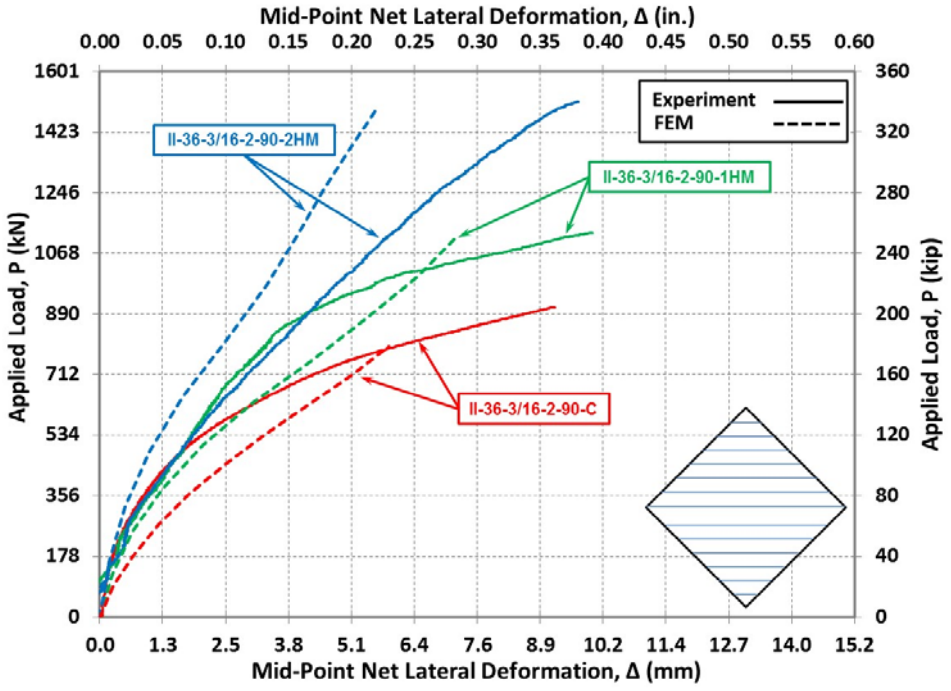

(b)

Figure 4-25: Comparison between experimental results and FE predictions at mid-point of set #2 specimens; applied load vs. a) horizontal steel strain, b)net lateral deformation

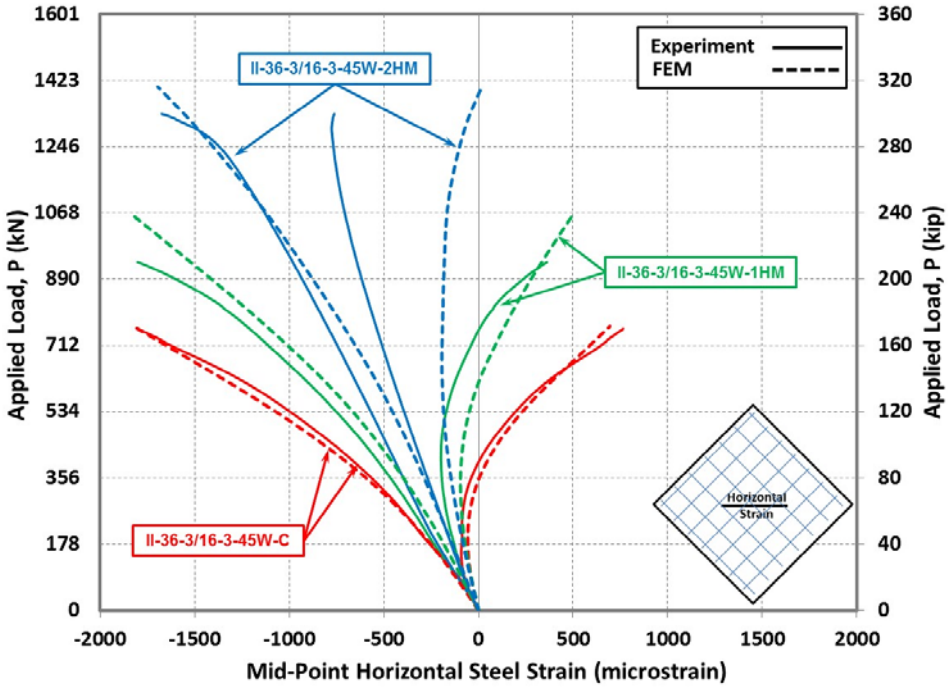

(a)

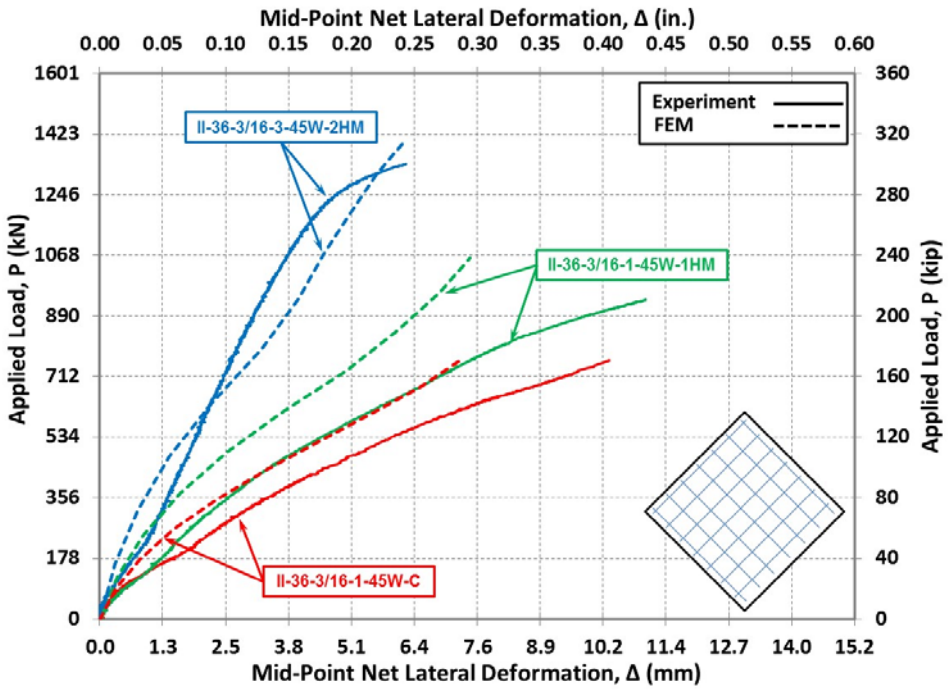

(b)

Figure 4-26: Comparison between experimental results and FE predictions at mid-point of set #3 specimens; applied load vs. a) horizontal steel strain, b)net lateral deformation

5 PARAMETRIC STUDIES

This chapter presents the use of the developed FE model is to study the effect of different parameters which were not considered in experimental program and are believed to influence the behavior of CFRP strengthening system. The FE model is used also as a tool to develop the appropriate design guideline for the proposed strengthening system. The following sections present results of the parametric studies which were considered for uniaxial compressive and shear loading conditions of the steel plates and used for formulation of the design guidelines.

5.1 PHASE I: UNIAXIAL COMPRESSIVE STRENGTHENING

The developed FE model was used to perform parametric study to evaluate the effects of the following parameters:

1. Boundary conditions.
2. Reinforcement ratio.
3. Slenderness ratio.
4. Elastic modulus of the CFRP strengthening material.

A total of 120 control and strengthened specimens with height of 915 mm (36 in.) and width of 510 mm (20 in.) were used in the nonlinear analysis. Two boundary conditions were used including pin-pin and fix-fix end conditions. Effect of reinforcement ratio was studied using one, two, and three layers of the CFRP strands. The plate thicknesses were varied from 6 mm (1/4 in.) to 19 mm (3/4 in.) covering a wide range of slenderness ratio ranging from 48 to 144. Three different elastic moduli were investigated, HM, IM and LM. The steel material was

idealized as a perfectly-plastic Grade 50 as shown in Figure 5-1 and was defined in ANSYS as Bilinear Isotropic Hardening material having no strain hardening after yielding. Mechanical properties used for CFRP composite and polyurea putty are used from Table 4-2 in Chapter 4. The CFRP composites were defined as Orthotropic Elasticity material and Pulyurea putty was defined as Isotropic-Elastic material. The value of out-of-straightness imperfection at mid-height of specimens was set to the calibrated value of 2 mm (0.08 in.) estimated from the experimental program.

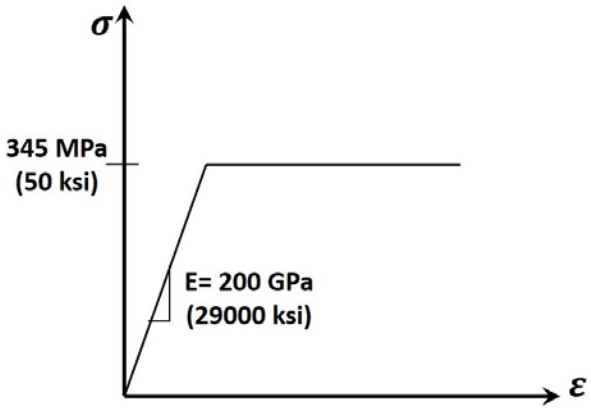

Figure 5-1: Stress-strain curve for the steel material used for parametric study of Phase I

Deflected shapes and stress contours distributed along the plate obtained from the FE model for two sample control plates with slenderness ratio of 48 using pin-pin and fix-fix end conditions are shown in Figure 5-2 and Figure 5-3 at the onset of buckling. The analyses clearly indicate that both plates experienced inelastic buckling where buckling occurred after the yielding of the steel. Generally, the pined end plates yield at mid-height; while, the fixed end plates yield at the mid-height and at fixed ends.

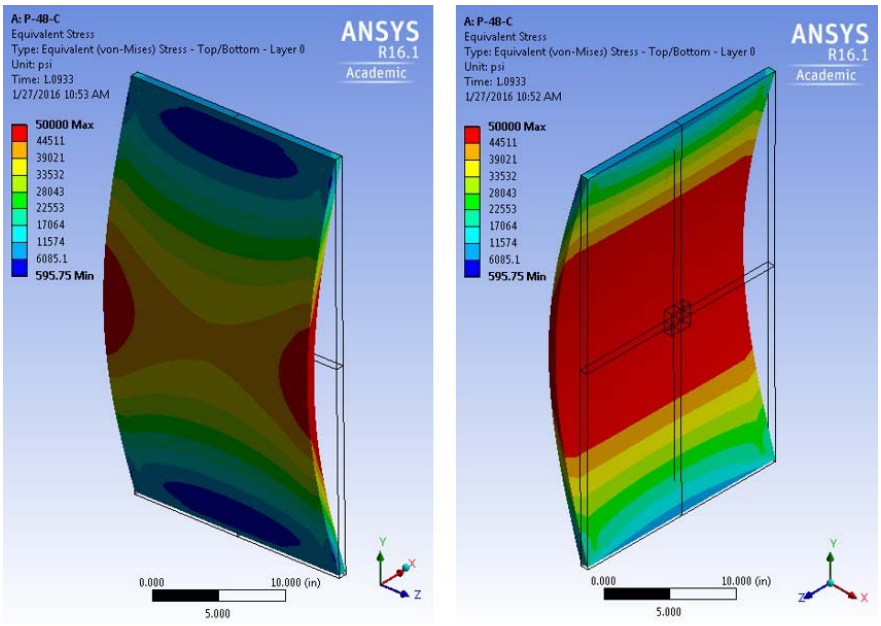

(a) (b)

Figure 5-2: Equivalent steel stress at buckling for pined end control specimen with slenderness ratio of 48, a) Front face , b) Back face

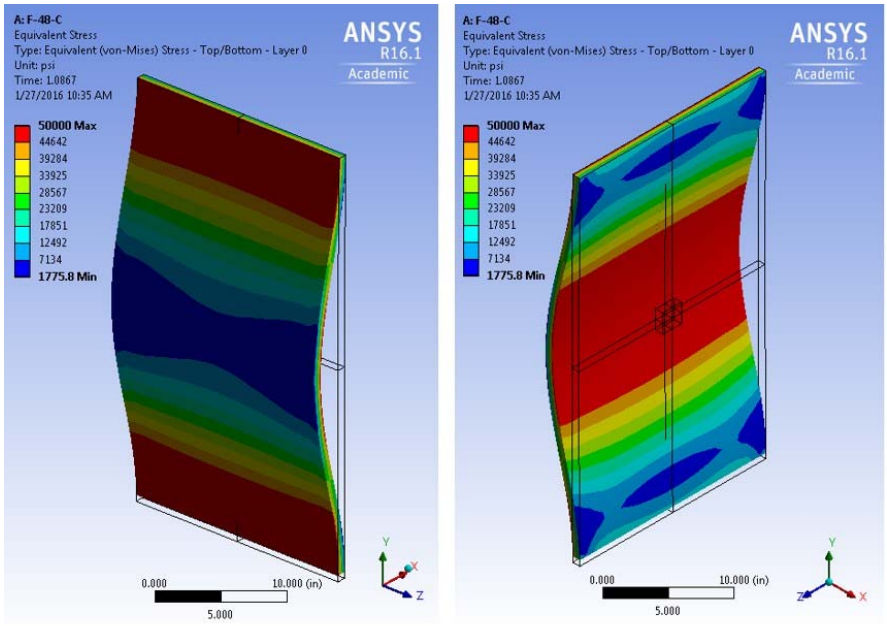

(a) (b)

Figure 5-3: Equivalent steel stress at buckling for fixed end control specimen with slenderness ratio of 48, a) Front face , b) Back face

Results of the analyses for the predicted buckling loads are given in Table 5-1 through Table 5-3 for the plates strengthened by HM, IM, and LM CFRP strands, respectively. The specimens in these tables are identified as follows. The first letter of specimen ID represents type of boundary condition, i.e., “P” is referred as pined ends condition and “F” is referred as fixed ends condition. The second number specifies the slenderness ratio of the plate. The last letter shows the strengthening condition. For the control plates, letter “C” is used. For the strengthened plate, number of layers at each face, followed by type of CFRP material are given, for example, “F-72-2HM” describes a strengthened plate fixed at both ends having a slenderness ratio of 72, strengthened by two layers of HM CFRP strands at each face.

Table 5-1: Predicted buckling load for steel plates strengthened with HM CFRP

Pin-Pin End Condition				Fix-Fix End Condition			
Specimen ID	Buckling Load			Specimen ID	Buckling Load		
	kN	kip	Ratio		kN	kip	Ratio
P-48-C	614	138	1.00	F-48-C	2062	464	1.00
P-48-1HM	774	174	1.26	F-48-1HM	2342	527	1.14
P-48-2HM	996	224	1.62	F-48-2HM	2924	657	1.42
P-48-3HM	1290	290	2.10	F-48-3HM	3706	833	1.80
P-58-C	369	83	1.00	F-58-C	1326	298	1.00
P-58-1HM	494	111	1.34	F-58-1HM	1628	366	1.23
P-58-2HM	681	153	1.84	F-58-2HM	2088	470	1.57
P-58-3HM	930	209	2.52	F-58-3HM	2789	627	2.10
P-72-C	196	44	1.00	F-72-C	735	165	1.00
P-72-1HM	289	65	1.48	F-72-1HM	1009	227	1.37
P-72-2HM	436	98	2.23	F-72-2HM	1399	315	1.90
P-72-3HM	649	146	3.32	F-72-3HM	1975	444	2.69
P-96-C	85	19	1.00	F-96-C	329	74	1.00
P-96-1HM	151	34	1.79	F-96-1HM	540	121	1.64
P-96-2HM	262	59	3.11	F-96-2HM	860	193	2.62
P-96-3HM	436	98	5.16	F-96-3HM	1332	300	4.05
P-115-C	49	11	1.00	F-115-C	195	44	1.00
P-115-1HM	102	23	2.09	F-115-1HM	370	83	1.89
P-115-2HM	200	45	4.09	F-115-2HM	653	147	3.34
P-115-3HM	351	79	7.18	F-115-3HM	1079	243	5.52
P-144C	27	6	1.00	F-144-C	103	23	1.00
P-144-1HM	67	15	2.50	F-144-1HM	241	54	2.35
P-144-2HM	147	33	5.50	F-144-2HM	487	109	4.75
P-144-3HM	285	64	10.67	F-144-3HM	869	195	8.47

Table 5-2: Predicted buckling load for steel plates strengthened with IM CFRP

Pin-Pin End Condition				Fix-Fix End Condition			
Specimen ID	Buckling Load			Specimen ID	Buckling Load		
	kN	kip	Ratio		kN	kip	Ratio
P-48-C	616	138	1.00	F-48-C	2062	464	1.00
P-48-1IM	752	169	1.22	F-48-1IM	2300	517	1.12
P-48-2IM	948	213	1.54	F-48-2IM	2787	627	1.35
P-48-3IM	1206	271	1.96	F-48-3IM	3476	781	1.69
P-58-C	368	83	1.00	F-58-C	1326	298	1.00
P-58-1IM	477	107	1.30	F-58-1IM	1582	356	1.19
P-58-2IM	640	144	1.74	F-58-2IM	1990	447	1.50
P-58-3IM	862	194	2.34	F-58-3IM	2616	588	1.97
P-72-C	195	44	1.00	F-72-C	735	165	1.00
P-72-1IM	277	62	1.42	F-72-1IM	973	219	1.32
P-72-2IM	407	91	2.08	F-72-2IM	1325	298	1.80
P-72-3IM	593	133	3.04	F-72-3IM	1839	413	2.50
P-96-C	85	19	1.00	F-96-C	329	74	1.00
P-96-1IM	142	32	1.66	F-96-1IM	515	116	1.57
P-96-2IM	241	54	2.82	F-96-2IM	803	181	2.44
P-96-3IM	393	88	4.59	F-96-3IM	1230	277	3.74
P-115-C	50	11	1.00	F-115-C	195	44	1.00
P-115-1IM	96	22	1.90	F-115-1IM	349	79	1.79
P-115-2IM	181	41	3.58	F-115-2IM	604	136	3.09
P-115-3IM	316	71	6.27	F-115-3IM	991	223	5.07
P-144C	27	6	1.00	F-144-C	103	23	1.00
P-144-1IM	62	14	2.29	F-144-1IM	225	51	2.19
P-144-2IM	133	30	4.96	F-144-2IM	445	100	4.34
P-144-3IM	253	57	9.41	F-144-3IM	794	178	7.74

Table 5-3: Predicted buckling load for steel plates strengthened with LM CFRP

Pin-Pin End Condition				Fix-Fix End Condition			
Specimen ID	Buckling Load			Specimen ID	Buckling Load		
	kN	kip	Ratio		kN	kip	Ratio
P-48-C	616	138	1.00	F-48-C	2062	464	1.00
P-48-1LM	697	157	1.13	F-48-1LM	2162	486	1.05
P-48-2LM	821	185	1.33	F-48-2LM	2452	551	1.19
P-48-3LM	984	221	1.60	F-48-3LM	2894	651	1.40
P-58-C	368	83	1.00	F-58-C	1326	298	1.00
P-58-1LM	434	98	1.18	F-58-1LM	1478	332	1.11
P-58-2LM	536	121	1.46	F-58-2LM	1737	391	1.31
P-58-3LM	678	152	1.84	F-58-3LM	2103	473	1.59
P-72-C	195	44	1.00	F-72-C	735	165	1.00
P-72-1LM	245	55	1.26	F-72-1LM	884	199	1.20
P-72-2LM	326	73	1.67	F-72-2LM	1119	252	1.52
P-72-3LM	445	100	2.28	F-72-3LM	1443	324	1.96
P-96-C	85	19	1.00	F-96-C	329	74	1.00
P-96-1LM	120	27	1.41	F-96-1LM	447	101	1.36
P-96-2LM	182	41	2.13	F-96-2LM	643	145	1.96
P-96-3LM	279	63	3.26	F-96-3LM	927	208	2.82
P-115-C	50	11	1.00	F-115-C	195	44	1.00
P-115-1LM	78	18	1.55	F-115-1LM	293	66	1.50
P-115-2LM	131	30	2.61	F-115-2LM	466	105	2.38
P-115-3LM	217	49	4.31	F-115-3LM	728	164	3.73
P-144C	27	6	1.00	F-144-C	103	23	1.00
P-144-1LM	48	11	1.79	F-144-1LM	181	41	1.76
P-144-2LM	93	21	3.45	F-144-2LM	329	74	3.21
P-144-3LM	168	38	6.26	F-144-3LM	568	128	5.54

Figure 5-6 through Figure 5-4 show the predicted buckling load ratio vs slenderness ratio of the steel plates strengthened by LM, IM, and HM CFRP strands, respectively. Each figure shows results of three reinforcement ratio for pinned and fixed end conditions. These figures can be used as a design tool to estimate the number of CFRP layers needed for required strengthening level. It should be noted the shown increase in the buckling capacity exceeds the realistic values needed for typical projects, however, the higher strengthening ratio are provided for the cases of severe corrosion where the thickness of the web significantly reduced. As a plate strengthening designer, for instance, to strengthen a pin ended steel plate with

slenderness ratio of 130 and there is a need to increase the buckling capacity four times, different strengthening scenarios may be used such as two layers of HM CFRP or three layers of IM CFRP or LM CFRP.

Results confirm that the effectiveness of CFRP strengthening system is highly pronounced for the plates with higher slenderness ratio, as observed in experimental program. This behavior is highly attributed to significant increase of the stiffness of the strengthened specimens in comparison to the control specimens for larger slenderness ratio. In terms of reinforcement ratio, increase in number of CFRP layers has a direct influence on increasing the buckling load. One layer of CFRP strand can increase the buckling capacity up to two times. Two layers can increase the buckling capacity up to five times. Since the failure is not governed by rupture or de-bonding of the material, adding number of layers of strengthening system increase the section stiffness and results in higher buckling capacity. Results also indicate that effect of strengthening system using one layer of CFRP strands is almost identical for different the two end conditions considered in this study. However, effectiveness of the strengthening system is more pronounced for the pined end conditions by adding more layers of CFRP material. Therefore, increase of buckling load ratio is enhanced using higher effective length factor (K). For example, having HM CFRP material and slenderness ratio of 144, the buckling load ratio increased from 4.75 to 5.5 for two layers of CFRP strands and from 8.5 to 10.6 for three layers of CFRP strands.

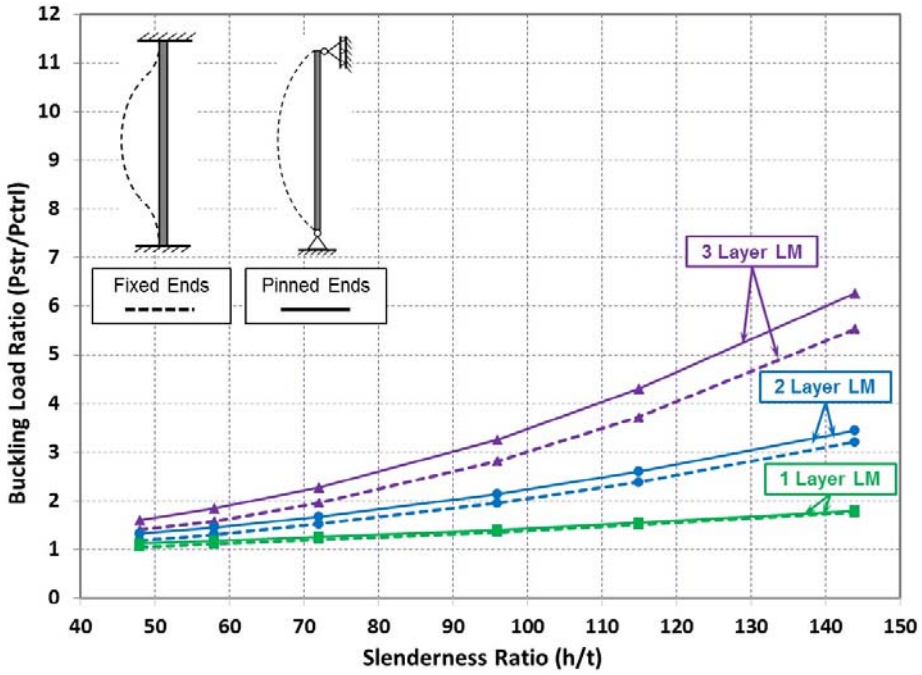

Figure 5-4: Buckling load ratio vs slenderness ratio of steel plates strengthened with LM CFRP

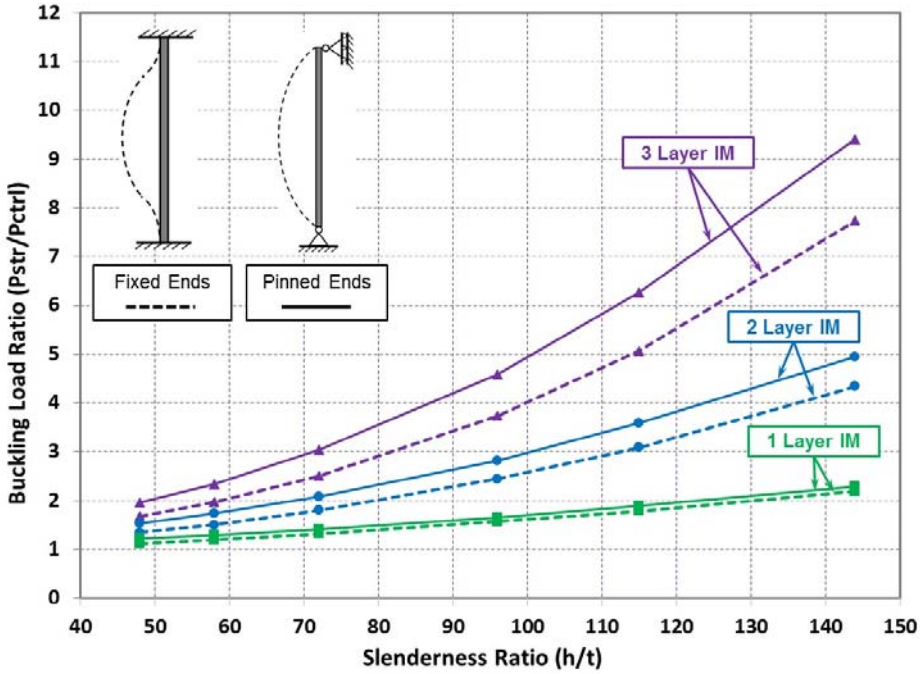

Figure 5-5: Buckling load ratio vs slenderness ratio of steel plates strengthened with IM CFRP

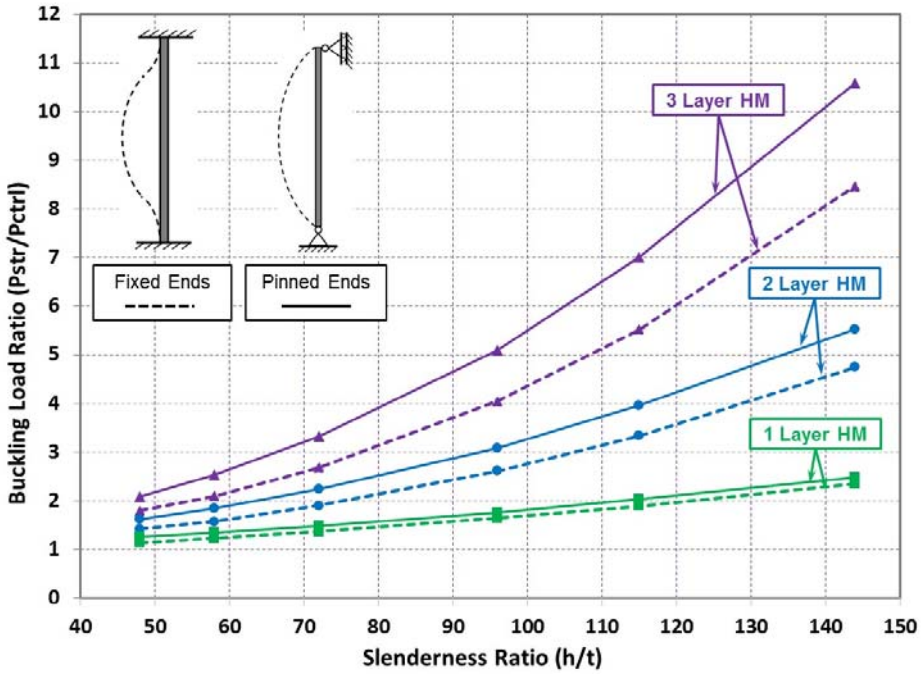

Figure 5-6: Buckling load ratio vs slenderness ratio of steel plates strengthened with HM CFRP

Effects of the elastic modulus of the CFRP material are presented in Figure 5-7 and Figure 5-8 for pinned end and fixed end conditions, respectively. Results indicate that HM CFRP is more effective for strengthening steel plates regardless to any end conditions, slenderness ratio and reinforcement ratio. This behavior is attributed to the fact that the buckling is a stiffness based problem, a CFRP material with higher elastic modulus results in higher compressive capacity.

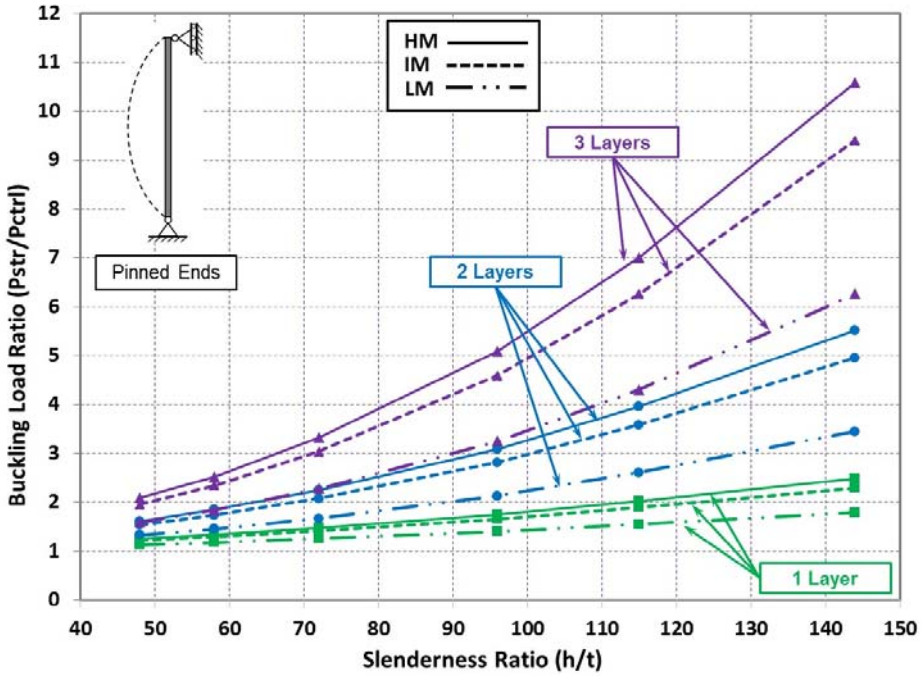

Figure 5-7: Buckling load ratio vs slenderness ratio of pinned end strengthened plates

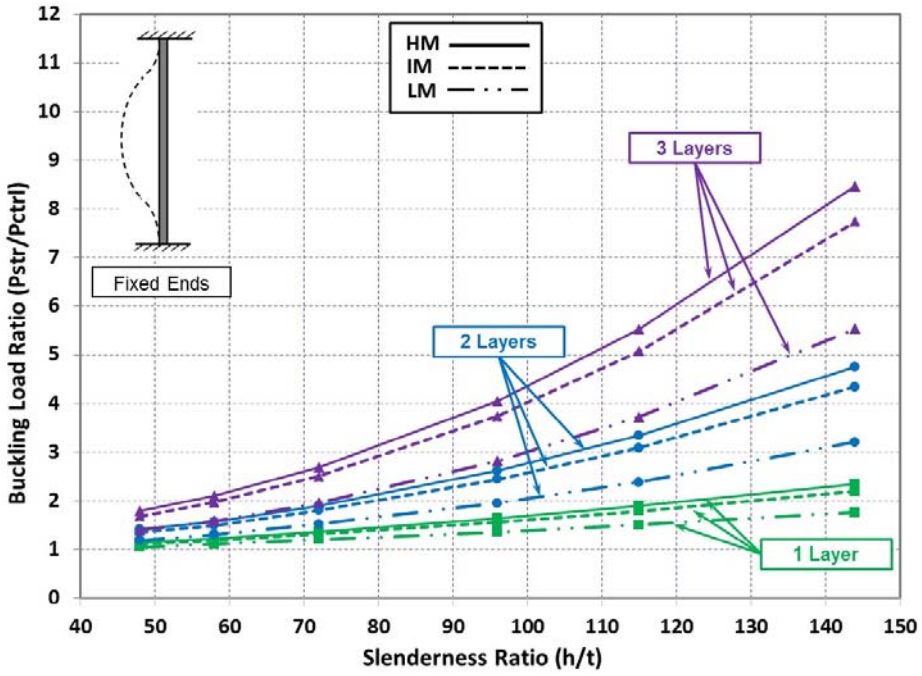

Figure 5-8: Buckling load ratio vs slenderness ratio of fixed end strengthened plates

5.1.1 Simple Analytical Approach

In this section, the theoretical buckling loads were determined using Euler buckling equations for steel columns. Since the steel and the CFRP strengthening system have different material properties, the transformed section method was used to determine the elastic buckling observed by the tested specimens. Use of the transferred section is due to the observed excellent perfect bond of the strengthening system to the steel substrate. The buckling load, P_{cr}, for each tested specimen was estimated using following equations,

$$P_{cr} = \frac{\pi^2 E_s I_t}{(KL)^2} \quad (1)$$

where,

$$I_t = I_s + \sum_{i=1}^{n} \frac{E_{fi}}{E_s} I_{fi} \quad (2)$$

K is effective buckling length factor, L is the total height of the plate, E_s and E_{fi} are elastic modulus of steel and the compressive elastic modulus of each CFRP layer, respectively. I_t, I_s, and I_{fi} are moment of inertia of the transformed cross-section, moment of inertia of steel, and moment of inertia of each CFRP layer. Compressive elastic modulus of CFRP of the witness panels was used in calculations. Resembling hinge-hinge boundary condition used in the experimental program, the buckling length factor, K, was set to one. The predicted buckling loads are compared to the measured values for all tested specimens, including the control and strengthened plates, as shown in Figure 5-9.

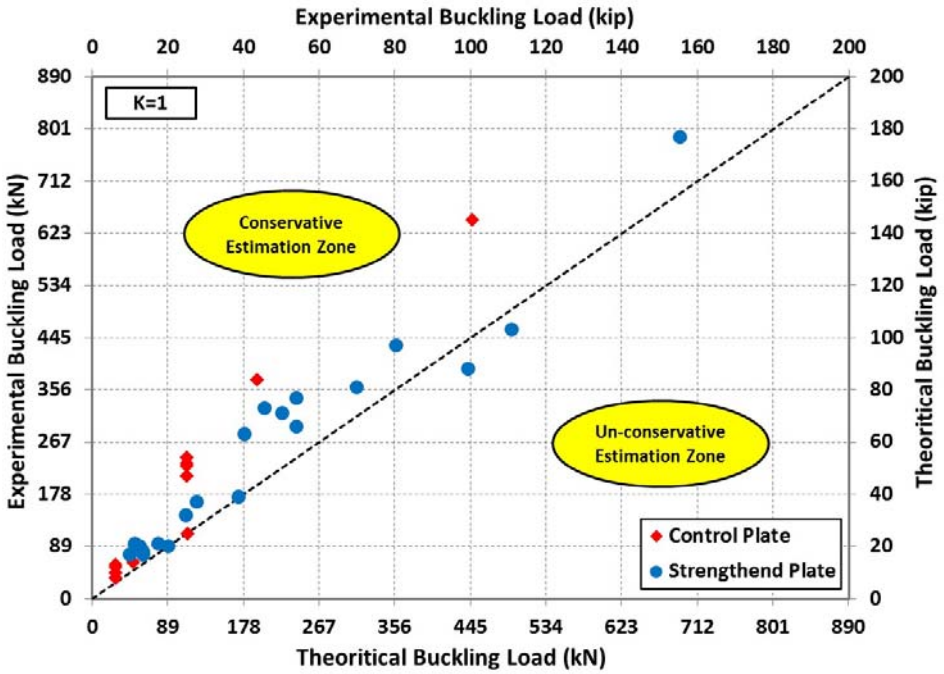

Figure 5-9: Comparison between measured and predicted buckling loads

The comparison shown in Figure 5-9 indicates that the buckling load can be adequately estimated using transformed section properties of the strengthened plate. The comparison could be improved by accounting for the friction between the pins and the sleeves which reduces the buckling length factor, K, and consequently increase the predicted values. For the design, the above analysis indicates that the buckling capacity can be accurately predicted by using the proper boundary conditions and the composite transformed section properties of the strengthened steel plates.

In addition, to have an estimation of the buckling length factors, K, the experimental buckling loads were matched with the predicted buckling loads using transformed section. The calibrated factors predicted for tested control and strengthened specimens are shown in Figure 5-10. Results clearly indicates reduction effects of the friction between the pins and the

sleeves on the buckling length factors. The calibrated values resulted in an average value equal to 0.85 to reproduce the predicted buckling loads and to compare with the measured values for all test specimens, as shown in Figure 5-11. Results show that buckling load predictions are more in agreement when using the reduced buckling length factor. However, for a given boundary condition similar to the experimental program, using pined end assumption with buckling length factor K=1, would end up with a more conservative design of strengthened steel plates.

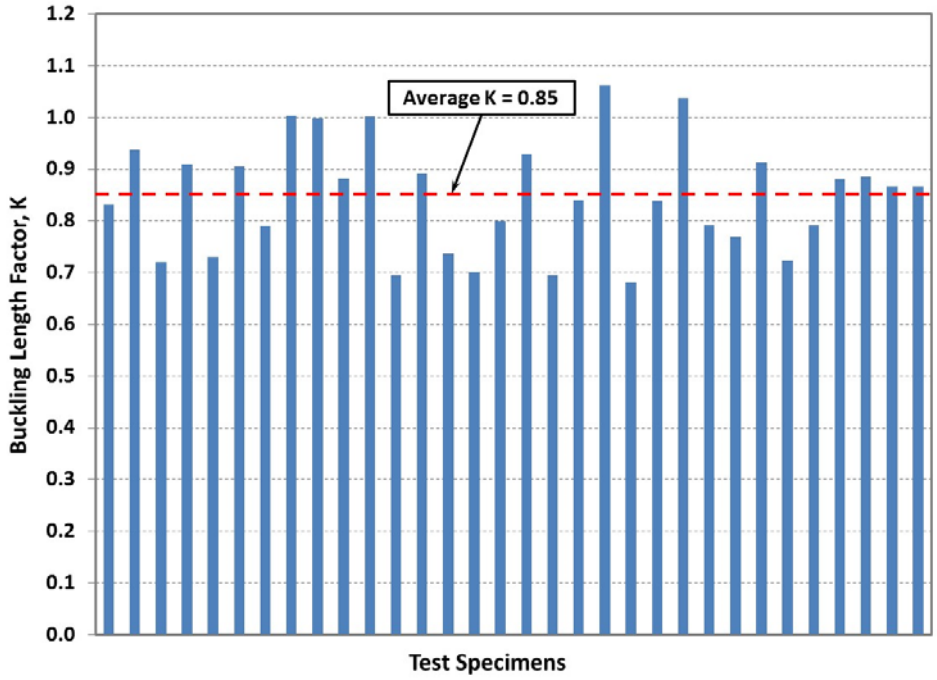

Figure 5-10: effective length factor obtained calibrated from test specimens

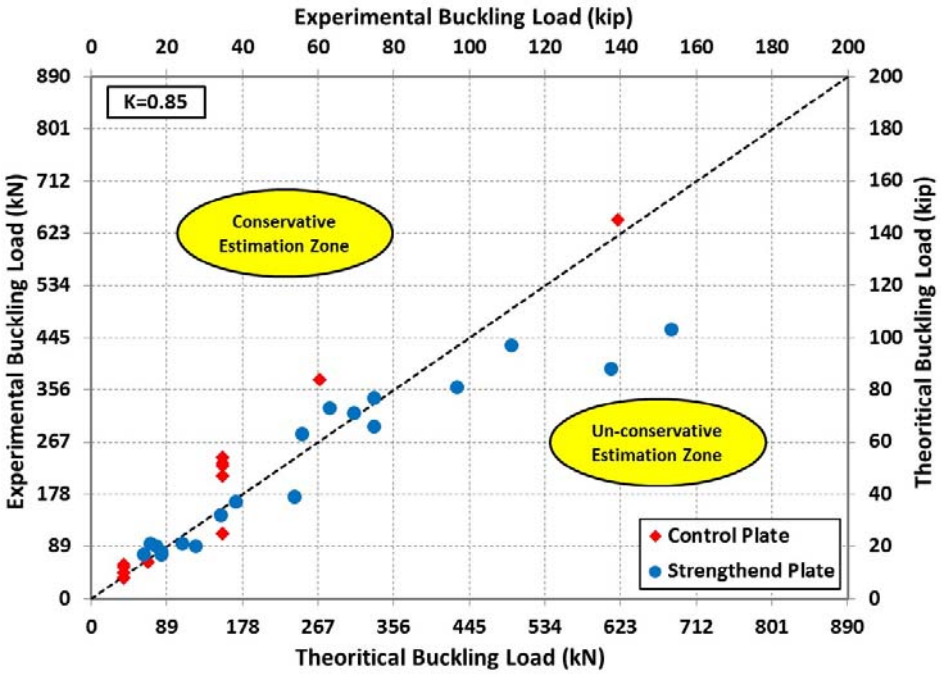

Figure 5-11: Comparison between measured and predicted buckling loads using calibrated average buckling length factor

5.2 PHASE II: SHEAR STRENGTHENING

The developed nonlinear FE model is used to study parameters not included in the experimental program including the following:

1. Behavior of wide range of slenderness ratio ranging from 44 to 192.
2. Behavior of the three CFRP strengthening materials, i.e. HM, IM, and LM under the above parameters.
3. Effect of applying combined tensile vertical and compressive horizontal load.
4. Effect of the orientation of CFRP strand.

A total of 49 square steel plates with dimensions of 915x915 mm (36x36 in.) were considered in the study. The steel material was idealized as a perfectly-plastic Grade 65 as shown in Figure 5-12 and defined in ANSYS as Bilinear Isotropic Hardening material with no strain hardening after yielding.

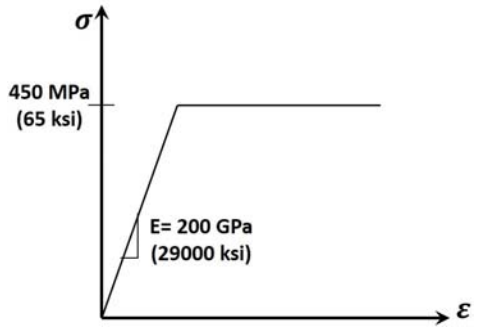

Figure 5-12: Stress-strain curve for the steel material used for Phase II parametric studies

Mechanical properties used for CFRP composite and polyurea putty were determined from Table 4-5 in Chapter 4. The CFRP composites were defined as Orthotropic Elasticity material and polyurea putty was defined as Isotropic Elastic material. The value of out-of-straightness

imperfection at the mid-point of the control and strengthened steel plates was assumed to be the average of the measured imperfections of the control specimens equal to 1 mm (0.04 in.) at the centroid of the plate. It should be noted that using higher values of the imperfections could lead to unreasonable high residual stresses close to plate yielding for plates with low slenderness ratio. To highlight the effectiveness of different parameters on the behavior of the strengthening system, the shear capacities prior to the plate yielding were compared. Bolts were assumed to have initial bearing contacts with the holes.

5.2.1.1 *Effect of Slenderness ratio, Reinforcement Ratio and CFRP Material*

To examine the effects of the slenderness ratio, plate thicknesses were varied from 5 mm (3/16 in.) to 19 mm (3/4 in.) covering a wide range of plate slenderness ratio ranging from 48 to 192. The selected FE model considered the steel plates subjected to diagonal vertical tensile load and CFRP strands with an angle of 45^{o} relative to the vertical tensile loads. Figure 5-13 shows the percentage increase in shear capacity vs slenderness ratio of steel plates strengthened by HM, IM, and LM CFRP strands. Results of two reinforcement ratio including one and two layers of the CFRP strands are compared. Shear capacities are compared at the load level prior to the yielding of the steel plate. Results confirm that the CFRP strengthening system is more effective for the plates with higher slenderness ratio. This behavior can be attributed to the increase in the CFRP to steel plate stiffness ratio for higher slenderness ratio. Reinforcement ratio has also noticeable effects on increase of shear capacity. Percentage increase in shear capacity is almost in direct correlation with increase in reinforcement ratio. For instance, doubling the reinforcement ratio almost doubles the percentage increase of the shear capacity.

The most effective material is confirmed as HM CFRP followed by IM CFRP for the shear strengthening of steel plates regardless to any slenderness ratio and reinforcement ratio. This behavior is attributed to the stiffer behavior of HM CFRP in both tensile and compressive directions compared to other two CFRP materials which results in higher shear capacity. The shown percentage increase of the shear capacity is realistic to the typical values required in practice.

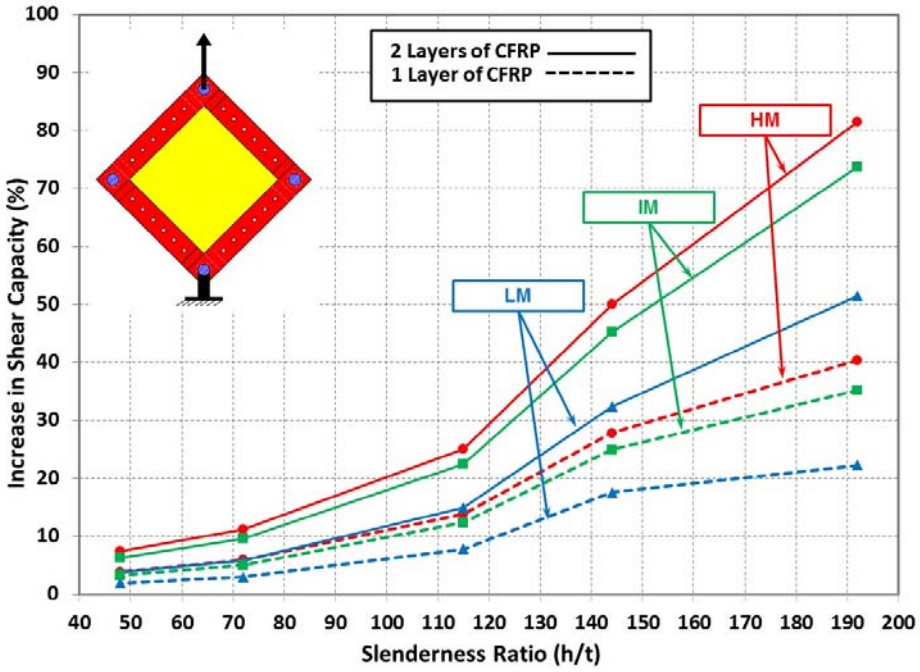

Figure 5-13: Percentage increase in shear capacity vs slenderness ratio of plates strengthened with one and two layers of HM, IM, and LM CFRP strands oriented 45º relative to the vertical tensile load

5.2.1.2 *Effect of the Shear Stress Distribution*

The experimental program simulated pure shear stresses by subjecting the steel plates to diagonal tensile vertical load. However, the state of pure shear may be also obtained by subjecting the steel plates to diagonal vertical tensile and diagonal horizontal compressive

loads, simultaneously. Subjecting the steel plates to the vertical tensile and horizontal compressive loads simultaneously, can distribute the shear stress to more uniform shape along with the plate edges as shown in Figure 5-14 (a). Distribution of shear stress using only diagonal tensile vertical load may become non-uniform as shown in Figure 5-14 (b). Therefore, in this section, the effectiveness of the strengthening system is examined using different shear stress distributions along with the edges of the steel plate.

For both loading conditions, the top pin was given an upward displacement and bottom pin was constraint from the translations and rotations. The right and left pins of the shear panel were subjected to horizontal compressive loads and were allowed to move in two directions. The applied displacements on the right and left pins were one half of the top pin displacement. Both right and left pins were set to move horizontally toward the centroid of the plate.

Induced shear forces, V, along with the steel plate edge was calculated using force components obtained from pins reactions and are schematically shown in Figure 5-15. The shear forces are derived from summation of load components projected to the frame legs.

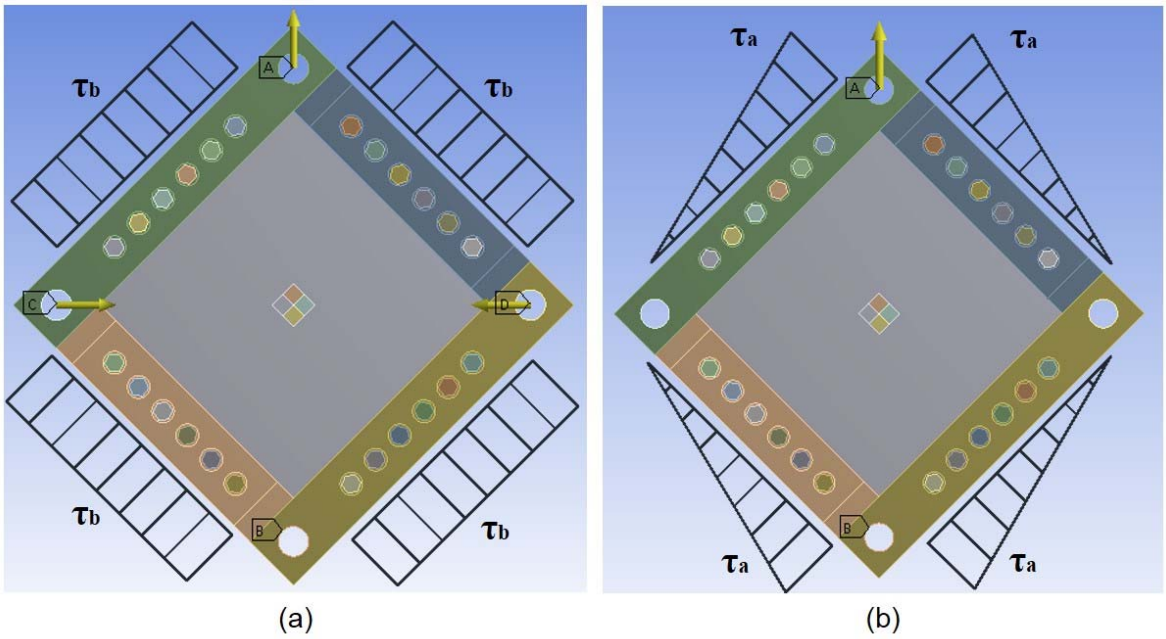

Figure 5-14: Loading conditions to simulate pure shear on steel plate, a) Applied vertical tension and horizontal compression, b) Applied vertical tension only

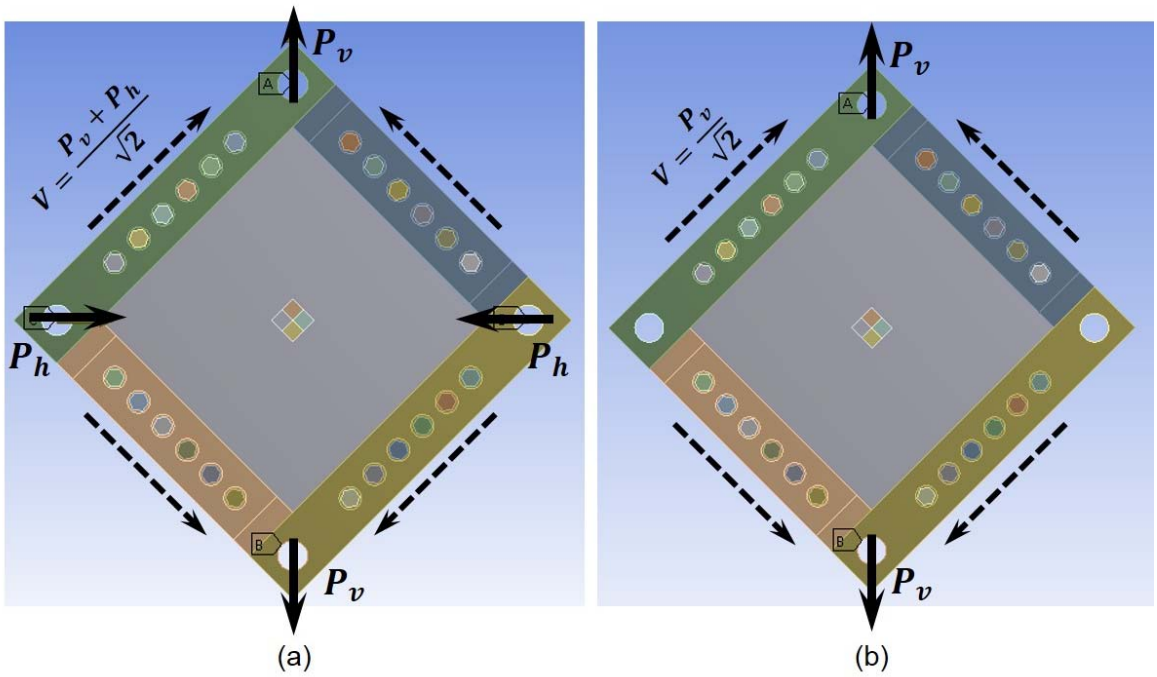

Figure 5-15: Induced shear forces on plate edges, a) Applied vertical tension and horizontal compression, b) Applied vertical tension only

The induced shear force, V, versus horizontal steel strain at mid-point of the steel plate under the two loading conditions are shown in Figure 5-16. Figures illustrate the results of the FE analysis of the plates strengthened with CFRP strands oriented with an angle of 45^{o} relative to the vertical tensile load. Each figure contains results of the control plate, plate strengthened with one layer and plate strengthened with two layers of HM CFRP strands. General behaviors confirm the effectiveness of the externally bonded CFRP material in increasing the shear capacity of the steel plates for both types of shear stress distributions. The strengthening system contributed to the load carrying capacity by highly reducing the horizontal strains at each load level which is resulted to an increase in shear capacity. Results indicate that with similar strengthening condition and at a given load, the induced horizontal steel strain of the panel subjected to the vertical tensile and horizontal compressive loads is higher than the panel subjected to vertical tensile load only. That behavior is attributed to the fact that presence of the horizontal load increases the horizontal steel strain.

Predicted results of shear capacity prior to the steel yielding obtained from the strengthened plates are also compared to the control plates and are given in Table 5-4 and shown as a bar chart in Figure 5-17. The specimens in these tables are identified as follows. The first letter of specimen ID represents type of loading condition, i.e., “T” is referred as tensile vertical load only and “TC” is referred as tensile vertical and horizontal compressive load condition. The second number specifies the slenderness ratio of the plate. The last letter shows the strengthening condition. For the control plates, letter “C” is used. For the strengthened plate, number of layers at each face, followed by type of CFRP material. The trend indicates that

increasing the reinforcement ratio of the CFRP strands contributes to higher shear capacity regardless to the loading conditions; since, it is dependent to the stiffness of the specimens. Therefore, general behavior indicates that the percentage increase in shear capacity is not dependent to the shear stress distribution along the edges of the steel plates. However, effectiveness of the strengthened plates with two layers of the CFRP strands is slightly more pronounced for the plates subjected to the rectangular shear stress distribution compared to the triangular shear stress distribution.

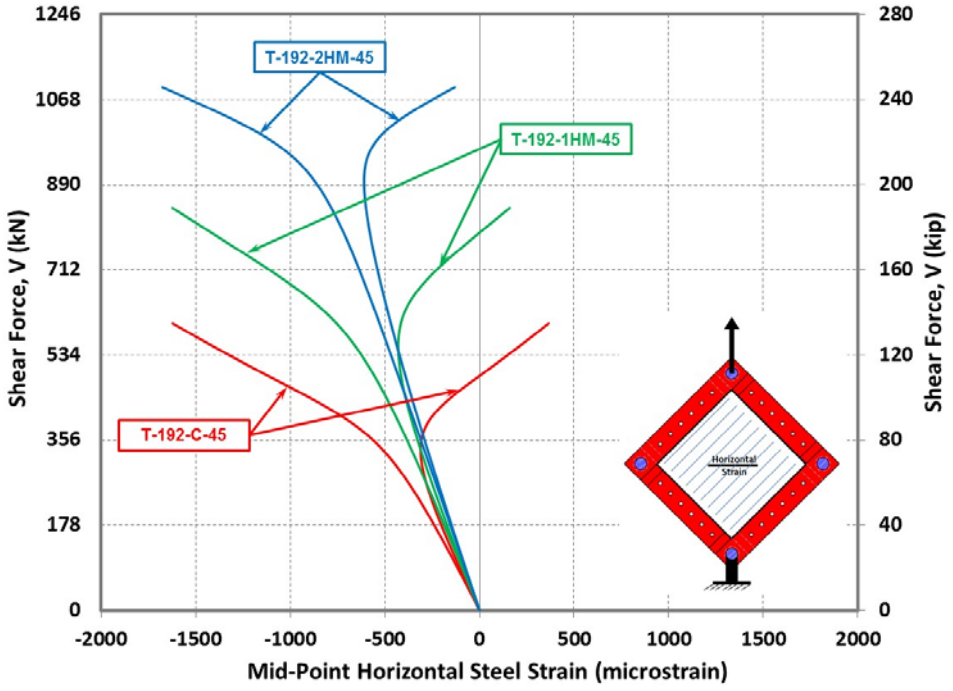

(a)

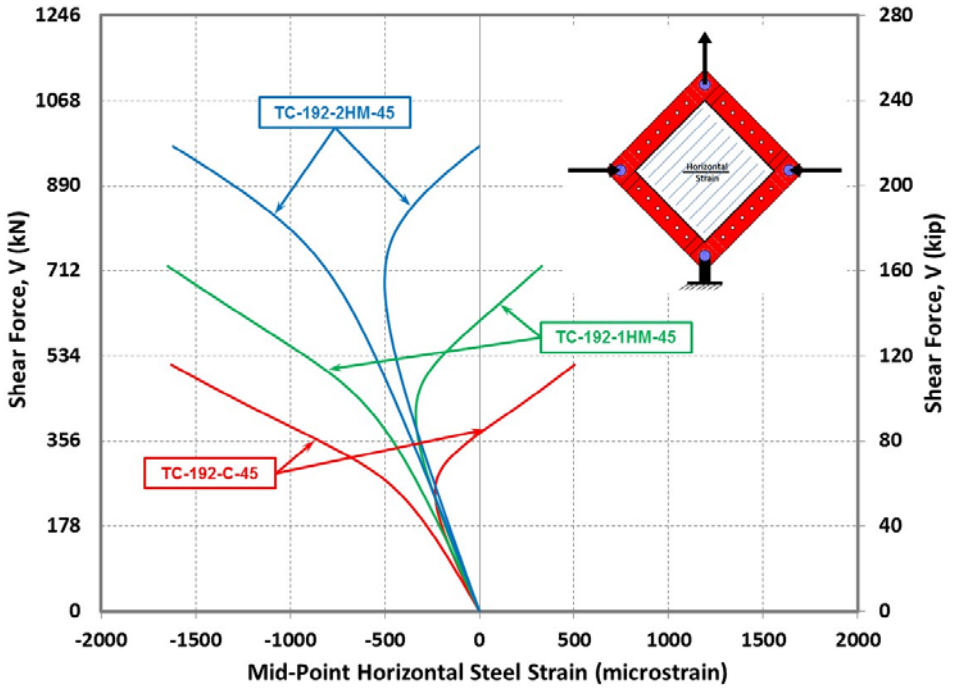

(b)

Figure 5-16: Applied load vs. horizontal steel strain at mid-point of the plates strengthened with 45 degree CFRP strands subjected to, a) Tensile load, b) Tensile and compressive loads

Table 5-4: Effect of loading conditions on shear capacity strengthened plates

Specimen ID	h/t	Loading Type	Fiber Orientation	No. of Layers	Plate Edge Shear Load		
					kips	kN	Increase (%)
T-192-C	192	Ten.	NO	NO	134	595	-
T-192-1HM-45		Ten.	45º	1	188	835	40
T-192-2HM-45		Ten.	45º	2	243	1080	82
TC-192-C		Ten. & Comp.	NO	NO	114	509	-
TC-192-1HM-45		Ten. & Comp.	45º	1	159	709	39
TC-192-2HM-45		Ten. & Comp.	45º	2	217	967	90
T-192-C	192	Ten.	NO	NO	134	595	-
T-192-1HM-90		Ten.	90º	1	198	882	48
T-192-2HM-90		Ten.	90º	2	257	1145	93
TC-192-C		Ten. & Comp.	NO	NO	114	509	-
TC-192-1HM-90		Ten. & Comp.	90º	1	169	750	47
TC-192-2HM-90		Ten. & Comp.	90º	2	233	1036	104
T-192-C	192	Ten.	NO	NO	134	595	-
T-192-1HM-45W		Ten.	45º	1	188	835	40
T-192-2HM-45W		Ten.	±45º	2	248	1104	86
TC-192-C		Ten. & Comp.	NO	NO	114	509	-
TC-192-1HM-45W		Ten. & Comp.	45º	1	159	709	39
TC-192-2HM-45W		Ten. & Comp.	±45º	2	223	993	95

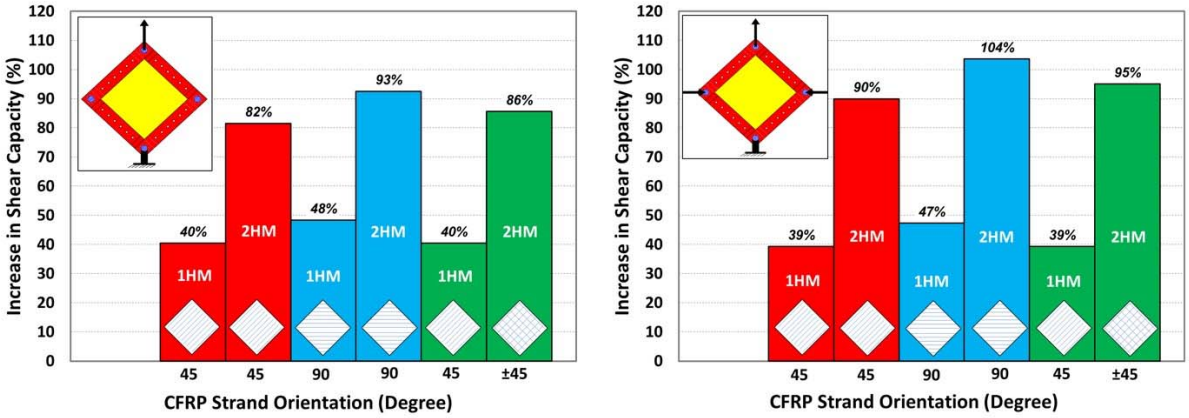

Figure 5-17: Shear capacity percentage increase of plates strengthened with one and two layers of HM CFRP strands under, a) Tensile load only, b) Tensile and compressive loads

5.2.1.3 *Effect of the CFRP Orientation*

The measured results of the experimental program previously showed that effect of the CFRP strengthening system is similar for plates strengthened with different orientations and selected reinforcement ratio as shown in in Chapter 3, Figure 3-113. However, detailed inspection of the test setup showed some misalignment of the steel plates with respect to the frame, not complete bearing of the bolts as well as different plate imperfections. Therefore, FE models were developed using different boundary conditions to determine the effectiveness of the CFRP orientations on the shear capacity of the strengthened steel plates. As shown in Figure 5-17 (a), for the steel plate subjected to similar loading condition as the experimental tests, FE predictions show that strengthened plates with CFRP strands oriented with an angle of 90^o can be slightly more effective than other orientations. This behavior can be mainly due to the bonding of the CFRP strands parallel to the direction of induced compressive stresses which results in shear buckling. However, cutting CFRP strands in the orientation of 90^o relative to the tensile stresses could produce significant wastes of the material. Therefore, it is recommended to use CFRP strands in the orientation of 45^o relative to the tensile stresses and additional layers in an orthogonal direction creating an angle of ±45^o relative to applied tensile load. This configuration for two layers of material efficiently decreases the effective length of the CFRP strands in compression and results in increasing the shear capacity and lateral stiffness of the strengthened plate compared with using two layers of CFRP strands both with an angle of 45^o.

5.2.2 Simple Analytical Approach

In this section, the theoretical shear load were determined using shear stress equation for section. Since the steel and the CFRP strengthening system have different material properties, the transformed section method was used to determine the shear load inducing shear yielding stress on the plate section. Use of the transferred section is due to the observed excellent perfect bond of the strengthening system to the steel substrate. The shear stress, τ, for the strengthened specimen with one and two layers of CFRP strands was estimated using following equations,

$$\tau = \frac{VQ}{It} \tag{3}$$

where,

$$I_t = I_s + \sum_{i=1}^{n} \frac{E_{fi}}{E_s} I_{fi} \tag{4}$$

$$t_t = t_s + \sum_{i=1}^{n} \frac{t_{fi}}{t_s} t_{fi} \tag{5}$$

V is shear force, Q is first moment of area, E_s and E_{fi} are elastic modulus of steel and the compressive elastic modulus of each CFRP layer, respectively. I_t, I_s, and I_{fi} are moment of inertia of the transformed cross-section, moment of inertia of steel, and moment of inertia of each CFRP layer. t_t, t_s, and t_{fi} are thickness of the transformed cross-section, moment of inertia of steel, and moment of inertia of each CFRP layer. Compressive elastic modulus of CFRP of the witness panels was used in calculations. The predicted shear forces of control specimen and strengthened specimens are compared and the percentage increase in shear strength are given in Table 5-5. The shear forces were predicted at shear stress equal to 60% of yield strength over the cross-section. The average measured percentage increase of the strengthened

specimens are also provided in the table. It is worth noting that the proposed analytical approach is not considering the effects of the CFRP strands orientation.

Table 5-5: Comparison between measured and predicted Shear capacities

Plate Designation	Analytical Approach			Measured Increase (%)		
	Shear Yielding		Increase (%)	Set#1 (45°)	Set#2 (90°)	Set#3 (±45°)
	kN	kip				
Control	781	176	-	-		
1 Layer HM Strengthened	978	220	25	36	23	24
2 Layer HM Strengthened	1175	264	51	65	67	79

The comparisons shown indicate that the shear load can be conservatively estimated using transformed section properties of the strengthened plate. For the design, the above analysis indicates that the shear capacity can be adequately predicted by using the composite transformed section properties of the strengthened steel plates.

6 SUMMARY AND CONCLUSION

This chapter provides the summary and conclusion of the research program undertaken to investigate the effectiveness of small-diameter CFRP strands to increase the shear capacity of web of steel girders. The research consists of a comprehensive experimental program and finite element modeling to study other parameters that were not considered in the experimental program. To evaluate the efficiency of the proposed small-diameter CFRP strands for shear strengthening of steel beams, their buckling behavior and the ability to undergo associated large deformations were initially investigated. This included strengthening of steel plates subjected to uniaxial compressive stresses and followed by strengthening of steel plates subjected to pure shear stresses.

6.1 SUMMARY

The proposed experimental program consisted of two phases. The first phase studied the effectiveness of the small-diameter CFRP strands to increase the uniaxial compressive capacity of steel plates. In this phase different slenderness ratio (h/t) of steel plates were considered. The selected ratios covered a wide spectrum of webs of typical steel bridge girders ranged from 48 to 154. Three types of CFRP strands high, intermediate and low elastic modulus, were examined to identify the most effective type of CFRP strands to increase the buckling capacity of steel plates. By applying layers of small-diameter CFRP strands, the effectiveness of using different reinforcement ratio of CFRP materials was examined. Furthermore, the effect of

using low-modulus polyurea putty on the de-bonding capacity of the CFRP strands was investigated.

The second phase of the experimental program examined the effectiveness of the proposed strengthening system to increase the shear capacity of the plates subjected to pure shear using unique test setup that is designed to simulate pure shear loading condition. The effect of using different fiber orientation and reinforcement ratio of CFRP strands were investigated in this phase.

The analytical investigation utilized commercially available FE models calibrated by the measured data. The models were used to study the effects of different parameters which were not considered in experimental program and believed to influence the behavior of CFRP strengthening system. The FE model was calibrated by the measured results of Phase I and extended to evaluate the effects of two boundary conditions including pin-pin and fix-fix end conditions, three reinforcement ratio, six slenderness ratio and three elastic modulus of the CFRP strengthening material on the compressive strength of the strengthened steel plates. Furthermore, the buckling load could be adequately estimated by Euler buckling equations using transformed section properties of the strengthened plate. The second phase of the analytical studies evaluated effects of strengthening system subjected to pure shear using wide range of five slenderness ratio, three CFRP strengthening materials, three orientations of CFRP strands, and combined tensile vertical and compressive horizontal loads.

6.2 CONCLUSIONS

Several conclusions were made from the measured behavior in the specimens tested in the experimental program. The conclusions are summarized as follows,

1. The small-diameter CFRP strands have proven to be an effective strengthening system for increasing the axial compressive and shear capacity of the steel plates.
2. The proposed strengthening system exhibits excellent bond characteristics in compression and in tension and eliminated any possible debonding at failure.
3. The effectiveness of the small-diameter CFRP strengthening system increased by increasing the slenderness ratio of the plates subjected to compressive or shear loads.
4. High-Modulus (HM) small-diameter CFRP strands provides a more effective strengthening system in comparison to Intermediate-Modulus (IM) and Low-Modulus (LM) CFRP strands for compressive and shear strengthening of steel plates.
5. Increase of CFRP reinforcement ratio increases the buckling and shear capacity of the strengthened plate.
6. The effectiveness of the proposed strengthening system on buckling capacity of steel plates is also a function of the boundary conditions and is increased by increase of effective length factor (K).
7. The initial lateral stiffness of steel specimen subjected to compressive or shear loads increases with the use of the CFRP strengthening system.
8. Polyurea putty has no significant effect on the bond characteristics and the efficiency of the CFRP strands strengthening system.

9. Increase in shear capacity of the strengthened steel plate with higher reinforcement ratio is slightly more pronounced for the plates subjected to the rectangular shear stress distribution compared to the triangular shear stress distribution.
10. It is recommended to use small-diameter CFRP strands for the shear strengthening of steel plates in an orientation parallel to the induced shear stresses. Additional layers of CFRP reinforcement is more effective if it is orthogonal to the bottom layer.
11. For design purposes, simple analytical approaches can be effectively used to estimate the buckling and shear capacity of the strengthened specimens using the transformed cross-section properties.
12. The percentage increase in buckling and shear capacity of the strengthened steel plates is effected by imperfections of the strengthened plate.

6.3 FUTURE WORKS

Future research may consider the following

- Full-scale testing of typical scaled steel bridge girders strengthened with CFRP strands to evaluate the effectiveness of the shear strengthening system for real bridges. The control steel girder specimens should be designed to fail in shear. Based on the results design guideline to predict the shear capacity of the actual strengthened steel girder should be proposed.
- Testing a combined flexural and shear strengthening of full-scale steel-concrete composite girders subjected to static loads.
- Determine the behavior of the proposed strengthening system under the effects of cyclic loads to evaluate the bond characteristics subjected to high cyclic deformation.
- Testing the durability and long-term behavior to determine possible degradation of strengthening system.

REFERENCES

[1] M. Dawood, D. Schnerch, E. Sumner, and S. Rizkalla, "Strengthening steel bridges with new high modulus CFRP materials," in *Third international conference on bridge maintenance, safety and management (IABMAS'06). Portugal*, 2006.

[2] G. Vasdravellis and B. Uy, "Shear Strength and Moment-Shear Interaction in Steel-Concrete Composite Beams," *Journal of Structural Engineering,* vol. 140, p. 04014084, 2014.

[3] A. P. Rathod and T. P. Vora, "FIBER REINFORCED POLYMER REINFORCEMENT FOR CONSTRUCTION-STATE OF THE ART REVIEW," *stress (Mpa),* vol. 276, p. 517.

[4] L. Ye, P. Feng, X. Lu, P. Qian, L. Lin, Y. Huang, *et al.*, "FRP in China: the state of FRP research, design guidelines and application in construction," in *FRP Composites in Civil Engineering-CICE 2004: Proceedings of the 2nd International Conference on FRP Composites in Civil Engineering-CICE 2004, 8-10 December 2004, Adelaide, Australia*, 2002, p. 109.

[5] A. Rahai and H. Akbarpour, "Experimental investigation on rectangular RC columns strengthened with CFRP composites under axial load and biaxial bending," *Composite Structures,* vol. 108, pp. 538-546, 2014.

[6] J. Ortigao, "FRP applications in geotechnical engineering," in *Proc. ASCE 4th Materials Engineering Conference, Washington DC*, 1996, pp. 535-544.

[7] S. M. Hejazi, M. Sheikhzadeh, S. M. Abtahi, and A. Zadhoush, "A simple review of soil reinforcement by using natural and synthetic fibers," *Construction and building materials,* vol. 30, pp. 100-116, 2012.

[8] S. A. Safavizadeh, "Fatigue and Fracture Characterization of GlasGrid® Reinforced Asphalt Concrete Pavement," Doctor of Philosophy, Civil Engineering, North Carolina State University, 2015.

[9] F. Canestrari, L. Belogi, G. Ferrotti, and A. Graziani, "Shear and flexural characterization of grid-reinforced asphalt pavements and relation with field distress evolution," *Materials and Structures,* vol. 48, pp. 959-975, 2015.

[10] S. A. Safavizadeh, A. Wargo, M. Guddati, and Y. R. Kim, "Investigating Reflective Cracking Mechanisms in Grid-Reinforced Asphalt Specimens: Use of Four-Point Bending Notched Beam Fatigue Tests and Digital Image Correlation," *Transportation Research Record: Journal of the Transportation Research Board,* pp. 29-38, 2015.

[11] L. C. Hollaway and M. Leeming, *Strengthening of reinforced concrete structures: Using externally-bonded FRP composites in structural and civil engineering*: Elsevier, 1999.

[12] F. Hosseini, B. Gencturk, S. Lahpour, and D. I. Gil, "An experimental investigation of innovative bridge columns with engineered cementitious composites and Cu–Al–Mn super-elastic alloys," *Smart Materials and Structures,* vol. 24, p. 085029, 2015.

[13] M. Hallaji and M. Pour-Ghaz, "A new sensing skin for qualitative damage detection in concrete elements: Rapid difference imaging with electrical resistance tomography," *NDT & E International,* vol. 68, pp. 13-21, 2014.

[14] N. Zolghadri, M. Halling, P. Barr, and S. Petroff, "Identification of Truck Types using Strain Sensors include Co-located Strain Gauges," in *Structures Congress 2013@ sBridging Your Passion with Your Profession*, 2013, pp. 363-375.

[15] N. Zolghadri, M. Halling, N. Johnson, and P. Barr, "Field Verification of Simplified Bridge Weigh-In-Motion Techniques," *J. Bridge Eng.,* 2016.

[16] X.-L. Zhao and L. Zhang, "State-of-the-art review on FRP strengthened steel structures," *Engineering Structures,* vol. 29, pp. 1808-1823, 2007.

[17] J. Teng, J. Chen, S. T. Smith, and L. Lam, "Behaviour and strength of FRP-strengthened RC structures: a state-of-the-art review," *Proceedings of the institution of civil engineers-structures and buildings,* vol. 156, pp. 51-62, 2003.

[18] C. Pellegrino and J. Sena-Cruz, "Design Procedures for the Use of Composites in Strengthening of Reinforced Concrete Structures."

[19] D. Schnerch, M. Dawood, S. Rizkalla, and E. Sumner, "Proposed design guidelines for strengthening of steel bridges with FRP materials," *Construction and building materials,* vol. 21, pp. 1001-1010, 2007.

[20] S. Rizkalla, M. Dawood, and D. Schnerch, "Development of a carbon fiber reinforced polymer system for strengthening steel structures," *Composites Part A: Applied Science and Manufacturing,* vol. 39, pp. 388-397, 2008.

[21] X.-L. Zhao, *FRP-Strengthened Metallic Structures*: CRC Press Taylor & Francis Group, LLC, 2014.

[22] X. Lu, J. Teng, L. Ye, and J. Jiang, "Bond–slip models for FRP sheets/plates bonded to concrete," *Engineering structures,* vol. 27, pp. 920-937, 2005.

[23] S. Xia and J. Teng, "Behaviour of FRP-to-steel bonded joints," in *Proceedings of the international symposium on bond behaviour of FRP in structures*, 2005, pp. 419-26.

[24] S. Fawzia, R. Al-Mahaidi, and X.-L. Zhao, "Experimental and finite element analysis of a double strap joint between steel plates and normal modulus CFRP," *Composite structures,* vol. 75, pp. 156-162, 2006.

[25] S. Fawzia, X.-L. Zhao, and R. Al-Mahaidi, "Bond–slip models for double strap joints strengthened by CFRP," *Composite Structures,* vol. 92, pp. 2137-2145, 2010.

[26] C. Wu, X. Zhao, W. H. Duan, and R. Al-Mahaidi, "Bond characteristics between ultra high modulus CFRP laminates and steel," *Thin-Walled Structures,* vol. 51, pp. 147-157, 2012.

[27] T. Yu, D. Fernando, J. Teng, and X. Zhao, "Experimental study on CFRP-to-steel bonded interfaces," *Composites Part B: Engineering,* vol. 43, pp. 2279-2289, 2012.

[28] D. Schnerch, K. Stanford, E. Sumner, and S. Rizkalla, "Bond behavior of CFRP strengthened steel bridges and structures," in *Proceedings of International Symposium on Bond Behavior of FRP in Structures, Hong Kong, China*, 2005.

[29] Schnerch, Dawood, Rizkalla, Sumner, and Stanford, "Bond behavior of CFRP strengthened steel structures," *Advances in Structural Engineering,* vol. 9, pp. 805-817, 2006.

[30] J. Teng, D. Fernando, T. Yu, and X. Zhao, "Debonding failures in CFRP-strengthened steel structures," in *Proceedings of the Third Asia-Pacific Conference on FRP in Structures*, 2012.

[31] J. Teng, D. Fernando, and T. Yu, "Finite element modelling of debonding failures in steel beams flexurally strengthened with CFRP laminates," *Engineering Structures,* vol. 86, pp. 213-224, 2015.

[32] E. Ghafoori and M. Motavalli, "Innovative CFRP-Prestressing System for Strengthening Metallic Structures," *Journal of Composites for Construction,* vol. 19, p. 04015006, 2015.

[33] D. Schnerch and S. Rizkalla, "Flexural strengthening of steel bridges with high modulus CFRP strips," *Journal of Bridge Engineering,* vol. 13, pp. 192-201, 2008.

[34] A. Fam, C. MacDougall, and A. Shaat, "Upgrading steel–concrete composite girders and repair of damaged steel beams using bonded CFRP laminates," *Thin-Walled Structures,* vol. 47, pp. 1122-1135, 2009.

[35] S. Tabrizi, H. Kazem, S. Rizkalla, and A. Kobayashi, "New small-diameter CFRP material for flexural strengthening of steel bridge girders," *Construction and Building Materials,* vol. 95, pp. 748-756, 2015.

[36] R. Sen, L. Liby, and G. Mullins, "Strengthening steel bridge sections using CFRP laminates," *Composites Part B: Engineering,* vol. 32, pp. 309-322, 2001.

[37] P. Colombi and C. Poggi, "An experimental, analytical and numerical study of the static behavior of steel beams reinforced by pultruded CFRP strips," *Composites Part B: Engineering,* vol. 37, pp. 64-73, 2006.

[38] H. Kazem, S. Tabrizi, H. Seliem, S. Rizkalla, and A. Kobayashi, "STRENGTHENING OF STEEL STRUCTURES USING SMALL-DIAMETER CFRP STRANDS," in *International Institute for FRP in Construction (IIFC)*, 2014.

[39] A. Shaat and A. Fam, "Axial loading tests on short and long hollow structural steel columns retrofitted using carbon fibre reinforced polymers," *Canadian Journal of Civil Engineering,* vol. 33, pp. 458-470, 2006.

[40] N. Silvestre, B. Young, and D. Camotim, "Non-linear behaviour and load-carrying capacity of CFRP-strengthened lipped channel steel columns," *Engineering Structures,* vol. 30, pp. 2613-2630, 2008.

[41] A. Shaat and A. Z. Fam, "Slender steel columns strengthened using high-modulus CFRP plates for buckling control," *Journal of Composites for Construction,* vol. 13, pp. 2-12, 2009.

[42] K. A. Harries, A. J. Peck, and E. J. Abraham, "Enhancing stability of structural steel sections using FRP," *Thin-Walled Structures,* vol. 47, pp. 1092-1101, 2009.

[43] X.-L. Zhao, D. Fernando, and R. Al-Mahaidi, "CFRP strengthened RHS subjected to transverse end bearing force," *Engineering structures,* vol. 28, pp. 1555-1565, 2006.

[44] X. Zhao and R. Al-Mahaidi, "Web buckling of lightsteel beams strengthened with CFRP subjected to end-bearing forces," *Thin-walled structures,* vol. 47, pp. 1029-1036, 2009.

[45] X. Zhao, "Tests on CFRP strengthened open sections subjected to end bearing forces," in *Proceedings of Asia Pacific conference on FRP in structures. Seoul, Korea*, 2009.

[46] J. Aguilera and A. Fam, "Bonded FRP plates for strengthening rectangular hollow steel section T-joints against web buckling induced by transverse compression," *Journal of Composites for Construction,* vol. 17, pp. 421-432, 2012.

[47] A. Patnaik, C. Bauer, and T. Srivatsan, "The extrinsic influence of carbon fibre reinforced plastic laminates to strengthen steel structures," *Sadhana,* vol. 33, pp. 261-272, 2008.

[48] A. M. Okeil, Y. Bingol, and M. R. Ferdous, "Novel technique for inhibiting buckling of thin-walled steel structures using pultruded glass FRP sections," *Journal of composites for construction,* vol. 13, pp. 547-557, 2009.

[49] A. Okeil, T. Ulger, and H. Babaizadeh, "Effect of adhesive type on Strengthening-By-Stiffening for shear-deficient thin-walled steel structures," *International Journal of Adhesion and Adhesives,* vol. 58, pp. 80-87, 2015.

[50] A. Okeil, T. Ulger, and H. Babaizadeh, "Performance of thin-walled steel beams strengthened with GFRP stiffeners bonded using two different adhesives," 2014.

[51] H. BabaizadehRoshanfekr, "FRP Stiffener Efficiency Coefficient for SBS Shear Strengthening Applications," Master of Science, Department of Civil and Environmental Engineering, Louisiana State University, 2012.

[52] K. Narmashiri, M. Z. Jumaat, and N. R. Sulong, "Shear strengthening of steel I-beams by using CFRP strips," *Scientific Research and Essays,* vol. 5, pp. 2155-2168, 2010.

[53] H. Kazem, L. Guaderrama, H. Selim, S. Rizkalla, and A. Kobayashi, "Strengthening of steel plates subjected to uniaxial compression using small-diameter CFRP strands," *Construction and Building Materials,* vol. 111, pp. 223-236, 2016.

[54] M. Alinia, A. Gheitasi, and S. Erfani, "Plastic shear buckling of unstiffened stocky plates," *Journal of Constructional Steel Research,* vol. 65, pp. 1631-1643, 2009.

[55] H. Kazem, S. Rizkalla, R. Seracino, and A. Kobayashi, "Small-Diameter CFRP Strands for Strengthening Steel Bridge Girder," in *The 12th International Symposium on Fiber Reinforced Polymers for Reinforced Concrete Structures (FRPRCS-12) & The 5th Asia-Pacific Conference on Fiber Reinforced Polymers in Structures (APFIS-2015) Joint Conference*, Nanjing, China, 14-16 December 2015.

[56] H. Kazem, S. Rizkalla, and A. Kobayashi, "Shear and Buckling Strengthening of Steel Bridge Girder Using Small-Diameter CFRP Strands," in *20th International Conference on Composite Materials*, Copenhagen, Denmark, 19-24th July 2015.

[57] E. H. Gaylord, C. N. Gaylord, and J. E. Stallmeyer, *Design of steel structures*, 1992.

[58] A. V. D. Neut, "Post Buckling Behavior of Structures," Delft-Nederland,July 1956.

[59] "ANSYS® Workbench Academic Research," v.16.1 ed, 2016, p. Finite Element Modeling Software.

[60] S. C. Tan, *Stress concentrations in laminated composites*: CRC Press, 1994.

[61] Y. Okuyama, T. Miyashita, T. Ogata, K. Fujino, K. Ogaki, Y. Hidekuma*, et al.*, "Mechanical Behavior of Plate Bonded FRP Sheets Under Uniaxial Compression Load," *APFIS2012,* 2012.

[62] H.-H. Lee, *Finite Element Simulations with ANSYS Workbench 16*: SDC publications, 2015.

[63] Available: http://www.applied.com/site.cfm/CoefficientsofFriction.cfm